Cover Page

Universiteit Leiden

Leiden University Repository

The handle http://hdl.handle.net/1887/58472 holds various files of this Leiden University dissertation.

Author: Witte, W.E.A. de
Title: Mechanistic modelling of drug target binding kinetics as determinant of the time course of drug action in vivo
Issue Date: 2017-12-19

Mechanistic modelling of drug target binding kinetics as determinant of the time course of drug action *in vivo*

Wilhelmus E. A. de Witte

The research described in this thesis is part of the K4DD (Kinetics for Drug Discovery) consortium which is supported by the Innovative Medicines Initiative Joint Undertaking (IMI JU) under grant agreement no 115366. The IMI JU is a project supported by the European Union's Seventh Framework Programme (FP7/2007–2013) and the European Federation of Pharmaceutical Industries and Associations (EFPIA).

The research was performed at the division of Pharmacology of the Leiden Academic Center for Drug Research, Leiden University, The Netherlands.

Publication of this thesis was financially supported by Cisbio and Greiner Bio-One.

Printed by GVO Printers and Designers B.V., Ede, The Netherlands

ISBN: 978-94-6332-278-2

©2017 Wilhelmus E.A. de Witte (WilbertdeW@gmail.com)

Copyright left-hand cover figure: Alex Antonio Ramirez Arias © 123RF.com

Copyright right-hand cover figure: molekuul © 123RF.com

No part of this thesis may be reproduced or transmitted in any form or by any means without written permission of the author and the publisher holding the copyright of the published articles

Mechanistic modelling of drug target binding kinetics as determinant of the time course of drug action *in vivo*

Proefschrift

ter verkrijging van

de graad van Doctor aan de Universiteit Leiden,

op gezag van Rector Magnificus Prof. mr. C.J.J.M. Stolker,

volgens besluit van het College voor Promoties

te verdedigen op 19 december 2017

klokke 15.00 uur

door

Wilhelmus Egbertus Arnout de Witte

Geboren te Harderwijk, Nederland

op 25 maart 1989

Promotoren:	Prof. Dr. M. Danhof
	Prof. Dr. P. H. van der Graaf
Co-promotor:	Dr. E. C. M. de Lange
Promotie commissie:	Prof. Dr. H. Irth (voorzitter)
	Prof. Dr. J.A. Bouwstra (secretaris)
	Prof. Dr. S. J. Charlton, University of Nottingham
	Prof. Dr. A. Vermeulen, Universiteit Gent
	Prof. Dr. A. P. IJzerman
	Dr. M. van der Stelt
	Dr. J. H. Proost

Table of contents

Section I: General introduction **6**

Chapter 1. Mechanistic models enable the rational use of in vitro drug-target binding kinetics for better drug effects in patients 6

Chapter 2. The long residing negligence of target saturation 30

Chapter 3. Mechanistic modelling of drug target binding kinetics as determinant of drug effect kinetics: Scope and intent of the investigations 39

Section II: Simulations, model analysis and experimental validation of the influence of binding kinetics on the time course of target occupancy **46**

Chapter 4. In vivo target residence time and kinetic selectivity: the association rate constant as determinant. 46

Chapter 5. The influence of drug distribution and drug-target binding on target occupancy: The rate-limiting step approximation 77

Chapter 6. Target and tissue selectivity prediction by integrated mechanistic pharmacokinetic-target binding and quantitative structure activity modelling 88

SECTION III. Simulations, model analysis and experimental validation of the influence of binding kinetics on the time course of drug action **119**

Chapter 7. Modelling the delay between PK and EEG effects of morphine in rats; binding kinetic versus effect compartment models 119

Chapter 8. In vitro and in silico analysis of the influence of D2 antagonist target binding kinetics on the cellular response to fluctuating dopamine concentrations 159

SECTION IV. Discussion, perspectives and conclusion **194**

Chapter 9. Mechanistic modelling of drug target binding kinetics as determinant of the time course of drug action in vivo: Discussion, perspectives and conclusion 194

Acknowledgements 207

Curriculum Vitae 208

List of publications 209

Chapter 1. Mechanistic models enable the rational use of *in vitro* drug-target binding kinetics for better drug effects in patients

Wilhelmus E.A. de Witte[1] , Yin Cheong Wong[1], Indira Nederpelt[2], Laura H. Heitman[2], Meindert Danhof[1], Piet H. van der Graaf[1], Ron A.H.J. Gilissen[3], Elizabeth C.M. de Lange[1*]

[1] Division of Pharmacology, Leiden Academic Centre for Drug Research, Leiden University, Einsteinweg 55, 2333 CC, Leiden, The Netherlands.
[2] Division of Medicinal Chemistry, Leiden Academic Centre for Drug Research, Leiden University, Einsteinweg 55, 2333 CC, Leiden, The Netherlands.
[3] Janssen Research and Development, A Division of Janssen Pharmaceutica N.V., Turnhoutseweg 30, Beerse 2340, Belgium

*corresponding author: ecmdelange@lacdr.leidenuniv.nl

Expert Opin Drug Discov 2016;11(1):45–63

Abstract

Introduction: Drug-target binding kinetics are major determinants of the time course of drug action for several drugs, as clearly described for the irreversible binders omeprazole and aspirin. This supports the increasing interest to incorporate newly developed high-throughput assays for drug-target binding kinetics in drug discovery. A meaningful application of *in vitro* drug-target binding kinetics in drug discovery requires insight in the relation between *in vivo* drug effect and *in vitro* measured drug-target binding kinetics.

Areas covered: In this review, the authors discuss both the relation between *in vitro* and *in vivo* measured binding kinetics and the relation between *in vivo* binding kinetics, target occupancy and effect profiles.
We conclude that more scientific evidence is required for the rational selection and development of drug-candidates on basis of *in vitro* estimates of drug-target binding kinetics.

Expert opinion: To elucidate the value of *in vitro* binding kinetics measurements, it is necessary to obtain information on system-specific properties which influence the kinetics of target occupancy and drug effect. Mathematical integration of this information enables the identification of drug-specific properties which lead to optimal target occupancy and drug effect in patients.

Abbreviations: GPCR: G-Protein Coupled Receptor, HTRF: Homogeneous Time-Resolved Fluorescence, NA: Not Available, PET: Positron Emission Tomography, SAW: Surface Acoustic Wave, SPECT: Single Photon Emission Computed Tomography, SPR: Surface Plasmon Resonance, TO: target occupancy.

1. Introduction

The rates of drug-target association and dissociation are essential determinants of the time course of target binding and drug effect. This is most clearly illustrated by the irreversible binders aspirin and omeprazole, which have shown a long-lasting effect in clinical practice [1–3]. Numerous other examples confirm that drug-target binding kinetics are important drug characteristics, as reviewed by others [4–6].

The relevance of drug-target binding arises from their connecting role between pharmacokinetics and pharmacodynamics. More precisely, for a given drug concentration profile, the kinetics of drug-target binding determine the time course of target occupancy and thus the time course of drug effect. The basic concepts of target equilibration kinetics are well established. The simplest mechanism to describe drug-target binding is depicted in equation 1,

$$T + L \underset{k_{off}}{\overset{k_{on}}{\rightleftharpoons}} TL \qquad (1)$$

in which T = target concentration, L = ligand concentration, k_{on} = the second order association rate constant, and k_{off} = the first order dissociation rate constant. However, more complex mechanisms have been described in which target activation and G-protein binding (for GPCR's) are incorporated [5,7]. Affinity, the ratio of the dissociation and association rate constants ($K_D = k_{off}/k_{on}$), is related to binding kinetics, but informs only on the extent of binding at equilibrium and gives no information on the required time to reach a new equilibrium.

The important role of drug-target binding kinetics as a determinant of target occupancy profiles has been known for long, and both *in vitro* and *in vivo* measurements of association and dissociation kinetics have been reported from the eighties of last century [8–10]. However, with the development of high-throughput *in vitro* methods for binding kinetics, such as SPR, the interest in the use of binding kinetics in drug discovery has been rising in the past ten years. This has also led to the development of structure-kinetics relationships (SKR's) for some drug classes [11,12]. The recent attention for binding kinetics in drug discovery focuses mostly on the drug-target dissociation rate, since a slow dissociation rate is expected to give a prolonged duration of drug action and improved efficacy [5,6,13–16].

While most recent publications express an expected benefit of incorporating drug-target binding kinetics in drug discovery, more critical studies have also been published. On basis of basic pharmacokinetic/pharmacodynamic simulations, Dahl and Akerud indicated that the relevance of binding kinetics in drug treatment depends on a drug's pharmacokinetics [15]. Several other studies have indicated that multiple other physiological processes can influence the impact of drug-target binding kinetics on drug effect, including endogenous competition, diffusion-limited binding and signal transduction [17–19]. While these simulations might contain oversimplifications and cannot be applied to all cases of drug treatment, it is important to realize that the impact of drug-target binding kinetics on drug action depends on multiple kinetic processes in the human body.

To incorporate the role of drug-target binding kinetics in this complexity of kinetic processes, mathematical models have been developed to describe and predict the time profile of drug effects for several drugs and targets [20–26]. These models have been used to estimate drug-target binding kinetics on basis of pharmacokinetic and pharmacodynamic data, which supports the relevance of drug-target binding kinetics for drug action.

In summary, the available literature indicates a growing interest in the application of screening techniques for binding kinetics in drug discovery and a context dependency for the impact of drug-target binding kinetics on drug effect. This poses the question under which conditions the *in vitro* screening of binding kinetics would further drug discovery and development. To answer this question, this review aims to investigate the value of *in vitro* binding kinetics measurements for the prediction of *in vivo* target occupancy and drug effect, using available literature with emphasis on two questions:

- What is the relation between *in vitro* measured binding kinetics and *in vivo* measured binding kinetics?
- To what extent do binding kinetics contribute to target occupancy and drug effect profiles *in vivo*?

To that end, first, the available methods to measure drug-target binding kinetics both *in vitro* and *in vivo* will be addressed and discussed. Second, we will discuss to what extent the estimates of these *in vitro* and *in vivo* methods provide comparable results, and what experimental conditions are required to enable translation of *in vitro* to *in vivo* binding kinetics. Third, we will discuss binding kinetics in a broader perspective, i.e. in the context of the other determinants of target occupancy and drug effect. Finally, the integration of all kinetic processes will be discussed, as well as their implementation in the various phases of drug discovery and development.

2. *In vitro* methodological approaches to measure binding kinetics

2.1 Labeled-ligand assays

Various methods are available to determine *in vitro* kinetic binding parameters of compounds of interest at their respective target. In this review, we will use “ligand” to refer to compounds of interest (either labeled or unlabeled) and we will use “tracer” to refer to labeled or unlabeled compounds with known binding characteristics intended to inform about the binding of compounds of interest. The methods as discussed below are summarized in table 1.

2.1.1 Radiolabel-based assays

The most commonly used and straightforward method to characterize target binding is the use of radioligand binding assays. These assays use a radiolabeled ligand and can directly measure the association and dissociation rates of the radiolabeled ligand. In addition to traditional association and dissociation experiments, other kinetic radiolabel-based binding assays such as a competition association assay are emerging. This type of assay is an indirect assay based on a theoretical model developed by Motulsky & Mahan in 1984 by which one can quantitatively determine the binding kinetics of unlabeled ligands in a competitive assay using only one radiotracer [16,27–29]. The competition association assay can also be used in a higher-throughput fashion with the recently developed dual-point competition association assay. Only two timepoints are selected here to measure radiotracer binding; the ratio of binding at both time points gives a qualitative measure of the ligands’ dissociation kinetics. This makes this simplified assay a suitable method for screening potential drug candidates with favorable dissociation kinetics [30].

2.1.2 Fluorescent label-based assays

Similarly, instead of using a radiolabeled tracer in a competition assay the tracer can also be fluorescently labeled and used in homogeneous time-resolved fluorescence (HTRF) assays. Similar to the radioligand competition assay, only one fluorescently labeled tracer is required and the binding kinetics of competitive ligands can be determined in an indirect fashion. This method is homogeneous since it requires no physical separation of bound and free ligand which enables continuous measurements and increases the throughput. HTRF assays are successfully applied in the determination of binding kinetics of dopamine D_2 receptor antagonist spiperone [31] and more recently for histamine H_1 receptor ligands [32] and GnRH receptor agonists [Nederpelt *et al.,* 2015, submitted for publication]. Of note, in addition to a fluorescently labeled tracer a fluorescently labeled receptor is needed for this method, as opposed to wild-type receptors for radioligand and radiotracer binding.

Table 1. Overview of *in vitro* methods to measure drug-target binding kinetics.

	***In vitro* methods**						
Technique	radioligand	radiotracer	HTRF	SPR	SAW	Organ bath	Washout
Throughput rate	Low	Low-medium	medium	medium	medium	Low	Low
Required labeling	Radiolabeled ligand	Radiolabeled tracer	Fluorescently labeled tracer	None	None	None	None
Receptor environment	Membrane fractions	Membrane fractions	Whole cells	Isolated	Isolated	Native tissue/ whole cells/ membrane fractions	Native tissue/ whole cells/ membrane fractions
Relation to ligand binding kinetics	Direct	Inferred from tracer binding	Inferred from tracer binding	Direct	Direct	Inferred from effect	Inferred from effect
Major confounding factors	Lack of intracellular environment	Lack of intracellular environment	Fluorescent labeling of target	Non-native target environment	Non-native target environment	Microkinetics, rebinding, signal transduction	Microkinetics, rebinding, signal transduction

SAW: Surface Acoustic Wave, HTRF: Homogenous Time-Resolved Fluorescence, SPR: Surface Plasmon Resonance

2.2 Label-free assays

Several label-fee methods can be applied for kinetic target binding measurements without the need of a labeled ligand or labeled tracer.

2.2.1 Surface plasmon resonance

The most instilled label-free measurement is surface plasmon resonance (SPR) spectroscopy [33]. This method has the potential to be medium-throughput and the capability to measure real-time quantitative binding kinetics of ligands for membrane proteins using relatively small quantities of protein. The traditional SPR method needs one immobilized binding component on a coated gold sensor chip during which the ligand in solution is flowed over the sensor chip. This induces a real time change in the refractive index on the sensor surface which is linear to the number of molecules bound [33–35].

2.2.2 Acoustic wave biosensor

Another label-free technology is the surface acoustic wave biosensor [36]. This methodology captures real-time mass changes on the surface, which result in a shifted phase and/or changed amplitude of a sound wave signal [37]. A disadvantage of these biophysical approaches for G protein-coupled receptors is that these receptors are integral membrane proteins that rapidly disintegrate when taken out of their natural environment, which is a prerequisite for these approaches. However, recent advances are made to overcome this problem [33].

2.3 Functional assays

Another way to determine drug-target binding kinetics is by use of functional assays. These assays provide an indirect measurement of binding kinetics by characterizing the time profile of drug effect. Although the use of functional assays is generally limited due to the indirect nature of these measurements, functional assays are valuable for the measurement of enzyme binding kinetics because of the direct relation between enzymatic product generation rates and enzyme inhibitor binding. Functional assays can be carried out in two different settings, either by resembling the classical ‘’organ bath’’ experiment or by washout experiments.

2.3.1 Organ bath

An organ bath experiment is only suitable to qualitatively examine binding kinetics of antagonists and requires pre-incubation of cells/tissues with antagonists prior their challenge with an agonist. With this method the distinction between so-called surmountable and insurmountable antagonists can be made, where the level of insurmountability by an antagonist is related to its receptor dissociation kinetics [18,38,39].

2.3.2 Washout

Functional washout experiments are suitable for predicting binding kinetics of both agonists and antagonists. In this type of experiments, the rate of decrease in effect after removal of the free ligand by repeated washing (washout) is measured. Agonists with fast dissociation kinetics will readily wash out and will show a right-ward shift in their potency, whereas agonists with slow dissociation kinetics will show insignificant shifts in their potency, and *vice versa* for antagonists. It should be stated that control experiments are necessary to confirm that the long-lasting effect of the ligand is due to long target binding versus other effect-prolonging factors (such as exo-site binding, membrane partitioning, rebinding or signal transduction [40–42].

3.1 In vivo methodological approaches to measure binding kinetics

3.1.1 General principle of target occupancy measurements

To obtain drug-target binding kinetics *in vivo,* target occupancy and target site concentrations are required. For most *in vivo* and *ex vivo* approaches, the target occupancy of a drug is measured indirectly by using a tracer. The administered drug competes at the same target site with the tracer and the reduction in specific binding of the tracer is used to calculate the target occupancy of the drug. The tracer can be an antagonist (more common) or agonist to the target, and can be radiolabeled (more common) or non-radiolabeled. The advantages and disadvantages of each approach will be briefly discussed, and the characteristics of each approach are summarized in table 2. We focus here mainly on methods which are in use for measurement of binding kinetics in the brain, since most methods have been used primarily for the brain targets.

3.1.2 Tissue homogenate method with radiolabeled tracer

The traditional way of measuring CNS target occupancy in preclinical animals is the brain homogenate method. At a pre-determined time point after radiotracer administration, the animal is sacrificed and the brain regions of interest (e.g. striatum for D_2 receptors) and the reference region (e.g. cerebellum which has relatively low D_2 receptor density, for the correction of non-specific binding of radiotracer to and uptake in brain tissue) are collected. These brain regions are then dissolved in a scintillation cocktail and the drug-induced change in radioactivity of the tracer is measured by a liquid scintillation counter. Literature reports suggest that the target occupancy values obtained by this method are comparable to that obtained by positron emission tomography (PET) imaging [43]. Compared with PET/SPECT (single-photon emission computed tomography) imaging, this method is associated with much lower costs and allows higher throughput in screening different compounds or different doses of a single compound. Nevertheless, since this method involves the terminal use of animals, a continuous target occupancy time profile within the same animal cannot be obtained, and multiple animals are needed for a single target occupancy time profile. Moreover, in addition to the receptors expressed on the membrane surface, intracellular or internalized receptors would also become accessible to the tracer when the tissue is homogenized, which might hamper the accuracy of target occupancy assessment for membrane-bound receptors [44].

Table 2. Overview of *in/ex vivo* methods to measure drug-target binding kinetics.

	In vivo methods					***Ex vivo* methods**	
Technique	PET scan	SPECT scan	Beta-microprobe	Tissue homogenate method with radiolabelled tracer	Tissue homogenate method with non-radiolabelled tracer	Single time-point, tissue homogenate method with radiolabelled tracer	Single time-point, tissue slice method with autoradiography imaging
Subjects	Living humans or animals	Living humans or animals	Living animals	Animals sacrificed at a specific post-drug dosing time point	Animals sacrificed at a specific post-drug dosing time point	Animals sacrificed at a specific post-drug dosing time point	Animals sacrificed at a specific post-drug dosing time point
Equipments	Cyclotrons and PET scanner	SPECT scanner	Positron-sensitive probe	Scintillation counter	Liquid chromatograph /mass spectrometer	Scintillation counter	Autoradiographic film, storage phosphor imager or beta-imager
Radiolabelled tracer needed?	Yes	Yes	Yes	Yes	No	Yes	Yes
Simultaneous TO determination for multiple receptors?	Difficult	Yes	No	No	Yes	No	Yes
Relation to drug binding kinetics	Inferred from tracer binding	Inferred from tracer binding	Inferred from tracer binding	Inferred from tracer binding from multiple tissue samples	Inferred from tracer binding from multiple tissue samples	Inferred from tracer binding from multiple tissue samples	Inferred from tracer binding from multiple tissue samples
Major confounding factors	Anesthesia, tracer metabolite interference	Anesthesia, tracer metabolite interference	Tissue damage, tracer metabolite interference	Tracer dose, dosing time of tracer, tracer metabolite	Tracer dose, dosing time of tracer	Tracer incubation period and temperature	Tracer incubation period and temperature

PET: Positron Emission Tomography, SPR: Surface Plasmon Resonance, SPECT: Single Photon Emission Computed Tomography, TO: target occupancy

3.1.3 Tissue homogenate method with non-radiolabeled tracer using LC/MS assays

The procedures of this method are the same as that with radiolabeled tracer as described above, except that a non-radiolabeled tracer (cold tracer) is administered to the animal and the absolute amount of the tracer in the brain tissues is quantified by LC/MS. The first report was presented by Phebus and colleagues, in which the drug-induced target occupancy of D_2, serotonin 2A and NK-1 receptors in rat was quantified using non-radiolabeled tracers [45]. They also demonstrated in rats that for the eight D_2-antagonists they had investigated, the doses required to achieve 50% target occupancy using this LC/MS method (cold raclopride as tracer) are comparable to those using the traditional brain homogenate method ([^{3}H]raclopride as tracer) [46]. This method offers several advantages; first, the parent, intact tracer in the brain tissue can be differentiated from the tracer metabolites, thus increasing the accuracy of tracer quantification. Second, the costs and hazards associated with radioactivity are avoided. Third, it allows separation and quantification of different tracers in one sample, and thus enables the simultaneous assessment of the target occupancy of different receptors [47].

The greatest concern of this method is the relatively high dose of the tracer that needs to be administered. Since the sensitivity of an LC/MS assay is lower than that of radioactivity counting, a much higher dose of the tracer is administered in order to achieve a quantifiable tissue concentration. This high tracer dose might distort the drug-induced target occupancy and might exert pharmacodynamics effects [48,49].

3.1.4 PET/SPECT imaging

PET and SPECT imaging are the most common approaches to measure drug target occupancy in living humans and other primates. After the administration of a very small dose of radiotracer for the desired target, scans are carried out by the PET or SPECT scanner before and after administration of the competing drug. The radioactivity at the region of interest is measured, from which the density of receptors (B_{max}) and the radiotracer binding affinity (K_D) are derived. The ratio of B_{max} and K_D is termed the binding potential. The target occupancy of the drug is calculated as the percentage reduction in binding potential after drug administration. Binding kinetic parameters (k_{on}, k_{off}) can be derived if the target occupancy and free drug PK at the binding site are available by fitting a mathematical model which describes binding kinetics according to scheme 1. However, the PET signal arises from the sum of free, specifically and non-specifically bound radiotracer, and free concentrations cannot be measured at the binding site. Instead of the free drug pharmacokinetics at the binding site, a reference tissue which is similar to the binding site but has no specific binding is commonly used [50,51]. PET/SPECT can be regarded as an *in vivo* version of autoradiography (discussed in the *ex vivo* section), with inferior spatial resolution but with the advantage that the pharmacokinetics of the tracer can be measured in a single experiment, or even in repeated studies on the same subject [52]. This also provides the possibility to obtain target occupancy values at different time points within the same subject. Over the past decade, there are considerable developments of both PET and SPECT systems with improved spatial resolution designed specifically for small-animal imaging (i.e. microPET and microSPECT).

A limiting factor in longitudinal PET/SPECT measurements is the half-life of the radioactive decay of the tracer (depending on the applied radiolabel), which can limit the duration of the experiment after tracer administration. This limited duration of the imaging decreases the suitability of PET/SPECT for measuring drugs with slow binding kinetics

One of the main concerns in PET/SPECT is that the anesthesia, applied to immobilize the animals before and during imaging, could hamper the accuracy of target occupancy assessment by, for example, altering the level of neurotransmitters [53]. Moreover, the use of anesthesia might also impose additional experimental variability (e.g. due to variable susceptibility to the anesthetic effect [54]).

Since both the tracer and the drug of interest interact with the same receptor, the observed effect cannot be completely attributed to the drug. Therefore, drug effect measurements are considered less useful, except for studies which are focused on the binding and effect of only the tracer. Depending on the target of interest, the required anesthesia can also interact with drug effects and make their measurement impossible or less useful.

3.1.5 Beta-microprobe

Another method of measuring a radiotracer in a living animal's brain is the use of a beta-microprobe. The microprobe captures beta/positron emission (similar to the PET detector) and is surgically implanted in the brain structures of interest, allowing *in vivo* measurement of local radioactivity concentrations within 1-2 millimeters from the probe. Reports on the application of beta-microprobe on target occupancy assessment are limited. Good correlations have been reported between *in vivo* beta-microprobe measurements and *ex vivo* brain homogenate and *in vivo* microPET measurements of respectively D_2 and $5HT_{1A}$ target occupancy in rat brain [55,56].

The potential advantages of beta-microprobe are that the target occupancy could be measured in awake, non-anesthetized animals and simultaneous assessment of drug-induced changes in behavior is allowed, which are critical for drugs that act on CNS receptors. Nevertheless, the surgical implantation procedures might interfere with the neurochemistry and the pharmacokinetics and pharmacodynamics of the drug and tracer. Implantation of the electrode into the brain would cause mechanical trauma and trigger both acute and chronic tissue responses, and the final outcome depends on factors such as the size, geometry and material of the probe, the insertion method, and the period after insertion [57]. Device implantation could also alter the release of neurotransmitters and neural activity [58]. While the previously developed beta-microprobes were based on a single pixel scheme that did not provide any spatial information on the radiotracer distribution [55], a new wireless probe was recently published, which contains 10 submillimeter pixels which allows the analysis of the spatial distribution of the radiotracer within the region of interest in freely moving rats [59].

3.2 Ex vivo approaches of target occupancy measurements

3.2.1 Tissue homogenate method with radiolabeled tracer

While for *in vivo* methods both the drug and the tracer are administered to the living animals, for *ex vivo* methods the tracer is added to the collected tissue from the drug-treated animal, and the amount of radiotracer bound to the target in the homogenate is measured by liquid scintillation counting. In this way tracers with unfavorable *in vivo* characteristics (e.g. slow equilibrium at target tissue, pharmacokinetic variability etc.) can be used and the costs of developing suitable tracers are reduced and the amount of tracer can be precisely controlled. However, the values of target occupancy obtained by this method are highly dependent on the binding conditions (particularly the time and temperature of tracer incubation) and tend to give an underestimation of drug-induced target occupancy [60]. This is mainly due to the dissociation of the drug from the receptor during the *ex vivo* tracer incubation and the tissue homogenization step, particularly for those drugs with a fast dissociation rate from the receptor. Therefore, a short incubation time and a radiotracer with a fast association rate is recommended [60].

3.2.2 Tissue slice autoradiography imaging

The procedures of this method are the same as that with tissue homogenate method described above, except that the animal tissue is sectioned into slices and the amount of radiotracer bound to the target is quantified by autoradiography. Unlike tissue homogenate, the tissue slice preparation maintains structural integrity. It offers higher spatial resolution than PET/SPECT imaging and thus allows the investigation of anatomical regions that are small in size. Traditionally, the radioactivity on the slice is captured by autoradiographic film, which requires a long exposure period (weeks) and thus is not considered as an efficient screening method for determining the target occupancy of compounds [61]. The introduction of storage phosphor imaging is a major improvement in *ex vivo* receptor autoradiography, which shortens the exposure time from weeks to days or even one day [62]. An alternative method is to use a beta-imager which uses a highly sensitive gaseous detector of beta particles. This allows the exposure time to be shortened to a few hours [63].

4. Comparison of *in vitro* and *in/ex vivo* measurements of binding kinetics

To investigate whether the current *in vitro* and *in vivo* measurements of binding kinetics deliver similar or translatable values, we performed a literature survey to identify compounds for which both *in vitro* and *in vivo* estimates of target association or dissociation rates were available. Since *in vivo* estimates are the least available, we started our search with *in vivo* estimates and continued to search for *in vitro* estimates of the same compounds. Since the number of compounds for which we could find *in vitro* and *in vivo* estimates of their target binding kinetics was very low, we decided to list all estimates we could find and discuss the reliability and comparability of the estimates below. The results of this search are listed in table 3.

Based on table 3, we can start to answer our first question:

- What is the relation between *in vitro* measured binding kinetics and *in vivo* measured binding kinetics?

From the results in table 3, it can be directly seen that the difference between *in vitro* and *in vivo* estimates of target dissociation rates can be quite substantial (up to 30 fold) and inconsistent (the ratio varies from 0.2 to 31). This clearly indicates that the use of *in vitro* measured target binding kinetics to predict *in vivo* binding profiles is not straightforward. Apart from the studies in table 3, another study was published in which no *in vivo* values for k_{on} and k_{off} were included, but *in vitro* values were used to predict target occupancy profiles of the CRF1 receptor in rats for several antagonists [23]. Although the *in vivo* results were not highly informative for the identification of the binding kinetics for some compounds in this study, the target occupancy profiles could be predicted reasonably well.

To investigate the origin of the observed difference between *in vitro* and *in vivo* binding studies, the experimental details need to be taken into account to identify which results are less reliable or comparable.

4.1 Temperature

Firstly, all *in vitro* estimates of association and dissociation rates which are not obtained at 37 °C cannot be compared directly to *in vivo* estimates, since these rates are temperature dependent in a compound specific manner [85–87]. Therefore entry 3, 9, 12, 13, 17, 18 and 19 from table 3 cannot be used to compare *in vitro* and *in vivo* dissociation rates.

4.2 Influence of *in vivo* displacer/competitor dose

Another important factor in the comparison between *in vitro* and *in vivo* estimates of target dissociation rates is the method by which the dissociation is induced. Drug-target dissociation can be induced in *in vitro* studies either by continuous washing, the so-called “infinite dilution” method, or by displacement of the drug by adding an excess of a competing ligand. These methods can give quite different results since washing cannot displace all free ligand molecules and diffusion-limited binding (or “rebinding”) can occur. Thus, comparisons between *in vitro* and *in vivo* estimates should use the same method of dissociation measurement [19]. However, in the *in vivo* setting, continuous washing cannot be applied and the amount of competing compound which can be added is limited by its toxicological effects. In the analysis of *in vivo* drug-target binding studies, computational models can be used to correct for remaining drug concentrations or partial displacement. However, this is often not done and assumptions have to be made about the effect of a displacer dose or of a remaining drug concentration. For entry 1, 3, 4, 8 and 10 from table 3, the rationale for the displacer dose was not clear, and model-based analysis was not used. These entries should therefore not be used to compare *in vitro* and *in vivo* dissociation rates. For entry 1, the *in vitro* experiment did not use either a displacer or continuous washing, which makes it even less appropriate for comparison with the *in vivo* experiment.

For entries 14-19 in table 3, the *in vivo* drug-target binding kinetic parameters are estimated from PK and PD data without target occupancy measurements. This makes these estimates indirect and subject to influences of signal transduction kinetics and other factors between PK and PD. Therefore, entry 14-19 cannot be used for a direct comparison of *in vitro* and *in vivo* binding kinetic parameters.

Table 3. Literature data on estimated binding kinetics from *in vitro* and *in vivo* studies.

#	Drug (target)	$t_{1/2}$[a] assoc. *in vitro*	$t_{1/2}$[a] dissoc. *in vitro*	*In vitro* system[b]	$t_{1/2}$[a] assoc. *in vivo.*	$t_{1/2}$[a] dissoc. *in vivo*	Observed binding parameter (method)	Ref.	Ratio *in vivo/ in vitro*	
									assoc.	dissoc.
1	^{3}H-CGP 12177 (β-AR)	7	99	I	NA	50	dog heart (PET)	[64],[65]	NA	0.5
2	^{125}I-epidepride (D_2R)	267	13	II	NA	53	rhesus monkey striatum (SPECT)	[66]	NA	4
3	^{18}F-desmethoxy fallypride (D_2R)	3[c]	9[c]	III	NA	12	rhesus monkey striatum (PET)	[67]	NA	1
4	^{18}F-fallypride (D_2R)	1[c]	13	III	NA	169	rhesus monkey striatum (PET)	[68]	NA	13
5	^{18}F-fallypride (D_2R)	1[c]	13	III	NA	18[d]	rhesus monkey brain (PET)	[68],[69]	NA	1
6	^{18}F-fallypride (D_2R)	1[c]	13	III	NA	30[d]	rhesus monkey brain (PET)	[68],[70]	NA	2
7	^{18}F-spiperone (D_2R)	NA	56	IV/V	NA	50[e]	baboon striatum (PET)	[71],[72]	NA	0.9
8	^{3}H-spiperone (D_2R)	5	20	III	1690	231	rat striatum (homogenate)	[73]	338	12
9	Olanzapine (D_2R)	9[j,k]	18[j]	IV	234	16	rat brain (homogenate)	[74],[75]	26	0.9
10	^{123}I-iomazenil ($GABA_A$)	2	2	VI	46	4	baboon brain (SPECT)	[76]	23	2
11	^{123}I-iomazenil ($GABA_A$)	2	2	VI	NA	4[f]	human brain (SPECT)	[76],[77]	NA	2
12	^{3}H-flumazenil ($GABA_A$)	NA	15[g]	IV	NA	4[f]	mouse brain (homogenate)	[60],[78]	NA	0.3
13	^{11}C-flumazenil ($GABA_A$)	0.4	1[h]	VII	NA	2[i]	human brain (PET)	[79],[80]	NA	2
14	Nitrendipine (Ca^{2+} channels)	1[c]	2	VIII	320	47	human blood pressure	[81],[20]	320	24
15	Benidipine (Ca^{2+} channels)	1	112	VIII	16	3465	human blood pressure	[81],[20]	16	31
16	Benidipine (Ca^{2+} channels)	1	112	VIII	28[l]	60[l]	human blood pressure	[81],[21]	28	0.5
17	Buprenorphine (opioid)	26[j]	43[j]	I	6	68	human respiration	[82],[83]	0.2	2
18	Buprenorphine (opioid)	26[j]	43[j]	I	3	8	rat respiration	[82],[84]	0.1	0.2
19	Buprenorphine (opioid)	26[j]	43[j]	I	135	18	cat nociception	[82],[22]	5	0.4

[a] $t_{1/2}$ assoc.: concentration-dependent association half-life in min•nM (at a constant concentration of free ligand or free target and with absence of dissociation), $t_{1/2}$ dissoc.: dissociation half-life in min (with absence of association). Values are obtained by calculating $0.693/k_{on}$ and $0.693/k_{off}$, respectively.

[b] I = transfected CHO cells, II = rat striatal membranes, III = rat striatal homogenate, IV = rat brain homogenate, V = guinea pig brain homogenate, VI = baboon occipital homogenate, VII = rat brain P2 fraction, VIII = rat cardiac membranes.

[c] this value was obtained at 25 °C.

[d] displayed value is the average from all brain regions as reported in the reference.

[e] displayed value is the average from all experiments as reported in the reference.

[f] displayed value is the average from all brain regions as reported in the reference, except for the pons, which had an insufficient significance.

[g] this value was obtained at 4 °C.

[h] this value was obtained at 22 °C.

[i] displayed value is the average from the three-compartment estimation from all brain regions as reported in the reference.

[j] this value was obtained at room temperature.

[k] The published k_{on} values in this reference seem to be erroneously calculated. The value in this table is obtained by dividing the measured k_{off} over K_i.

[l] This value was based on a model fit on drug effect data of heart rate. The same model was also fitted on blood pressure which resulted in a similar but dose dependent estimate, which was ignored.

PET: Postiron Emission Tomography, SPECT: Single Photon Emission Computed Tomography, NA: Not Available.

4.3 Most valid comparisons

To evaluate the difference between *in vitro* and *in vivo* estimates of association and dissociation rates, we should only use the most valid comparisons, restricting table 3 to entries 2,5,6,7 and 11. Now the ratio between *in vitro* and *in vivo* estimates varies between 0.9 and 4 which is considerably better, but based only on four compounds and two targets. Moreover, it should be noted that these entries include only one entry for which the comparison is made with human binding data. Also, all observations from table 3 originate from GPCRs and therefore, none of the studies used isolated receptors. One could speculate that the correlation between *in vitro* and *in vivo* estimates is better for membrane-bound targets than for soluble targets since the membrane-bound receptors are mostly measured in membrane fractions and therefore retain some of their natural environment, whereas soluble targets can be completely purified. However, the natural exposure of membrane-bound receptors to the differential composition of extracellular and intracellular fluids cannot be reproduced in homogenized *in vitro* experiments, while the homogeneous environment of soluble targets can be replicated *in vitro*.

4.4 Summary

The amount of available literature data to compare *in vitro* and *in vivo* estimates for drug-target dissociation rates in a valid manner is too low to draw general conclusions about the predictive value of the *in vitro* drug-target dissociation estimates. This is even more so for drug-target association rates. Moreover, differences in experimental approach and conditions, and differences in data analysis hamper the comparison of *in vitro* and *in vivo* binding kinetics data. These differences include most frequently a difference in temperature (i.e. *in vitro* experiment not at 37 °C), difference in dissociation method (washout vs. displacement) and analysis method (model-based parameter estimation vs. graphical methods). Therefore, the current *in vitro* estimates of drug-target binding kinetics cannot be translated reliably into *in vivo* binding kinetics due to a lack of available information on comparability and due to methodological differences between *in vitro* and *in vivo* experiments.

5. Missing links in the translation between in vitro and in vivo binding kinetics

The differential results that have been observed from *in vitro* and *in vivo* studies can be explained by a multitude of differences between the extremely complex *in vivo* situation and the much more simplified *in vitro* environment. Possible explanations include factors that are poorly understood, such as the *in vivo* occurrence of complicated ligand interactions with multiple targets, allosteric binding sites, exosites and subcellular compartments or organelles, but also complex target interactions with other proteins (homo- and heterodimerisation), and other cell membrane and intra- and extracellular fluid constituents, such as ions. Moreover, the *in vivo* three-dimensional structure of multiple cell types is rarely replicated *in vitro* and unknown contributors to the observed *in vivo* target binding kinetics cannot be excluded.

However, the following section is focused on the better understood contributors to *in vivo* target binding kinetics and how these can be accounted for in the design and analysis of both *in vitro* and *in vivo* experiments

5.1 Experimental conditions in in vitro and in vivo studies of binding kinetics

As described in the previous section, the comparison of *in vitro* and *in vivo* binding kinetic parameters is often hampered by differential experimental conditions between in *in vitro* and *in vivo* studies. We will discuss here the most relevant experimental conditions which can hamper the translation between *in vitro* and *in vivo* measured binding kinetics. These are: *in vitro* temperature, *in vivo* displacement method and the presence of endogenous ligand.

5.1.1 Temperature

One very important *in vitro* and *ex vivo* experimental condition is the temperature. Since both drug-target association and dissociation rate are temperature dependent in a compound-specific manner [85–87], translation of binding kinetics from one temperature to another temperature cannot be done unless the temperature dependency has been determined for that specific compound. Moreover, since the target conformation might be temperature dependent as well, the Arrhenius plots of k_{on} and k_{off} are not necessarily linear. A few literature examples are available of linear Arrhenius plots for k_{on} and k_{off} [87–89]. Therefore, it is highly relevant to obtain *in vitro* binding parameters at 37 °C, or to obtain a linear Arrhenius plot at lower temperatures.

5.1.2 Displacer/competitor

Another condition that may affect translational success is the presence or absence of a displacer/competitor. To account for this, it is necessary to obtain both *in vitro* and *in vivo* estimates for k_{off} in the presence of a displacer. If both experiments are done in the absence of a displacer, translation can still be hampered because of differential diffusion rates and target clustering in the two experiments, leading to different diffusion-limited binding (“rebinding”).

5.1.3 Endogenous ligand

The presence of an endogenous ligand is also influencing the rate of drug-target association and dissociation. An endogenous ligand can be present both *in vitro* and *in vivo.* To enable an accurate *in vivo* and *in vitro* estimation of drug-target k_{on} and k_{off} in the presence of an endogenous ligand, the concentration profile over time during the experiment and the binding kinetics of the endogenous ligand need to be known.

5.2 Integrated analysis of multiple determinants of in vivo target occupancy and drug effect

In order to use *in vitro* binding kinetic data to predict *in vivo* target occupancy and effect kinetics, all kinetic processes which influence the *in vivo* kinetics of drug effect need to be taken into account (see also section 7). These include pharmacokinetics, endogenous competition, diffusion-limited binding, non-specific binding, target turnover and signal transduction. Each of these processes will be discussed in the following section.

5.2.1 Pharmacokinetics

One of the clearest examples for the need to integrate all kinetic processes for the prediction of *in vivo* target occupancies is the role of pharmacokinetics: If the drug concentration in the human body has a constant profile, an equilibrium situation will be reached and a slow dissociation rate will not prolong the target occupancy anymore. On basis of a very simple relation between pharmacokinetics and binding kinetics, one can expect a slow dissociation rate to be prolonging target occupancy only when its dissociation rate is slower than its elimination rate (figure 2, upper panels) [15,19]. However, this might be an oversimplification, and other processes need to be integrated as well [19].

5.2.2 Endogenous competition

Another process which is important for the role of binding kinetics is endogenous competition. The presence of a varying concentration of endogenous ligand can make a drug's binding kinetics more important, also when its dissociation half-life does not exceed its plasma elimination half-life (figure 1) [14,18,90–92]. Since endogenous ligands usually have a varying concentration, endogenous competition might be relevant for the binding kinetics of most agonists and antagonists. A hypothesis in this direction was already published by Kapur and Seeman before the recent interest in binding kinetics [92]. In their publication, fast dissociating dopamine antagonists were suggested to be less resistant to dopamine signaling, thereby preventing side effects from over-suppression of dopamine signaling.

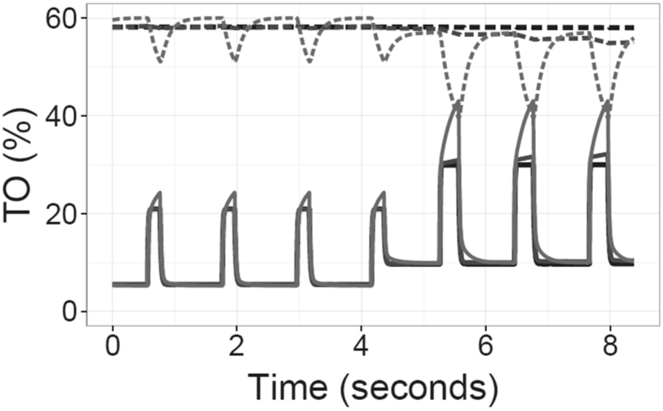

Figure 1. The influence of drug-target binding kinetics on drug (dashed lines) and dopamine (solid lines) target occupancy (TO) is influenced by endogenous competition, as simulated by Vauquelin et al [18]. *A constant drug concentration and pulsatile dopamine concentration are used, and the system is allowed to reach equilibrium before t = 0. The dopamine concentrations rise after 4 seconds to represent a high activity period. The drug target dissociation rate (k_{off}) changes from 181 min^{-1} (light grey) to 6.03 min^{-1} (dark grey), and 0.181 min^{-1} (black).*

5.2.3 Diffusion-limited binding

A kinetic process which has got only limited attention for its effect on target occupancy profiles is diffusion-limited binding. If the effective diffusion of a drug around its target is limited, the chance that it will re-associate to its target before diffusing into the tissue (often called 'rebinding') will increase and thus the target occupancy will decrease slower than expected from its binding kinetics and tissue concentration. Although the possible significance of diffusion and diffusion-limited binding (or 'rebinding') has already been indicated in studies with rats, humans and *in vitro* over three decades ago [9,10,93], there is no general practice of taking this into account in either *in vitro* or *in vivo* studies. As reported several times by Vauquelin and his colleagues, based on literature, experimental and theoretical findings, "rebinding" can have a significant impact on the estimated k_{off} value in *in vitro* and *in vivo* studies, and therefore needs to be taken into account in the design and analysis of these studies (figure 2) [19,40,94–96].

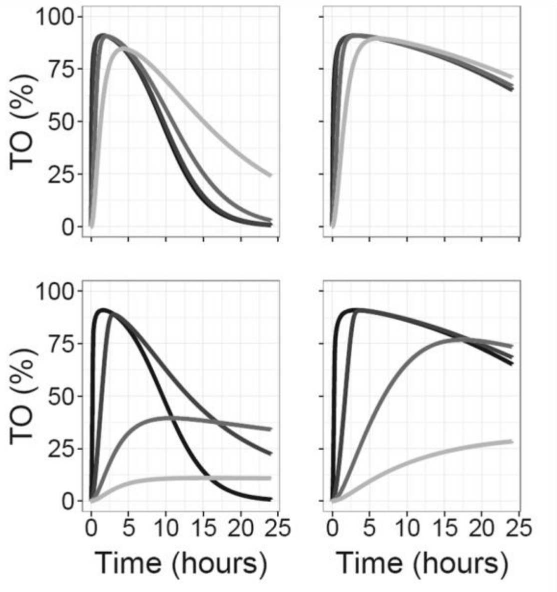

Figure 2. The influence of drug-target binding kinetics on target occupancy (TO) depends on both pharmacokinetics and diffusion-limited binding, as simulated by Vauquelin et al [19]*. The drug target dissociation rate (k_{off}) changes from 83 hr^{-1} (black) to 2.1 hr^{-1} (dark grey), 0.35 hr^{-1} (grey), and 0.087 hr^{-1} (light grey). The drug elimination rate constant is 0.35 hr^{-1} for the left panel and 0.087 hr^{-1} for the right panel.*

5.2.4 Non-specific binding

Another kinetic process which can influence the profile of target occupancy is non-specific binding. Non-specifically bound drug can act as a reservoir which releases drug upon decreasing free drug concentrations, thereby decreasing the effective elimination rate. Moreover, if the release of non-specifically bound drug is slow, this can become the rate determining factor for the rate of drug elimination from either the plasma or the target tissue (figure 3) [97,98].

5.2.5 Target turnover

The rate of target synthesis and degradation can also influence the profile of target occupancy, since the breakdown of occupied target and synthesis of new (unoccupied) target decreases the occupied fraction. Thus, target turnover provides a suitable explanation for the limited duration of the antiplatelet effect of the irreversible binder aspirin [1]. Moreover, target synthesis and degradation can be regulated and function as feedback mechanisms [99–103]. A high rate of target turnover can limit the impact of a decreasing dissociation rate constant and can increase the impact of the association rate constant (figure 4).

5.2.6 Signal transduction

Apart from these multiple factors which influence the target occupancy profiles, another step is required to predict effect kinetics from target occupancy profiles. To do this, the kinetics of all signal transduction steps need to be taken into account. The significance of signal transduction kinetics with respect to binding kinetics has been indicated by a simulation study of binding kinetics, enzyme inhibition and several signal transduction pathways [17]. However, since signal transduction can have various mechanisms and includes feedback mechanisms, the influence of signal transduction on the role of drug-target binding kinetics can differ greatly between targets.

Although the kinetics of signal transduction can be important, direct relationships between target occupancy and drug effect have been characterized for a few targets. However, *in vivo* target occupancy and drug effect are rarely measured simultaneously, and mathematical models are often required to estimate the relationship between target occupancy and effect from pharmacokinetic and pharmacodynamic data.

One example where *in vivo* target occupancy and drug effect were measured simultaneously for the dopamine D_2 receptor demonstrated the typical hyperbolical relationship [104]. However, linear relationships between target occupancy and effect have been used by mathematical models as well, for example to describe drug effect for calcium channel blockers and DPP-4 inhibitors [20, 26].

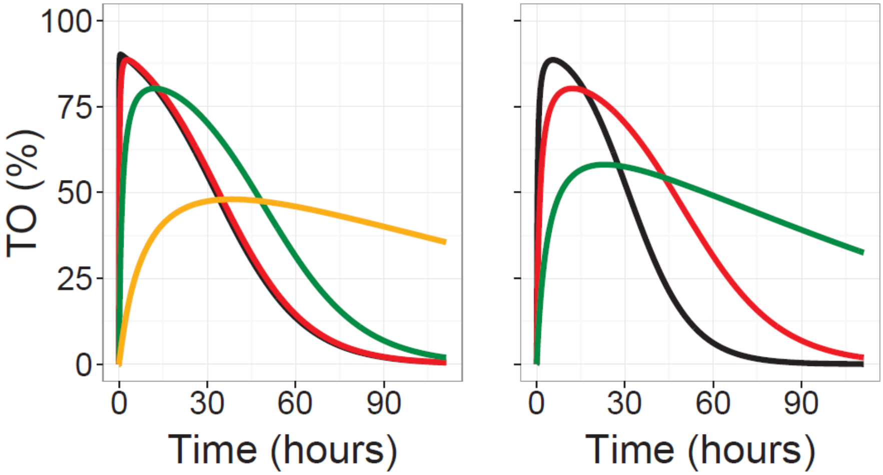

Figure 3. The target occupancy (TO) profile can be influenced by non-specific binding of the drug, as simulated for lipid and protein binding in the brain by Peletier et al [97]*. The drug target dissociation rate constant (k_{off}) is 36 $hr^{-1}$for all lines. For the left panel, the drug-protein dissociation rate constant changes from 1000 sec^{-1} (black) to 100 sec^{-1} (red), 10 sec^{-1} (green), and 1 sec^{-1} (orange). For the right panel, the drug-lipid dissociation rate constant changes from 500 sec^{-1} (black) to 100 sec^{-1} (red) and 20 sec^{-1} (green). The drug-protein and the drug-lipid affinity change in the same way as the dissociation rate constants, since both drug-protein and drug-lipid association rate constants remain unchanged.*

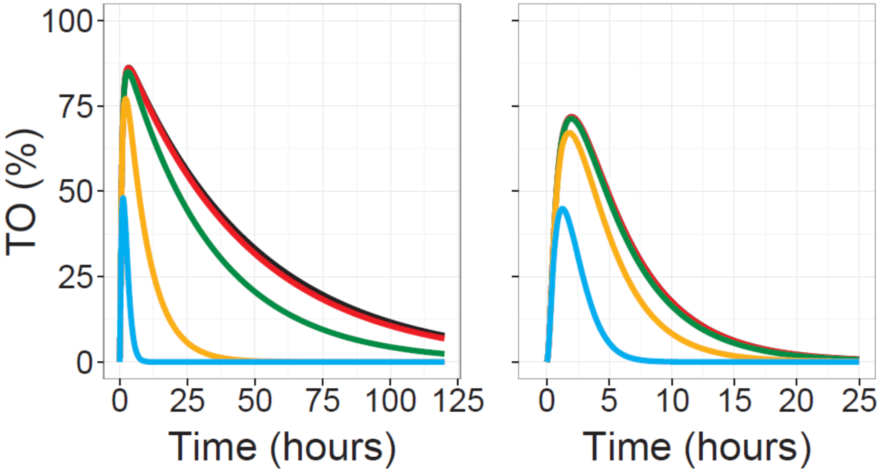

Figure 4. The influence of drug-target binding kinetics on target occupancy (TO) can be influenced by target turnover, as described by the model of Hong et al. for the antiplatelet effect of aspirin and ibuprofen [1]*. The drug target dissociation rate (k_{off}) changes from 0 (black line representing aspirin) to 0.001 hr^{-1} (red), 0.01 hr^{-1} (green), 0.1 hr^{-1} (orange) and 1 hr^{-1}(blue). The target degradation rate constant (k_{deg}) is 0.02 hr^{-1}(as identified for aspirin and ibuprofen) for the left panel and 0.2 hr^{-1} for the right panel (note the different time scale). The target synthesis rate constant (k_{syn}) was adjusted accordingly to obtain a steady state target concentration of 25 nM for both panels: $k_{syn} = 25 * k_{deg}$.*

5.2.7 Integrated mathematical modeling

To incorporate all the processes as described above for the prediction of target occupancy and drug effect and to use these predictions for the selection of the best drug candidates, quantitative mathematical description and integration of all these processes is essential.

Mathematical models have made use of drug-target binding kinetics in the previous decades to describe and predict the time course of drug effect [20–26]. These mathematical models most often use differential equations to describe the rate with which concentrations change, rather than describing the absolute value of a concentration for any time point. The use of differential equations requires solving of the differential equations for each time profile and each initial value, but it also allows the integration of numerous processes in a relatively simple way. As an example, the decrease in drug concentration due to elimination is often described by an equation like equation 2, where dC/dt is the change in drug concentration per time unit, C is the drug concentration and k_{el} is the elimination rate constant.

$$\frac{dC}{dt} = -k_{el} * C \qquad (2)$$

Equation 2 means that if k_{el} = 0.1/min, for example, the drug concentration decreases with 10% every minute (if you solve the equation by taking time steps of 1 minute). For compartmental models, differential equations are used to describe the concentration in each compartment, and each compartment is considered to be homogeneous. For example, if the distribution of a drug over the body is fast or limited, the concentration profile of a drug in plasma can often be described by a one-compartment model with absorption and elimination. Such a compartmental approach can be used to describe drug-target binding by adding one or more compartments which represent the drug-target complex and assuming homogeneous distribution of the target in one of the pharmacokinetic compartments. This approach has been used for the simulations of figure 1-4, where binding was simulated from a single compartment for figure 2 and 4, from a brain compartment for figure 3 while a constant concentration was used for figure 1. Although these simulations are based on simplifying assumptions such as homogeneity, they provide a conceptual insight in the impact of the described processes on the relation between drug-target binding kinetics and target occupancy.

A special field where drug-target binding kinetics are taken into account as standard practice is the field of target mediated drug disposition (TMDD). TMDD describes the pharmacokinetics of drugs (mostly biologicals) which are distributed and eliminated predominantly when bound to their target. In this situation, binding kinetics are required to describe the drugs pharmacokinetics, since the pharmacokinetics depend on the binding and the dissociation is often relatively slow [105–108]. Mathematical analysis of a TMDD model revealed that k_{on} had a more pronounced impact on the maximal target occupancy than k_{off} [109]. Another field where drug-target binding kinetics are commonly incorporated in mathematical models is in the analysis of positron emission tomography (PET) data (see table 3). In all these examples and in the simulations shown in figure 1-4, mathematical models have demonstrated their potential to further our understanding of the role of drug-target binding kinetics in their complex physiological context.

6. Conclusion

On basis of the sparse amount of available literature estimates for drug-target binding kinetics, no conclusions can be made on how well *in vivo* binding kinetics are reflected in *in vitro* experiments. Moreover, differences in conditions, methodology and analysis avoid the comparison of available *in vitro* and *in vivo* estimates in many cases.

Next to the relation between *in vitro* and *in vivo* estimates of binding kinetics, the relation between *in vivo* binding kinetics and *in vivo* target occupancy and effect kinetics is also uncertain. This relation can be influenced by pharmacokinetics, endogenous competition, target tissue diffusion, non-specific binding, signal transduction and other factors. A quantitative integration by means of mathematical models can greatly enhance our understanding of the role of drug-target binding kinetics in this context.

This implies that more scientific support is required for the rational selection and development of drug-candidates on basis of *in vitro* estimates of drug-target binding kinetics.

7. Expert opinion: Towards an integrated approach for translational binding kinetics analysis in drug discovery and development.

The aforementioned determinants of target occupancy are related to each other, and need to be taken into account in an integrated manner. The use of compartmental modeling, as applied commonly in PK/PD modeling, is an important tool to facilitate the integration of all kinetic processes which are involved in the generation of drug effect (figure 5). The value of such models for all stages of drug discovery and development is increasingly recognized [110–112].

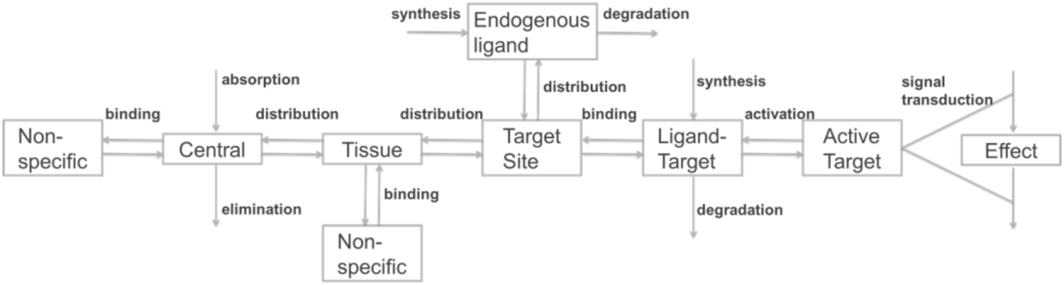

Figure 5. Schematic representation of the interconnected kinetic processes which determine target occupancy and effect kinetics. The central compartment represents the blood, the target site compartment represents the direct environment around the target, from where binding occurs.

The feasibility of such an integrative approach in (the early phases of) drug discovery and development may seem limited by its complex and time-consuming nature. However, it is important to note that some of these kinetic processes are system-specific processes (e.g. endogenous competition, target turnover and signal transduction). These system-specific processes are equal for all new compounds and will not decrease the screening throughput in drug discovery. The integrated analysis of these system-specific processes can thus be used to define which drug specific kinetic parameters (e.g. drug-target association and dissociation rate, non-specific binding rates and pharmacokinetic parameters) are most relevant per target/drug class to screen for. During the drug discovery process, the screening can start with only the most important parameter and be gradually extended to the other relevant parameters to refine the compound selection. The integrated analysis of all contributors to drug effect will not only improve compound selection, but it will also enable drug-candidate optimization on the most relevant parameters and optimization of drug dosing and sampling times in (pre)clinical investigations.

7.2 Context-dependency of binding kinetics values

To enable the integrated analysis of the kinetic processes which determine a drug's effect kinetics, specific information on all of these separate processes is required. This urges the performance of both *in vitro* and *in vivo* experiments which deliver drug- and system specific parameters for all kinetic processes. This is necessary to avoid experiments which inform only on the combined effect of multiple processes and thus deliver context-dependent information. For example, if an *in vivo* binding study is analyzed to determine only the rate with which the target occupancy inclines and declines after a certain dose, process-specific information is lacking because no specific information is collected about the pharmacokinetics or binding kinetics. This applies also to *in vitro* experiments. If a washout experiment is used to estimate the dissociation rate without a competing ligand, the obtained estimate can be a combined parameter for both dissociation and diffusion, because 'rebinding' can occur [96]. The occurrence of multiple kinetic processes during one experiment is not necessarily problematic, as long as the results can be analyzed in a process-specific manner to enable optimal translation to different experimental or clinical conditions. This type of process-specific analysis can be obtained by using physiologically based PK/PD models with process-specific parameters.

7.3 Need for an integrated approach

Although experiments are available and in use to estimate the rate constants of the above mentioned kinetic processes, there is hardly any information available about what the relative contribution of each of those processes is in the determination of target occupancy profiles during the various scenarios of drug treatment. To enable the prediction of *in vivo* target occupancy and effect profiles, integrated analysis of experimental data and increased theoretical insight in the role of all contributors to target occupancy and effect are required. Mathematical models which describe the mechanisms of all relevant processes can be of great value to both analyze experimental data and simulate various cases of drug treatment in a comprehensive and integrated fashion. Increasing knowledge of the drivers of drug effect is of critical importance to select the best drug candidates in drug discovery, to optimize drug therapy in drug development and improve the health of those in need of medicines.

8. Acknowledgements

The K4DD project is supported by the Innovative Medicines Initiative Joint Undertaking (IMI JU) under grant agreement no 115366, resources of which are composed of financial contribution from the European Union's Seventh Framework Programme (FP7/2007-2013) and EFPIA companies' in kind contribution.

References

1. Hong Y, Gengo FM, Rainka MM, et al. Population pharmacodynamic modelling of aspirin- and ibuprofen-induced inhibition of platelet aggregation in healthy subjects. Clin Pharmacokinet 2008;47(2):129–37
2. Katashima M, Yamamoto K, Tokuma Y, et al. Comparative pharmacokinetic/pharmacodynamic analysis of proton pump inhibitors omeprazole, lansoprazole and pantoprazole, in humans. Eur J Drug Metab Pharmacokinet 1998;23(1):19–26
3. Äbelö A, Holstein B, Eriksson UG, et al. Gastric acid secretion in the dog: A mechanism-based pharmacodynamic model for histamine stimulation and irreversible inhibition by omeprazole. J Pharmacokinet Pharmacodyn 2002;29(4):365–82
4. Copeland RA. The dynamics of drug-target interactions: drug-target residence time and its impact on efficacy and safety. Expert Opin Drug Discov 2010;5(4):305–10
5. Tummino PJ, Copeland RA. Residence Time of Receptor-Ligand Complexes and Its Effect on Biological Function. Biochemistry 2008;47(20):5481–92
6. Swinney DC. The role of binding kinetics in therapeutically useful drug action. Curr Opin Drug Discov Devel 2009;12(1):31–9
7. Kinzer-Ursem TL, Linderman JJ. Both ligand- and cell-specific parameters control ligand agonism in a kinetic model of g protein-coupled receptor signaling. PLoS Comput Biol 2007;3(1):84–94
8. Leysen JE, Gomeren W. Different kinetic properties of neuroleptic receptor binding in the rat striatum and frontal cortex. Life Sci 1978;23(5):447–52
9. Perry DC, Mullis KB, Oie S, et al. Opiate antagonist receptor binding in vivo: evidence for a new receptor binding model. Brain Res 1980;199(1):49–61
10. Syrota A, Paillotin G, Davy JM, et al. Kinetics of in vivo binding of antagonist to muscarinic cholinergic receptor in the human heart studied by positron emission tomography. Life Sci 1984;35(9):937–45
11. Guo D, Xia L, van Veldhoven JPD, et al. Binding Kinetics of ZM241385 Derivatives at the Human Adenosine A2A Receptor. ChemMedChem 2014;9(4):752–61
12. Schneider E V, Böttcher J, Huber R, et al. Structure-kinetic relationship study of CDK8/CycC specific compounds. Proc Natl Acad Sci U S A 2013;110(20):8081–6
13. Copeland RA, Pompliano DL, Meek TD. Drug-target residence time and its implications for lead optimization. Nat Rev Drug Discov 2006;5(9):730–9
14. Vauquelin G, Van Liefde I. Slow antagonist dissociation and long-lasting in vivo receptor protection. Trends Pharmacol Sci 2006;27(7):356–9
15. Dahl G, Akerud T. Pharmacokinetics and the drug-target residence time concept. Drug Discov Today 2013;18(15-16):697–707
16. Guo D, Hillger JM, IJzerman AP, et al. Drug-target residence time - a case for G protein-coupled receptors. Med Res Rev 2014;34(4):856–92
17. Yin N, Pei J, Lai L. A comprehensive analysis of the influence of drug binding kinetics on drug action at molecular and systems levels. Mol Biosyst 2013;9(6):1381–9
18. Vauquelin G, Bostoen S, Vanderheyden P, et al. Clozapine, atypical antipsychotics, and the benefits of fast-off D2 dopamine receptor antagonism. Naunyn Schmiedebergs Arch Pharmacol 2012;385(4):337–72
19. Vauquelin G. Rebinding : or why drugs may act longer in vivo than expected from their in vitro target residence time. Expert Opin Drug Discov 2010;5(10):927–41
20. Shimada S, Nakajima Y, Yamamoto K, et al. Comparative Pharmacodynamics of Eight Calcium Channel Blocking Agents in Japanese Essential Hypertensive Patients. Biol Pharm Bull 1996;19(3):430–7
21. Yun H-Y, Yun M-H, Kang W, et al. Pharmacokinetics and pharmacodynamics of benidipine using a slow receptor-binding model. J Clin Pharm Ther 2005;30(6):541–7
22. Steagall PVM, Pelligand L, Giordano T, et al. Pharmacokinetic and pharmacodynamic modelling of intravenous, intramuscular and subcutaneous buprenorphine in conscious cats. Vet Anaesth Analg 2013;40(1):83–95
23. Ramsey SJ, Attkins NJ, Fish R, et al. Quantitative pharmacological analysis of antagonist binding kinetics at CRF1 receptors in vitro and in vivo. Br J Pharmacol 2011;164(3):992–1007
24. Yassen A, Olofsen E, Dahan A, et al. Pharmacokinetic-Pharmacodynamic Modeling of the Antinociceptive Effect of Buprenorphine and Fentanyl in Rats : Role of Receptor Equilibration Kinetics. J Pharmacol Exp Ther 2005;313(3):1136–49
25. Äbelö A, Andersson M, Holmberg AA, et al. Application of a combined effect compartment and binding model for gastric acid inhibition of AR-HO47108: A potassium competitive acid blocker, and its active metabolite AR-HO47116 in the dog. Eur J Pharm Sci 2006;29(2):91–101
26. Landersdorfer CB, He YL, Jusko WJ. Mechanism-based population pharmacokinetic modelling in diabetes: Vildagliptin as a tight binding inhibitor and substrate of dipeptidyl peptidase IV. Br J Clin Pharmacol 2012;73(3):391–401
27. Guo D, Mulder-Krieger T, IJzerman AP, et al. Functional efficacy of adenosine A_2A receptor agonists is positively correlated to their receptor residence time. Br J Pharmacol 2012;166(6):1846–59

28. Motulsky HJ, Mahan LC. The Kinetics of Competitive Radioligand Binding Predicted Mass Action by the Law of Mass Action. Mol Pharmacol 1984;25(1):1–9
29. Zweemer AJM, Nederpelt I, Vrieling H, et al. Multiple binding sites for small-molecule antagonists at the CC chemokine receptor 2. Mol Pharmacol 2013;84(4):551–61
30. Guo D, van Dorp EJH, Mulder-Krieger T, et al. Dual-point competition association assay: a fast and high-throughput kinetic screening method for assessing ligand-receptor binding kinetics. J Biomol Screen 2013;18(3):309–20
31. Mathis G, Pierre N, Tardieu J. Determination of association(kon) and dissociation(koff) rate constants of Spiperone on the Dopamine D2 receptor using the Tag-lite® platform. 2011. p. SBS 17th Annual Conference. Orlando, USA
32. Schiele F, Ayaz P, Fernández-Montalván A. A universal, homogenous assay for high throughput determination of binding kinetics. Anal Biochem 2014;468:42–9
33. Patching SG. Surface plasmon resonance spectroscopy for characterisation of membrane protein-ligand interactions and its potential for drug discovery. Biochim Biophys Acta 2014;1838(1A):43–55
34. Rich RL, Myszka DG. Higher-throughput, label-free, real-time molecular interaction analysis. Anal Biochem 2007;361(1):1–6
35. Shiau AK, Massari ME, Ozbal CC. Back to basics: label-free technologies for small molecule screening. Comb Chem High Throughput Screen 2008;11(3):231–7
36. Gronewold TMA, Baumgartner A, Hierer J, et al. Kinetic Binding Analysis of Aptamers Targeting HIV-1 Proteins by a Combination of a Microbalance Array and Mass Spectrometry (MAMS). J Proteome Res 2009;8(7):3568–77
37. Gronewold TMA. Surface acoustic wave sensors in the bioanalytical field: recent trends and challenges. Anal Chim Acta 2007;603(2):119–28
38. Kenakin T, Jenkinson S, Watson C. Determining the potency and molecular mechanism of action of insurmountable antagonists. J Pharmacol Exp Ther 2006;319(2):710–23
39. Vauquelin G, Fierens F, Verheijen I, et al. Insurmountable AT 1 receptor antagonism : the need for different antagonist binding states of the receptor Glutamate signalling in the lung. Trends Pharmacol Sci 2001;22(7):343–4
40. Szczuka A, Wennerberg M, Packeu A, et al. Molecular mechanisms for the persistent bronchodilatory effect of the beta 2-adrenoceptor agonist salmeterol. Br J Pharmacol 2009;158(1):183–94
41. Lindström E, von Mentzer B, Påhlman I, et al. Neurokinin 1 receptor antagonists: correlation between in vitro receptor interaction and in vivo efficacy. J Pharmacol Exp Ther 2007;322(3):1286–93
42. Le MT, Pugsley MK, Vauquelin G, et al. Molecular characterisation of the interactions between olmesartan and telmisartan and the human angiotensin II AT1 receptor. Br J Pharmacol 2007;151(7):952–62
43. Atack JR, Wong DF, Fryer TD, et al. Benzodiazepine binding site occupancy by the novel GABAA receptor subtype-selective drug 7-(1,1-dimethylethyl)-6-(2-ethyl-2H-1,2,4-triazol-3-ylmethoxy)-3-(2-fluorophenyl)-1,2,4-triazolo[4,3-b]pyridazine (TPA023) in rats, primates, and humans. J Pharmacol Exp Ther 2010;332(1):17–25
44. Laruelle M. Measuring Dopamine Synaptic Transmission with Molecular Imaging and Pharmacological Challenges : The State of the Art. Neuromethods 2012;71:163–203
45. Chernet E, Martin LJ, Li D, et al. Use of LC/MS to assess brain tracer distribution in preclinical, in vivo receptor occupancy studies: dopamine D2, serotonin 2A and NK-1 receptors as examples. Life Sci 2005;78(4):340–6
46. Barth VN. Typical and atypical antipsychotics: Relationships between rat in vivo dopamine D(2) receptor occupancy assessed using LC/MS and changes in neurochemistry and catalepsy. Section Title: Mammalian Hormones. 2006.
47. Need AB, McKinzie JH, Mitch CH, et al. In vivo rat brain opioid receptor binding of LY255582 assessed with a novel method using LC/MS/MS and the administration of three tracers simultaneously. Life Sci 2007;81(17-18):1389–96
48. Hume SP, Gunn RN, Jones T. Pharmacological constraints associated with positron emission tomographic scanning of small laboratory animals. Eur J Nucl Med 1998;25(2):173–6
49. Kung M-P, Kung HF. Mass effect of injected dose in small rodent imaging by SPECT and PET. Nucl Med Biol 2005;32(7):673–8
50. Hume SP, Myers R, Bloomfield PM, et al. Quantitation of carbon-11-labeled raclopride in rat striatum using positron emission tomography. Synapse 1992;12(1):47–54
51. Tantawy MN, Jones CK, Baldwin RM, et al. [(18)F]Fallypride dopamine D2 receptor studies using delayed microPET scans and a modified Logan plot. Nucl Med Biol 2009;36(8):931–40
52. Lancelot S, Zimmer L. Small-animal positron emission tomography as a tool for neuropharmacology. Trends Pharmacol Sci 2010;31(9):411–7
53. Müller CP, Pum ME, Amato D, et al. The in vivo neurochemistry of the brain during general anesthesia. J Neurochem 2011;119(3):419–46
54. Schiffer WK, Mirrione MM, Biegon A, et al. Serial microPET measures of the metabolic reaction to a microdialysis probe implant. J Neurosci Methods 2006;155(2):272–84

55. Ginovart N, Sun W, Wilson AA, et al. Quantitative Validation of an Intracerebral beta-Sensitive Microprobe System to Determine in Vivo Drug-Induced Receptor Occupancy Using [11C]Raclopride in Rats. Synapse 2004;52(2):89–99

56. Balasse L, Maerk J, Pain F, et al. PIXSIC, a Pixelated β(+)-Sensitive Probe for Radiopharmacological Investigations in Rat Brain: Binding Studies with [(18)F]MPPF. Mol imaging Biol 2014;

57. Polikov VS, Tresco PA, Reichert WM. Response of brain tissue to chronically implanted neural electrodes. J Neurosci Methods 2005;148(1):1–18

58. Wang Y, Michael AC. Microdialysis probes alter presynaptic regulation of dopamine terminals in rat striatum. J Neurosci Methods 2012;208(1):34–9

59. Märk J, Benoit D, Balasse L, et al. A wireless beta-microprobe based on pixelated silicon for in vivo brain studies in freely moving rats. Phys Med Biol 2013;58(13):4483–500

60. Li J, Fish RL, Cook SM, et al. Comparison of in vivo and ex vivo [3H]flumazenil binding assays to determine occupancy at the benzodiazepine binding site of rat brain GABAA receptors. Neuropharmacology 2006;51(1):168–72

61. Schotte A, Janssen PF, Gommeren W, et al. Risperidone compared with new and reference antipsychotic drugs: in vitro and in vivo receptor binding. Psychopharmacology (Berl) 1996;124(1-2):57–73

62. Lengyel K, Pieschl R, Strong T, et al. Ex vivo assessment of binding site occupancy of monoamine reuptake inhibitors: methodology and biological significance. Neuropharmacology 2008;55(1):63–70

63. Langlois X, te Riele P, Wintmolders C, et al. Use of the beta-imager for rapid ex vivo autoradiography exemplified with central nervous system penetrating neurokinin 3 antagonists. J Pharmacol Exp Ther 2001;299(2):712–7

64. Baker JG, Hall IP, Hill SJ. Pharmacological characterization of CGP 12177 at the human beta(2)-adrenoceptor. Br J Pharmacol 2002;137(3):400–8

65. Delforge J, Syrota A, Lançon JP, et al. Cardiac beta-adrenergic receptor density measured in vivo using PET, CGP 12177, and a new graphical method. J Nucl Med 1991;32(4):739–48

66. Kessler RM, Votaw JR, Schmidt DE, et al. High affinity dopamine D2 receptor radioligands. 3. [123I] and [125I]epidepride: in vivo studies in rhesus monkey brain and comparison with in vitro pharmacokinetics in rat brain. Life Sci 1993;53(3):241–50

67. Mukherjee J, Yang ZY, Brown T, et al. 18F-desmethoxyfallypride: a fluorine-18 labeled radiotracer with properties similar to carbon-11 raclopride for PET imaging studies of dopamine D2 receptors. Life Sci 1996;59(8):669–78

68. Mukherjee J, Yang Z-Y, Lew R, et al. Evaluation of d -Amphetamine Effects on the Binding of Dopamine D-2 Receptor Radioligand , 18F-Fallypride in Nonhuman Primates Using Positron Emission Tomography. Synapse 1997;27(1):1–13

69. Christian BT, Narayanan T, Shi B, et al. Measuring the in vivo binding parameters of [18F]-fallypride in monkeys using a PET multiple-injection protocol. J Cereb blood flow Metab 2004;24(3):309–22

70. Vandehey NT, Moirano JM, Converse AK, et al. High-affinity dopamine D2/D3 PET radioligands 18F-fallypride and 11C-FLB457: a comparison of kinetics in extrastriatal regions using a multiple-injection protocol. J Cereb blood flow Metab 2010;30(5):994–1007

71. Leysen JE, Gommeren W. Drug-Receptor Dissociation Time , New Tool for Drug Research : Receptor Binding Affinity and Drug-Receptor Dissociation Profiles of Serotonin-S2 , Dopamine-D2 , Histamine-HI Antagonists , and Opiates. Drug Dev Res 1986;131:119–31

72. Perlmutter JS, Kilbourn MR, Welch MJ, et al. Non-Steady-State Measurement of in vivo Receptor Binding with Positron Emission Tomography :"Dose Response" Analysis. J Neurosci 1989;9(7):2344–52

73. Leslie CA, Bennett JP. [3H]spiperone binds selectively to rat striatal D2 dopamine receptors in vivo: a kinetic and pharmacological analysis. Brain Res 1987;407(2):253–62

74. Kapur S, Seeman P. Antipsychotic agents differ in how fast they come off the dopamine D2 receptors. Implications for atypical antipsychotic action. J Psychiatry Neurosci 2000;25(2):161–6

75. Johnson M, Kozielska M, Pilla Reddy V, et al. Mechanism-based pharmacokinetic-pharmacodynamic modeling of the dopamine D2 receptor occupancy of olanzapine in rats. Pharm Res 2011;28(10):2490–504

76. Laruelle M, Abi-Dargham A, Ai-Tikriti MS, et al. SPECT Quantification of [123I] lomazenil Binding to Benzodiazepine Receptors in Nonhuman Primates : II . Equilibrium Analysis of Constant Infusion Experiments and Correlation with In Vitro Parameters. J Cereb blood flow Metab 1994;14(3):453–65

77. Millet P, Graf C, Moulin M, et al. SPECT quantification of benzodiazepine receptor concentration using a dual-ligand approach. J Nucl Med 2006;47(5):783–92

78. Sakiyama Y, Saito M, Inoue O. Acute treatment with pentobarbital alters the kinetics of in vivo receptor binding in the mouse brain. Nucl Med Biol 2006;33(4):535–41

79. Sihver W, Sihver S, Bergström M, et al. Aspects for In Vitro Characterization of Receptor Ligands : Receptor Binding Using 11C-Labeled A Detailed Study with the Benzodiazepine Receptor Antagonist [11C] Ro 15-1788. Nucl Med Biol 1997;24(8):723–31

80. Koeppe RA, Holthoff VA, Frey KA, et al. Compartmental analysis of [11C]flumazenil kinetics for the estimation of ligand transport rate and receptor distribution using positron emission tomography. J Cereb blood flow Metab 1991;11(5):735–44

81. Ishii A, Toyama J. Binding Properties of (+/-)[3H] Benidipine Hydrochloride to Rat Heart Membranes. J Cardiovasc Pharmacol 1993;21(2):191–6

82. Cassel JA, Daubert JD, DeHaven RN. [(3)H]Alvimopan binding to the mu opioid receptor: comparative binding kinetics of opioid antagonists. Eur J Pharmacol 2005;520(1-3):29–36

83. Yassen A, Olofsen E, Romberg R, et al. Mechanism-based PK/PD modeling of the respiratory depressant effect of buprenorphine and fentanyl in healthy volunteers. Clin Pharmacol Ther 2007;81(1):50–8

84. Yassen A, Kan J, Olofsen E, et al. Mechanism-Based Pharmacokinetic-Pharmacodynamic Modeling of the Respiratory-Depressant Effect of Buprenorphine and Fentanyl in Rats. 2006;319(2):682–92

85. Casadó V, Allende G, Mallol J, et al. Thermodynamic analysis of agonist and antagonist binding to membrane-bound and solubilized A1 adenosine receptors. J Pharmacol Exp Ther 1993;266(3):1463–74

86. Langlois X, Megens A, Lavreysen H, et al. Pharmacology of JNJ-37822681, a specific and fast-dissociating D2 antagonist for the treatment of schizophrenia. J Pharmacol Exp Ther 2012;342(1):91–105

87. Treherne JM, Young JM. Temperature-dependence of the kinetics of the binding the histamine H 1 -receptor : comparison with the kinetics of [3H] -mepyramine. Br J Pharmacol 1988;94(3):811–22

88. Wallace RM, Young JM. Temperature Dependence Related Compounds of the Binding of [3H]Mepyramine to the Histamine H1 Receptor. Mol Pharmacol 1983;23(1):60–6

89. Sakai S. Effect of hormones on dissociation of prolactin from the rabbit mammary gland prolactin receptor. Biochem J 1991;279:461–5

90. Endres CJ, Kolachana BS, Saunders RC, et al. Kinetic modeling of [11C]raclopride: combined PET-microdialysis studies. J Cereb blood flow Metab 1997;17(9):932–42

91. Morris ED, Yoder KK. Positron emission tomography displacement sensitivity: predicting binding potential change for positron emission tomography tracers based on their kinetic characteristics. J Cereb blood flow Metab 2007;27(3):606–17

92. Kapur S, Seeman P. Does Fast Dissociation From the Dopamine D 2 Receptor Explain the Action of Atypical Antipsychotics ?: A New Hypothesis. Am J Psychiatry 2001;158(3):360–9

93. Wiley HS. Anomalous Binding of Epidermal Growth Factor to A431 Cells Is Due to the Effect of High Receptor Densities and a Saturable Endocytic System. J Cell Biol 1988;107(2):801–10

94. Packeu A, Wennerberg M, Balendran A, et al. Estimation of the dissociation rate of unlabelled ligand-receptor complexes by a “two-step” competition binding approach. Br J Pharmacol 2010;161(6):1311–28

95. Vauquelin G, Van Liefde I. Radioligand dissociation measurements: potential interference of rebinding and allosteric mechanisms and physiological relevance of the biological model systems. Expert Opin Drug Discov 2012;7(7):583–95

96. Vauquelin G, Charlton SJ. Long-lasting target binding and rebinding as mechanisms to prolong in vivo drug action. Br J Pharmacol 2010;161(3):488–508

97. Peletier LA, Benson N, van der Graaf PH. Impact of protein binding on receptor occupancy: a two-compartment model. J Theor Biol 2010;265(4):657–71

98. Proost JH, Wierda JM, Meijer DK. An extended pharmacokinetic/pharmacodynamic model describing quantitatively the influence of plasma protein binding, tissue binding, and receptor binding on the potency and time course of action of drugs. J Pharmacokinet Biopharm 1996;24(1):45–77

99. Kim KM, Valenzano KJ, Robinson SR, et al. Differential regulation of the dopamine D2 and D3 receptors by G protein-coupled receptor kinases and beta-arrestins. J Biol Chem 2001;276(40):37409–14

100. Macey TA, Gurevich V V, Neve KA. Preferential Interaction between the Dopamine D2 Receptor and Arrestin2 in Neostriatal Neurons. Mol Pharmacol 2004;66(6):1635–42

101. Paspalas CD, Rakic P, Goldman-Rakic PS. Internalization of D2 dopamine receptors is clathrin-dependent and select to dendro-axonic appositions in primate prefrontal cortex. Eur J Neurosci 2006;24(5):1395–403

102. Dang VC, Christie MJ. Mechanisms of rapid opioid receptor desensitization, resensitization and tolerance in brain neurons. Br J Pharmacol 2012;165(6):1704–16

103. Skinbjerg M, Liow J-S, Seneca N, et al. D2 dopamine receptor internalization prolongs the decrease of radioligand binding after amphetamine: a PET study in a receptor internalization-deficient mouse model. Neuroimage 2010;50(4):1402–7

104. Haraguchi K, Ito K, Kotaki H, et al. Prediction of drug-induced catalepsy based on dopamine D1, D2, and muscarinic acetylcholine receptor occupancies. Drug Metab Dispos 1997;25(6):675–84

105. Mager DE, Jusko WJ. General pharmacokinetic model for drugs exhibiting target-mediated drug disposition. J Pharmacokinet Pharmacodyn 2001;28(6):507–32

106. Eppler SM, Combs DL, Henry TD, et al. A target-mediated model to describe the pharmacokinetics and hemodynamic effects of recombinant human vascular endothelial growth factor in humans. Clin Pharmacol Ther 2002;72(1):20–32

107. Jin F, Krzyzanski W. Pharmacokinetic model of target-mediated disposition of thrombopoietin. AAPS J 2004;6(1):86–93

108. Retlich S, Duval V, Graefe-Mody U, et al. Impact of target-mediated drug disposition on Linagliptin pharmacokinetics and DPP-4 inhibition in type 2 diabetic patients. J Clin Pharmacol 2010;50(8):873–85

109. Aston PJ, Derks G, Raji A, et al. Mathematical analysis of the pharmacokinetic-pharmacodynamic (PKPD) behaviour of monoclonal antibodies: Predicting in vivo potency. J Theor Biol 2011;281(1):113–21

110. Zhang L, Sinha V, Forgue ST, et al. Model-based drug development: the road to quantitative pharmacology. J Pharmacokinet Pharmacodyn 2006;33(3):369–93

111. Stone JA, Banfield C, Pfister M, et al. Model-Based Drug Development Survey Finds Pharmacometrics Impacting Decision Making in the Pharmaceutical Industry. J Clin Pharmacol 2010;50(S9):20S – 30S

112. Van der Graaf PH, Gabrielsson J. Pharmacokinetic – pharmacodynamic reasoning in drug discovery and early development. Future Med Chem 2009;1(8):1371–4

Chapter 2. The long residing negligence of target saturation

Wilhelmus E.A. de Witte[1*], Meindert Danhof[1], Piet H. van der Graaf[1,2], Elizabeth C.M. de Lange[1]

[1] Division of Pharmacology, Leiden Academic Centre for Drug Research, Leiden University, 2333 CC Leiden, The Netherlands

[2] Certara Quantitative Systems Pharmacology, Canterbury Innovation Centre, Canterbury CT2 7FG, United Kingdom

* correspondence: wilbertdew@gmail.com

Manuscript under revision for Nature Reviews Drug Discovery

The interaction between a drug and its biological target molecule is a key step in the causal chain between drug dosing and drug effect in the human body. The strength of this interaction may be represented by the drug-target dissociation constant (K_D), which describes the drug concentration that results in 50% target occupancy (i.e. the percentage of target molecules that is bound to a drug molecule) in equilibrium. However, the K_D does not inform on the rate at which target binding equilibrium is reached after a change in the drug concentration. The kinetics of target binding is described by two rate constants: the second order association rate constant k_{on} and the first order dissociation rate constant k_{off}. From the value of k_{off}, the average time that each drug molecule spends bound at the target after drug-target association (the drug-target residence time or RT) can be calculated as $1/k_{off}$.

The significance of drug-target residence time has received increasing attention in drug discovery following the publication of an Opinion article in 2006, which discussed the beneficial effect of a long dissociation half-life on (selective) prolongation of target occupancy (*Nat. Rev. Drug Discov.* **5,** 730–9 (2006))[1]. However, the role of target saturation (i.e. target occupancy close to 100%) on prolongation of target occupancy was not fully considered in this, as well as other subsequent publications.[2–5]

By using simulations, we demonstrate the impact of target saturation on prolongation of target occupancy and show that lack of consideration of this role may contribute to inaccurate conclusions about the influence of drug-target binding kinetics.[1,2,4,5] Moreover, we demonstrate that stating that a drug-target dissociation rate constant lower than the pharmacokinetic elimination rate constant prolongs the duration of target occupancy[3,6,7], does not incorporate the role of target saturation and therefore does not always hold, especially if target occupancy values are higher than 50%. However, it should be noted that not all simulations demonstrating the influence of k_{off} on the duration of target occupancy are misleading because of target saturation. Most notably, when differential equation models are used and the k_{off} is changed simultaneously with the k_{on} to keep the K_D constant, the target saturation is not obscuring the influence of k_{off} on the duration of target occupancy.[6,8]

The fact that a higher drug concentration leads to an increased duration of drug effects has been described in quantitative terms in the early days of PKPD modelling.[9,10] More recently, the relationship between target saturation and the duration of target occupancy has also been explained quantitatively with respect to drug-target binding kinetics.[11,12]The role of target saturation that we describe here should be taken into account for the decision whether or not to select drug candidates with low k_{off} values in drug discovery and for understanding the role of drug-target binding kinetics in pharmacotherapy.

In the initial opinion article of Copeland et al.[1], the influence of target saturation has been attributed to a low dissociation rate constant for the calculated target occupancy.[13] However, in fact, the high dissociation rate constants ($0.009 - 1.0\ s^{-1}$) compared to the low elimination rate constant of the unbound drug ($0.0002\ s^{-1}$) indicate that the observed long duration of target occupancy cannot be influenced by the dissociation rate constant.[6,11] Later publications from these authors[2,4] showed that the target occupancy was calculated according to the equilibrium equation[4], which challenges the conclusions about the role of binding kinetics, since this assumes binding equilibrium has been reached.[14]

To demonstrate that the duration of target occupancy in the simulations of Copeland et al.[1] is influenced by target saturation, we have performed similar simulations with a simple single-step drug-target binding model (Figure 1). Changing the value of the association rate constant (k_{on}) instead of the dissociation rate constant (k_{off}), resulted in similar target occupancy profiles as observed in the simulations of Copeland et al[1]. This means that the duration of target occupancy is mostly influenced by the affinity and not by the binding kinetics. To exclude the influence of the drug target affinity, we performed additional simulations with a constant affinity. In these simulations, k_{off} had to be lower than $2\ h^{-1}$ to prolong the occupancy significantly (Figure 2).

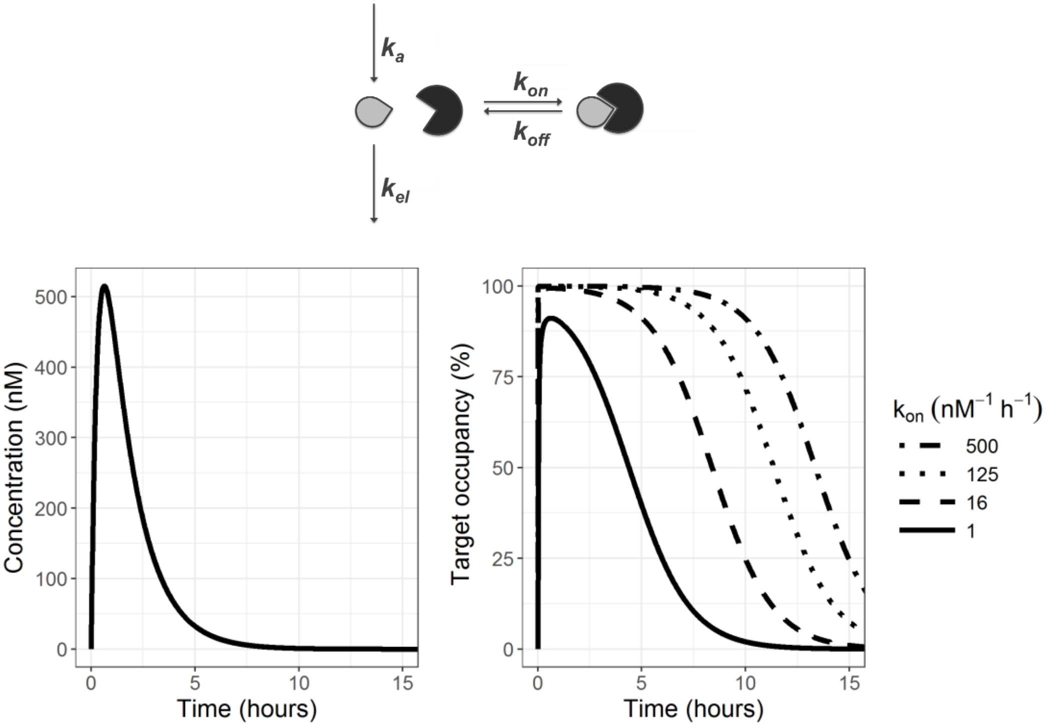

Figure 1. Simulations of plasma drug concentrations (left panel) and the resulting target occupancy profiles (right panel) for different values of k_{on}. All plasma concentration profiles overlap. The model structure is provided at the top. Here, k_a and k_{el} represent the first-order absorption constant (3.0 hr^{-1}) and elimination rate constant (0.69 h^{-1}), respectively. The value of k_{off} was fixed at 50 h^{-1} and the target concentration at 1 pM. For the associated differential equations, see supplementary information S1, and for the R simulation script see supplementary information S2. Note: similar simulations can be performed online at: wilbertdewitte.shinyapps.io/absorption_binding_elimination.

As shown in figure 2, a k_{off} value of 2 h^{-1} results in almost the same duration of target occupancy as a k_{off} value of 36 h^{-1}. To find the k_{off} value that gives a significant prolongation of target occupancy, we identified for what values of target occupancy the elimination rate constant (k_{el}) of the drug from plasma would have less influence on the duration of target occupancy than the k_{off}. The horizontal lines in figure 2 demonstrate that slow drug-target dissociation is the main determinant of the duration of target occupancy if both the dissociation rate constant and the target occupancy have values such that

$$BF < 1 - k_{off} / k_{el}$$

in which *BF* is the target fraction bound.[11,15] It should be noted that this equation is an approximation of the simple drug-target binding model and only holds for this model if the target concentration is lower than the ratio k_{el}/k_{on}, as described previously (which provides this equation in a slightly modified form as Equation 2).[11] However, the target occupancy versus time curves in figure 1 and figure 2 are independent from this approximation, as they are simulated with the full differential equation model. From this equation, it follows that when the clinical situation requires a target occupancy that, for example, should continuously be above 90%, the k_{off} needs to be more than tenfold smaller than the k_{el} for it to become the main determinant of the duration of target occupancy.[15] This equation also indicates that if $k_{off} > k_{el}$, the required target occupancy would be negative, which means that the k_{off} cannot be the main determinant of the duration of target occupancy for this condition.

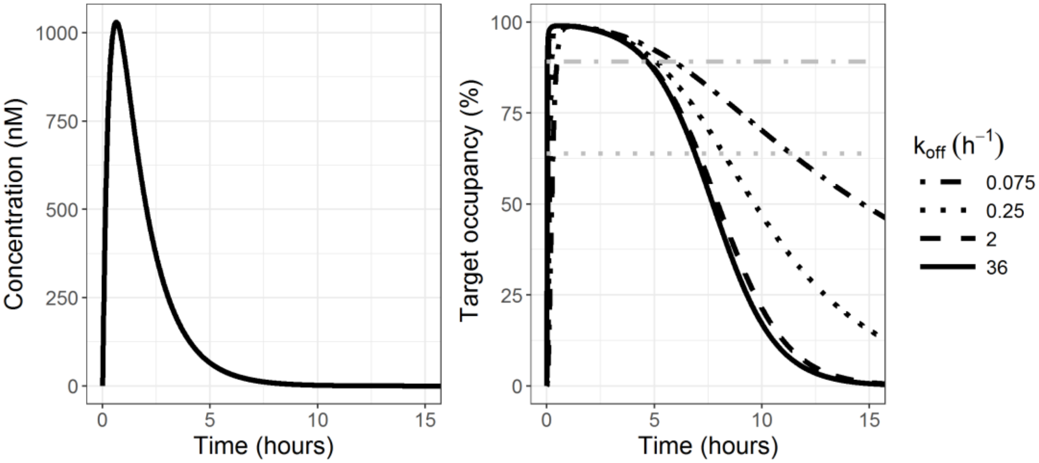

Figure 2. Simulations of plasma drug concentrations (left panel) and the resulting target occupancy profiles (right panel) for different values of k_{off}. All plasma concentration profiles overlap. The K_D was set at 10 nM for all simulations, resulting in k_{on} values of 3.6 (solid), 0.2 (dashed), 0.025 (dotted) and 0.0075 nM^{-1} h^{-1} (dash-dotted). The absorption and elimination rate constants k_a and k_{el} were 3.0 and 0.69 h^{-1}, respectively, and the concentration of the target was set at 1 pM. The grey lines denote the situation where the target fraction bound equals $1 - k_{off} / k_{el}$ for the corresponding line type (see text). Below that line, the condition is met for which k_{off} is the main determinant of the decline rate of target occupancy.

Our findings demonstrate the importance of target saturation on the duration of drug effects *in vivo*. These findings can directly be applied to the selection of drug candidates. A clear example where our insights should have been applied is the study of Lindström et al.[5] In this study, the *in vivo* drug effects of three NK1 antagonists are compared with their pharmacokinetics. Aprepitant demonstrated a much longer duration of drug effect, which can clearly be attributed to target saturation, considering the equation described above and the shape of the drug effect *versus* time curve (i.e. first a flat section close to the maximal effect and a subsequent rapid decline of the drug effect). In contrast, the authors conclude that the duration of the effect of Aprepitant cannot be explained by its pharmacokinetics. The other two compounds in this study did not show this target saturation and the authors conclude that this is likely explained by their faster binding kinetics. Aprepitant was therefore concluded to be the preferable drug of the three drugs due to its duration of effect. However, our findings above indicate that the other drugs may also exhibit this duration of effect at higher drug concentrations.

Our insights can also be applied to the decision as to whether to include target binding kinetics in hit or lead selection. For CCR2 antagonists, an occupancy of above 90% is considered to be required for a sufficient drug effect. This means that the dissociation half-life needs to be 10 times larger than the plasma elimination half-life. Together with an average plasma half-life of 5 hours[6], this means that the dissociation half-life needs to be 50 hours or longer before it becomes the main determinant of the duration of drug effect. In combination with the knowledge that such long dissociation half-lives are rarely observed[11], this suggests that inclusion of drug target binding kinetics for CCR2 antagonist screening should not be prioritized. In conclusion, target saturation is an important factor that should be included in the analysis of the influence of drug-target binding kinetics on target occupancy. By doing so, drug discovery scientists would be better equipped to decide on the relevance of drug-target binding kinetics for each specific project, depending on the required level of target occupancy and the (predicted) pharmacokinetics.

Acknowledgements

The authors are part of the K4DD consortium, which is supported by the Innovative Medicines Initiative Joint Undertaking (IMI JU) under grant agreement no 115366. The IMI JU is a project supported by the EU's Seventh Framework Programme (FP7/2007–2013) and the European Federation of Pharmaceutical Industries and Associations (EFPIA).

References

1. Copeland RA, Pompliano DL, Meek TD. Drug-target residence time and its implications for lead optimization. Nat Rev Drug Discov 2006;5(9):730–9
2. Copeland RA. The dynamics of drug-target interactions: drug-target residence time and its impact on efficacy and safety. Expert Opin Drug Discov 2010;5(4):305–10
3. Copeland RA. The drug-target residence time model: a 10-year retrospective. Nat Rev Drug Discov 2016;15(2):87–95
4. Tummino PJ, Copeland RA. Residence Time of Receptor-Ligand Complexes and Its Effect on Biological Function. Biochemistry 2008;47(20):5481–92
5. Lindström E, von Mentzer B, Påhlman I, et al. Neurokinin 1 receptor antagonists: correlation between in vitro receptor interaction and in vivo efficacy. J Pharmacol Exp Ther 2007;322(3):1286–93
6. Dahl G, Akerud T. Pharmacokinetics and the drug-target residence time concept. Drug Discov Today 2013;18(15–16):697–707
7. Vauquelin G, Van Liefde I. Slow antagonist dissociation and long-lasting in vivo receptor protection. Trends Pharmacol Sci 2006;27(7):356–9
8. Tonge PJ. Drug-Target Kinetics in Drug Discovery. ACS Chem Neurosci 2017;epub ahead of print
9. Levy G. Kinetics of pharmacologic effects. Clin Pharmacol Ther 1966;7(3):362–72
10. Levy G. Kinetics of drug action: An overview. J Allergy Cinical Immunol 1986;78(4):754–61
11. de Witte WEA, Danhof M, van der Graaf PH, et al. In vivo Target Residence Time and Kinetic Selectivity: The Association Rate Constant as Determinant. Trends Pharmacol Sci 2016;37(10):831–42
12. Szczuka A, Wennerberg M, Packeu A, et al. Molecular mechanisms for the persistent bronchodilatory effect of the beta 2-adrenoceptor agonist salmeterol. Br J Pharmacol 2009;158(1):183–94
13. Folmer RHA. Drug target residence time: a misleading concept. Drug Discov Today 2017;6446(17)
14. Mager DE, Krzyzanski W. Quasi-Equilibrium Pharmacokinetic Model for Drugs Exhibiting Target-Mediated Drug Disposition. Pharm Res 2005;22(10):1589–96
15. Bot I, Ortiz Zacarías N V., de Witte WEA, et al. A novel CCR2 antagonist inhibits atherogenesis in apoE deficient mice by achieving high receptor occupancy. Sci Rep 2017;7(1):52

Supplementary information S1. Differential equations for Figure 1 and Figure 2.

The concentrations in the depot and the plasma compartment were modeled according to equation S.1 - S.3. In these equations, [*DEP*] is the drug concentration in the depot compartment, [*C*] is the unbound drug concentration in the plasma compartment, [*R*] is the unbound target concentration in the plasma compartment, [R_{tot}] is the total target concentration and [*LR*] is the bound drug concentration. k_a is the first order absorption rate constant, k_{el} is the first order elimination rate constant, k_{on} is the second order drug-target association rate constant and k_{off} is the first order drug-target dissociation rate constant. For this model, the total target concentration is assumed to be constant, which allows the calculation of the free target concentration according to equation S.4. All initial concentrations were equal to zero and the dose was administered in the depot compartment.

$$\frac{d[DEP]}{dt} = -k_a \cdot [DEP] \tag{S.1}$$

$$\frac{d[C]}{dt} = k_a \cdot [DEP] - k_{el} \cdot [C] - k_{on} \cdot [C] \cdot [R] + k_{off} \cdot [LR] \tag{S.2}$$

$$\frac{d[LR]}{dt} = k_{on} \cdot [C] \cdot [R] - k_{off} \cdot [LR] \tag{S.3}$$

$$[R] = [R_{tot}] - [LR] \tag{S.4}$$

Supplementary information S2. R script for the simulations for Figure 1 and Figure 2.

```
# The following packages are required for the script below.
# Please install those by removing the hashtag and running the install commands below
# install.packages("deSolve")
# install.packages("ggplot2",dependencies = T)
# install.packages("gridExtra")
# install.packages("grid")
####################
library(deSolve)
library(ggplot2)
library(gridExtra)
library(grid)
rm(list = ls())  #clear environment
#---------------------------------------------------------
# parameters
#---------------------------------------------------------
parameters = c(
  ka = 3,
  kel = 0.693,        #h-1
  kon = 1,                                                    #nM-1 h-1
  koff = 50,        #h-1
  Kd = expression(koff/kon),
  Rtot = 0.001, #nM
                dose =  800,
  dosetime = 0  )
#---------------------------------------------------------
# ODE solving function
#---------------------------------------------------------
solveivro<-function(allparams2){
    allparams2<-lapply(allparams2,FUN=eval,envir=allparams2)
    #---------------------------------------------------------
  # initial states
  #---------------------------------------------------------
   state<-  c(
    D = 0,
    C = 0,
    RL = 0    )
  #---------------------------------------------------------
  # ODE system plus dosing function
  #---------------------------------------------------------
    ivro <<- function(t, state, allparams2) {
    with(as.list(c(state, allparams2)),{
      dD = -ka*D
      dC =  - kon*C*(Rtot-RL)  + koff*RL - kel*C  +ka*D
      dRL=     kon*C*(Rtot-RL)  - koff*RL

            list(c(dD,dC,dRL))    })  }
  eventdat<-data.frame(var = "D",
                    time = with(allparams2,{dosetime}),
                    value = with(allparams2,{dose}),
                    method = "add"
                    )#dosing regiments
   time<-  seq(0,  24, by = 0.01)
  out <-  lsoda(y = state, times = time, func = ivro, parms = allparams2,
              events = list(data = eventdat))
   #---------------------------------------------------------
  # derived output
  #---------------------------------------------------------
  dout <- as.data.frame(out)
  outpar<-c(as.list(dout),as.list(allparams2))
  outderpar <- within(outpar, {
     TO = RL/Rtot      })
    outder<-outderpar[names(outderpar)[!(names(outderpar)%in%names(allparams2))]]
  doutder<-as.data.frame(outder)
  return(doutder)
} #end function solveivro
##########################################################
# changing parameters for additional simulations
##########################################################
params<-as.list(parameters)
changedpars1<-within(params, {  kon=16 })
changedpars2<-within(params, {  kon=125 })
changedpars3<-within(params, {  kon=500 })
##########################################################
# executing the additional simulations
##########################################################
doutder1<-NULL
doutder1<-solveivro(as.list(params))
doutder2<-NULL
doutder2<-solveivro(changedpars1)
doutder3<-NULL
doutder3<-solveivro(changedpars2)
doutder4<-NULL
doutder4<-solveivro(changedpars3)
#---------------------------------------------------------
# plots over time
#---------------------------------------------------------
# plot pharmacokinetics over time ----------------------------------------------------------------------
plotpk<-ggplot()+
  geom_line(data=(data=doutder1),aes(y=C,x=time),lty=1,size=1.5)+
  geom_line(data=(data=doutder2),aes(y=C,x=time),lty=1,size=1.5, col = 1)+
  geom_line(data=(data=doutder3),aes(y=C,x=time),lty=1,size=1.5, col = 1)+
  geom_line(data=(data=doutder4),aes(y=C,x=time),lty=1,size=1.5, col = 1)+
  ylab("Concentration (nM)")+ xlab("Time (hours)")+
  theme_bw()+theme(text=element_text(size=15))+
  coord_cartesian(xlim = c(0,15)    )
plotpk
# plot target occupancy over time ----------------------------------------------------------------------
cbbPalette <- c("#000000", "#E69F00", "#56B4E9", "#009E73", "#F0E442", "#0072B2", "#D55E00", "#CC79A7")
plotTO<-ggplot()+
    geom_line(data=data.frame(doutder1,col=factor(1,levels = c(1,2,3,4))),aes(y=TO*100,x=time, col=col),lty=1,size=1.5)+
    geom_line(data=data.frame(doutder2,col=factor(2,levels = c(1,2,3,4))),aes(y=TO*100,x=time, col=col),lty=1,size=1.5)+
   geom_line(data=data.frame(doutder3,col=factor(3,levels = c(1,2,3,4))),aes(y=TO*100,x=time, col=col),lty=1,size=1.5)+
  geom_line(data=data.frame(doutder4,col=factor(4,levels = c(1,2,3,4))),aes(y=TO*100,x=time, col=col),lty=1,size=1.5)+
  ylab(" Target occupancy (%)")+ xlab("Time (hours)")+
  theme_bw()+theme(text=element_text(size=15),plot.margin = unit(c(5,5,5,5),"mm"))+
  scale_color_manual(name= expression(k[on]~(nM^-1~h^-1)),values = cbbPalette, breaks=c(4,3,2,1), labels =
                c(500,125,16,1))+
  coord_cartesian(ylim = c(0,100),xlim = c(0,15)
  )
plotTO
##########################################################
# changing parameters for additional simulations
##########################################################
changedpars8<-within(params, {  kon = 3.6
koff = 36.00
dose = 1600})
changedpars9<-within(params, {  kon = 0.2
koff = 2.00
dose = 1600})
```

```
changedpars10<-within(params, {  kon = 0.025
koff = 0.25
dose = 1600})
changedpars11<-within(params, {  kon = 0.0075
koff = 0.075
dose = 1600})

#########################################################
# executing additional simulations
#########################################################
doutder9<-NULL
doutder9<-solveivro(as.list(changedpars8))
doutder10<-NULL
doutder10<-solveivro(changedpars9)
doutder11<-NULL
doutder11<-solveivro(changedpars10)
doutder12<-NULL
doutder12<-solveivro(changedpars11)
# plot pharmacokinetics over time -----------------------------------------------------------------------
plotpk3<-ggplot()+
  geom_line(data=(data=doutder9),aes(y=C,x=time),lty=1,size=1.5)+
  geom_line(data=(data=doutder10),aes(y=C,x=time),lty=1,size=1.5, col = 1)+
  geom_line(data=(data=doutder11),aes(y=C,x=time),lty=1,size=1.5, col = 1)+
  geom_line(data=(data=doutder12),aes(y=C,x=time),lty=1,size=1.5, col = 1)+
  ylab("Concentration (nM)")+ xlab("Time (hours)")+
  theme_bw()+theme(text=element_text(size=15))+
  coord_cartesian(xlim = c(0,15)  )
plotpk3
# plot target occupancy over time -----------------------------------------------------------------------
plotTO3<-ggplot()+
  geom_line(data=(data=data.frame(doutder9,col=factor(1))),aes(y=TO*100,x=time,col=col),lty=1,size=1.5)+
  geom_line(data=(data=data.frame(doutder10,col=factor(2))),aes(y=TO*100,x=time,col=col),lty=1,size=1.5)+
  geom_line(data=(data=data.frame(doutder11,col=factor(3))),aes(y=TO*100,x=time,col=col),lty=1,size=1.5)+
  geom_line(data=(data=data.frame(doutder12,col=factor(4))),aes(y=TO*100,x=time,col=col),lty=1,size=1.5)+
  geom_line(aes(y=rep((1-0.075/0.693)*100,2),x=c(0,15)),lty=2, col = cbbPalette[4],size=1.5)+
  geom_line(aes(y=rep((1-0.25/0.693)*100,2),x=c(0,15)),lty=2, col = cbbPalette[3],size=1.5)+
  ylab(" Target occupancy (%)")+ xlab("Time (hours)")+
  theme_bw()+theme(text=element_text(size=15))+
  scale_color_manual(name= expression(k[off]~(h^-1)),values = cbbPalette, breaks=c(4,3,2,1),
                   labels = c(0.075,0.25,2,36))+
  coord_cartesian(ylim = c(0,100),xlim = c(0,15)
  )
plotTO3
fig1<-cbind(ggplotGrob(plotpk), ggplotGrob(plotTO),size="first")
grid.newpage()
grid.draw(fig1)
fig2<-cbind(ggplotGrob(plotpk3), ggplotGrob(plotTO3),size="first")
grid.newpage()
grid.draw(fig2)

tiff("fig1.tiff",width = 9, height = 4, units = "in", res = 300)
grid.newpage()
grid.draw(fig1)
dev.off()


tiff("fig2.tiff",width = 9, height = 4, units = "in", res = 300)
grid.newpage()
grid.draw(fig2)
dev.off()
```

Chapter 3. Mechanistic modelling of drug target binding kinetics as determinant of the time course of drug action *in vivo*

Scope and intent of the investigations

General introduction

Drug-target binding kinetics refers to the kinetics of the central event in pharmacology: target engagement. The kinetics of this event can be described in its simplest form according to equation 1, in which k_{on} is the second order association rate constant, k_{off} is the first order dissociation rate constant, L is the concentration of the ligand (i.e. a drug or an endogenous ligand), R is the concentration of the target and LR is the concentration of the bound ligand-target complex. The equilibrium dissociation constant (K_D) is given by the ratio k_{off}/k_{on}.

$$L + R \underset{k_{off}}{\overset{k_{on}}{\rightleftarrows}} LR \qquad \text{Eq. 1}$$

The mathematical description of drug target binding according to equation 1 is regularly incorporated in the models that describe the pharmacokinetic profile of monoclonal antibodies and their associated pharmacodynamic profiles in so-called target mediated drug disposition (TMDD) models.[1–3] For small molecules however, the role of drug-target binding kinetics has also been incorporated [4–7] but this effect is most often assumed to be negligible in both PKPD modelling practices and in the design and development of new molecules.

With the publication of Copeland et al. in 2006 [8], a new interest was initiated to utilize drug-target binding kinetics and especially the drug-target dissociation rate constant (k_{off}) or its reciprocal value that expresses the mean target residence time (RT) of each drug molecule on the target after drug-target association. In this regard, especially a low k_{off} value was proposed to be a desirable property for new drug candidates.

The reasons why a low k_{off} value is considered as a desirable drug property are diverse:

- A lower k_{off} can lead to a slower decline of target occupancy and as a result, a prolongation of the drug effect, compared to a drug with rapid target equilibration kinetics.[9,10]
- Differences in target equilibration kinetics at different targets may result in an improved selectivity of action over time, a phenomenon which is often referred to as kinetic selectivity.[8,11]
- The value of k_{off} may affect fluctuations in target occupancy upon repeated dosing and/or in the situation of fluctuating endogenous ligands concentration, with potentially a more favourable efficacy/safety balance.[12]
- A low k_{off} gives rise to longer binding of each drug molecule to the target molecule, which could improve the efficacy of signal transduction.[13,14]

In this thesis, we focus on the first three points, which are all focused on the duration of target occupancy as determinant of the duration of drug effect. As outlined in **chapter 1**, the duration of target occupancy is not only influenced by the drug-target binding kinetics but also by all other kinetic factors that connect drug dosing to drug effect [15]:

First of all, after a drug enters the body and is absorbed into the blood circulation, the elimination and distribution of a drug are the main determinants for how quickly the drug concentrations decline. If the drug concentration is declining slowly compared to the k_{off}, the duration of target occupancy is hardly influenced by the value of k_{off}.

Secondly, the distribution into and out of the tissue where the target resides can also affect the time course of target occupancy and, similar to a slow elimination from plasma, slow distribution out of the target tissue compared to drug-target dissociation reduces the influence of the k_{off} value on the duration target occupancy.

Thirdly, the concentration profile and target binding kinetics of endogenous ligands can also influence the time course of drug-target occupancy. If a drug is bound to the target, a steep increase in the endogenous ligand concentration would lead to faster displacement of the drug by endogenous ligand binding for drugs with a higher k_{off} value compared to drugs with a lower k_{off} value.

Fourthly, the target synthesis and degradation rate constants can influence the time course of target occupancy, especially when the target turnover is fast, compared to drug target dissociation. In essence, target turnover functions as an additional dissociation mechanism (since drug-bound target is degraded and unbound target is synthesized) and determines the duration of target occupancy if it is much faster than the drug-target dissociation. On top of this influence of target turnover on the effective drug-target dissociation, the degradation of target-bound drug also functions as additional elimination mechanism of the drug, which is described in Target-Mediated Drug Disposition models.[2]

Finally, signal transduction and homeostatic feedback kinetics can influence the time course of drug action, as well as the factors that affect the time course of target occupancy described above. Especially a slow turnover of one of the signalling molecules in a signalling cascade, compared to the fluctuations in target occupancy, will decrease the fluctuations of the drug effect compared to a fast turnover of all signalling molecules.

In this respect, it is important to emphasize that prolonged target occupancy compared to the plasma pharmacokinetics is not defined by a lower log-linear tangent of the target occupancy versus time curve at a given time point, compared to the log-linear slope of plasma concentrations. As explained in **chapter 2**, if the target occupancy is close to 100 %, the log-linear tangent of target occupancy *versus* time profile is lower than the log-linear slope of the plasma concentration *versus* time profile, even if target binding is fast and results in an immediate binding equilibrium. This is a result of the non-linear drug concentration *versus* equilibrium target occupancy relationship.

The aim of our studies was to investigate how the influences of drug-target binding kinetics on the time course of the target occupancy (**Section II**) and the drug effect (**Section III**) depend on the other kinetic processes that constitute the PKPD context of drug-target binding kinetics.

Section II. Simulations, model analysis and experimental validation of the influence of binding kinetics on the time course of target occupancy

In **Section II**, we first investigate how, upon single dose administration, the time course of the target occupancy depends on one hand on the drug-target binding kinetics and on the other hand also on the pharmacokinetics, in particular the elimination rate constant and the tissue distribution kinetics. Secondly, we apply this insight and study how this affects the selectivity of action of a drug and the ability to discriminate between a drug-target binding model and a biophase distribution model to account for hysteresis in PKPD modeling.

Kinetics of *in vivo* target occupancy: impact of drug distribution and elimination *versus* target binding kinetics

To understand the influence of the drug-target dissociation rate constant (k_{off}) on the time course of target occupancy and its dependence on the plasma elimination rate constant (k_{el}), one cannot just compare the k_{off} with the k_{el} and conclude that the lowest rate constant determines the decline rate of target occupancy, as suggested previously [10]. The problem with this approach is that it does not take into account that the decline of drug concentrations over time are influenced by drug target binding, as is well documented for biologics [1,2] and has been described as rebinding for small molecules on a local scale [9]. In **chapter 4**, we therefore investigate when, on the one hand the elimination rate constant and the tissue distribution kinetics and on the other hand, the drug-target dissociation become the rate-limiting step in the decline of target occupancy, taking into account the important role of the total target concentration. This rate-limiting step refers to the slowest step in a chain of reactions that determines the overall rate of the whole chain of reactions, which is a concept often applied in chemistry.[16]

To explore the interrelationships between the pharmacokinetics and the target association and dissociation kinetics as determinants of the time course of target occupancy, we approximate two minimal pharmacokinetic target binding models, with first order elimination from the central compartment, in which the target binding either takes place in the only pharmacokinetic (plasma) compartment or in a peripheral tissue compartment connected to the plasma by linear distribution kinetics. These approximations are obtained by formalizing the rate-limiting step concept as described in the previous paragraph to obtain algebraic equations for the tangent of the target occupancy *versus* time curve for a given value of target occupancy.

The obtained approximations are subsequently used to visualise the influence of the values of k_{on} and k_{off}, relative to the elimination rate constant, on the time course of target occupancy for a wide range of k_{on} and k_{off} values and to calculate the influence of the elimination rate constant, the tissue distribution rate constants and the target concentration on the duration of target occupancy. With this analysis, we show that at concentrations of a drug target which largely exceed the K_D value, the values of k_{off} and the k_{on} have an equal effect on the duration of target occupancy, which is thus driven by the K_D and in equilibrium under these conditions.

Chapter 5 focuses on the role of rebinding as determinant of the duration of target occupancy and the mathematical approximation of this phenomenon. More specifically, we compared the rate-limiting step approximation, with the steady-state approximation. The rate-limiting step approximation assumes that the slowest step in the chain from drug-target dissociation, drug distribution and drug elimination determines the duration of target occupancy, as described in chapter 4, whereas the steady-state approximation is based on the assumption that the target site concentrations are in steady-state and dependent on the target-bound concentration.[17–19]. In **chapter 5**, we investigate how the rate limiting step approximation differs from the steady-state equation. To do so, we rewrite our rate-limiting step approximation equations in the same format as the steady-state approximation equations, compare these equations and perform simulations to investigate which approximation provides the most similar results to the full pharmacokinetic-target binding model. We demonstrate that the rate-limiting step approximation performs best in most situations and performs much better if the steady state assumption does not hold: if the drug-target dissociation is fast compared to the distribution out of the target site and the drug-target association. Based on these findings, we propose that either the rate-limiting step approximation or the full differential equation model is used, rather than the steady-state approximation.

Selectivity of action: target selectivity *vs* tissue selectivity

As explained before, one of the proposed benefits of a low k_{off} value for a small molecule drug is that it could dissociate slower from the therapeutic target compared to the secondary-target (kinetic selectivity). However, the results in chapter 4 indicate that for drugs with a high target concentration compared to the K_D value, a low k_{off} value would still lead to equilibrium target binding. This implies that kinetic selectivity would be decreased or absent for drugs with a high target concentration and low K_D value. On the other hand, if a high target concentration compared to the K_D value leads to an increased target site concentration compared to the plasma concentration, this could lead to increased tissue selectivity for tissues with high target concentrations. The aim of **chapter 6** is therefore to explore the influence of tissue distribution kinetics, drug-target binding kinetics, and target concentrations on the time course of target and tissue selectivity. To that end, we perform simulations in three minimal physiologically-based pharmacokinetic models and combine those with target binding kinetics models. The first model is designed to investigate target selectivity, where we lump all tissues without drug-target binding except the eliminating organ and the plasma, and incorporate one tissue with drug-target binding to two different targets. The second model is designed to investigate tissue selectivity and differs from the first model in that it has two tissues with drug-target binding and that only one target type is incorporated in both tissues. The third model is a more specific case study that combines drug-target binding to 4 different targets in 3 different brain areas.

With these simulations, we describe that the characteristics that determine the decline of target occupancy, as identified in chapter 4, could similarly be identified in the more complex models for target and tissue selectivity. We describe the influence of target expression levels and the affinity constant K_D on target and tissue selectivity. The identification of a context-dependent optimal K_D value rather than aiming to minimize the K_D increases the value of K_D predictions in early drug discovery. Therefore, we developed a Quantitative Structure Activity Relationship (QSAR) with a random forest model based on public affinity values for the CB1, 5-HT1a, mGlu5 and TRPV1 targets. Combined with the target concentrations for these targets in 3 different brain areas, we simulate the target occupancy profiles for Rimonabant, CP-55490 and Δ^8 THC, CB1 ligands which have approximately tenfold different K_D values for the CB1 receptor. In these studies, the dose was adjusted to obtain similar equilibrium CB1 occupancy for all three compounds. When steady state occupancy was reached, all compounds showed selectivity for the different targets according to the difference in their K_D values for the different targets. We also describe that the higher affinity compounds Rimonabant and CP-55490 showed a much slower approach to steady-state occupancy in the brain regions with the highest target expression compared to Δ^8 THC, which led to a change in target selectivity across tissues in the first week of treatment. We thus show the advantage and propose the application of combined computational methods to predict target and tissue selectivity in the earliest phase of drug discovery and generate understanding of multiple target binding in multiple target tissues.

SECTION III. Simulations, model analysis and experimental validation of the influence of binding kinetics on the time course of drug action

In chapter 4, 5 and 6, we show how the influence of drug-target binding kinetics on the time course of target occupancy is dependent on the pharmacokinetics and target concentrations. This invokes the question when a drug-target binding model can be discriminated from linear target site distribution models and when these models provide similar drug effect profiles. To investigate this, in **chapter 7** we fit an effect compartment model, a target binding model and a combined effect compartment-target binding model to a historical morphine PKPD dataset in rats. This dataset contained plasma and brain extracellular fluid (ECF) morphine concentrations and EEG amplitudes as pharmacodynamic endpoint. In addition, we perform simulations with a one compartment PK model with drug-target binding to identify for what parameter values the time to the maximal target occupancy ($Tmax_{TO}$) changed significantly with a tenfold increase in the dose. We describe that the differentiation between the target binding and effect compartment model is difficult, both if the plasma concentrations or the brain concentrations are assumed to be directly linked to the target binding/effect compartment. Moreover, our simulations show that the shift in $Tmax_{TO}$ with increasing dose is only observed for intermediate k_{off} values around the elimination rate constant and for low K_D values relative to the target concentrations. We conclude that successful target binding or effect compartment model fits are not supportive for the relevance of target binding or target site distribution, respectively. The target binding model should be considered more often as alternative to the effect compartment model to obtain the best model and to generate the possibility to inform the *in vivo* model with *in vitro* parameters.

So far, we have focused on the role of target binding kinetics as a determinant of the time course of the target occupancy and the selectivity of action in a stationary system without homeostatic feedback, where a constant drug concentration leads to a constant drug effect. In reality, fluctuations of the drug effect may occur, also with constant drug concentration. Such fluctuations may result from fluctuations in the release of neurotransmitters or from homeostatic feedback mechanisms. In Section III, we study how the influence of drug-target binding kinetics depends on the concentration profile and target binding kinetics of endogenous ligands, on the signal transduction and on homeostatic feedback. We investigate this question in **chapter 8** based on the *in vitro* binding kinetics and cAMP response data for 17 dopamine D_2 antagonists. The relation between drug-target binding kinetics, endogenous competition and signal transduction is especially relevant for D_2 antagonists since it has been postulated in the “fast-off” hypothesis that a high antagonist k_{off} value would reduce their side effects by partially allowing the endogenous dopamine binding to the D_2 receptor.[20] This hypothesis has been investigated with a more detailed simulation study for fluctuating dopamine concentrations, but the signal transduction and feedback kinetics were not taken into account in that study.[12] Therefore, we firstly develop a minimal mechanistic model that included antagonist and dopamine binding kinetics to the D_2 receptor, the synthesis and degradation of cyclic adenosine monophosphate (cAMP) and the synthesis and degradation of phosphodiesterase (PDE), which provides negative feedback on cAMP concentrations. This model is fitted to the *in vitro* cAMP response data of all 17 D_2 antagonists and subsequently used to simulate the response to fluctuating dopamine concentrations with a wide variety of fluctuation frequencies, as observed *in vivo*.[21] We find that the influence of the antagonist k_{off} on the amplitude of the induced cAMP fluctuations is restricted by both the cAMP degradation rate constant and the dopamine k_{off} which also means that an antagonist k_{off} higher than one of these values does not influence the cAMP fluctuations. This means that to study the relevance of the k_{off} value, the signal transduction kinetics, endogenous ligand binding kinetics and the homeostatic feedback kinetics need to be taken into account, especially for fluctuating endogenous ligand concentrations.

In **chapter 9**, we discuss how the findings in this thesis affect our understanding of the influence of drug-target binding kinetics on the time course of target occupancy and drug effect. We conclude that this is dependent on the pharmacokinetic and pharmacodynamic context and that modeling and simulation can be a valuable tool to increase the understanding of the complex biological system that determines the relevance of drug-target binding kinetics for the time course of drug action.

References

1. Dua P, Hawkins E, van der Graaf P. A Tutorial on Target-Mediated Drug Disposition (TMDD) Models. CPT Pharmacometrics Syst Pharmacol 2015;4(6):324–37
2. Levy G. Pharmacologic target-mediated drug disposition. Clin Pharmacol Ther 1994;56(3):248–52
3. Cheung WK, Levy G. Comparative pharmacokinetics of coumarin anticoagulants XLIX: Nonlinear tissue distribution of S-warfarin in rats. J Pharm Sci 1989;78(7):541–6
4. Yassen A, Olofsen E, Dahan A, et al. Pharmacokinetic-Pharmacodynamic Modeling of the Antinociceptive Effect of Buprenorphine and Fentanyl in Rats : Role of Receptor Equilibration Kinetics. J Pharmacol Exp Ther 2005;313(3):1136–49
5. Ploeger BA, Van Der Graaf PH, Danhof M. Incorporating Receptor Theory in Mechanism-Based Pharmacokinetic-Pharmacodynamic (PK-PD) Modeling. Drug Metab Pharmacokinet 2009;24(1):3–15
6. Landersdorfer CB, He YL, Jusko WJ. Mechanism-based population pharmacokinetic modelling in diabetes: Vildagliptin as a tight binding inhibitor and substrate of dipeptidyl peptidase IV. Br J Clin Pharmacol 2012;73(3):391–401
7. Ramsey SJ, Attkins NJ, Fish R, et al. Quantitative pharmacological analysis of antagonist binding kinetics at CRF1 receptors in vitro and in vivo. Br J Pharmacol 2011;164(3):992–1007
8. Copeland RA, Pompliano DL, Meek TD. Drug-target residence time and its implications for lead optimization. Nat Rev Drug Discov 2006;5(9):730–9
9. Vauquelin G, Charlton SJ. Long-lasting target binding and rebinding as mechanisms to prolong in vivo drug action. Br J Pharmacol 2010;161(3):488–508
10. Dahl G, Akerud T. Pharmacokinetics and the drug-target residence time concept. Drug Discov Today 2013;18(15–16):697–707
11. Tummino PJ, Copeland RA. Residence Time of Receptor-Ligand Complexes and Its Effect on Biological Function. Biochemistry 2008;47(20):5481–92
12. Vauquelin G, Bostoen S, Vanderheyden P, et al. Clozapine, atypical antipsychotics, and the benefits of fast-off D2 dopamine receptor antagonism. Naunyn Schmiedebergs Arch Pharmacol 2012;385(4):337–72
13. Sykes DA, Dowling MR, Charlton SJ. Exploring the Mechanism of Agonist Efficacy : A Relationship between Efficacy and Agonist Dissociation Rate at the Muscarinic M 3 Receptor. 2009;76(3):543–51
14. Guo D, Mulder-Krieger T, IJzerman AP, et al. Functional efficacy of adenosine A$_2$A receptor agonists is positively correlated to their receptor residence time. Br J Pharmacol 2012;166(6):1846–59
15. Danhof M. Systems pharmacology - Towards the modeling of network interactions. Eur J Pharm Sci 2016;94:4–14
16. Campbell CT. Finding the Rate-Determining Step in a Mechanism: Comparing DeDonder Relations with The “Degree of Rate Control.” J Catal 2001;204(2):520–4
17. DeLisi C. The biophysics of ligand-receptor interactions. Quaterly Rev Biophys 1980;13(2):201–30
18. Coombs D, Goldstein B. Effects of the geometry of the immunological synapse on the delivery of effector molecules. Biophys J 2004;87(4):2215–20
19. Vauquelin G. Rebinding : or why drugs may act longer in vivo than expected from their in vitro target residence time. Expert Opin Drug Discov 2010;5(10):927–41
20. Kapur S, Seeman P. Does Fast Dissociation From the Dopamine D 2 Receptor Explain the Action of Atypical Antipsychotics ?: A New Hypothesis. Am J Psychiatry 2001;158(3):360–9
21. Schultz W. Multiple dopamine functions at different time courses. Annu Rev Neurosci 2007;30(1):259–88

Chapter 4. *In vivo* target residence time and kinetic selectivity: the association rate constant as determinant.

Wilhelmus E.A. de Witte[1], Meindert Danhof[1], Piet H. van der Graaf[1,2], Elizabeth C.M. de Lange[1*]

[1] Division of Pharmacology, Leiden Academic Centre for Drug Research, Leiden University, 2333 CC Leiden, The Netherlands

[2] Certara Quantitative Systems Pharmacology, Canterbury Innovation Centre, Canterbury CT2 7FG, United Kingdom

* Correspondence: ecmdelange@lacdr.leidenuniv.nl

Trends Pharmacol Sci 2016;37(10):831–42

Abstract

It is generally accepted that, in conjunction with pharmacokinetics, the first-order rate constant of target dissociation is a major determinant of the time course and duration of *in vivo* target occupancy. Here we show that the second-order rate constant of target association can be equally important. On the basis of the commonly used mathematical models for drug-target binding, it is shown that a high target association rate constant can increase the (local) concentration of the drug, which decreases the rate of decline of target occupancy. The increased drug concentration can also lead to increased off-target binding and decreased selectivity. Therefore, both the kinetics of target association and dissociation need to be taken into account in the selection of drug candidates with optimal pharmacodynamic properties.

Glossary

Endogenous ligand; A compound that is naturally present in the body and functions by binding to a certain receptor.

Endogenous competition; Binding of an endogenous ligand to the same binding site as a drug.

Kinetic selectivity; Differential kinetics of a compound for binding to intended and unintended targets. Most often considered beneficial if the residence time on the intended target is longer than the residence time on the unintended targets

Non-specific binding; Drug binding to proteins, lipids or other materials that do not initiate signaling. Often unsaturated.

Pharmacokinetics; The combination of all processes that influence the concentration of a drug over time, including absorption, distribution, metabolism and excretion in all body compartments.

Pharmacodynamics; The combination of all processes that influence the relation between drug concentrations and drug effects.

Residence time; The average time each drug molecule remains bound to the target after the binding event, calculated as $1/k_{off}$.

Rebinding; The occurrence of multiple binding events during the dissociation phase, as a consequence of increasing unbound drug and target concentrations due to dissociation. Mostly used to describe the increased local drug concentration due to dissociation and limited diffusion near the drug target, for example in a synapse.

Signal transduction; The cascade of (cellular) reactions that is initiated by receptor activation and leads to the eventual effect.

Target-Mediated Drug Disposition; Extensive drug-target binding that influences the pharmacokinetic characteristics of a drug.

Target occupancy; The fraction of target that is bound to a drug or ligand molecule.

Target Turnover; Synthesis and degradation of a drug target leading to continuous regeneration of unbound target molecules.

Optimisation of *in vivo* drug-target binding kinetics for drug discovery

To optimise the duration of drug action for its therapeutic use, developers have primarily focused on modification of pharmacokinetic parameters. However, an alternative approach is to optimise the duration of drug action by the modification of drug-target binding kinetics.

The target association and dissociation rate constants are important determinants of both the time course and the extent of drug effects, and their values can be measured in high-throughput *in vitro* systems. This has led to the inclusion of drug-target binding kinetics as a selection criterion in the evaluation of drug candidates in drug discovery [1,2].

Although drug-target binding kinetics can be optimised for different purposes regarding the magnitude and the kinetics of both wanted and unwanted drug effects [3–7], the most frequently proposed application is to prolong the duration of action by prolonging the **target occupancy** (see Glossary). Generally, the emphasis has been put on an increase of the target **residence time** through a reduction of the rate of target dissociation [8–10].

However, as drugs act in the human body, which is a complex and dynamic biological system, the duration of drug action is also influenced by other factors. These factors include the time course of the drug concentration (**pharmacokinetics**), the rates of synthesis and breakdown of the target molecule (**target turnover**), the concentrations of **endogenous ligands** competing for the same target, and the kinetics of the **signal transduction** [11].

Of these factors, the pharmacokinetics of the drug and the drug-target binding kinetics are the most frequently considered determinants of the time course of target occupancy. It is generally believed that the drug-target dissociation will only prolong target occupancy if it is slower than the rate of elimination of the drug [10].

While this rule of thumb offers a valuable approach to evaluate the role of drug-target binding kinetics, it does not account for all aspects of the complex interaction between the drug and its target. An important factor in this respect is that binding to the target can modify the local pharmacokinetics of the drug. In this way, binding of the drug to the target may lead to a decrease in the free drug concentration, while dissociation from the target may lead to an increase of the free drug concentration. This process is commonly referred to as "**target-mediated drug disposition**" or TMDD. The quantitative significance of this effect depends on the ratio of target-bound and unbound drug concentrations, which in turn depends on the target affinity of the drug and the concentration of the target in the biological system. Particularly for drugs with a high affinity for the target, target binding may reduce the elimination of the drug, as reflected in a long terminal phase in the decrease of the unbound plasma concentration, as has been demonstrated for warfarin and other drugs (Box 2) [12–19].

The influence of drug-target binding kinetics has not only been described for unbound drug concentrations in plasma, but also for unbound drug concentrations in the local environment of the target, such as a synapse or a cell membrane. In the local context, this interaction is commonly referred to as "diffusion-limited binding", "**rebinding**" or drug-target binding from a "micro compartment" [20–24].

To understand the role of drug-target binding kinetics, others have analysed when binding equilibrium can be assumed in a TMDD model with target binding in plasma [17] and what the role of binding kinetics is when rebinding occurs [22]. Most recently, Vauquelin *et al.* demonstrated in a simulation study that both the drug-target association and dissociation rate constant have a similar impact on the duration of target occupancy if rebinding occurs [25]. However, an integrated analysis that indicates when binding kinetics are most relevant in a pharmacokinetic context, including tissue distribution, is currently missing.

Our aim here is to obtain such an integrated analysis. We firstly present an approximation to understand and visualize the role of drug-target binding kinetics if binding occurs in plasma. Subsequently, we expand this approximation to binding in a tissue. We obtain simple algebraic expressions to calculate when the drug-target dissociation rate is determining the duration of target occupancy for both binding in plasma and in tissues. Thus, we provide a connection of model-based insights from TMDD and rebinding models to predict the role of drug-target binding kinetics for drugs that bind to targets in the blood or in more peripheral tissues.

Drug-target binding *in vivo*: where does it happen?

The commonly used mathematical models for drug-target binding were analysed in this study to yield a quantitative insight in the relative impact of drug-target binding kinetics and pharmacokinetics on the time course of target occupancy *in vivo*. The simplest model considers the situation where drug-target binding and elimination of the unbound drug occur simultaneously from the blood or from a tissue that is in fast equilibrium with the blood. This is schematically represented by Model 1 (Figure 1). The central compartment represents the blood and all organs that equilibrate quickly with the blood (see Box 1 for more information). Similar models have been used to describe binding to enzymes and binding to centrally expressed targets [26,27]. Note that absorption is not incorporated in this model and the dose is administered directly in the central compartment to represent intravenous dosing or very fast absorption.

Although drug-target binding from the blood is commonly seen for circulating enzymes or receptors on circulating cells, many drug targets are only expressed in specific tissues, such as the brain. For such targets, Model 2 (see Figure 1) might be more relevant. Model 2 is a common model for distribution into a specific tissue and binding to a drug target which is localised only in this tissue. This model has been used for a long time, for example to describe dopamine D_2 receptor binding in the human brain and β-Adrenergic receptor binding in the human heart [28,29]. The central compartment represents the blood and all organs that equilibrate quickly with the blood. Absorption is not incorporated in this model and the dose is given directly in the central compartment to represent intravenous dosing or very fast absorption.

Simultaneous elimination and drug-target binding: what's the difference?

The influence of pharmacokinetics on the role of drug-target binding kinetics has been acknowledged previously. This influence has been summarized in the general paradigm that the rate of drug-target dissociation has to be slower than the rate of elimination of the unbound drug to prolong the duration of target occupancy. However, this general rule does not take into account the possible influence of drug-target binding on unbound drug concentration profiles. The influence of drug-target binding on the unbound drug concentration is known to be most pronounced for drugs with high affinities or high target concentrations (i.e. if the ratio of the target concentration and the affinity exceeds 1, see Box 2) [12]. As the interaction between pharmacokinetics and drug-target binding depends on the dissociation constant (K_D), decreasing the drug-target dissociation rate constant (k_{off}) or increasing the drug-target association rate constant (k_{on}) will both have a similar impact on the unbound drug concentrations (Box 1 and Box 2). As a consequence, changing the k_{on} of a drug can have the same impact on the duration of target occupancy as changing the k_{off}. However, the impact of k_{on} and k_{off} on the initial increase of target occupancy might be different. The comparable impact on the duration of target occupancy of changing only k_{off} (left panels) or only k_{on} (right panels) is illustrated in Figure 2. The different rows in Figure 2 demonstrate that the impact of k_{on} and k_{off} on the duration of target occupancy depends on the target concentration and the elimination rate constant k_{el}: In the first row, where the target concentration is 10 nM, the impact of k_{on} and k_{off} is very similar, but in the second row, where the target concentration has changed to 1 nM, the impact of k_{on} and k_{off} is different, as can be seen most clearly for the yellow and the blue line. In the bottom row, where the target concentration stays 1 nM and the elimination rate constant changes from 1 to 0.1 h^{-1}, the impact of k_{on} and k_{off} on the duration of target occupancy is again similar.

Box 1. Drug-target binding in compartmental models.

Compartmental models are the most common form of mathematical models in pharmacology. In these models, the different locations and states in which the drug can occur are lumped into one or more compartments. Differential equations are used to describe the time profile in each compartment (see Supplemental Information S1 for the differential equations of Model 1 and Model 2). The underlying assumptions of a compartmental description of drug-target binding are the following:

1. *Homogeneity within each compartment: Although the represented biological systems are clearly non-homogeneous, the assumption of homogeneity can be used if equilibration within each compartment is sufficiently fast.*

2. *Drug-target binding occurs in the unbound drug compartment: As the drug target has to reside in the same location as the unbound drug to enable drug-target binding, the volume of the ligand-receptor compartment and the volume of the unbound drug compartment that drives the drug-target binding (i.e. the tissue compartment for Model 2) are assumed to be the same.*

Model 1 connects the drug concentration to the target binding according to the law of mass action. The law of mass action states that the rate of elementary (single-step) chemical reactions is proportional to the product of the concentrations of the reactants. This results in the familiar equations that describe the drug-target association rate as the product of the drug-target association rate constant k_{on}*, the unbound target concentration [R] and the unbound ligand concentration [L], while the drug-target dissociation rate is the product of the dissociation rate constant* k_{off} *and the bound ligand concentration [RL]. As the drug-target association and dissociation rates are equal in equilibrium, this leads to the common equilibrium equation for the dissociation constant* K_D*:*

$$K_D = \frac{[L] \cdot [R]}{[LR]} = \frac{k_{off}}{k_{on}}$$

In a closed system (without drug or target elimination) with a low target concentration (as in most in vitro *binding experiments) [L] can be assumed to be constant and much larger than [R]. This has led to analytical expressions that describe the drug-target binding profile in vitro, such as published by Motulsky and Mahan* [39]. *For the in vivo situation, [L] is not constant, because high target concentrations can lead to depletion of the ligand upon binding, and because of drug elimination. Thus,* in vivo *drug-target binding cannot be simplified in the same way as* in vitro *drug-target binding.*

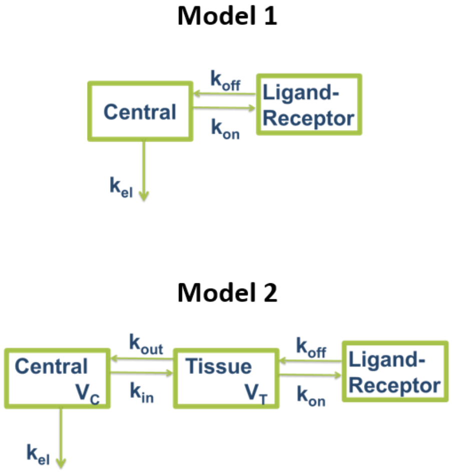

Figure 1. Schematic representation of the two models that are used in this study. Model 1 describes drug-target binding in the central compartment (representing blood and quickly equilibrating tissues) with the second-order association rate constant k_{on} *and the first order dissociation rate constant* k_{off}*. Elimination of the drug from the body (by excretion or metabolism) is described by the first order rate constant* k_{el}*. Model 2 describes drug-target binding from a tissue, and distribution into and out of the tissue is described by the first-order rate constants* k_{in} *and* k_{out}*, respectively. The differential equations of Model 1 and 2 can be found in Supplemental Information S1.*

Box 2. Target-Mediated Drug Disposition.

To describe the influence of extensive drug-target binding on the pharmacokinetic profile of the drug, the term “Target-Mediated Drug Disposition” (TMDD) was introduced by Levy et al. *in 1994*[35]*. Extensive target binding occurs mainly when the ratio of total target concentration/dissociation constant* K_D *is larger than 1, as a consequence of the law of mass action. For example, if the unbound concentration of a drug in binding equilibrium is 5 nM, the total target concentration is 50 nM and the* K_D *is 5 nM, 50 % of the target will be occupied, which corresponds to 25 nM. This means that the concentration of the bound drug is five times larger than the concentration of the unbound drug. As most drugs can only be eliminated if they are unbound, this extensive target binding leads to a slower elimination of drug from the body, compared to the situation without extensive target binding. This extensive target binding decreases if the target becomes saturated. If the drug concentration is increased from 5 to 500 nM for the example of a target concentration of 50 nM and a* K_D *of 5 nM, the equilibrium occupancy becomes 99%, corresponding to a target-bound drug concentration of 50 nM. This means that the concentration of bound drug is now ten times smaller than the concentration of the unbound drug. The impact of extensive target binding on free drug concentrations in plasma is most apparent if the average target concentration is high in the whole body. This has led to the frequent application of TMDD models to describe the plasma concentration profile of antibodies, as they often bind with high affinity to centrally expressed targets* [14]*. Since the degradation/internalization of target-bound antibodies often contributes significantly to the elimination of the total amount of antibody, TMDD models often incorporate these processes* [16]*. If extensive target binding only occurs locally and not in the whole body, this can lead to a longer effect compared to what is expected on basis of unbound plasma concentrations.*

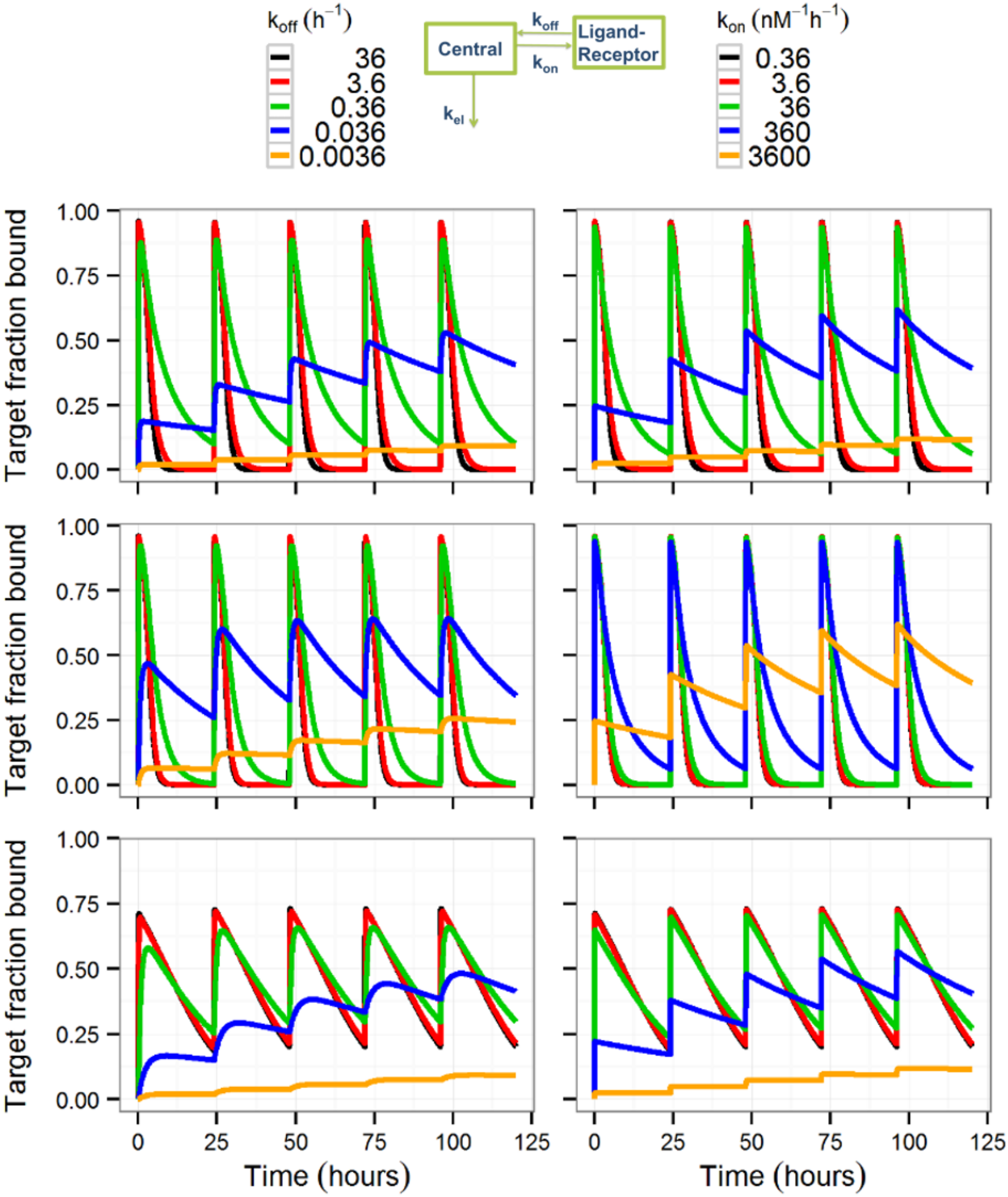

*Figure 2. Simulation of the target fraction bound for drug-target binding in the blood (Model 1). The simulated affinities are increased by changing either the dissociation rate constant k_{off} (left panels) or the association rate constant k_{on} (right panels). The k_{on} was 0.36 $nM^{-1}h^{-1}$ for all lines in the left panels and the k_{off} was 36 h^{-1} for all lines in the right panels. The initial concentration is 25*K_D for the top and middle row and 2.5*K_D for the bottom row, to achieve similar maximal occupancies in all panels. K_D is the drug-target dissociation equilibrium constant and k_{el} is the drug elimination rate constant. [R_{tot}] = total target concentration. Top row: [R_{tot}] = 10 nM, k_{el} 1 h^{-1}, middle row: [R_{tot}] = 1 nM, k_{el} 1 h^{-1}, bottom row: [R_{tot}] = 1 nM, k_{el} 0.1 h^{-1}.*

The influence of pharmacokinetics, target concentration, and affinity on drug-target binding kinetics requires simultaneous analysis of the influence of all parameters. To focus on the duration of target occupancy, we derived an approximation of the decrease of target occupancy after it maximal value. This decrease of target occupancy is described here as the derivative of the target fraction bound (BF) vs. time curve. As the decrease of target occupancy often follows an exponential decline, the derivative is calculated for the semi logarithmic target fraction bound (BF) vs. time curve, where the target fraction bound is on the logarithmic axis. The derivative of the semi logarithmic target fraction bound (BF) vs. time curve, called λ_{TO} here, is not always constant over time as it depends on the saturation of drug-target binding: If the drug concentration is much higher than the affinity and all target molecules are bound to the drug, a relatively small proportion of the drug is bound to the target and the elimination of the drug is not limited by target binding. Also, if target binding is saturated and the unbound drug concentration decreases with a certain percentage, the target fraction bound decreases much less than that percentage. However, a fractional decrease in the unbound drug concentration will result in a similar decrease in the target fraction bound if the target fraction bound is low and binding is not saturated. As an example, if the unbound drug concentration decreases 90% from 500 to 50 nM for a drug with a K_D of 5.0 nM, the corresponding equilibrium bound fraction decreases 7%: from 0.99 to 0.91. If the unbound drug concentration decreases 90% from 50 to 0.50 nM for a drug with a K_D of 5.0 nM, the corresponding equilibrium bound fraction decreases 82%: from 0.50 to 0.091, (see also box 2 and Supplemental Information S2). As the derivative of the semi logarithmic target fraction bound (BF) vs. time curve, λ_{TO}, depends on the saturation of drug-target binding, it can be expressed as a function of the target fraction bound: λ_{TO}(BF).

Our approximation is based on the assumption that the process that results in the slowest decrease of target occupancy (elimination or dissociation) will determine the decrease of target occupancy as rate-limiting step. To predict which of these processes is the rate-limiting step in the decrease of target occupancy, one needs to take into account that only elimination of the unbound drug occurs, and elimination is thus limited by drug-target binding. Moreover, incorporation of the influence of drug-target target saturation on the relationship between the decline of unbound and target-bound drug concentrations is required. As demonstrated in Supplemental Information S2, the derivative of the semi logarithmic target fraction bound (BF) vs. time curve, as function of BF, λ_{TO}(BF), can be approximated on this basis. The resulting approximation of λ_{TO}(BF) for the physiological range of parameter values for Model 1 reveals 3 different situations for the influence of drug-target binding kinetics on the duration of target occupancy:

1) Only the k_{off} determines the duration of target occupancy. This is the case if drug-target dissociation is the rate-limiting step for the decrease of the target occupancy.

2) Both k_{off} and k_{on} influence the duration of target occupancy equally. The duration of target occupancy is determined by the dissociation constant K_D, the elimination rate constant k_{el}, and the total target concentration$[R_{tot}]$.

3) Only the elimination rate constant k_{el} determines the duration of target occupancy.

Which of these situations applies for a specific drug depends on the value of k_{on} and k_{off}, but also on the target concentration and the pharmacokinetic parameters. The situation where drug-target dissociation is rate limiting and k_{off} the only determinant for the decrease of target occupancy requires both a low value for k_{on} and k_{off}. On basis of our approximation, we could identify a constant for the value of k_{off} and k_{on} that results in drug elimination as the rate-limiting step in the decrease of target occupancy. The constants that approximate the threshold value of k_{on} and k_{off} for the rate-limiting step, K_{RLon} and K_{RLoff}(BF), are given by Equation 1 and 2 (which are derived as equation S25 and S26). It should be noted that the K_{RLon} is independent of target saturation while K_{RLoff}(BF) is dependent on target saturation and thus given as function of the target fraction bound (BF).

Equation 1

$$\boldsymbol{K_{RLon} = \frac{k_{el}}{k_{on} \cdot [R_{tot}]}}$$

Equation 2

$$K_{RLoff}(BF) = \frac{k_{el} \cdot (1 - BF)}{k_{off}}$$

If K_{RLon} and $K_{RLoff}(BF)$ are both greater than 1, dissociation is the rate-limiting step in the decrease of target occupancy, which is than determined by k_{off}. If either of these constants is smaller than 1, elimination is the rate-limiting step in the decrease of target occupancy.

If elimination is the rate-limiting step in the decrease of target occupancy, the decrease rate can be either determined by the kel alone, or by k_{el}, k_{on} and k_{off}. The maximal value of k_{off} that leads to an elimination rate that is significantly influenced by k_{el}, k_{off} and k_{on} is given in Equation 3 (derived as equation S28).

Equation 3

$$k_{off} = k_{on} \cdot [R_{tot}] \cdot (1 - BF)$$

Equations 1-3 provide the basis to identify which of the situations regarding the influence of drug-target binding kinetics on the duration of target occupancy applies, as visualised in Figure 3.

The analysis of Model 1 as presented in Figure 3 provides several general insights for drug discovery:

1) Increasing the k_{on} can increase the duration of target occupancy (indicated by the changing color in the horizontal direction), even if the k_{off} is higher than the k_{el}.

2) If the k_{on} or the k_{off} is sufficiently high to result in a K_{RLon} or $K_{RLoff}(BF) > 1$, decreasing the k_{off} has the same impact on the duration of target occupancy as increasing the k_{on} (indicated by the diagonal color bands in the lower right corner).

3) If both the k_{off} and the k_{on} value are sufficiently low to make both K_{RLon} and $K_{RLoff}(BF) < 1$, drug-target dissociation is rate-limiting and k_{off} determines the duration of target occupancy (as indicated by the horizontal color bands in the lower left corner). A rate-limiting drug-target dissociation is required to obtain a slower decline of target occupancy than expected on basis of the unbound drug concentration and the drug-target affinity. This means that only a combination of a low k_{off} and a low k_{on} could lead to longer binding to the intended than to the unintended target (which also requires a lower dissociation rate from the intended compared to the dissociation rate from the unintended target, i.e. **kinetic selectivity**) [1,30].

Model 1 applies to drugs which have their target in the blood or in a tissue that equilibrates rapidly with blood. Mainly targets that are expressed in the blood, such as circulating enzymes (HSP90, Factor X) have target concentrations higher or similar to the highest target concentration of 20 nM in Figure 3 [26,31].

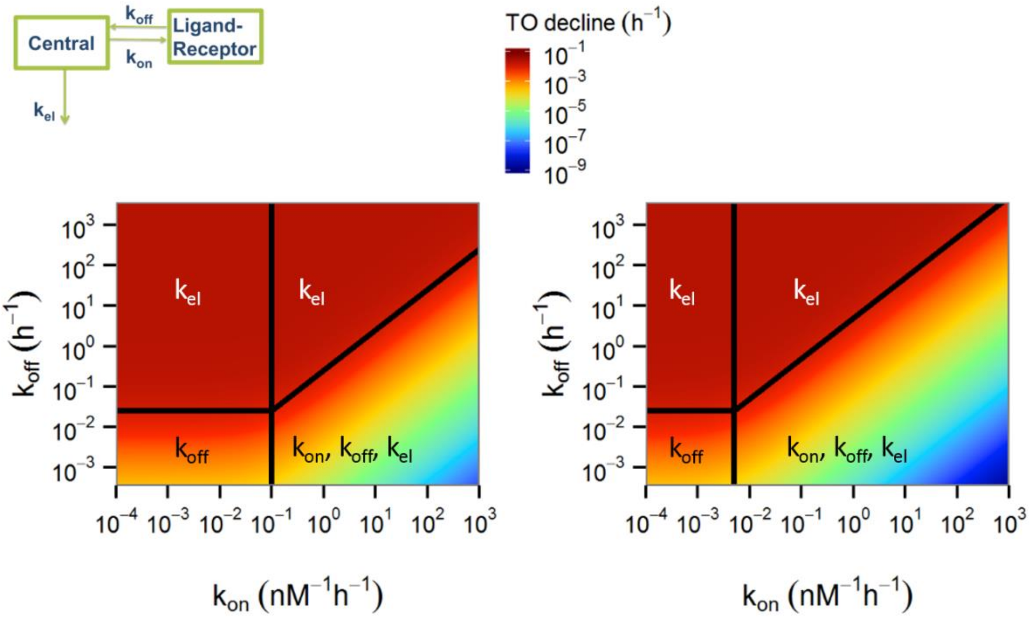

Figure 3. Approximation of the decline in target occupancy using Model 1. The total target concentration is 1 nM (left panel) and 20 nM (right panel), the elimination rate constant is 0.1/h and the target fraction bound is 0.75, to represent a clinically relevant degree of target occupancy. Colors represent the decrease of target occupancy ($\lambda_{TO}(BF)$) as calculated according to Supplemental Information S2 (Equation S19). The vertical line is given for K_{RLon} = 1 (see Equation 1), the horizontal line is given by $K_{RLoff}(BF)$ = 1 (see Equation 2) and the diagonal line is given by Equation 3. In these equations, k_{el} is the elimination rate constant, $[R_{tot}]$ is total target concentration and BF is the bound fraction of the target. The annotations indicate which parameters influence the decrease in target occupancy in the corresponding segment of the plot. This figure is an approximation of Model 1 (insert) (Supplemental Information S2).

Is the impact of drug-target binding kinetics different for target binding in a tissue?

To expand our understanding of drug-target binding, a similar analysis was performed for drugs that bind only in a specific tissue, similarly as was done for drug-target binding from the blood. The results of this analysis can be found in Supplemental Information S3. One of the main differences with the analysis for Model 1 is that the drug distribution from the tissue to the central compartment can be rate limiting for Model 2. A high value of k_{on} still leads to an equal impact of k_{on} and k_{off} on the decline of target occupancy in the same way as for Model 1 if drug distribution out of the tissue is rate-limiting, but this is not necessarily reflected in the unbound plasma concentration versus time profile. Moreover, rate-limiting elimination can similarly influence the duration of target occupancy due to extensive target binding, but this occurs only at high target concentrations in the tissue, as the fraction of the total amount of drug in the body that is bound to the target decreases for decreasing volumes of the drug-target binding tissue.

To understand what our analysis means for drug discovery, our equations have been applied to a combination of common pharmacokinetic parameters (Figure 4, key figure). A small literature survey was performed to find a common value for the total tissue target concentration. The target concentration for common targets such as µ-opioid [23], adenosine [32], dopamine D2 [28], GABA [33], 5-HT [34], and Vitamin K epoxide reductase [35] varied between 2 [34] and 2000 [35] nM, with most values in the range between

10 and 100 nM. As can be seen in Figure 4, our analysis reveals a very similar influence of the drug-target binding kinetics for drug-target binding in tissue compared to drug-target binding in the blood (Figure 4).

To investigate how the combination of k_{on} and k_{off} values of drug discovery compounds relate to the expected determinants of the duration of target occupancy, all compounds from the K4DD (kinetics for drug discovery http://www.k4dd.eu) consortium database were included in Figure 4. This K4DD database is brought together by both industry and academia and consists of *in vitro* binding kinetics measurements of small molecule drug discovery compounds on different targets, including kinases and GPCRs. We will refer to this data set as the “discovery dataset”.

Moreover, a literature dataset of compounds with known drug-target binding kinetics which were developed into drugs or drug candidates, as published by Dahl and Akerud [10], was also included in Figure 4. Below, we will refer to this dataset as the “candidate dataset”. The data in Figure 4 show that the majority of compounds from both datasets have high k_{on} values for the common pharmacokinetic parameters and target concentration and would be expected to have an equal influence of both k_{on} and k_{off} on the duration of target occupancy. Moreover, as the drug distribution is rate limiting for the decline of target occupancy for a high value of k_{on} and the given pharmacokinetic parameters and target concentration in Figure 4, binding equilibrium will be reached and no kinetic selectivity is expected over unintended targets that are located in the same tissue as the intended target. Interestingly, comparison of the discovery and the candidate dataset shows a similar distribution of k_{on} values in both datasets, but a distribution of k_{off} values which is approximately one order of magnitude lower for the candidate dataset. The differential distribution for k_{off} but not for k_{on} in these datasets can have multiple explanations. As indicated by others, k_{on} is often less sensitive to chemical modifications of similar compounds or for biological modifications of the target compared to k_{off} [36]. Also, the selection of drug (candidates) was based on the availability of drug-target binding kinetics, which could lead to a biased dataset for compounds where the drug-target binding kinetics plays a more significant role. Moreover, achieving a high affinity in drug discovery and development by changing the k_{on} is limited by the diffusion-limited maximal value of k_{on}, whereas the k_{off} has no theoretical minimum until irreversible binding is reached [37].

The similar values for k_{on} in both datasets correspond with our finding that an increasing k_{on} can increase the duration of target occupancy but at the cost of increasing the (local) drug concentrations, which can result in increased side effects. Moreover, the observation of lower k_{off} values in the candidate dataset indicates that a low k_{off} value might contribute to successful drug development. Dahl and Akerud observed that the drug-target dissociation for most compounds in the candidate dataset is slower than the plasma elimination, which means in their analysis that the elimination rate determines the duration of target occupancy (assuming there is no rebinding). In our analysis, the high k_{on} values in the candidate and in the discovery dataset result in a decline of target occupancy that is influenced by the elimination rate constant and the binding affinity and that the resultant decline of target occupancy can be slower than the elimination and the dissociation rates.

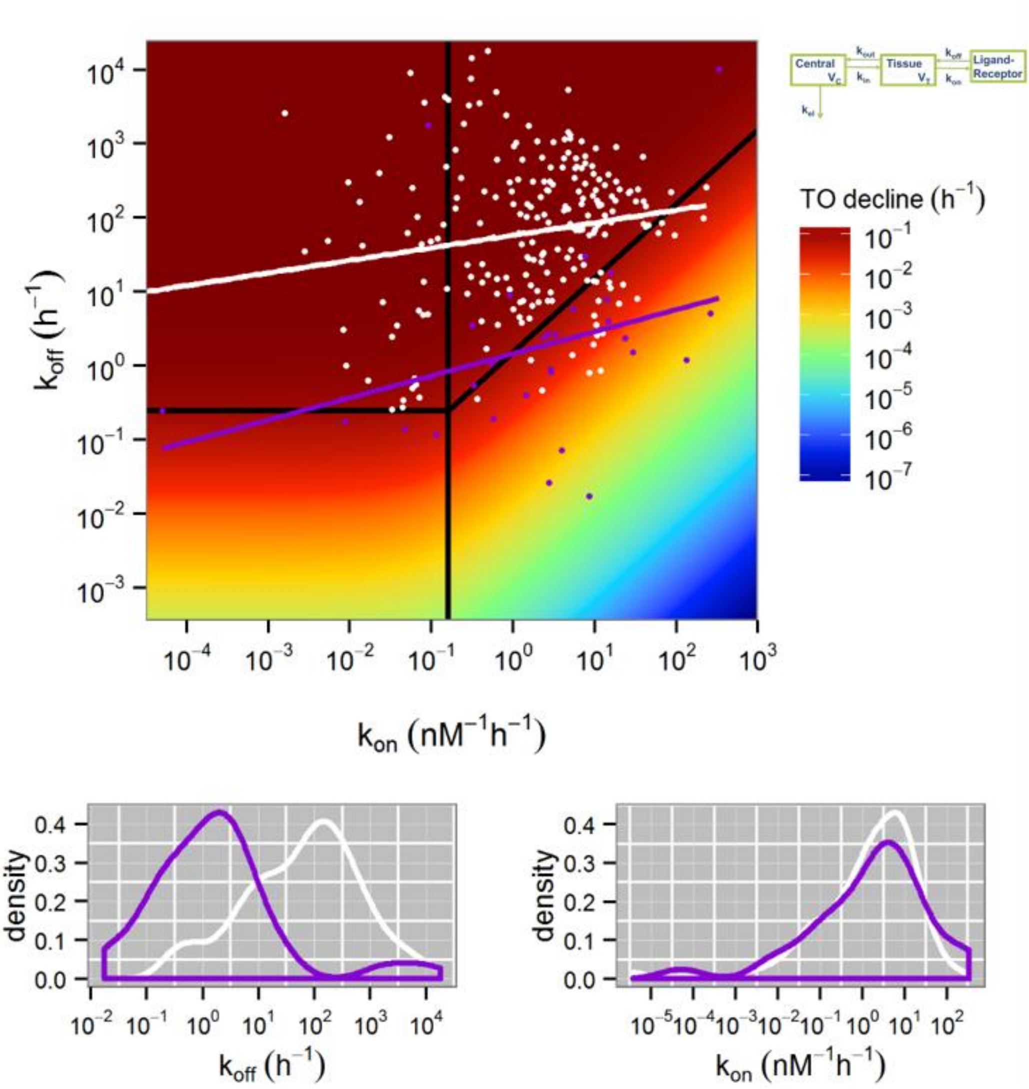

Figure 4. Calculated duration of target occupancy for drug-target binding in a tissue (Model 2). Top panel: Relation between drug-target binding kinetics and the duration of target occupancy for binding in tissue. The points and their linear regressions provide an overview of the distribution of binding kinetics measurements of all compounds in the drug discovery compound database of the K4DD consortium (white) or the drug (candidate) dataset from the review published by Dahl and Akerud (purple). The colors and black lines depend on the pharmacokinetic parameters according to equation S35 in Supplemental Information S3 and are based on Model 2 (insert) with the following parameter values: $[R_{tot}] = 50$ nM, $k_{el} = 0.5$/hr, $k_{in} = 0.2$/hr, $V_C = 40$ L, $V_T = 1$ L, BF = 0.5. $[R_{tot}]$ is the total target concentration, k_{el} is the elimination rate constant, k_{in} is the brain to plasma distribution rate constant, V_C is the volume of the central compartment, V_T is the volume of the tissue and BF is the bound fraction of the target. Bottom panels: distribution of the dissociation (left) and association (right) rate constants of both datasets with the corresponding colors in the top panel. The distribution of the parameter values of each dataset is plotted as the estimated probability density function.

Optimising drug-target binding kinetics: to what end?

Both for drug-target binding in plasma and in tissue, our analysis indicates that high k_{on} values can decrease the target occupancy decline below the elimination and dissociation rates. However, this increased duration of target occupancy is caused by increased (local) drug concentrations unless both k_{off} and k_{on} are low. This means that the optimal value for k_{on} depends on the target, the drug class and the drug-specific pharmacokinetic, **pharmacodynamic** and toxicity processes.

If an increased duration of target occupancy is desired, this can be achieved by both increasing the k_{on} or by decreasing the k_{off}. If the k_{on} is high enough, k_{on} and k_{off} have the same impact on the duration of target occupancy (Figure 2, top and bottom row), but not on the initial increase rate of target occupancy after dosing (Figure 2, bottom row). Moreover, a high value of k_{on} will lead to increased local drug concentrations and a rate-limiting role for the pharmacokinetics, which can result in increased off-target binding and decreased selectivity. How drug target binding can influence only local drug concentrations is illustrated by our simulations for diprenorphine (Supplemental Information S4 and S5).

Our analysis is based on a simplification of the complex biological system that determines the duration of target occupancy, see Outstanding Questions. Three important factors that can play a role in the kinetics of target occupancy are **non-specific binding**, **endogenous competition** and **target turnover**. Non-specific binding could influence the relevance of our analysis as a high percentage of non-specific binding could mean that the impact of specific binding on drug concentrations decreases for drugs with extensive non-specific binding. Also, the presence of an endogenous ligand that competes for binding to the drug target will reduce the number of available target molecules and thus decrease the impact of drug-target binding. Moreover, the synthesis and degradation of the target and drug-target complex can increase the decline of target occupancy and thus decrease the impact of drug-target binding. However, our analysis provides a quantitative improvement of the commonly used consideration that only a drug-target dissociation rate lower than the plasma elimination rate can influence the duration of target occupancy [10,36].

Apart from these complications, the validity of our findings depends on the validity of our assumptions and mathematical method. However, mathematical and experimental findings that explored the interaction between local concentrations in the target vicinity and drug-target binding(“rebinding”) also pointed towards the importance of k_{on} in similar equations [20–22,38]. Moreover, published [3H] diprenorphine plasma and brain concentrations were fitted with Model 2 for this study, and subsequent simulations with varying drug-target binding kinetics revealed an equal impact of k_{on} and k_{off} on the target occupancy profile over time, as expected from our analysis (Supplemental Information S4 and S5). Supplemental Information S4 supports the relevance of the analysed model, Model 2, as it is able to describe the experimental data of diprenorphine plasma and brain concentration. Supplemental Information S5 supports the necessary assumptions that were made to analyse Model 2, as the role of binding kinetics in the full model corresponds with the predicted role of binding kinetics from our approximation. Finally, comparison of approximated and simulated target occupancy vs. time derivatives indicated a high accuracy of our approximation and a high relevance of our assumptions, except for the combination of low association, dissociation and elimination rate constants with low target concentrations (Supplemental Information S6). Altogether, this supports the relevance and validity of our analysis.

To enable the rational use of drug-target binding kinetics in drug discovery, the whole kinetic context between drug dosing and effect should be taken into account. The algebraic equations as presented in this study provide a first step to integrate and understand both pharmacokinetics and drug-target binding kinetics. If the pharmacokinetic parameters are unknown, commonly observed values can be used, as demonstrated in Figure 4. If more detailed information is required on both the duration and the extent of target occupancy, simulations of the compartmental models can be performed easily.

Concluding Remarks

Comprehensive analysis of the commonly used models for drug-target binding reveals that high drug-target association rate constants result in longer target occupancy than expected on basis of the drug-target dissociation and the drug elimination rate constants. The k_{on} value that separates high and low values of k_{on} increases with increasing target concentration and with decreasing drug elimination and distribution rate constants and can be calculated algebraically. High values of k_{on}, for common pharmacokinetic parameter values, are observed frequently for both drug discovery and drug (candidate) compounds and result in an equal impact of both k_{on} and k_{off} on the duration of target occupancy. However, these high k_{on} values can lead to more off-target toxicity. Comparison of drug discovery and drug (candidate) compounds shows similar distributions of k_{on} while k_{off} is approximately one order of magnitude smaller for the drug (candidate) compounds.

The target occupancy versus time profile can only be predicted if the target concentration and the rate constants of drug binding, elimination and distribution are taken into account, which often results in an equal impact of k_{on} and k_{off} on the duration of target occupancy.

Our findings demonstrate that optimizing the drug discovery requires mechanistic knowledge of the intended mechanism of action, including the in vivo concentration of the drug target. Moreover, the role of the drug-target association rate constant (k_{on}) should be taken into account in the optimization of the duration of drug effects. Although this study does not include all relevant processes that can influence the duration of drug effects following administration of a drug (see Outstanding Questions box), the presented integration of target binding and pharmacokinetics is an important step towards a more rational selection of drug candidates.

Acknowledgements

The authors wish to thank professor L. A. Peletier for critically reading the manuscript and providing useful feedback.

The authors are part of the K4DD (Kinetics for Drug Discovery) consortium which is supported by the Innovative Medicines Initiative Joint Undertaking (IMI JU) under grant agreement no 115366. The IMI JU is a project supported by the European Union’s Seventh Framework Programme (FP7/2007–2013) and the European Federation of Pharmaceutical Industries and Associations (EFPIA).

References

1. Copeland RA, Pompliano DL, Meek TD. Drug-target residence time and its implications for lead optimization. Nat Rev Drug Discov 2006;5(9):730–9
2. Shiau AK, Massari ME, Ozbal CC. Back to basics: label-free technologies for small molecule screening. Comb Chem High Throughput Screen 2008;11(3):231–7
3. Swinney DC. The role of binding kinetics in therapeutically useful drug action. Curr Opin Drug Discov Devel 2009;12(1):31–9
4. Langlois X, Megens A, Lavreysen H, et al. Pharmacology of JNJ-37822681, a specific and fast-dissociating D2 antagonist for the treatment of schizophrenia. J Pharmacol Exp Ther 2012;342(1):91–105
5. Kapur S, Seeman P. Does Fast Dissociation From the Dopamine D 2 Receptor Explain the Action of Atypical Antipsychotics ?: A New Hypothesis. Am J Psychiatry 2001;158(3):360–9
6. Sykes DA, Dowling MR, Charlton SJ. Exploring the mechanism of agonist efficacy: a relationship between efficacy and agonist dissociation rate at the muscarinic M3 receptor. Mol Pharmacol 2009;76(3):543–51
7. Sykes DA, Riddy DM, Stamp C, et al. Investigating the molecular mechanisms through which FTY720-P causes persistent S1P1 receptor internalization. Br J Pharmacol 2014;171(21):4797–807
8. Copeland RA. The dynamics of drug-target interactions: drug-target residence time and its impact on efficacy and safety. Expert Opin Drug Discov 2010;5(4):305–10
9. Guo D, Hillger JM, IJzerman AP, et al. Drug-target residence time - a case for G protein-coupled receptors. Med Res Rev 2014;34(4):856–92
10. Dahl G, Akerud T. Pharmacokinetics and the drug-target residence time concept. Drug Discov Today 2013;18(15–16):697–707
11. de Witte WEA, Wong YC, Nederpelt I, et al. Mechanistic models enable the rational use of in vitro drug-target binding kinetics for better drug effects in patients. Expert Opin Drug Discov 2016;11(1):45–63
12. Wagner JG. A new generalized nonlinear pharmacokinetic model and its implications. In: Wagner JG, editor. Biopharmaceutics and Relevant Pharmacokinetics Hamilton, IL; 1971. p. 302–17
13. Mager DE, Jusko WJ. General pharmacokinetic model for drugs exhibiting target-mediated drug disposition. J Pharmacokinet Pharmacodyn 2001;28(6):507–32
14. Dua P, Hawkins E, van der Graaf P. A Tutorial on Target-Mediated Drug Disposition (TMDD) Models. CPT Pharmacometrics Syst Pharmacol 2015;4(6):324–37
15. Mager DE, Krzyzanski W. Quasi-Equilibrium Pharmacokinetic Model for Drugs Exhibiting Target-Mediated Drug Disposition. Pharm Res 2005;22(10):1589–96
16. Peletier LA, Gabrielsson J. Dynamics of target-mediated drug disposition: characteristic profiles and parameter identification. J Pharmacokinet Pharmacodyn 2012;39(5):429–51
17. Ma P. Theoretical considerations of target-mediated drug disposition models: simplifications and approximations. Pharm Res 2012;29(3):866–82
18. Abraham AK, Krzyzanski W, Mager DE. Partial derivative-based sensitivity analysis of models describing target-mediated drug disposition. AAPS J 2007;9(2):E181-9
19. Aston PJ, Derks G, Raji A, et al. Mathematical analysis of the pharmacokinetic-pharmacodynamic (PKPD) behaviour of monoclonal antibodies: Predicting in vivo potency. J Theor Biol 2011;281(1):113–21
20. Coombs D, Goldstein B. Effects of the geometry of the immunological synapse on the delivery of effector molecules. Biophys J 2004;87(4):2215–20
21. DeLisi C. The biophysics of ligand-receptor interactions. Quaterly Rev Biophys 1980;13(2):201–30
22. Vauquelin G. Rebinding : or why drugs may act longer in vivo than expected from their in vitro target residence time. Expert Opin Drug Discov 2010;5(10):927–41
23. Perry DC, Mullis KB, Oie S, et al. Opiate antagonist receptor binding in vivo: evidence for a new receptor binding model. Brain Res 1980;199(1):49–61
24. Szczuka A, Wennerberg M, Packeu A, et al. Molecular mechanisms for the persistent bronchodilatory effect of the beta 2-adrenoceptor agonist salmeterol. Br J Pharmacol 2009;158(1):183–94
25. Vauquelin G. Impact of target binding kinetics on in vivo drug efficacy: koff, kon and rebinding. [Internet]. British Journal of Pharmacology. 2016. Epub ahead of print p
26. Yamazaki S, Shen Z, Jiang Y, et al. Application of target-mediated drug disposition model to small molecule heat shock protein 90 inhibitors. Drug Metab Dispos 2013;41(6):1285–94
27. Francis RJ, Brown AN, Kler L, et al. Pharmacokinetics of the converting enzyme inhibitor cilazapril in normal volunteers and the relationship to enzyme inhibition: Development of a mathematical model. J Cardiovasc Pharmacol 1987;9(1):32–8
28. Farde L, Eriksson L, Blomquist G, et al. Kinetic Analysis of Central [llC] Raclopride Binding to D2-Dopamine Receptors Studied by PET-A Comparison to the Equilibrium Analysis. J Cereb Blood Flow Metab 1989;9(5):696–708

29. Doze P, Elsinga PH, van Waarde A, et al. Quantification of β-adrenoceptor density in the human heart with (S)-[11 C]CGP 12388 and a tracer kinetic model. Eur J Nucl Med Mol Imaging 2002;29(3):295–304
30. Guo D, Dijksteel GS, Van Duijl T, et al. Equilibrium and kinetic selectivity profiling on the human adenosine receptors. Biochem Pharmacol 2016;105:34–41
31. Fair DS, Edgington TS. Heterogeneity of hereditary and acquired factor X deficiencies by combined immunochemical and functional analyses. Br J Haematol 1985;59(2):235–48
32. Bruns RF, Daly JW, Snyder SH. Adenosine receptors in brain membranes: Binding of N6-cyclohexy[3H]adenosine and 1,3-diethyl-8-[3H]phenylxanthine. Proc Natl Acad Sci USA 1980;77(9):5547–51
33. Millet P, Graf C, Moulin M, et al. SPECT quantification of benzodiazepine receptor concentration using a dual-ligand approach. J Nucl Med 2006;47(5):783–92
34. Costes N, Merlet I, Zimmer L, et al. Modeling [18 F]MPPF Positron Emission Tomography Kinetics for the Determination of 5-Hydroxytryptamine(1A) Receptor Concentration With Multiinjection. J Cereb Blood Flow Metab 2002;22(6):753–65
35. Levy G. Pharmacologic target-mediated drug disposition. Clin Pharmacol Ther 1994;56(3):248–52
36. Copeland RA. The drug-target residence time model: a 10-year retrospective. Nat Rev Drug Discov 2016;15(2):87–95
37. Zhou G-Q, Zhong W-Z. Diffusion-Controlled Reactions of Enzymes. A Comparison between Chou’s Model and Alberty-Hammes-Eigen’s Model. Eur J Biochem 1982;387(2–3):383–7
38. Goldstein B, Dembo M. Approximating the effects of diffusion on reversible reactions at the cell surface: ligand-receptor kinetics. Biophys J 1995;68(4):1222–30
39. Motulsky HJ, Mahan LC. The Kinetics of Competitive Radioligand Binding Predicted Mass Action by the Law of Mass Action. Mol Pharmacol 1984;25(1):1–9

Supplemental Information

Inventory of Supplemental Information

Appendix S1. Differential equations of models 1 and 2, related to Box 1 and Figure 1. (page 2)

Appendix S2. Approximation and analysis of model 1, related to Figure 3. (page 5)

Appendix S3. Approximation and analysis of model 2, related to Figure 4. (page 10)

Appendix S4. Experimental validation of model 2, related to Figure 4. (page 15)

Appendix S5. Simulation example of local concentrations determining target occupancy, related to Figure 4. (page 17)

Appendix S6. Accuracy of the approximation of model 1, related to Figure 3. (page 19)

Supplemental references. (page 23)

Appendix S1. Differential equations of models 1 and 2, related to Box 1 and Figure 1.

Used parameters

k_{el} = first order drug elimination rate constant
k_{in} = first order drug distribution rate constant into the tissue
k_{out} = first order drug elimination rate constant out of the tissue
k_{off} = first order drug-target dissociation rate constant
k_{on} = second order drug-target association rate constant
C = unbound drug in the central compartment
T = unbound drug in the tissue compartment
LR = drug-target complex
L_{tot} = total drug in de body = C + T + LR
R_{free} = unbound target
R_{tot} = total target = R_{free} + LR
[] = concentration
A = amount

Model 1

The rate of change in the amount of drug in the central compartment of model 1, AC, is given by Equation S1, where k_{el} and k_{off} are the first order rate constants describing elimination and drug-target dissociation, respectively, where k_{on} is the second order drug-target association rate constant, [R_{free}] is the unbound target concentration and ALR is the amount of drug-target complex. Drug absorption and non-specific binding are not taken into account.

Equation S1

$$\frac{dAC}{dt} = -k_{el} \cdot AC - k_{on} \cdot AC \cdot \left[R_{free}\right] + k_{off} \cdot ALR$$

The rate of change of the unbound receptor concentration [R_{free}], is given by Equation S2 and the rate of change in the amount of drug-target complex, ALR, is given by Equation S3

Equation S2

$$\frac{d[R_{free}]}{dt} = -k_{on} \cdot [C] \cdot \left[R_{free}\right] + k_{off} \cdot [LR]$$

Equation S3

$$\frac{dALR}{dt} = k_{on} \cdot AC \cdot \left[R_{free}\right] - k_{off} \cdot ALR$$

As the total target concentration is constant in this model, [R_{free}] can be calculated from the total target concentration [R_{tot}] and the bound target concentration [LR] as in Equation S4:

Equation S4

$$\left[R_{free}\right] = [R_{tot}] - [\mathrm{LR}]$$

Model 2

For model 2, the rate of change in the amount of drug in the central compartment, AC, is described by Equation S5, where k_{out} and k_{in} are the first order rate constants describing distribution into and distribution out of the tissue, respectively, and AT is the amount of drug in the tissue. Drug absorption and non-specific binding are not taken into account.

Equation S5

$$\frac{dAC}{dt} = -k_{el} \cdot AC - k_{in} \cdot AC + k_{out} \cdot AT$$

The rate of change in the amount of drug in the tissue, AT, is described by Equation S6.

Equation S6

$$\frac{dAT}{dt} = k_{in} \cdot AC - k_{out} \cdot AT - k_{on} \cdot AT \cdot [R_{free}] + k_{off} \cdot ALR$$

the rate of change of the unbound receptor concentration [R_{free}], is given by Equation S7

Equation S7

$$\frac{d[R_{free}]}{dt} = -k_{on} \cdot [T] \cdot [R_{free}] + k_{off} \cdot [LR]$$

The rate of change in the amount of drug-target complex in the tissue, ALR, is described by Equation S8.

Equation S8

$$\frac{dALR}{dt} = k_{on} \cdot AT \cdot [R_{free}] - k_{off} \cdot ALR$$

The total target concentration is constant in this model, so [R_{free}] can be calculated from the total target concentration [R_{tot}] and the bound target concentration [LR] as in Equation S9:

Equation S9

$$[R_{free}] = [R_{tot}] - [\mathrm{LR}]$$

All simulations were performed in Berkeley Madonna, version 8.3.18, while visualisations were performed in R, version 3.1.1[1].

Appendix S2. Approximation and analysis of model 1, related to Figure 1.

As known since the study of Wagner et al[2], the terminal log-linear slope of a PK curve with fast binding equilibrium (λ_z) is given by Equation S10.

Equation S10

$$\boldsymbol{\lambda_z = \frac{k_{el}}{1 + \frac{[R_{tot}]}{K_D}}}$$

As explained in box 2, the extensive target binding that leads to a decreased terminal slope of the plasma concentration depends on the ratio of $[R_{tot}]$ and K_D. Equation S10 can be derived as in Equation S12 by assuming that the free target concentration equals the total target concentration, since the slope of only the last part of the PK curve is derived. For earlier phases of the PK curve, the target binding might be saturated, leading to a decreased extent of target binding and a steeper PK curve. This saturated part of the PK curve is of interest, as most drugs require a substantial target saturation to be efficacious, especially if the drug is an antagonist.

To make Equation S10 valid for the whole part of the PK curve where equilibrium between bound and unbound drug concentration can be assumed, the value of the target fraction bound (BF) needs to be incorporated as in Equation S13. Here, λ_{el}(BF) describes the derivative of the drug concentration profile over time on semi-log scale (i.e. ln(drug concentration) vs. time), as a function of the target fraction bound. This can be derived by recognizing that the total amount of drug decreases with the same rate as the free amount of drug, and by assuming drug-target binding is fast and in equilibrium, as in Equation S12.

Equation S11

$$BF = \frac{[LR]}{[R_{tot}]}$$

Equation S12

$$\boldsymbol{\frac{dAL_{tot}}{dt} = -k_{el} \cdot AL_{tot} \cdot \frac{AC}{AL_{tot}} = -AL_{tot} \cdot \frac{k_{el}}{1 + [R_{tot}] \cdot \frac{1 - BF}{K_D}}}$$

Equation S13

$$\boldsymbol{\lambda_{el}(BF) = \frac{k_{el}}{1 + [R_{tot}] \cdot \frac{1 - BF}{K_D}}}$$

The derivative of the semi-logarithmic drug concentration-time curve, λ_{el}(BF), is important for the duration of target occupancy, as the rate-limiting (i.e. the slowest) step in the decline of target occupancy can be either the drug-target dissociation or the decline of the free drug concentration.

To calculate the derivative for the semi logarithmic target fraction bound vs. time curve as function of the target fraction bound, λ_{TO}(BF), it is important to realise that λ_{el}(BF) and λ_{TO}(BF) are equal to each other if elimination is rate limiting in the decline of target occupancy and if the target fraction bound is low. If target binding is saturated (i.e. BF is high), the decline of the unbound target concentration is higher, as explained above and in box 2, but the decline of the bound target fraction is lower. As an example, if the unbound drug concentration decreases 90% from 500 to 50 nM for a drug with a K_D of 5.0 nM, the corresponding equilibrium bound fraction decreases 7%: from 0.99 to 0.91. If the unbound drug concentration decreases 90% from 50 to 0.50 nM for a drug with a K_D of 5.0 nM, the corresponding equilibrium bound fraction decreases 82%: from 0.50 to 0.091. To calculate the derivative for the semi-loarithmic target fraction bound vs. time curve if elimination is rate-limiting λ_{elTO}(BF) from λ_{el}(BF), the relationship between unbound concentration needs to be taken into account. This relationship can be derived from the law of mass action (box 1) as in Equation S14:

Equation S14

$$\boldsymbol{BF} = \frac{\frac{\boldsymbol{L}}{\boldsymbol{K_D}}}{\boldsymbol{1} + \frac{\boldsymbol{L}}{\boldsymbol{K_D}}}$$

As we intend to calculate λ_{elTO}(BF) from λ_{el}(BF), which are both derivatives on a semi-log scale, we need to obtain the derivative of the logarithm of the BF-unbound concentration relationship, as a function of BF. Thus, we first convert Equation S14 to Equation S15 to obtain the logarithm of BF as function of the logartithm of L/K_D, which results in Equation S16 after taking the derivative with respect to ln(L/K_D).

Equation S15

$$\ln(\boldsymbol{BF}) = \ln\left(\frac{\boldsymbol{e}^{\ln\frac{\boldsymbol{L}}{\boldsymbol{K_D}}}}{\boldsymbol{1} + \boldsymbol{e}^{\ln\frac{\boldsymbol{L}}{\boldsymbol{K_D}}}}\right)$$

Equation S16

$$\frac{\boldsymbol{d}\ln(\boldsymbol{BF})}{\boldsymbol{d}\ln\left(\frac{\boldsymbol{L}}{\boldsymbol{K_D}}\right)} = \frac{\boldsymbol{1}}{\boldsymbol{1} + \boldsymbol{e}^{\ln\frac{\boldsymbol{L}}{\boldsymbol{K_D}}}} = \frac{\boldsymbol{1}}{\boldsymbol{1} + \frac{\boldsymbol{L}}{\boldsymbol{K_D}}}$$

Equation S16 can be rewritten as a function of BF using Equation S14:

Equation S17

$$\frac{\boldsymbol{d}\ln(\boldsymbol{BF})}{\boldsymbol{d}\ln\left(\frac{\boldsymbol{L}}{\boldsymbol{K_D}}\right)} = \frac{\boldsymbol{1}}{\boldsymbol{1} + \frac{\boldsymbol{BF}}{\boldsymbol{1} - \boldsymbol{BF}}} = \boldsymbol{1} - \boldsymbol{BF}$$

Thus, Equation S18 can be used to obtain λ_{elTO}(BF) from λ_{el}(BF):

Equation S18

$$\boldsymbol{\lambda_{elTO}}(\boldsymbol{BF}) = (\boldsymbol{1} - \boldsymbol{BF}) \cdot \boldsymbol{\lambda_{el}}(\boldsymbol{BF}) = \frac{(\boldsymbol{1} - \boldsymbol{BF}) \cdot \boldsymbol{k_{el}}}{\boldsymbol{1} + [\boldsymbol{R_{tot}}] \cdot \frac{\boldsymbol{1} - \boldsymbol{BF}}{\boldsymbol{K_D}}}$$

As said before, the decline of the target fraction bound over time can be determined by two processes: dissociation and elimination. Thus, λ_{elTO}(BF) can be compared directly to k_{off}, which is the slope of the target fraction bound vs. time plot on semi-log scale if drug-target dissociation is rate-limiting in the decline of the target fraction bound.

By selecting the smallest of λ_{elTO}(BF) and k_{off}, Equation S19 can be used to calculate λ_{TO}(BF), the slope of the target fraction bound vs. time plot on semi-log scale. In other words, Equation S19 represents our assumption that the decline of target occupancy is determined by the process that gives rise to the slowest decline of target occupancy.

Equation S19

$$\boldsymbol{\lambda_{TO}}(\boldsymbol{BF}) = \frac{\boldsymbol{1}}{\frac{\boldsymbol{1}}{\boldsymbol{\lambda_{elTO}}(\boldsymbol{BF})} + \frac{\boldsymbol{1}}{\boldsymbol{k_{off}}}}$$

To find for what parameter values elimination is the rate-limiting step in the decline of the target fraction bound, Equation S20 can be solved for the parameter of interest.

Equation S20

$$\frac{\boldsymbol{k_{el}\cdot(1-BF)}}{\boldsymbol{1\ +\ [R_{tot}]\cdot\ \frac{1-BF}{K_D}}} < \boldsymbol{k_{off}}$$

Equation S20 can be solved for k_{on} (by rewriting K_D as k_{off}/ k_{on}, deviding both sides by k_{off} and rewriting the resultant fraction) to find the required value of k_{on} to make elimination the rate-limiting step in the decline of the target fraction bound as in Equation S21.

Equation S21

$$\boldsymbol{k_{on}} > \frac{\boldsymbol{k_{el}\cdot(1-BF)-k_{off}}}{\boldsymbol{[R_{tot}]\cdot(1-BF)}}$$

To obtain from Equation S21 the value of k_{on} for which elimination is rate-limiting in the decline of BF for all possible values of k_{off}, it can be reduced to Equation S22 by substituting k_{off} = 0 into Equation S21. Equation S22 equals Equation S23.

Equation S22

$$\boldsymbol{k_{on}} > \frac{\boldsymbol{k_{el}\cdot(1-BF)}}{\boldsymbol{[R_{tot}]\cdot(1-BF)}}$$

Equation S23

$$\boldsymbol{k_{on}} > \frac{\boldsymbol{k_{el}}}{\boldsymbol{[R_{tot}]}}$$

Equation S20 can also be used to find the value of k_{off} for which elimination becomes the rate-limiting step, for all values of k_{on}, as it can be reduced to Equation S24 by substituting k_{on} = 0 into Equation S20.

Equation S24

$$\boldsymbol{k_{off} < k_{el}\cdot(1-BF)}$$

Equations 23 and 24 can be rewritten to obtain K_{RLon} and K_{RLoff}(BF), which are the corresponding constants that indicate elimination as rate-limiting step if either K_{RLon} or K_{RLoff}(BF) are smaller than 1, as in Equation S25 and S26.

Equation S25

$$\boldsymbol{K_{RLon}} = \frac{\boldsymbol{k_{el}}}{\boldsymbol{k_{on}\cdot[R_{tot}]}}$$

Equation S26

$$\boldsymbol{K_{RLoff}(BF)} = \frac{\boldsymbol{k_{el}\cdot(1-BF)}}{\boldsymbol{k_{off}}}$$

The k_{off} value that marks the transition where the slope of target occupancy for a rate-limiting elimination (λ_{elTO}(BF)) starts to be strongly influenced by the affinity can be derived from Equation S18 and is given by Equation S27, which can be rewritten as Equation S28.

Equation S27

$$\frac{[\boldsymbol{R_{tot}}] \cdot (\mathbf{1} - \boldsymbol{BF})}{\boldsymbol{K_D}} = \mathbf{1}$$

Equation S28

$$\boldsymbol{k_{off}} = [\boldsymbol{R_{tot}}] \cdot (\mathbf{1} - \boldsymbol{BF}) \cdot \boldsymbol{k_{on}}$$

The threshold values as obtained in equations 25, 26 and 28 provide the relation of Figure 3 with all the parameters of model 1 that are not explicitly incorporated in Figure 3: [R_{tot}], BF and k_{el}.

Appendix S3. Approximation and analysis of model 2, related to Figure 4.

Since model 2 is similar to model 1, the prediction of the derivative of the target fraction bound (λ_{TO}(BF)) over time as function of the target fraction bound (BF) for model 2 has similar components as for model 1. Since model 2 has three compartments, three processes can be rate-limiting for the decrease of the target fraction bound; drug-target dissociation, unbound drug distribution and unbound drug elimination. If drug-target dissociation is rate limiting, λ_{TO}(BF) is equal to k_{off}. If the unbound drug distribution from tissue to plasma is rate limiting, the distribution is influenced by drug-target binding in a similar way as the elimination is influenced by drug-target binding (see Equation S13) for model 1. The resultant derivative for the unbound concentration in tissue vs time curve on semi logarithmic scale, as function of the target fraction bound, λ_{out}(BF), is thus given by Equation S29.

Equation S29

$$\boldsymbol{\lambda_{out}(BF) \; = \; \frac{k_{out}}{1 \; + \; [R_{tot}] \cdot \dfrac{1 - BF}{K_D}}}$$

If the unbound drug elimination is rate limiting, the derivative for the unbound concentration in the blood vs time curve on semi logarithmic scale, as function of the target fraction bound, λ_{el}(BF)is influenced again by the fraction of the drug that resides in the central compartment. This fraction is for model 2 not only determined by the drug target binding, but also by the tissue distribution. If passive diffusion is assumed to be the only mechanism of drug distribution, leading to equal equilibrium concentrations in both tissue and plasma, the ratio of the amount of drug in the central compartment (AC) and the total amount of drug in the body (L_{tot}) in equilibrium is given by Equation S30, which can be rewritten as Equation S31.

Equation S30

$$\boldsymbol{\frac{AC}{AL_{tot}} = \frac{V_C}{V_C + V_T + V_T \cdot \dfrac{[LR]}{[T]}}}$$

Equation S31

$$\boldsymbol{\frac{AC}{AL_{tot}} = \frac{V_C}{V_C + V_T \cdot \left(1 + \; [R_{tot}] * \dfrac{1 - BF}{K_D}\right)}}$$

With the ratio of amounts of drug in the central compartment and in the total body as in Equation S31, λ_{el}(BF) is given by Equation S32.

Equation S32

$$\boldsymbol{\lambda_{el}(BF) = \; k_{el} \; \cdot \frac{V_C}{V_C + V_T \cdot \left(1 + \; [R_{tot}] \cdot \dfrac{1 - BF}{K_D}\right)}}$$

As λ_{out}(BF) and λ_{el}(BF) represent the derivatives of the unbound drug concentration vs time profile on semi logarithmic scale, Equation S17 can be used to get the corresponding derivatives of the bound drug concentration vs time profile on semi logarithmic scale, as in equations 33 and 34.

With the values of k_{off}, λ_{outTO}(BF) and λ_{elTO}(BF), the derivative of the target fraction bound vs. time on semi logarithmic scale can be approximated according to Equation S35.

Equation S33

$$\boldsymbol{\lambda_{outTO}(BF) = \; \cdot \frac{k_{out} \; \cdot (1 - BF)}{1 + \; [R_{tot}] \cdot \dfrac{1 - BF}{K_D}}}$$

Equation S34

$$\lambda_{elTO}(BF) = k_{el} \cdot (1 - BF) \cdot \frac{V_C}{V_C + V_T \cdot \left(1 + [R_{tot}] \cdot \frac{1 - BF}{K_D}\right)}$$

Equation S35

$$\lambda_{TO}(BF) = \frac{1}{\frac{1}{\lambda_{elTO}(BF)} + \frac{1}{\lambda_{outTO}(BF)} + \frac{1}{k_{off}}}$$

Equation S35 can be used to identify the rate-limiting step in the decline of the target fraction bound similarly as Equation S19, but the dependency on the parameters is more complex as there are three possible rate-limiting steps. To find the maximal k_{on} value for which drug-target dissociation is the rate limiting step in the decline of the target fraction bound, either λ_{outTO}(BF) or λ_{elTO}(BF) needs to be smaller than k_{off}, as described by Equation S36.

Equation S36

$$\frac{k_{el} \cdot (1 - BF) \cdot V_C}{V_C + V_T \cdot \left(1 + [R_{tot}] \cdot \frac{1 - BF}{K_D}\right)} < k_{off} \text{ or } \frac{k_{out} \cdot (1 - BF)}{1 + [R_{tot}] \cdot \frac{1 - BF}{K_D}} < k_{off}$$

This equation is solved in the same way as Equation S20 to obtain the minimal value of k_{on} for which no value of k_{off} results in dissociation as the rate-limiting step in the decrease of the target fraction bound, which gives Equation S37. Equation S37 comprises two components as well, which can be rewritten to two more simple equations as in Equation S38 and Equation S39 where *min{}* is an operation that selects the minimal value of its input values.

Equation S37

$$k_{on} > \frac{k_{el} \cdot \frac{V_C}{V_T}}{[R_{tot}]} \text{ or } k_{on} > \frac{k_{out}}{[R_{tot}]}$$

Equation S38

$$k_{on} > \frac{k_{minon}}{[R_{tot}]}$$

Equation S39

$$k_{minon} = min\left\{k_{el} \cdot \frac{V_C}{V_T}, k_{out}\right\}$$

Equation S36 can also be used to find the minimal value of k_{off} for which no values of k_{on} result in dissociation as the rate-limiting step in the decline of the target fraction bound in a similar way as Equation S20 by substituting $k_{on} = 0$ into Equation S36. As a result, Equation S40 is obtained. The value of k_{off} for which dissociation is not rate-limiting for all values of k_{on} is given by Equation S41 and S42.

Equation S40

$$\boldsymbol{k_{off} > k_{el} \cdot (1 - BF) \cdot \frac{V_C}{V_C + V_T} \; or \; k_{off} > k_{out} \cdot (1 - BF)}$$

Equation S41

$$\boldsymbol{k_{off} = k_{minoff}}$$

Equation S42

$$\boldsymbol{k_{minoff} = min\left\{k_{el} \cdot (1 - BF) \cdot \frac{V_C}{V_C + V_T}, k_{out} \cdot (1 - BF)\right\}}$$

The k_{off} value that marks the transition where the decline of occupancy for a rate-limiting elimination (λ_{elTO}(BF)) or rate-limiting distribution (λ_{outTO}(BF)) starts to be strongly influenced by the affinity can be derived from Equation S33 and S34 and is given by Equation S43 for λ_{elTO}(BF) and Equation S44 for λ_{outTO}(BF).

Equation S43

$$\boldsymbol{\frac{V_T \cdot [R_{tot}] \cdot (1 - BF)}{K_D} = V_C + V_T}$$

Equation S44

$$\boldsymbol{\frac{[R_{tot}] \cdot (1 - BF)}{K_D} = 1}$$

Equations 43 and 44 can be rewritten as Equation S45 and S46, respectively

Equation S45

$$\boldsymbol{k_{off} = \frac{V_C + V_T}{V_T} \cdot k_{on} \cdot [R_{tot}] \cdot (1 - BF)}$$

Equation S46

$$\boldsymbol{k_{off} = k_{on} \cdot [R_{tot}] \cdot (1 - BF)}$$

S45 and 46 can be summarized by Equation S47.

Equation S47

$$\boldsymbol{k_{off} = \frac{k_{minoff}}{k_{minon}} \cdot k_{on} \cdot [R_{tot}]}$$

Appendix S4. Experimental validation of model 2, related to Figure 4.

Model 2 was fitted to describe digitised literature summary data of [^{3}H]diprenorphine brain and serum concentrations[3] with NONMEM version 7.3, ADVAN6 [4]. The results of our model fit and the obtained literature data are plotted in Figure S1, and the estimated parameter values are given in table S1.

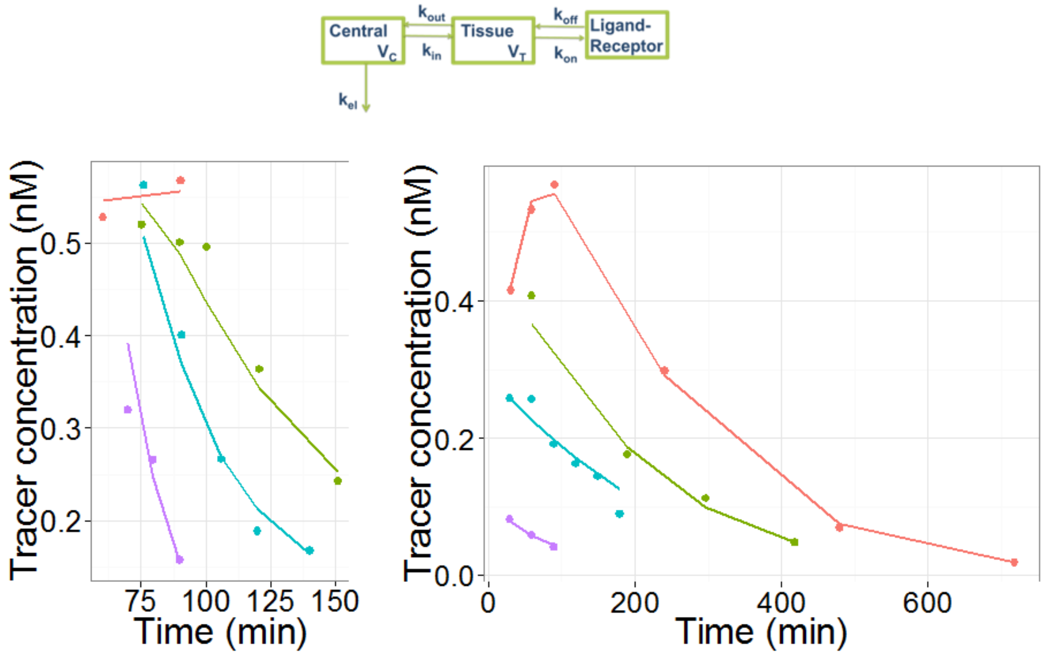

Figure S1. NONMEM fits of model 2 (lines) of [^{3}H] diprenorphine brain radioactivity data after administration of a tracer and unlabeled dose of diprenorphine as obtained from Perry et al. (points) [3]. Unlabeled diprenorphine was administered at t=60 min (left panel) or at t=0 (right panel) at different doses: 0 (red), 24 (green), 50 (blue), 500 (purple) nmol/kg. The tracer dose was 0.10 nmol Top: model structure of model 2, which was used to fit these data.

Table S1. Parameter estimates for [^{3}H]diprenorphine. Proportional errors were 0.6% and 9% with uncertainties of 29% and 19% in plasma and brain, respectively.

Parameter	**Estimate (% CV)**
k_{el} (h^{-1})	0.96 (0.6)
k_{in} (h^{-1})	0.29 (4.1)
k_{out} (h^{-1})	17 (5.5)
k_{on} ($nM^{-1}h^{-1}$)	5.6 (4.7)
k_{off} (h^{-1})	4.0 (3.8)
[R_{tot}] (nM)	20 (4.0)
V_C (L)	2.9 (0.6)
V_T (L)	0.022 (4.0)

Appendix S5. Simulation example of local concentrations determining target occupancy, related to Figure 4.

To simulate the relative impact of k_{on} and k_{off} in a relevant set of parameters, obtained from *in vivo* measurements, we used the parameter values as obtained from fitting model 2 to literature diprenorphine data (see appendix S5). In these simulations, either k_{on} or k_{off} were changed which means that the K_D changed accordingly. To compensate the effect of a changing K_D on the extent of target binding in equilibrium and to obtain relevant target occupancies, the dose was normalized for the K_D. On basis of our approximations, we would expect a similar impact of k_{on} and k_{off} on the duration of target occupancy for these parameter values, which was confirmed by our simulations, see Figure S2. These simulations also demonstrate clearly that only the local (i.e. brain) free drug concentrations are affected by drug-target binding, while the plasma free drug concentrations remain mainly unaffected (Figure S2).

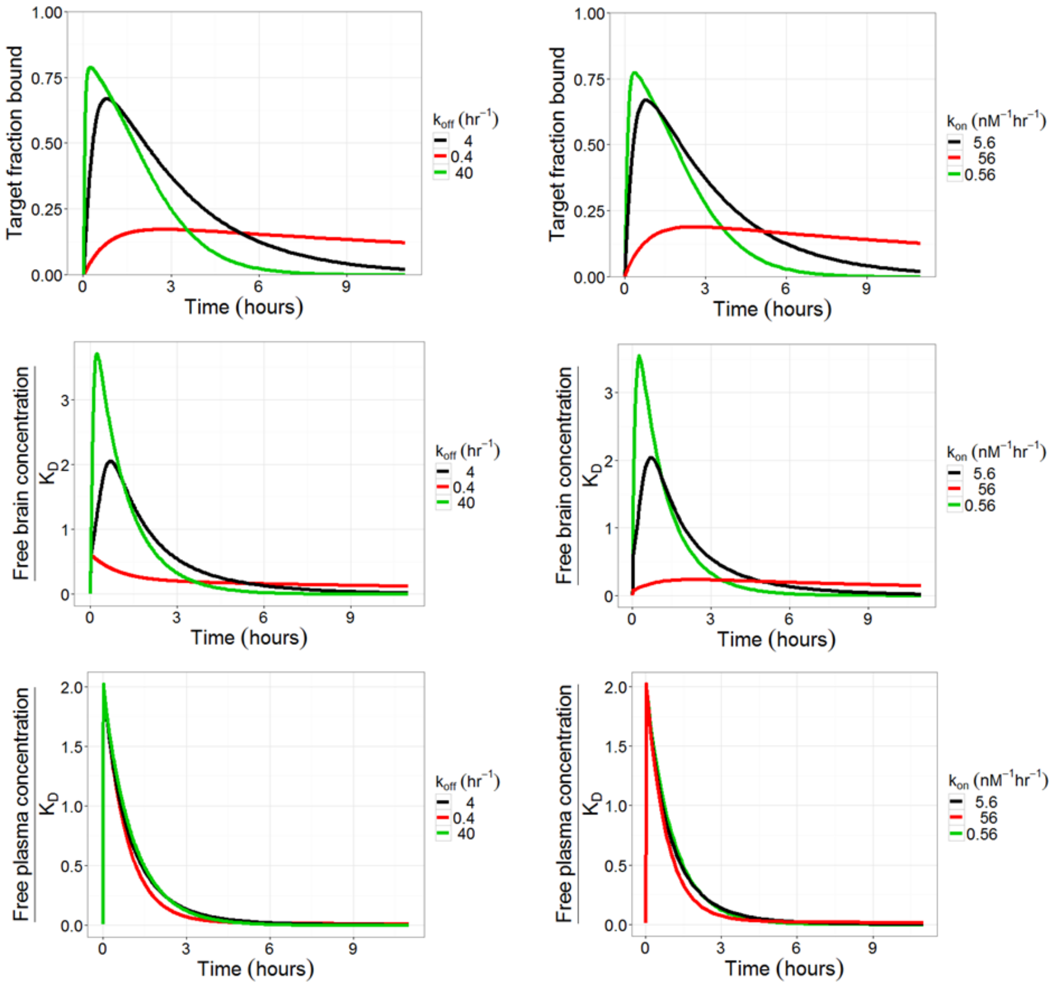

*Figure S2. Simulated target binding of diprenorphine (black lines) and 2 hypothetical drugs (red and green lines) with a 10-fold decrease and increase in k_{off} (left-hand panels) or k_{on} (right-hand panels). The other parameter values remain constant: k_{el} = 0.96, k_{in} = 0.29, k_{out} = 17, V_C = 2.9 L, V_T = 0.022 L. The dose was normalised for the affinity: dose = K_D*5.9 nmol.*

Appendix S6. Accuracy of the approximation of model 1, related to Figure 3.

To identify the accuracy of our approximation of the derivative of the semi logarithmic target occupancy curve, simulation studies (“observed slope”) were compared with the results of the approximation, the “approximated slope” for different target concentrations, dissociation and elimination rate constants. To obtain a normalized measure for the accuracy of our approximation, we used the ratio of the approximated and simulated slope, which equals 1 for a perfect approximation. First, we analysed the accuracy over time for a regular set of pharmacokinetic and binding kinetic parameters, with a low target concentration, see Figure S3. The initial phase of the target occupancy is not predicted accurately for the simulation with a low k_{off} value as the time to reach maximum target occupancy is increased by a low k_{off}, and our approximation is only meant for the decreasing phase of the target occupancy profile. This initial phase is longer for combinations of low k_{off}, k_{on}*[R_{tot}] and k_{el}. This can be seen in Figure S4, where a low elimination rate (0.1/hr) constant leads to inaccurate predictions at 24 hours post dosing for low target concentrations, compared to a high elimination rate constant(1/hr). This inaccuracy is still only present for the low target concentrations if the elimination rate constant is further decreased to an extremely low value (0.001/hr), see Figure S5. Furthermore, our approximation can introduce a underestimation of the derivative of the semi logarithmic target fraction bound vs time curve of up to two fold. This underestimation is especially observed for low target concentrations.

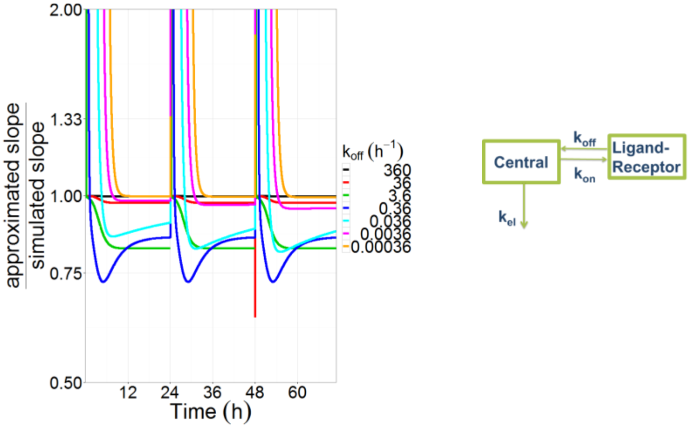

*Figure S3. Simulations with model 1 for the time-dependent accuracy of Equation S19 for various values of k_{off} after repeated dosing. k_{el} = 1/hr, k_{on} = 0.36/(nM*hr), [R_{tot}]= 1nM*

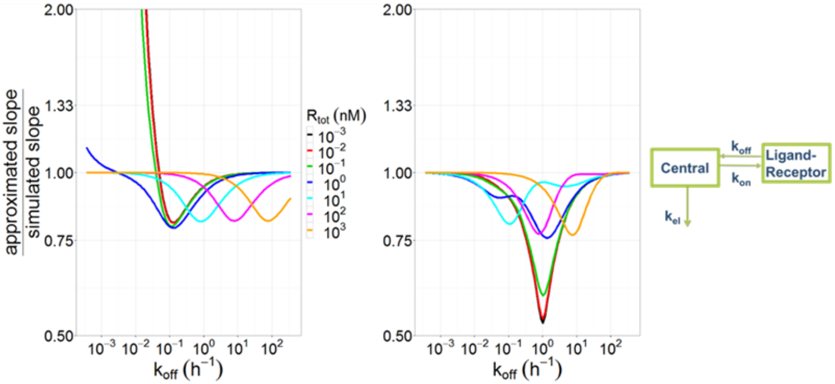

*Figure S4. The accuracy of equation S19 for model 1 at 24 hours post dosing depends on the value of k_{off}, [R_{tot}]and k_{el}. k_{el} = 0.1/hr (left panel) and 1/hr (right panel), k_{on} = 0.36/(nM*hr).*

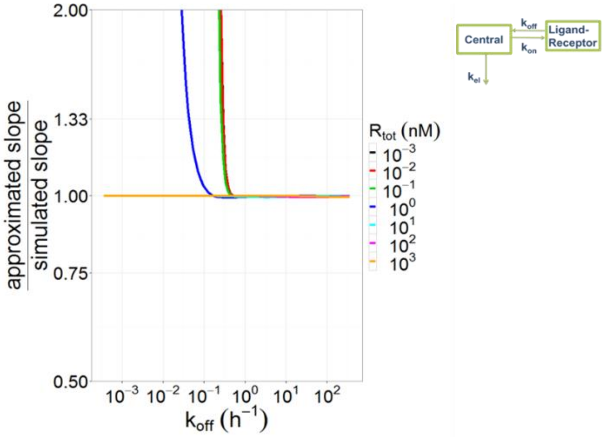

*Figure S5. The accuracy of Equation S19 for model 1 at 24 hours post dosing depends on the value of k_{off}, [R_{tot}] and k_{el}. k_{el} = 0.001/hr, k_{on} = 0.36/(nM*hr).*

Supplemental References

1. R Core Team. R: A language and environment for statistical computing. R Found Stat Comput Vienna, Austria URL http//wwwR-project.org/ 2013;
2. Wagner JG. A new generalized nonlinear pharmacokinetic model and its implications. In: Wagner JG, editor. Biopharmaceutics and Relevant Pharmacokinetics Hamilton, IL; 1971. p. 302–17
3. Perry DC, Mullis KB, Oie S, et al. Opiate antagonist receptor binding in vivo: evidence for a new receptor binding model. Brain Res 1980;199(1):49–61
4. Beal S, Sheiner LB, Boeckmann A, et al. NONMEM 7.3.0 Users Guides. (1989-2013). Icon Development Solutions

Chapter 5. The influence of drug distribution and drug-target binding on target occupancy: The rate-limiting step approximation

W.E.A. de Witte[a], G.Vauquelin[b], P.H. van der Graaf[a,c], E.C.M de Lange[a*]

[a] Division of Pharmacology, Leiden Academic Centre for Drug Research, Leiden University, 2333 CC Leiden, The Netherlands
[b] Department of Molecular and Biochemical Pharmacology, Vrije Universiteit Brussel, Brussels, Belgium
[c] Certara Quantitative Systems Pharmacology, Canterbury Innovation Centre, Canterbury CT2 7FG, United Kingdom

* Correspondence: ecmdelange@lacdr.leidenuniv.nl

Eur J Pharm Sci 2017;epub ahead of print

Abstract

The influence of drug-target binding kinetics on target occupancy can be influenced by drug distribution and diffusion around the target, often referred to as “rebinding” or “diffusion-limited binding”. This gives rise to a decreased decline of the drug-target complex concentration as a result of a locally higher drug concentration that arises around the target, which leads to prolonged target exposure to the drug. This phenomenon has been approximated by the *steady-state approximation*, assuming a steady-state concentration around the target. Recently, a *rate-limiting step approximation* of drug distribution and drug-target binding has been published. However, a comparison between both approaches has not been made so far.

In this study, the *rate-limiting step approximation* has been rewritten into the same mathematical format as the *steady-state approximation* in order to compare the performance of both approaches for the investigation of the influence of drug-target binding kinetics on target occupancy.

While both approximations clearly indicated the importance of k_{on} and high target concentrations, it was shown that the *rate-limiting step approximation* is more accurate than the *steady-state approximation*, especially when dissociation is fast compared to association and distribution out of the binding compartment.

It is therefore concluded that the new *rate-limiting step approximation* is to be preferred for assessing the influence of binding kinetics on local target site concentrations and target occupancy.

Introduction

Although drug-target binding kinetics (the association and dissociation rate constants) are important determinants of the kinetics of drug action [1–4], their role can be influenced by rebinding or diffusion-limited binding. [5–7] The term rebinding has been introduced to describe the result of a (micro-)environment around the target site which is not in instantaneous equilibrium with the plasma or target tissue, and where a concentration difference between target site and plasma or target tissue concentrations can be enhanced by drug-target binding. This local target site concentration can thus induce a delay in both drug-target association and dissociation and should therefore be considered in the analysis and prediction of the relationship between drug-target binding kinetics and target occupancy. This is especially important when *in vitro* values for drug-target binding are used to explain or predict *in vivo* target occupancy and effect.

The local concentration that drives rebinding has been approached historically from different perspectives. The biophysical approach started by describing diffusion around clustered receptors on a spherical or planar surface, which was subsequently discretized by dividing the space surrounding the receptor into the target vicinity and the bulk solution [8,9]. The pharmacological approach started from *in vitro*/*in vivo* observations of target binding that could not be explained by drug-target binding from bulk/tissue concentrations, which was solved by assuming the existence of a micro-compartment surrounding the target [10–12]. The effect compartment model is a less mechanistic and more general approach that is often used in PKPD modelling to explain a delay between drug concentrations and drug effect. In this approach, the drug concentrations in a hypothetical compartment drives the drug effect. The effect compartment model is most often combined with the assumption of fast target binding in the effect compartment (resulting in a “Emax model”) [13–16], although binding kinetics have also been incorporated in the effect compartment model [17,18].

The mathematical models that have been proposed from the different approaches as listed above share a similar compartmental structure and give rise to similar equations. In these models, the compartment in which binding takes place (in this paper referred to as the binding compartment) represents the target site, which is the (micro-) environment that surrounds the target.[5,9,11,17,19,20] An approximation of these compartmental models has been derived previously by assuming quasi steady-state in the binding compartment [19] and has been used since for simulation studies.[5,6] We will refer to this approximation as the *steady-state approximation*. A recent comparison between the *steady-state approximation* of rebinding and the effect compartment model (which has the same mathematical structure as the full two-compartment model from which the *steady-state approximation* is derived) indicated that the *steady-state approximation* is not capturing the behavior of the effect compartment model for fast dissociating ligands.[6]

A recently published approximation for describing target binding from a local (tissue) compartment, assumed that the overall decline of target occupancy is most influenced by the slowest process (the rate-limiting step).[7] We will refer to this approximation as the *rate-limiting step approximation*.

The *rate-limiting step approximation* has not yet been compared with the *steady-state approximation* as described by deLisi (deLisi, 1980). In this study, we use the *rate limiting step approximation* and the *steady-state approximation* of drug distribution and drug-target binding and compare their ability to capture the behavior of the original compartmental model, from which both models are derived.

Methods

To allow comparison of the *steady-state approximation* and the *rate-limiting step approximation* of drug-target binding and drug distribution as proposed here, both approximations should be written in the same mathematical format. In appendix A, the steady-state rebinding formula is rewritten in our format of choice, resulting in equation 1.

$$\mathrm{df}_1 = \frac{k_{out}}{k_{out} + k_{on} \cdot N}$$

In equation 1, df_1 is the delay factor for Model 3 that is multiplied with k_{off} and k_{on} to account for the influence of the local concentration, k_{out} is the first-order distribution or diffusion rate constant from the micro compartment into plasma, k_{on} is the second-order association rate constant and N is the unbound target concentration. In appendix B, our rate-limiting step formula for rebinding is derived from our previously published approximation of target binding, tissue distribution and plasma elimination, resulting in equation 2.

$$\mathrm{df}_2 = \frac{k_{out} \cdot (1 - BF)}{k_{off} + k_{out} \cdot (1 - BF) + k_{on} \cdot N}$$

In Equation 2, *df₂* is the delay factor for Model 4, the additional parameter *BF* is the fraction of target that is bound to the drug and k_{off} is the first-order dissociation rate constant. It should be noted that k_{out} is used to replace the drug distribution rate constant that has been called k_{-} or just k in the biophysical approach, k_{out} in the mechanistic pharmacological approach and k_{eo} in the non-mechanistic PKPD modelling approach.

Our *rate-limiting step approximation* of target binding was intended to approximate the duration of target occupancy after its maximal value and is thus applicable to calculate the delay factor for k_{off}. However, both k_{off} and k_{on} need to be multiplied with the same delay factor to ensure that rebinding does not affect equilibrium target occupancy. Multiplying k_{on} and k_{off} with the same factor is also common practice in previous rebinding studies.[6,9]

To assess the performance of the *rate-limiting step approximation* and to compare this with the recently published evaluation of the *steady-state approximation*, four different mathematical models were compared.

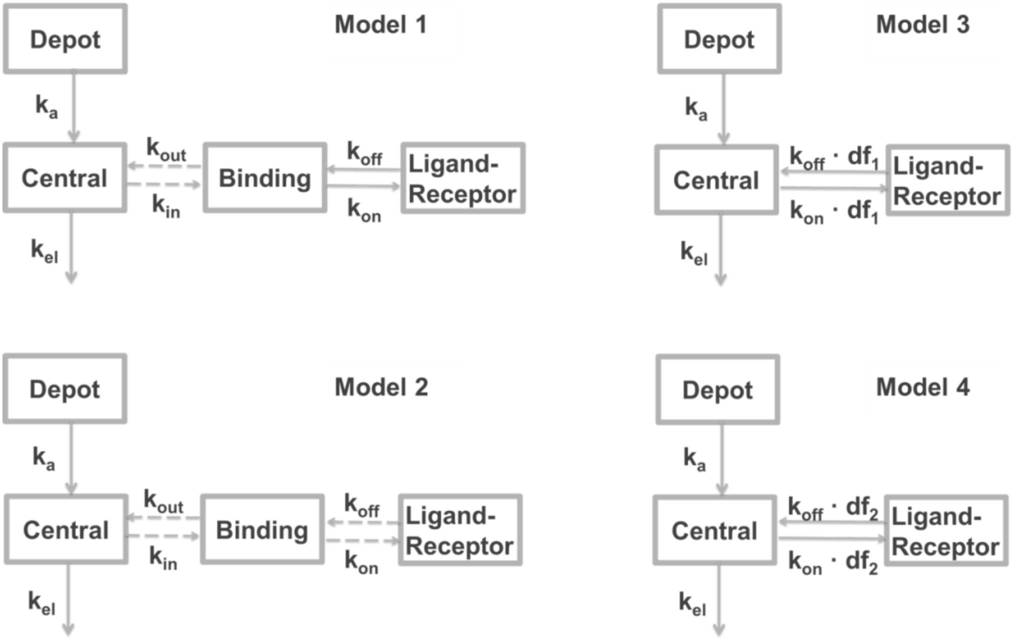

Figure 1. Schematic representation of all model structures that are used for simulations. Model 1 and Model 2 share a similar model structure, as depicted in the left panels. Model 3 and Model 4 share the model structure as depicted in the right panels. Dashed arrows indicate the absence of mass transfer between compartments. The binding compartment in Model 1 and Model 2 is assumed to be very small and the mass transfer between the Central and Binding compartment is ignored. This allows the direct modelling of the concentrations in the Binding compartment and the assumption that k_{out} equals k_{in}.

Model 1 (fig 1) is the full compartmental model that consists of a depot compartment from which absorption into plasma occurs, a central compartment representing the blood, a binding compartment in which binding occurs and a ligand-receptor compartment that represents ligand in the target-bound state. Since rebinding is often hypothesized to occur from a small “micro-compartment”, the mass transfer from plasma to this compartment was assumed to be negligible and was excluded from the model equations. However, since rebinding can result in accumulation or depletion of ligand in the binding compartment, mass transfer was incorporated in the model equations describing the concentration in the binding compartment.

Model 2 (fig 1) is equal to Model 1, except that it does not take into account mass transfer between the binding compartment and the target-bound compartment. This model was required for comparison with the previous publication on the performance of the steady-state rebinding formula in which Model 2 was compared to Model 3 [6].
Model 3 (fig 1) encompasses an absorption and central compartment in the same way as Model 1, but drug-target binding is now driven by the plasma concentrations. Both k_{on} and k_{off} are multiplied by the delay factor, according to the steady-state approximation (equation 1).
Model 4 (fig 1) is the same as model 3, but k_{on} and k_{off} are now multiplied by the delay factor according to the newly derived rate-limiting step approximation (equation 2).
As Model 1 is the original compartmental model that is approximated by Model 3 and Model 4, we can assess the performance of Model 3 and Model 4 by comparing the simulation outcomes of these models to the outcome of Model 1. More similarity to Model 1 means a more accurate approximation. Model 2 is included for comparison with the recent publication of Vauquelin [6], in which Model 2 was compared to Model 3. Also, the parameter values for k_{on}, k_{off}, k_{out}, k_{el} and k_a were set to the same values as for the simulations in the study of Vauquelin [6]. In contrast to the publication of Vauquelin, the delay factor is calculated from equation 1 and 2, where k_{out} is used both for simulation of distribution to the binding compartment and for calculation of the delay factor. The total target concentration was chosen to yield similar results as in the recent publication of Vauquelin.[6]
The differential equations for all models are given in appendix C. The initial concentration in the absorption compartment was $15 \cdot K_D$ in all simulations. The differential equations were solved by using the lsoda solving method in the deSolve package in R, version 3.3.1[21,22].

Results

The only differences between equation 1 and 2 are the addition of k_{off} in the denominator and the correction for the influence of target saturation in the factor (1-*BF*). Since $k_{off} + k_{out} \cdot (1\text{-}BF) + k_{on} \cdot N$ reduces to $k_{out} \cdot (1\text{-}BF) + k_{on} \cdot N$ if $k_{off} << k_{out} \cdot (1\text{-}BF) + k_{on} \cdot N$, equation 1 and 2 only give similar results for the delay factor *df* if k_{off} is relatively small compared to $k_{out} \cdot (1\text{-}BF)$ or $k_{on} \cdot N$. This corresponds to the steady-state approximation that is used to derive equation 1, which assumes that the concentration in the binding compartment adapts quickly to the surrounding concentrations. This requires that the rate at which the drug is distributed out of the binding compartment (determined by $k_{out} \cdot (1\text{-}BF)$ and $k_{on} \cdot N$) is relatively large compared to the rate at which drug is distributed into the binding compartment (determined by k_{off}). It should be noted that the influence of the saturation factor (1-*BF*) only has a major influence for high values of target occupancy.
The performance of our *rate-limiting step approximation* has been visualized in figure 2 and 3. Figure 2A demonstrates that both approximations (steady-state: Model 3 and rate-limiting step: Model 4) produce similar results as Model 1, although Model 4 seems to approximate Model 1 a bit better than Model 3 does. In figure 2B, the difference between Model 3 and Model 4 is clearly demonstrated for the simulations with the lowest values of k_{out} and Model 4 performs much better for the parameter values that were used for figure 2B (i.e. high k_{off}, low affinity and average receptor concentration). The mismatch between Model 3 and Model 1 in figure 2B is not only the result of the high dissociation rate constant: if the target concentration is set to 1 pM instead of 1 nM, a similar mismatch as in figure 2B is observed, as demonstrated in figure 2C. As can be derived from equation 1 and 2, the same effect is observed when the k_{on} value is lowered instead of the target concentration (data not shown). Similarly, the mismatch between Model 3 and Model 1 in figure 2B can be almost completely reversed by a thousand-fold increase in the target concentration or the k_{on} (figure 2D).

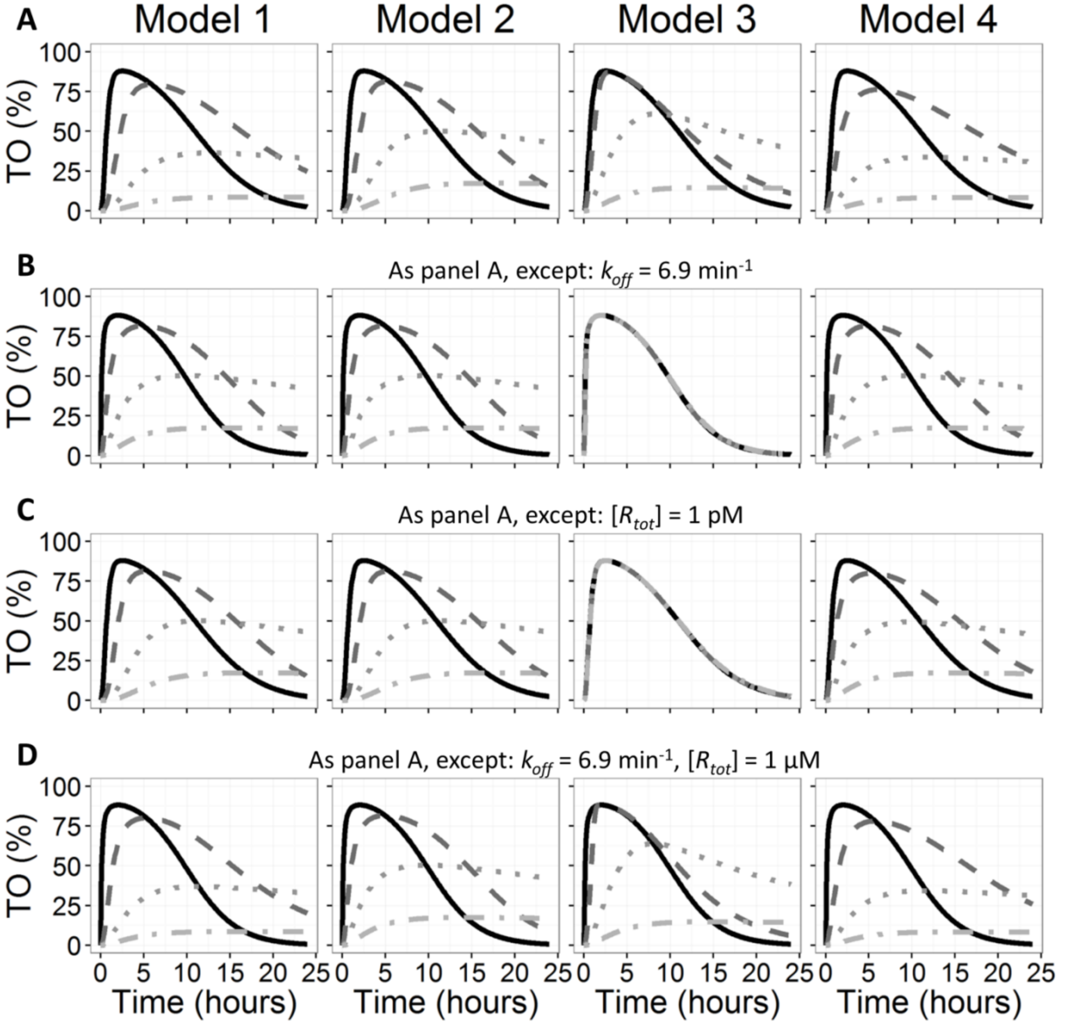

Figure 2. Comparative simulations of target occupancy (TO) over time for the models 1-4. Unless otherwise indicated above the panels, the parameter values remain the same as for panel A: k_{out} = 10 (solid line), 0.0047 (dashed line), 0.0005 (dotted line) or 0.000087 (dash-dotted line) min^{-1}. k_{off} = 0.0069 min^{-1}, k_{on} = $1 \cdot 10^7$ M^{-1} ·min^{-1}, [R_{tot}] = 1 nM, k_a = 0.0115 min^{-1} and k_{el} = 0.00575 min^{-1}. The different grey tones are used for visual distinction of the lines.

The performance of our *rate-limiting step approximation* of rebinding was also investigated in the context in which rebinding formulas are frequently applied: in simulations of the influence of k_{off} on target occupancy. Figure 3A demonstrates that the influence of k_{off} is much better approximated by Model 4 than by Model 3. Although Model 4 also shows a mismatch in the increase rate of target occupancy for the lowest k_{off} values, the duration of target occupancy and the influence of k_{off} thereon resembles Model 1 closely (note the increase in the simulation duration).

For a more typical drug treatment situation, with nanomolar drug-target affinity and target concentration and a moderate delay in distribution from plasma to the binding site, both Model 3 and Model 4 produce comparable results with Model 1, as illustrated in figure 3B. The result of incorporating a correction for target saturation in our *rate-limiting step approximation* is illustrated in figure 3C and 3D: While for figure 3C Model 3 and Model 4 result in similar simulations, an increased dose results in a mismatch between Model 3 and Model 1, which is not observed for Model 4.

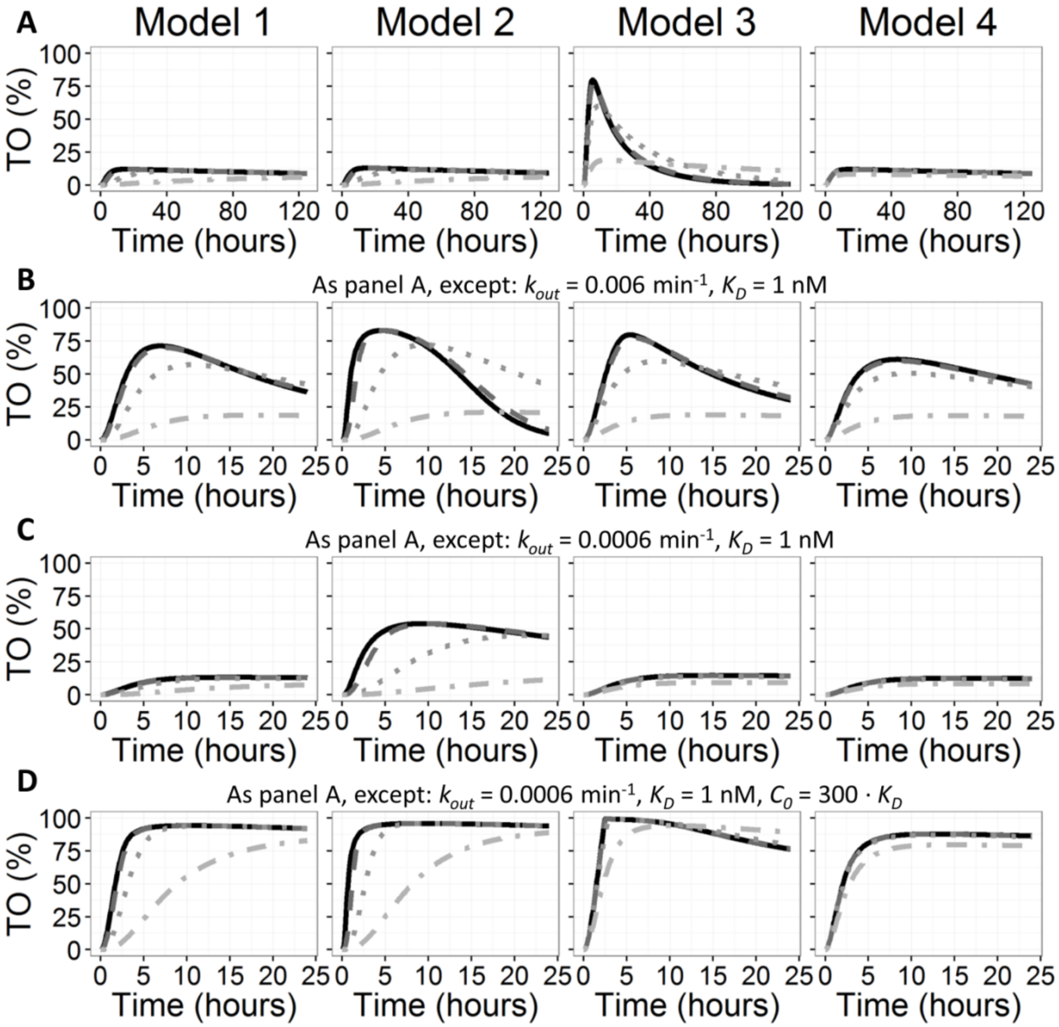

Figure 3. Comparative simulations of target occupancy (TO) over time for the different models. Unless otherwise indicated above the panels, the parameter values remain the same as for panel A: k_{off} = 0.1 (solid line), 0.01 (dashed line), 0.001 (dotted line) or 0.0001 (dash-dotted line) min^{-1}. k_{out} = 0.00006 min^{-1}, $K_D = 1 \cdot 10^{-7}$ M, $[R_{tot}]$ = 10 nM, k_a = 0.0115 min^{-1}, k_{el} = 0.00575 min^{-1} and C_0 (the initial concentration) = $15 \cdot K_D$. The different grey tones are used for visual distinction of the lines.

Discussion

The *rate-limiting step approximation* for drug distribution and drug-target binding that we propose here on basis of our previous publication differs significantly from the *steady-state approximation* when the dissociation rate constant (k_{off}) is high, compared to the distribution rate constant (k_{out}) and the product of the association rate constant and the unbound target concentration ($k_{on} \cdot N$). This difference results in an improved approximation of the original compartmental model (Model 1), from which both approximations are derived.

The improved robustness of the *rate-limiting step approximation* compared to the *steady-state approximation* that we demonstrated here, yields a mathematically reliable simulation of the influence of k_{on} and k_{off} for a wider range of pharmacological situations. Moreover, our new approximation can help to understand the role of the relevant parameters and to interpret the observed influence of rebinding from *in vivo*, *in vitro* or *in silico* data. For example, the *steady-state approximation* results in a decline of target occupancy that is linearly related to k_{off} as long as the drug elimination from plasma is not rate-limiting (equation 1). This is not in line with the intuitive thinking that the distribution/diffusion out of the target vicinity could also be determining the decrease of target occupancy, which would make k_{off} less influential. With our *rate-limiting step approximation*, this intuitive thought is confirmed and the influence of k_{off} on the decline rate of target occupancy decreases when k_{off} becomes relatively large. Also, a correct approximation of binding and distribution is essential if this approximation is used to discriminate between various mechanisms that can explain the duration of drug action or target occupancy.

While the *rate-limiting step approximation* as presented here is a more robust approximation than the *steady-state approximation*, the difference between these two approximations is most significant when the extent of influence of drug distribution is low (since the product of target concentration and k_{on} has to be relatively small). We do not provide a rigorous mathematical proof here that the *rate-limiting step approximation* is better than the *steady-state approximation*. However, the determining equations and the simulations make clear that the *rate-limiting step approximation* can be significantly different and more accurate for conditions with limited rebinding, slow distribution out of the binding compartment and relatively fast dissociation. An approximation of the full rebinding model, such as the two approximations discussed here, is not required for simulations or model fitting of drug distribution and drug-target binding, since the full compartmental model (Model 1) can be used. However, the previous use of the *steady-state approximation* demonstrates the value of *the rate-limiting step approximation* for investigations in the role of drug-target binding kinetics and rebinding.

In conclusion, the rate-limiting step approximation provides an improved approximation of drug-target binding and drug distribution which can be used as an alternative for the existing *steady-state approximation*. Using the *rate-limiting step approximation* as presented here is especially important when dissociation is fast compared to association and distribution out of the binding compartment.

Acknowledgements

This research is part of the K4DD (Kinetics for Drug Discovery) consortium which is supported by the Innovative Medicines Initiative Joint Undertaking (IMI JU) under grant agreement no 115366. The IMI JU is a project supported by the European Union's Seventh Framework Programme (FP7/2007–2013) and the European Federation of Pharmaceutical Industries and Associations (EFPIA).

Appendices

Appendix A: Rewriting the *steady-state approximation* of rebinding

In the *steady-state approximation* of rebinding, both k_{on} and k_{off} are multiplied with the delay factor df_1 that is defined in equation A.1, where all parameters are defined as explained in methods[6]:

$$df_1 = \frac{1}{1 + \frac{k_{on} \cdot N}{k_{out}}}$$

Equation A.1 can be rewritten as equation A.2, which equals equation A.3, which provides equation 1 of the main text.

$$df_1 = \frac{1}{\frac{k_{out} + k_{on} \cdot N}{k_{out}}}$$

$$df_1 = \frac{k_{out}}{k_{out} + k_{on} \cdot N}$$

Appendix B: Derivation of the *rate-limiting step approximation* of target binding and drug distribution.

For the *rate-limiting step approximation*, our previously published approximation of pharmacokinetics and target binding was used as the starting point [7]. From this publication, equation S35 is the most relevant which is given as equation B.1 here. In equation B.1, $\lambda_{TO}(BF)$ is the fractional decrease in target occupancy, as a function of the target fraction bound (*BF*). $\lambda_{elTO}(BF)$ is the value that $\lambda_{TO}(BF)$ would have if the elimination would be rate limiting and thus determining the decrease of target occupancy. $\lambda_{outTO}(BF)$ is the value that $\lambda_{TO}(BF)$ would have if drug distribution from the binding compartment to plasma would be rate limiting. $\lambda_{TO}(BF)$ equals the reverse rate constant $k_{off} \cdot df$ from equation 1 and 2 if there would be no drug in plasma, i.e. if the elimination rate would be extremely high. Such a high elimination rate can be assumed for equation 1 and 2, since these equations are meant for models that simulate plasma concentrations separately. Assuming an extremely high elimination rate constant leads to an extremely high value of $\lambda_{elTO}(BF)$, which reduces equation B.1 to equation B.2.

$$\lambda_{TO}(BF) = \frac{1}{\frac{1}{\lambda_{elTO}(BF)} + \frac{1}{\lambda_{outTO}(BF)} + \frac{1}{k_{off}}} \tag{B.1}$$

$$\lambda_{TO}(BF) = \frac{1}{\frac{1}{\lambda_{outTO}(BF)} + \frac{1}{k_{off}}} \tag{B.2}$$

Since $\lambda_{outTO}(BF)$ is given by equation B.3 according to our previous publication (equation S33), equation B.2 equals equation B.4, which can be rewritten as equation B.5.

$$\lambda_{outTO}(BF) = \frac{k_{out} \cdot (1-BF)}{1 + [R_{tot}] \cdot \frac{1-BF}{K_D}} \tag{B.3}$$

$$\lambda_{TO}(BF) = \frac{1}{\frac{1}{\frac{k_{out} \cdot (1-BF)}{1 + [R_{tot}] \cdot \frac{1-BF}{K_D}}} + \frac{1}{k_{off}}} \tag{B.4}$$

$$\lambda_{TO}(BF) = \frac{1}{\frac{1 + [R_{tot}] \cdot \frac{1-BF}{K_D}}{k_{out} \cdot (1-BF)} + \frac{1}{k_{off}}} \tag{B.5}$$

Equation B.5 can be rewritten as equation B.6 by realizing that K_D equals the ratio of k_{off} to k_{on} and by multiplying each fraction by unity in such a way that the denominators become equal and the two fractions can be summed as in equation B.7. Equation B.7 equals equation B.8 and since $[R_{tot}] \cdot (1-BF)$ is equal to the unbound target concentration, equation B.8 provides equation 2.

$$\lambda_{TO}(BF) = \frac{1}{\frac{k_{off} + [R_{tot}] \cdot \frac{1-BF}{\left(\frac{k_{off}}{k_{on}}\right)} \cdot k_{off}}{k_{out} \cdot (1-BF) \cdot k_{off}} + \frac{k_{out} \cdot (1-BF)}{k_{out} \cdot (1-BF) \cdot k_{off}}} \tag{B.6}$$

$$\lambda_{TO}(BF) = \frac{1}{\frac{k_{off} + [R_{tot}] \cdot (1-BF) \cdot k_{on} + k_{out} \cdot (1-BF)}{k_{out} \cdot (1-BF) \cdot k_{off}}} \tag{B.7}$$

$$\lambda_{TO}(BF) = \frac{k_{out} \cdot (1-BF) \cdot k_{off}}{k_{off} + [R_{tot}] \cdot (1-BF) \cdot k_{on} + k_{out} \cdot (1-BF)} \tag{B.8}$$

Appendix C: Differential equations of the four different models as used for the simulations.

The concentrations in the depot and the central compartment were modeled in the same way for all four models according to equation C.1 and C.2, respectively. In these equations, [*DEP*] is the drug concentration in the depot compartment, [*C*] is the drug concentration in the central compartment, k_a is the first-order absorption rate constant and k_{el} is the first-order elimination rate constant.

$$\frac{d[DEP]}{dt} = -k_a \cdot [DEP] \tag{C.1}$$

$$\frac{d[C]}{dt} = k_a \cdot [DEP] - k_{el} \cdot [C] \tag{C.2}$$

The concentration in the binding compartment is only explicitly simulated in Model 1 and Model 2 according to equations C.3 and C.4, respectively. Here, [*B*] denotes the drug concentration in the binding compartment, [*N*] denotes the unbound target concentration (which is calculated by assuming the total target concentration is constant), [*LR*] denotes the drug that is bound to the target, k_{out} is the first-order distribution constant between the binding compartment and plasma, k_{on} is the second-order association rate constant and k_{off} is the first-order dissociation rate constant.

Model 1:
$$\frac{d[B]}{dt} = k_{out} \cdot ([C] - [B]) - k_{on} \cdot [B] \cdot [N] + k_{off} \cdot [LR] \tag{C.3}$$

Model 2:
$$\frac{d[B]}{dt} = k_{out} \cdot ([C] - [B]) \tag{C.4}$$

The concentration of the target-bound drug is calculated identically for Model 1 and Model 2 according to equation C.5:

Model 1, Model 2:
$$\frac{d[LR]}{dt} = k_{on} \cdot [B] \cdot [N] - k_{off} \cdot [LR] \tag{C.5}$$

For Model 3 and Model 4 the target bound drug is calculated according to equation C.6 and C.7, where *BF* denotes the fraction of the target that is bound to the drug.

Model 3:
$$\frac{d[LR]}{dt} = \left(k_{on} \cdot [C] \cdot [N] - k_{off} \cdot [LR]\right) \cdot \frac{k_{out}}{k_{out} + k_{on} \cdot N} \tag{C.6}$$

Model 4:
$$\frac{d[LR]}{dt} = \left(k_{on} \cdot [C] \cdot [N] - k_{off} \cdot [LR]\right) \cdot \frac{k_{out} \cdot (1-BF)}{k_{off} + k_{out} \cdot (1-BF) + k_{on} \cdot N} \tag{C.7}$$

References

1. Johnson M, Kozielska M, Pilla Reddy V, et al. Mechanism-based pharmacokinetic-pharmacodynamic modeling of the dopamine D2 receptor occupancy of olanzapine in rats. Pharm Res 2011;28(10):2490–504
2. Copeland RA, Pompliano DL, Meek TD. Drug-target residence time and its implications for lead optimization. Nat Rev Drug Discov 2006;5(9):730–9
3. Yassen A, Olofsen E, Kan J, et al. Animal-to-human extrapolation of the pharmacokinetic and pharmacodynamic properties of buprenorphine. Clin Pharmacokinet 2007;46(5):433–47
4. Dahl G, Akerud T. Pharmacokinetics and the drug-target residence time concept. Drug Discov Today 2013;18(15–16):697–707
5. Vauquelin G, Charlton SJ. Long-lasting target binding and rebinding as mechanisms to prolong in vivo drug action. Br J Pharmacol 2010;161(3):488–508
6. Vauquelin G. Impact of target binding kinetics on in vivo drug efficacy: k off , k on and rebinding. Br J Pharmacol 2016;173(15):2319–34
7. de Witte WEA, Danhof M, van der Graaf PH, et al. In vivo Target Residence Time and Kinetic Selectivity: The Association Rate Constant as Determinant. Trends Pharmacol Sci 2016;37(10):831–42
8. Goldstein B, Dembo M. Approximating the effects of diffusion on reversible reactions at the cell surface: ligand-receptor kinetics. Biophys J 1995;68(4):1222–30
9. Coombs D, Goldstein B. Effects of the geometry of the immunological synapse on the delivery of effector molecules. Biophys J 2004;87(4):2215–20
10. De Meyts P. Cooperative properties of hormone receptors in cell membranes. J Supramol Struct 1976;4(2):241–58
11. Perry DC, Mullis KB, Oie S, et al. Opiate antagonist receptor binding in vivo: evidence for a new receptor binding model. Brain Res 1980;199(1):49–61
12. Frost JJ, Wagner HN. Kinetics of Binding to Opiate Receptors In Vivo Predicted From In Vitro Parameters. Brain Res 1984;305(1):1–11
13. Cleton A, de Greef HJ, Edelbroek PM, et al. Application of a combined “effect compartment/indirect response model” to the central nervous system effects of tiagabine in the rat. J Pharmacokinet Biopharm 1999;27(3):301–23
14. Groenendaal D, Freijer J, Rosier A, et al. Pharmacokinetic/pharmacodynamic modelling of the EEG effects of opioids: the role of complex biophase distribution kinetics. Eur J Pharm Sci 2008;34(2–3):149–63
15. Francheteau P, Steimer JL, Merdjan H, et al. A mathematical model for dynamics of cardiovascular drug action: Application to intravenous dihydropyridines in healthy volunteers. J Pharmacokinet Biopharm 1993;21(5):489–514
16. Nolan ER, Feng MR, Koup JR, et al. A novel predictive pharmacokinetic/pharmacodynamic model of repolarization prolongation derived from the effects of terfenadine, cisapride and E-4031 in the conscious chronic av node--ablated, His bundle-paced dog. J Pharmacol Toxicol Methods 2006;53(1):1–10
17. Yassen A, Olofsen E, Dahan A, et al. Pharmacokinetic-Pharmacodynamic Modeling of the Antinociceptive Effect of Buprenorphine and Fentanyl in Rats : Role of Receptor Equilibration Kinetics. J Pharmacol Exp Ther 2005;313(3):1136–49
18. Äbelö A, Andersson M, Holmberg AA, et al. Application of a combined effect compartment and binding model for gastric acid inhibition of AR-HO47108: A potassium competitive acid blocker, and its active metabolite AR-HO47116 in the dog. Eur J Pharm Sci 2006;29(2):91–101
19. DeLisi C. The biophysics of ligand-receptor interactions. Quaterly Rev Biophys 1980;13(2):201–30
20. Vauquelin G. Rebinding : or why drugs may act longer in vivo than expected from their in vitro target residence time. Expert Opin Drug Discov 2010;5(10):927–41
21. R Core Team. R: A language and environment for statistical computing. R Found Stat Comput Vienna, Austria URL http//wwwR-project.org/ 2013;
22. Soetaert K, Petzoldt T, Setzer RW. Solving Differential Equations in R: Package deSolve. J Stat Softw 2010;33(9):1–25

Chapter 6. Target and tissue selectivity prediction by integrated mechanistic pharmacokinetic-target binding and quantitative structure activity modelling

Anna H.C. Vlot*[a], Wilhelmus E. A. de Witte* [a], Meindert Danhof [a], Piet H. van der Graaf [a,b], Gerard J.P. van Westen [c], Elizabeth C. M. de Lange@ [a].

[a] Division of Pharmacology, Leiden Academic Centre for Drug Research, Leiden University, Einsteinweg 55, 2333 CC, Leiden, The Netherlands.
[b] Certara Quantitative Systems Pharmacology, Canterbury Innovation Centre, Canterbury CT2 7FG, United Kingdom
[c] Division of Medicinal Chemistry, Leiden Academic Centre for Drug Research, Leiden University, Einsteinweg 55, 2333 CC, Leiden, The Netherlands.

*These authors contributed equally

@ Correspondence: ecmdelange@lacdr.leidenuniv.nl

Manuscript under revision for the British Journal of Pharmacology

Abstract

Selectivity is an important attribute of effective and safe drugs, and prediction of *in vivo* target and tissue selectivity would likely improve drug development success rates. However, a lack of understanding of the underlying (pharmacological) mechanisms and availability of directly applicable predictive methods complicates the prediction of selectivity. We explore the value of combining physiologically based pharmacokinetic (PBPK) modelling with quantitative structure-activity relationship (QSAR) modelling to predict the influence of the target dissociation constant (K_D) and the target dissociation rate constant on target and tissue selectivity. The K_D values of CB1 ligands in the ChEMBL database are predicted by QSAR random forest (RF) modelling for the CB1 receptor and known off-targets (TRPV1, mGlu5, 5-HT1a). Of these CB1 ligands, Rimonabant, an inverse agonist at the CB1 receptor, CP-55940, a selective agonist for the CB1 and CB2 receptor and Δ^8-tetrahydrocanabinol, one of the active ingredients of cannabis, were selected for simulations of target occupancy for CB1, TRPV1, mGlu5 and 5-HT1a in three brain regions, to illustrate the principles of the combined PBPK-QSAR modelling. Our combined PBPK and target binding modelling demonstrated that the optimal values of the K_D and k_{off} for target and tissue selectivity were dependent on target concentration and tissue distribution kinetics. Interestingly, in many cases the optimal K_D value is not the lowest K_D value, suggesting that optimisation towards high drug-target affinity can decrease the benefit-risk ratio. The presented integrative structure-pharmacokinetic-pharmacodynamic modelling provides an improved understanding of tissue and target selectivity.

Introduction

Selectivity is an important attribute of successful drugs since highly selective compounds are less likely to mediate side-effects.[1] On the other hand, targeting multiple targets simultaneously is increasingly considered as a valuable option to exert sufficient effect on a complex biological system.[2,3] Regardless the desired degree of selectivity, understanding and prediction of the target binding to multiple targets in multiple tissues is essential for the optimisation of pharmacotherapy. In this article, we differentiate between two types of selectivity: target selectivity and tissue selectivity. Target selectivity is defined as a difference in target binding to different receptors and tissue selectivity is defined as a difference in target binding to the same target in different tissues. Additionally, a distinction is made between equilibrium selectivity and kinetic selectivity. Equilibrium selectivity refers to differential target binding while target binding is in equilibrium with the free drug concentration around the target. This equilibrium binding is described for single step target binding without target turnover according to Equation 1, in which K_D is the dissociation constant, [L] is the unbound drug concentration, [R] is the unbound target concentration, [LR] is the bound drug-target complex concentration, k_{off} is the first order target dissociation rate constant and k_{on} is the second order target association rate constant.

$$K_D = \frac{[L]\cdot[R]}{[LR]} = \frac{k_{off}}{k_{on}} \quad (1)$$

Equilibrium target selectivity is thus driven by differential K_D values for the different targets. Kinetic selectivity, however, refers to a difference of the duration of target occupancy, which can be achieved by differential k_{off} values.[4] Differential k_{off} values do not always result in a differential duration of target occupancy *in vivo* since the plasma and local pharmacokinetics can also be rate-limiting for the duration of target occupancy.[5,6] As kinetic selectivity has previously been equated with differential k_{off} values[7], we will refer to differential k_{off} values as *in vitro* kinetic selectivity, while we will refer to an *in vivo* difference in the duration of target occupancy due to slow dissociation as *in vivo* kinetic selectivity.

A previous study that analysed a minimal mechanistic model for drug elimination, tissue distribution and target binding showed that an increase in drug-target affinity decreases the chance of observing *in vivo* kinetic selectivity, especially for slow tissue distribution and a high target concentration.[6] On that basis, it is expected that the optimal K_D for target and tissue selectivity is dependent on the target concentration, tissue distribution kinetics and binding kinetics. This contrasts with the current practice of drug discovery and development which often aims at a minimal value for the K_D and k_{off} and a maximal ratio to the off-target K_D and k_{off} value if selectivity is concerned.

The minimal mechanistic model that was analysed in the study of de Witte et al.[6] did not consider i) the effects of slow distribution of a drug into tissues where no target binding takes place nor ii) the limiting role that blood flow can have on tissue distribution. In order to capture the influence of these pharmacokinetic mechanisms, physiologically based pharmacokinetic (PBPK) models can be used. In these models, a distinction is made between system-specific properties and drug-specific properties. In this type of analysis, the values of system-specific parameters such as blood flows and volumes for each organ are based on the physiological literature data, while the values of drug-specific parameters, such as partition coefficients and protein binding are often based on *in vitro* data or on Quantitative Structure Activity Relationships (QSARs).[8] As such, these models allow the prediction of plasma and tissue unbound drug concentrations. The influence of drug-target binding on free drug concentrations has been described frequently with target-mediated drug disposition (TMDD) models. [9] The combination of PBPK and TMDD modelling has been reported in the literature previously but is not generally used in selectivity optimisation. [10–13] To obtain the drug-specific properties that determine the values of the partitioning parameters in PBPK models either experimental data for each individual drug or quantitative structure-activity relationships (QSAR) are required. These QSARs enable the prediction of partitioning parameters from the molecular structure. While these QSARs are often used in PBPK modelling to predict non-specific tissue distribution parameters, the prediction of specific target binding parameters is currently not incorporated in PBPK modelling, based on the assumption that the amount of drug bound to its biological target is negligible relative to the total amount of drug in the body. [14–17]

QSAR models may be either regression or classification models which predict a response variable from a set of predictor values. In regression models, these predictor values are related to a continuous response variable (e.g. a K_D value), while in classification models the predictor values relate to a categorical variable (e.g. labelled “active” or “inactive”). The predictor values represent the molecular structure and molecular properties, and the response variable is an activity value, such as the K_D in the case of affinity. Machine learning methods such as support vector machines (SVMs), decision trees such as random forests (RFs) and deep neural networks (DNNs) are generally used to obtain a predictive learning model.[18–20] The training of these models is based on prior data, which means that their performance is greatly dependent on data quality and availability. A suitable database for bioactivity data is available in the ChEMBL, which can be used to obtain predictive QSAR models. [21,22]

Integration of drug-target binding prediction and pharmacokinetic modelling allows for the prediction of the selectivity profile for a given ligand directly from its molecular structure. As such, this modelling approach may provide information on a ligand’s efficacy and safety *in vivo* during the very early stage of drug development. This is especially relevant in systems that contain off-targets or targets that are also expressed in organs were no drug effect is desired. An example of the latter system is the cannabinoid system, of which the cannabinoid receptor CB1 is a major component. The CB1 receptor is widely expressed throughout the body but mainly found in the brain where it mediates a broad range of effects in health and disease. [23,24] Many off-targets have been identified for CB1 ligands, including the vanilloid receptor TRPV1, the metabotropic glutamate receptor mGlu5, and the serotonin receptor 5-HT1a. [25,26] Activity at these receptors, predominantly in the brain, may amplify or counteract effects at the CB1 receptor. TRPV1, for example, has been suggested to have an effect opposite of that of CB1 in anxiety and depression, which are common side effects observed for CB1 antagonists, and mGlu5 is a major player in the GABA-system, which is the target system for CB1 mediated therapies in Parkinson’s disease. [27–29] The mechanisms underlying functional *in vivo* selectivity are diverse and complex, but computational elucidation of off-target affinities and their integration in combined PBPK-TMDD modelling could help to identify safety concerns early in drug discovery and development, which would improve decision making in (pre)clinical drug development.

This article describes an approach towards the development of an integrative predictive modelling for drug selectivity. Firstly, the main determinants of *in vivo* equilibrium and kinetic selectivity, are identified by minimal PBPK-TMDD modelling and simulation. Secondly, the development and validation of a Random Forest based QSAR (QSAR-RF) model for the prediction of K_D values is described. Lastly, an example of the use of predicted K_D values in PBPK-TMDD modelling is provided for the combined *in vivo* target and tissue selectivity of Rimonabant, a prototype antagonist at the CB1 receptor.

Materials and Methods

1 Software

All simulations were performed in RStudio Version 1.0.136 coupled to R version 3.4.0. [30,31] Physicochemical property prediction and QSAR modelling were performed in Pipeline Pilot version 2016. [32]

2 Pharmacological Models

Three PBPK-TMDD models were developed: a minimal PBPK-TMDD model for simulation of target selectivity (**Model I, Figure 1**), a minimal PBPK-TMDD model for simulation of tissue selectivity (**Model II, Figure 2**) , and an integrated brain PBPK-TMDD model for simulation of selectivity across brain regions and between targets using K_D values predicted in a QSAR-RF (**3.3 QSAR**) (**Model III, Figure 3**).

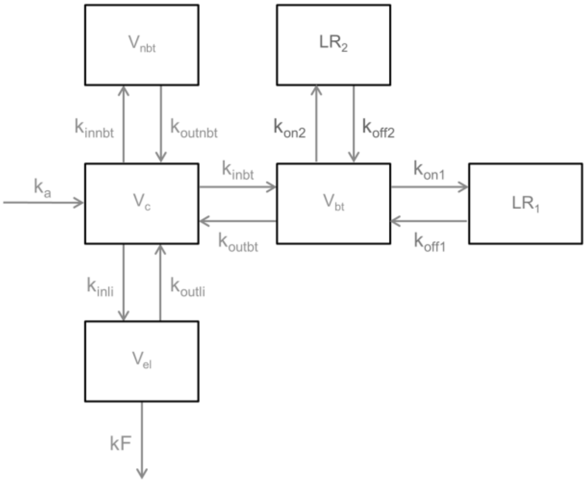

V_{nbt}
LR_2
k_{innbt}
k_{outnbt}
k_{on2}
k_{off2}
k_a
V_c
k_{inbt}
V_{bt}
k_{on1}
LR_1
k_{outbt}
k_{off1}
k_{inli}
k_{outli}
V_{el}
kF

Figure 1. Schematic overview of the minimal target selectivity model (Model I). k_a = rate of absorption (h^{-1}), k_{in} = inwards distribution rate (h^{-1}), k_{out} = outwards distribution rate, k_{on} = association rate ($nM^{-1}h^{-1}$), k_{off} = dissociation rate (h^{-1}), kF = forward rate of elimination constant (h^{-1}), LR = ligand-receptor complex, V = tissue volume (L), nbt = non-binding tissue, c = central compartment, bt = binding tissue, el = eliminating tissue.

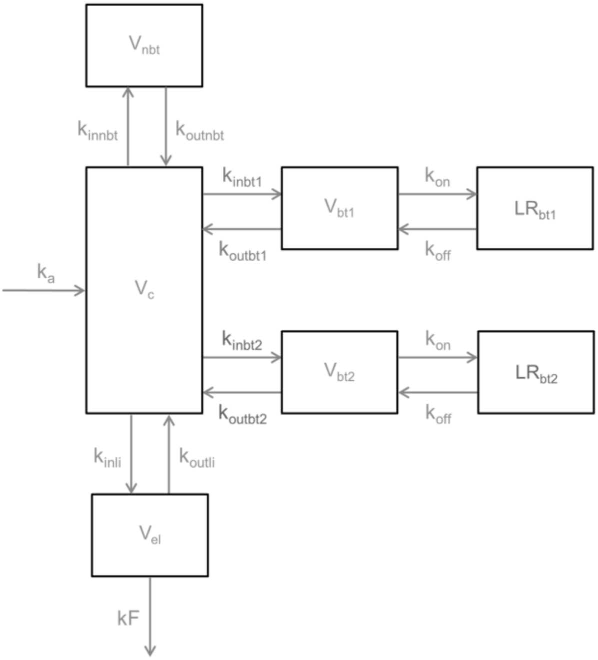

V_{nbt}
k_{innbt}
k_{outnbt}
k_{inbt1}
k_{on}
V_{bt1}
LR_{bt1}
k_{outbt1}
k_{off}
k_a
V_c
k_{inbt2}
k_{on}
V_{bt2}
LR_{bt2}
k_{outbt2}
k_{off}
k_{inli}
k_{outli}
V_{el}
kF

Figure 2. Schematic overview of the minimal tissue selectivity model (Model II). k_a = rate of absorption (h^{-1}), k_{in} = inwards distribution rate (h^{-1}), k_{out} = outwards distribution rate, k_{on} = association rate ($nM^{-1}h^{-1}$), k_{off} = dissociation rate (h^{-1}), kF = forward rate of elimination constant (h^{-1}), LR = ligand-receptor complex, V = tissue volume (L), nbt = non-binding tissue, c = central compartment, bt = binding tissue, el = elimination tissue.

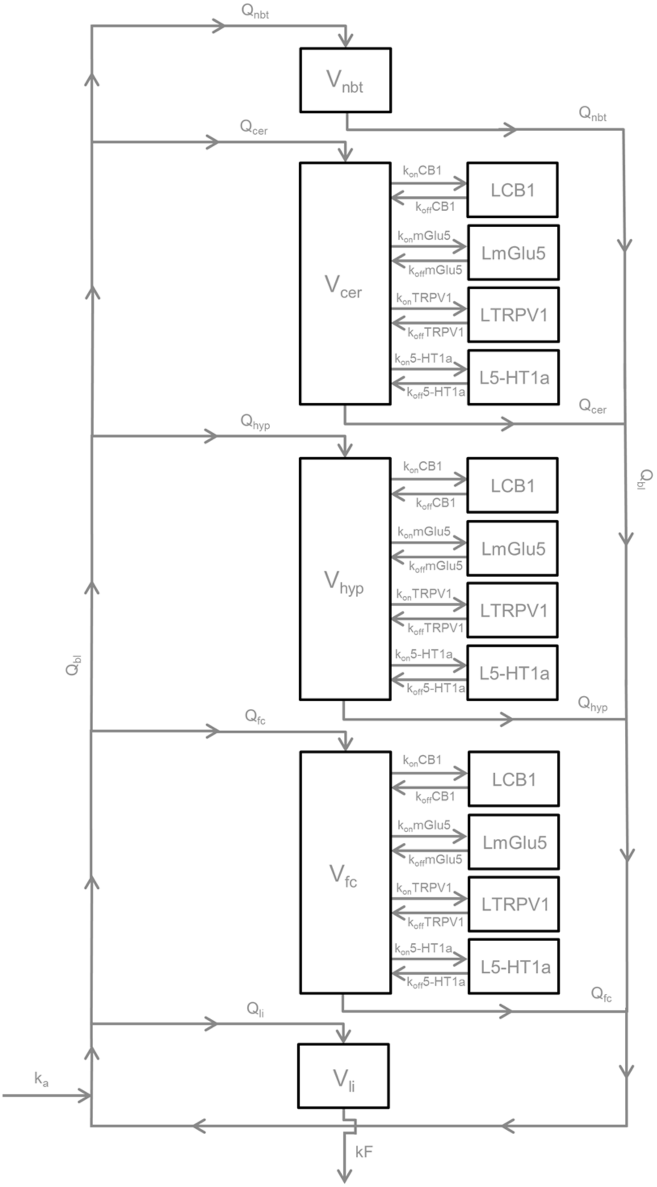
Q_{nbt}
V_{nbt}
Q_{nbt}
Q_{cer}
V_{cer}
k_{on}CB1
k_{off}CB1
LCB1
k_{on}mGlu5
k_{off}mGlu5
LmGlu5
k_{on}TRPV1
k_{off}TRPV1
LTRPV1
k_{on}5-HT1a
k_{off}5-HT1a
L5-HT1a
Q_{cer}
Q_{hyp}
Q_{bl}
V_{hyp}
k_{on}CB1
k_{off}CB1
LCB1
k_{on}mGlu5
k_{off}mGlu5
LmGlu5
k_{on}TRPV1
k_{off}TRPV1
LTRPV1
k_{on}5-HT1a
k_{off}5-HT1a
L5-HT1a
Q_{bl}
Q_{hyp}
Q_{fc}
V_{fc}
k_{on}CB1
k_{off}CB1
LCB1
k_{on}mGlu5
k_{off}mGlu5
LmGlu5
k_{on}TRPV1
k_{off}TRPV1
LTRPV1
k_{on}5-HT1a
k_{off}5-HT1a
L5-HT1a
Q_{fc}
Q_{li}
k_a
V_{li}
kF

Figure 3. Schematic model of the brain PBPK-TMDD model. k_a = rate of absorption (h^{-1}), Q = blood flow (L/h), k_{on} = association rate ($nM^{-1}h^{-1}$), k_{off} = dissociation rate (h^{-1}), kF = forward rate of elimination constant (h^{-1}), LR (with R = CB1, mGlu5, TRPV1 or 5-HT1a) = ligand-receptor complex, V = tissue volume (L), nbt = non-binding tissue, c = central compartment, bt = binding tissue, li = liver, cer = cerebellum, hyp = hypothalamus, fc = frontal cortex.

2.1 Parameters

2.1.1 Model I and II

All physiological values of the system-specific parameters were obtained from literature.[33–38] The heart was used as a reference organ for the determination of distribution into and out of the binding tissue. An overview of all model parameters is supplied in Supplemental 1.

2.1.2 Model III

All physiological values of the system-specific parameters were obtained from literature.[33–38] Target site distribution in the brain was characterized by the average effective flow through the target site as obtained from literature values from brain extra-cellular fluid flow to the cerebrospinal fluid as estimated for 9 drugs.[39] The conversion of these values as well as an overview of all parameters are supplied in Supplemental 1.

Receptor densities of CB1, mGlu5, TRPV1, and 5-HT1a in the cerebellum, hypothalamus, and frontal cortex were obtained from the literature for all four receptors, except the receptor concentration of mGlu5 in hypothalamus and 5-HT1a in cerebellum, which were not reported in the literature. [40–44] The mGlu5 receptor concentration in the hypothalamus was filled in with the averages of the other brain regions since differences between brain regions for the other receptors did not differ drastically. The 5-HT1a receptor concentration in cerebellum was set to the low value of 0.01 nM as it was reported to be unidentifiable.[43] Receptor concentrations in rats and humans were used interchangeably since no complete set of receptor densities could be obtained for either rats or humans. Values found in literature have shown to differ no more than ten-fold. [41,45] TRPV1 concentrations were given in ng/mg lysate and converted to pmol/mg protein by linear conversion. For this, the receptor concentration in ng/mg lysate and fmol/mg protein in the hypothalamus as reported in the literature was used. [42,46] The receptor density in the hypothalamus in fmol/mg was divided by the receptor density in ng/mg lysate and the resulting coefficient was used to transform the receptor density in ng/mg lysate of the cerebellum, hypothalamus and frontal cortex to the corresponding receptor density in fmol/mg. CB1 and TRPV1 concentrations in pmol/mg, were then converted to nM using a conservative (i.e. the lowest published) estimate of protein concentration in wet tissue of 100 mg/mL from literature. [47–49] An overview of the target concentrations is presented in

Table 1. An overview of the conversions and all target concentrations can be found in Supplemental 2.

Table 1. Receptor concentrations for the brain PBPK-TMDD model

	$R_{tot,cer}$ (nM)	$R_{tot,hyp}$ (nM)	$R_{tot,fc}$ (nM)
CB1	527	248	529
mGlu5	5.1	16	25
TRPV1	19	13	12
5-HT1a	0.01	2.37	1.7

* cer = cerebellum, hyp = hypothalamus, fc = frontal cortex

Tissue-blood partition coefficients were calculated according to Poulin & Theil 2000 (**Equation (2)**). [50] The required physicochemical parameters (logP, logSo) [51] were determined in Pipeline Pilot. An overview of all parameters is supplied in Supplemental 3.

$$(2) \quad P_{t:b} = \frac{[S_o*N_t]+[(S_w*0.7P_t)+(S_o*0.3P_t)]+[S_w*W_t]}{[S_o*N_b]+[(S_w*0.7P_b)+(S_o*0.3P_b)]+[S_w*W_b]}$$

where:

$P_{t:b}$ = predicted value of the tissue-blood partition coefficient
S_o = the solubility of the ligand in n-octanol (mol*m_{-3})
S_w = the solubility of the ligand in water (mol*m_{-3})
N_b = the neutral lipid content of blood (as fraction of blood volume)
N_t = the neutral lipid content of the tissue (as fraction of tissue volume)
P_b = the phospholipid content of blood (as fraction of blood volume)
P_t = the phospholipid content of the tissue (as fraction of tissue volume)
W_b = the water content of blood (as fraction of blood volume)
W_t = the water content of the tissue (as fraction of tissue volume)

2.2 Simulations

Model I

Model I was used to investigate the influence of K_D, target concentration (R_{tot}) and k_{off} on *in vivo* target selectivity. To this end, four different simulations (a,b,c,d) were performed. In all four simulations, the k_{off} at the first target (R1) was set to 0.01 h^{-1} and the k_{off} at the second target (R2) was set to 10 h^{-1} while both the K_D and R_{tot} were the same for both targets. An overview of the parameter values that were varied in these simulations can be found in **Table 2**. An overview of all other parameters can be found in Supplemental 1.

Table 2. Parameter values for *in vivo* target selectivity simulations with Model I.

	Model I				**Model II**			
	K_D	R_{tot}	k_{off} R1	k_{off} R2	K_D	$R_{tot}1$	$R_{tot}2$	k_{off}
a	10	25	0.01	10	10	25	0.025	10
b	0.01	25	0.01	10	1	25	0.025	10
c	10	0.25	0.01	10	0.1	25	0.025	10
d	0.01	0.25	0.01	10	0.01	25	0.025	10

* R1 is target 1, R2 is target 2, K_D and Rtot are given in nM, k_{off} is given in h^{-1}

Model II

This model was used to perform simulations to investigate the influence of K_D, target concentration (R_{tot}) and tissue distribution (k_{in}) on *in vivo* tissue selectivity. To this end, four different simulations were performed for a k_{in} value of 8.6 h^{-1} (fast tissue distribution) and for a k_{in} value of 0.86 h^{-1} (slow tissue distribution). An overview of the variable parameter values can be found in Table 2. An overview of all other parameters can be found in Supplemental 1.

Model III

Simulations were performed for Rimonabant, Δ^8 tetrahydrocannabinol (Δ^8 THC) and CP-55940 in a minimal-PBPK-TMDD model (Figure 3). The K_D at the selected targets (CB1, mGlu5, TRPV1, and 5-HT1a) was predicted by a QSAR per target model trained on the complete pChEMBL dataset per target. A fast dissociation from the receptor was assumed for all compounds by setting the k_{off} value to 10 h^{-1} at all receptors. Simulations were performed for a time span of 7 days during which a dose was administered every 24 hours.

In order to investigate the influence of increasing drug-target affinity without a change in equilibrium selectivity, additional simulations were performed in which the ratio between the different K_D values for the different receptors was kept the same while adjusting the absolute K_D values by a factor 10 and 100. Simulations were performed for a time span of 7 days with dosing once every 24 hours. The dose was scaled for the K_D to obtain similar equilibrium occupancies in all simulations.

3 QSAR

A Random Forest QSAR per target model was developed using the Random Forest package from CRAN. [52]

3.1 Data selection

Bio-activity data from ChEMBL22 was used for the development of the QSAR model.[53] High quality data was selected by setting assay confidence at 9 and requiring an assigned pChEMBL value for all data points.[22] This means that a direct single protein target is assigned to the ligand. PubChem database data and potential duplicates were excluded from the dataset. Bioactivity data from ChEMBL was limited to four different constants: K_D, K_i, IC_{50} and EC_{50}. It has been shown previously that K_i and IC_{50} can be combined for modelling.[54] In order to check if these constants could be used interchangeably, a statistical analysis of their pChEMBL values was performed. In this analysis, the mean, standard deviation (SD), median and median absolute deviation (MAD) were analysed within and between all four constants. An overview of all results is provided in Supplemental 4. Since from this analysis it could be concluded that the deviation between pChEMBL values between K_D and K_i do not differ significantly from the deviation within the K_D dataset, both K_D and K_i values were used in the model development.

The molecular structure of the ligands was extracted from the molfile and physicochemical properties and FCFP_6 circular fingerprints were calculated in Pipeline Pilot.[55] The FCFP_6 fingerprints were then converted to 768 feature properties for use in model training. Selection was performed based on the relative frequency of substructures per target, where the optimal frequency was close to being present in 50% of the ligands.

The complete dataset was split into a training set (70%) and validation set (30%). This split was performed seven times, each time with a different seed (111, 222, …, 777) in order to create seven different datasets. In this way, the model training and validation could be performed 7 times, allowing for reproducibility analysis of the model performance results.

3.2 Training

For each target, a Random Forest model consisting of 500 trees was trained using the seven different training sets. The models were trained on a predefined set of properties consisting of log(P), molecular weight, number of proton donors, number of proton acceptors, number of rotatable bonds, number of atoms, number of rings, number of aromatic rings, molecular solubility, molecular surface area, molecular polar surface area and the 768 FCFP_6 fingerprint properties that describe the molecular structure in more detail.

3.3 Validation

The model performance was validated internally and externally using the corresponding validation dataset per seed, as described above. Internal validation was performed by an out-of-bag (OOB) estimate and presented as the average R^2 regression coefficient and the root-mean-squared error (RMSE). [56] The OOB estimate method uses subsamples from the training dataset to determine the mean prediction error of the RF model. The RMSE is a value that measures the average magnitude of the error and is presented by the same unit as the dependent variable, which in this case is the pChEMBL value (-log K_D/K_i in M). External validation was performed by a regression validation of the validation dataset against the predicted pChEMBL values. These results are also presented as the average R^2 regression coefficient and the RMSE.

Results

1. Model I

The simulations in Figure 4 show *in vivo* kinetic target selectivity in all simulations, due to a difference in the k_{off} value for target 1 and target 2. However, the extent of the observed selectivity is dependent on the K_D value and target concentration. Given that optimisation is often performed towards lower k_{off} values, the target at which k_{off} is 0.01 h^{-1} is considered as the desired therapeutic target. Initially, target selectivity for the off-target is observed, but this selectivity reverses to selectivity for the therapeutic target over time in all simulations, except in Figure 4b, where the K_D is low and the target concentration is high. As it would be unlikely in drug development to develop two drugs with a 1000-fold different binding kinetics but the same K_D value, we also performed these simulations with 100-fold different binding kinetics and 10-fold different K_D values as presented in supplemental 5. In these figures, the same trend is observed, although the residual selectivity is higher due to the difference in K_D values.

In summary, we observed that both a high target concentration and a low K_D value decrease the *in vivo* kinetic target selectivity.

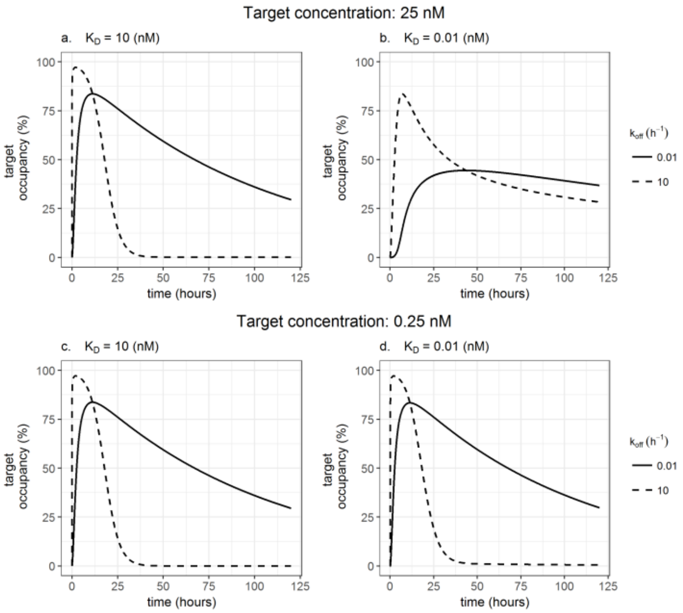

Figure 4. Target concentration and K_D determine the extent of in vivo kinetic target selectivity in Model I. Target selectivity is characterised by a difference in target occupancy between target 1 (solid) and target 2 (dashed). The parameter values for these simulations can be found in Supplemental 1.

2. Model II

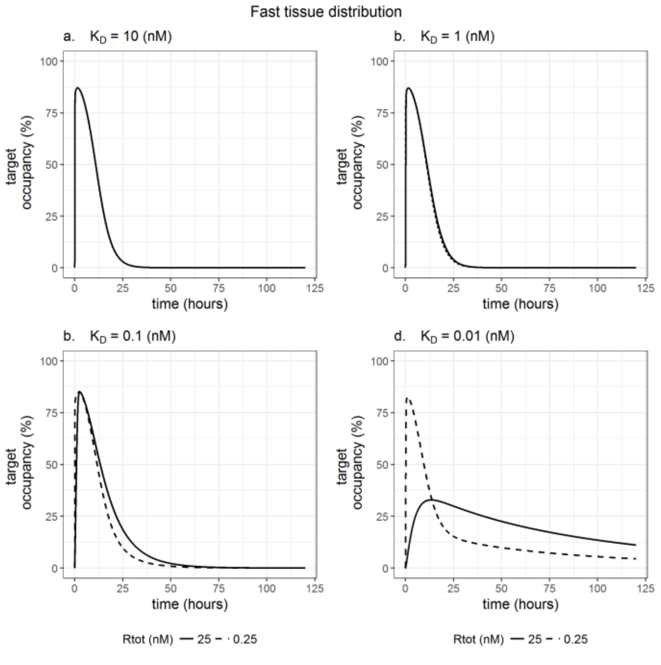

Figure 5. Tissue selectivity reverses to off-target selectivity as K_D decreases in Model II. k_{in} is 8.6 h^{-1}. Tissue selectivity is characterised by a difference in target occupancy between target 1 (solid) and target 2 (dashed). The parameter values for these simulations can be found in Supplemental 1.

For the simulations presented in Figure 5**,** no difference in k_{off} or K_D values between the two target sites could be included, since the ligand binds to the same target and the differences in target occupancy arise due to a difference in the target concentration. No selectivity is observed for the higher K_D values (10 and 1 nM), and only marginal selectivity is observed for lower K_D-values (0.1 nM and 0.01 nM). Assuming that the target concentration in the target tissue is higher than the target concentration in the off-target tissue, the lowest simulated K_D-values showed selectivity in the first 12 hours to the off-target tissue after which selectivity for the target tissue is observed (Figure 5d). Marginal selectivity for the target tissue is observed for a K_D value of 0.1 nM (Figure 5c). Taken together, this means that the K_D and receptor concentrations influence the extent of *in vivo* tissue selectivity.

The simulations in Figure 5 were performed for fast tissue distribution based on the reported blood flow of well-perfused organs in the human body.[37]

Figure 6 shows the simulation results for slower tissue distribution, representing limited perfusion of the target site (e.g. in a synaptic cleft) or the presence of diffusion barriers (e.g. for intracellular or CNS targets). In these figures, the same patterns are observed as for fast tissue distribution, but the observed selectivity is greater and the affinity for maximal selectivity for the target-rich tissue is lower.

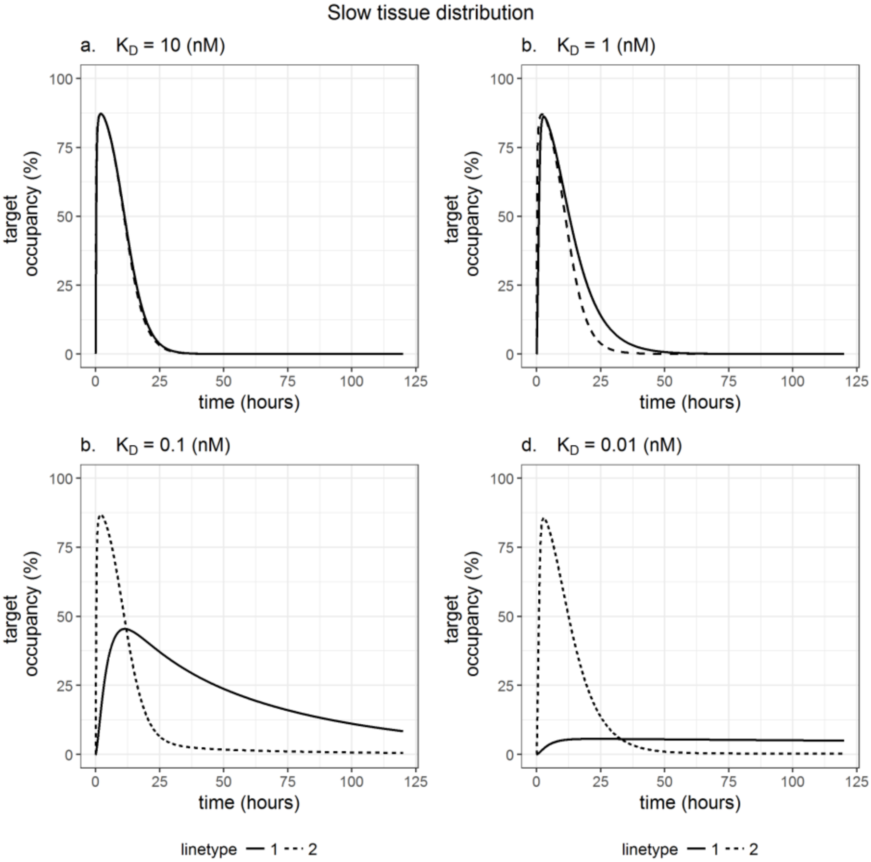

Figure 6. Slower tissue distribution amplifies the influence of K_D on tissue selectivity in Model II. k_{in} is 0.86 h^{-1}. Tissue selectivity is characterised by a difference in target occupancy between target 1 (solid) and target 2 (dashed). The parameter values can be found in Supplemental 1.

3 QSAR-RF

From the simulations described above, it follows that there is an optimal K_D for both tissue selectivity and target selectivity. To facilitate the optimisation of the K_D, we aimed to predict the K_D value from the molecular structure with predictive QSAR modelling. In this study, a QSAR-RF model was developed. The results of the internal and external validation are given in **Figure 7**. For the OOB validation, R^2 values range from 0.57 to 0.70, with an average of 0.63 (SD 0.04) and RMSE values range between 0.64 and 0.83 with an average of 0.69 (SD 0.05). For external regression validation, the R^2 values range from 0.50 to 0.73 with an average of 0.62 (SD 0.05) and RMSE values ranging between 0.9 and 0.64 with an average of 0.71 (SD 0.06). These values indicate good model performance, since the error in public data is around 0.44 for pK_i data. Moreover, based on this error it has been shown that the theoretical maximal achievable R^2 value then becomes 0.81 for the perfect model. [57–59] A full overview of the results is supplied in Supplemental 4.

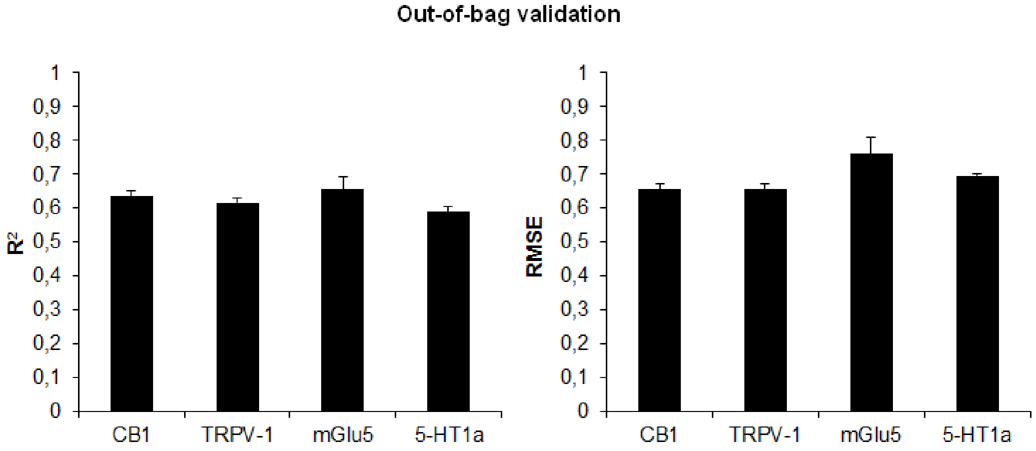
Out-of-bag validation

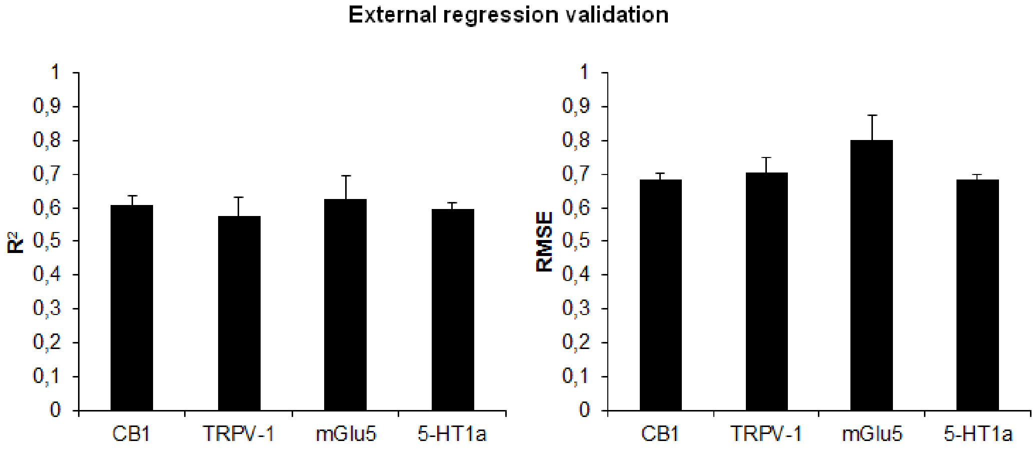
External regression validation

Figure 7. QSAR RF model performance regression validation. Internal out-of-bag validation resulted in an average R^2 value of 0.63 ± 0.06 (SD 0.04), with an RMSE of 0.69 ± 0.1 (SD 0.05). External regression validation gave an average R^2 value of 0.62 ± 0.12 (SD 0.05) with an RMSE of 0.71 ± 0.13 (SD 0.06).

4 Model III

To reflect a drug discovery/candidate selection scenario, the developed QSAR model was used to predict the affinity of the molecules Rimonabant, Δ^8 tetrahydrocannabinol (Δ^8 THC) and CP-55940 for the four selected receptors (CB1, TRPV1, mGlu5, 5-HT1a, **Figure 8**). These K_D values were then used to predict the selectivity over different brain regions (cerebellum, hypothalamus and the frontal cortex). The results of these simulations are given in **Figure 8**. For the target occupancy of Δ^8 THC, the compound with the lowest CB1 affinity, no selectivity is observed between brain regions. The target occupancy for the higher affinity compounds Rimonabant and CP-55490 show a slower increase of target occupancy in the brain regions with the highest target concentrations, the cerebellum and frontal cortex compared to the hypothalamus. The difference in target occupancy between the brain regions is similar for all targets, which results in a change in target selectivity across brain regions. Two days after the start of Rimonabant dosing, for example, the simulated target occupancy at TRPV1 in the hypothalamus is similar to the CB1 target occupancy in cerebellum and frontal cortex.

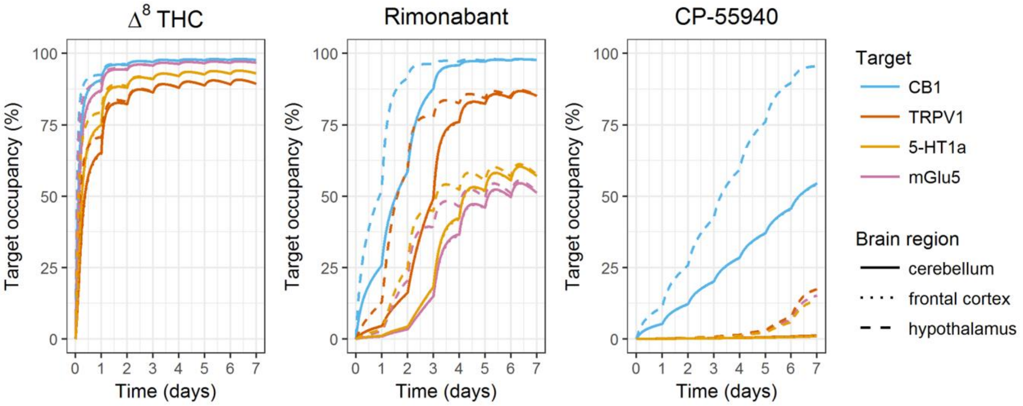

	K_D (± RMSE)	K_D (± RMSE)	K_D (± RMSE)
CB1	43 (9-208)	5 (1-25)	1 (0.2-5)
TRPV1	225 (45-1126)	38 (8-193)	107 (21-534)
5-HT1a	142 (30-682)	166 (35-796)	146 (30-698)
mGlu5	63 (10-396)	211 (33-1331)	125 (20-788)

Figure 8. Simulated PK-profile for Rimonabant in cerebellum, frontal cortex and hypothalamus. Predicted K_D values of Δ^8-THC, Rimonabant and CP-55940 at the CB1, 5-HT1a, mGlu5 and TRPV1 receptor were used in these simulations. k_{off} values were assumed to be 10 h^{-1}. A dose of 10^4 nM was administered every 24 hours. $R_{tot,cer,CB1}$ = 527 nM, $R_{tot,cer,mGlu5}$ = 5.1 nM, $R_{tot,cer,TRPV1}$ = 19 nM, $R_{tot,cer,5\text{-}HT1a}$ = 0.01, $R_{tot,hyp,CB1}$ = 248 nM, $R_{tot,hyp,mGlu5}$ = 16 nM, $R_{tot,hyp,TRPV1}$ = 13 nM, $R_{tot,hyp,5\text{-}HT1a}$ = 2.37, $R_{tot,fc,CB1}$ = 529 nM, $R_{tot,fc,mGlu5}$ = 25 nM, $R_{tot,fc,TRPV1}$ = 12 nM, $R_{tot,fc,5\text{-}HT1a}$ = 1.7.

For CP-55940, it takes more than 7 days to reach the maximal occupancies in the cerebellum and frontal cortex, while this delay would be even more extensive for lower doses. It should be noted that equilibrium selectivity (i.e. the difference in K_D values for the different receptors) is different for the compounds in Figure 8. To obtain a better view of the role of the value of the K_D as such, rather than the K_D ratio between targets, the simulations for Rimonabant were repeated with the same K_D ratio between targets and tenfold increased and decreased K_D values, as shown in Supplemental 6, Figure I. Additionally, to explore the influence of error propagation from the QSAR model into model III, simulations were performed for the lowest and highest K_D value within the RMSE based K_D(±) prediction range as shown in Supplemental 6, Figure II. Summarizing the results, it is consistently found that the selectivity profile changes drastically over time while this would not be expected based on plasma concentrations and K_D values alone.

Discussion

In this study, we have shown that the integration of target binding and PBPK modelling demonstrates the importance of target concentrations, target site distribution kinetics, the K_D and k_{off} for both *in vivo* target selectivity and tissue selectivity. We observe that a low K_D, in combination with a high target concentration, decreased the kinetic target selectivity. Moreover, we find that an increasing K_D can both increase and decrease tissue selectivity, dependent on the target concentration and tissue distribution. The demonstrated mechanistic modelling can thus be instrumental to find an optimal K_D value for a specific target/therapeutic area. To utlize this approach most effectively, our QSAR model to predict CB1 and off-target K_D values can be used to predict tissue and target selectivity directly from the molecular structure. Using this combination of models, our simulations for the CB1 ligands confirm that lower K_D values for all targets can decrease the CB1 and brain region selectivity significantly during the first days of treatment.

Our results suggest that optimisation towards high drug-target affinity and slow drug-target dissociation, as is commonly performed within the current drug development paradigm, may not result in the most selective compounds. While this study demonstrates the influence of target concentrations on the target occupancy in different tissues, the influence of target concentrations on the occupancy-response relationship has previously been described as driving factor for tissue selectivity of partial agonists.[60–62] For the development of more selective drugs, target concentrations of both the intended target and off-targets as well as distribution to the target tissue/target site should be taken into consideration. In this respect, it is important to consider that distribution to the target site is not only dependent on distribution into the target tissue, but also on the localisation of the target within this tissue (e.g. in the blood stream or intracellularly). Moreover, factors such as target concentrations and tissue distribution may be altered in a disease state, which is important for the translation from healthy volunteers to patients.[24,63–65] Finally, it should be considered that there is an increased interest towards allosteric modulation in CNS drug discovery due to the potential benefits with regard to selectivity and side effects.[66] However, it has also been shown that allosteric modulators display different physicochemical and efficacy (K_i *versus* ligand efficacy) profiles compared to orthosteric ligands.[67] These parameters can be included in the modelling approach for future studies.

The methods described in this study provide valuable insights for drugs in later stages of the drug development process. The selectivity profiles in **Figure 8**, for example, would result in underestimation of CB1 selectivity in (pre)clinical studies, if only the first 7 days were studied. This might lead to the unnecessary discontinuation of the development of valuable drug candidates. Moreover, the slowly increasing target occupancy for high affinity drugs such as CP-55940 might lead to a clinically undesired delay and unfavourable selectivity between the initiation of treatment and the onset of the therapeutic effect. This can potentially be mitigated by a higher dose (i.e. a loading dose), which can be lowered as soon as steady state occupancy is reached. Since monitoring of occupancy levels in the clinic is hardly feasible, this would required in-depth knowledge of the mechanisms and predicted occupancy profile as described in this study. Moreover, it should be noted that the target occupancy will decline only slowly after discontinuation of treatment and that it might take several days or even weeks for these high affinity drugs before the target occupancy is back to insignificant levels. This could be counteracted in the clinic by administration of a competitive antagonist or agonist to displace the drug from the receptor and enhance the clearance out of the target binding tissue.

The simulations in this study were all based on physiological parameter values as obtained from PBPK models and target concentration literature. However, additional assumptions were sometimes necessary. For the simulations in Figure 6, the tissue distribution of the drug was not based on the blood flow trough well-perfused organs, as for the other figures, but we assumed a delayed distribution due to, for example, limited diffusion into a synaptic cleft or the cytosol. The magnitude of this delay is compound and target specific and this assumption will thus only hold for a limited number of compounds. Secondly, the simulation in Figure 8 assumed fast binding kinetics as the actual binding kinetics of Rimonabant have been reported to be complex and therefore hard to accurately determine in *in vitro* studies.[68,69] The assumption of fast binding kinetics is supported by the the short dissociation half-life as reported by Packeu *et al*.[70] Additionally, this assumption will be valid for any drug for which the binding kinetics are not rate-limiting compared to the pharmacokinetics, but slower binding kinetics could change the outcome of the simulations, as shown in Figure 4 and in previous studies. [5,6] Thirdly, a number of assumptions concerning (interspecies) translatability of target densities were made in order to obtain useful target densities for the simulations in Figure 8. In general, the quality of absolute tissue-specific target concentration data, rather than relative expression values, might be limited. This is illustrated by the large deviations between experimental tissue density results found in the literature between PET-studies and tissue 'no wash' assay experiments. [41,71] Furthermore, the limited amount of information on target-site distribution for the simulations in Figure 8 limits the predictive value of these simulations. These simulations should therefore be considered as a prediction of the relevant parameters for combined target and tissue selectivity for a realistic set of traget concentrations and K_D values, rather than a precise prediction of target occupancy values for the simulated CB1 ligands. One of the most striking findings in our study is that increasing the K_D in drug development can both increase and decrease the target and tissue selectivity. This demonstrates the relevance of target concentrations and tissue distribution, and the valuable role of mechanistic modeling.

The prediction error that is observed for the K_D predictions of the developed QSAR model introduces an extra level of uncertainty into the overall reliability of the selectivity predictions. The largest RMSE value in this study was found for the mGlu5 QSAR, with an average value of 0.8. This value relates to the deviation of the predictions from the actual pChEMBL value, and has the same unit as the dependent variable, which in this case is the -log K_D. This uncertainty is therefore carried on into the pharmacological simulations. From the simulations performed with the highest and lowest value within the K_D prediction range of Rimonabant, it can be concluded that this propagation of error does influence the observed selectivity profile. This error is limited to the extent of selectivity and the distribution across brain regions during the first one to four days. However, part of this error is already present in the public data that was used to train our QSAR model, in which a larger standard deviation is found compared to the Rimonabant predictions at the CB1 receptor from the QSAR model (Supplemental 4, Figure I). Additionally, having the ability to predict the selectivity profile in the earliest stages of drug disovery justifies the use of predictions with significant uncertainty. Moreover, both the overrepresentation and underrepresentation of structural features or scaffolds in the ChEMBL database might decrease the predictive power for new compounds that do not share these structural features.

Although the predictive value of the presented models is limited by the assumptions we made, the presented insight into the influence of the target concentration and tissue distribution kinetics is in line with the previous analysis of more simple models with only one target and one tissue.[6] Moreover, the relevance of incorporating target binding in PBPK models for the accurate prediction of tissue concentrations has been demonstrated before.[13] The basic principle behind the role of the K_D and target concentration on the duration of occupancy is the high concentration of target-bound drug concentrations compared to unbound drug concentrations at the target site. This is mainly relevant for for drugs with a high K_D and target concentration and at a target occupancy that is not completely saturated. If this target occupancy is increasing, drug-target association will deplete the unbound target site concentration, and if the occupancy is decreasing, drug-target dissociation will increase the unbound target site concentration compared to plasma concentrations.

In summary, the information presented in this study provides new insights into the mechanisms underlying *in vivo* target and tissue selectivity, specifically in relation to drug-target affinity, target concentration, tissue and target-site distribution, as well as binding kinetics. The study provides situations in which selectivity is expected to occur, which may aid as a lead towards creating ligands with the desired selectivity profile. Additionally, the demonstrated integration of mechanistic modelling and machine learning could enable the incorporation of these insights in the earliest phases of drug discovery. The need for this model-based selectivity optimisation is especially valuable for therapeutic areas in which an optimal target or tissue selectivity profile is difficult to obtain (e.g. in oncology) and might be less valuable for therapeutic areas were selectivity is less challenging and the traditional minimisation of the K_D is desired (e.g. for antibiotic/antiviral targets that are not expressed in human cells).

Conclusions

Simulations performed in semi-physiological pharmacological models with target binding revealed an important role for the target concentration and tissue distribution, next to the K_D and k_{off} values, in determining the extent of selectivity. Interestingly, it was observed that the optimal selectivity is not observed for the drug that displays the highest drug-target affinity when assuming that the desired target concentrations are high and the desired binding kinetics are slow. Additionally, it was observed that kinetic selectivity is unlikely when the target concentrations and the drug-target affinity are high, while tissue selectivity is first increased and then decreased for increasing target concentrations and drug-target affinities. The context-dependent optimum of drug-target affinity in determining the extent of selectivity demonstrates the value of K_D prediction for drug development. Taken together, this study demonstrates the potential of integrative predictive modelling in providing improved strategies to optimize drug candidates for maximal *in vivo* selectivity.

Acknowledgements

The authors are part of the K4DD consortium, which is supported by the Innovative Medicines Initiative Joint Undertaking (IMI JU) under grant agreement no 115366. The IMI JU is a project supported by the EU's Seventh Framework Programme (FP7/2007–2013) and the European Federation of Pharmaceutical Industries and Associations (EFPIA).

References

1. Bowes J, Brown AJ, Hamon J, et al. Reducing safety-related drug attrition: the use of in vitro pharmacological profiling. Nat Rev Drug Discov 2012;11(12):909–22
2. Benson N, Metelkin E, Demin O, et al. A systems pharmacology perspective on the clinical development of Fatty Acid amide hydrolase inhibitors for pain. CPT pharmacometrics Syst Pharmacol 2014;3:e91
3. Yuraszeck T, Kasichayanula S, Benjamin JE. Translation and Clinical Development of Bispecific T-cell Engaging Antibodies for Cancer Treatment. Clin Pharmacol Ther 2017;101(5):634–45
4. Copeland RA, Pompliano DL, Meek TD. Drug-target residence time and its implications for lead optimization. Nat Rev Drug Discov 2006;5(9):730–9
5. Dahl G, Akerud T. Pharmacokinetics and the drug-target residence time concept. Drug Discov Today 2013;18(15–16):697–707
6. de Witte WEA, Danhof M, van der Graaf PH, et al. In vivo Target Residence Time and Kinetic Selectivity: The Association Rate Constant as Determinant. Trends Pharmacol Sci 2016;37(10):831–42
7. Guo D, Dijksteel GS, Van Duijl T, et al. Equilibrium and kinetic selectivity profiling on the human adenosine receptors. Biochem Pharmacol 2016;105:34–41
8. Rostami-Hodjegan A. Physiologically based pharmacokinetics joined with in vitro-in vivo extrapolation of ADME: a marriage under the arch of systems pharmacology. Clin Pharmacol Ther 2012;92(1):50–61
9. Mager DE, Krzyzanski W. General Pharmacokinetic Model for Drugs Exhibiting Target-Mediated Drug Disposition. Pharm Res 2005;22(10):1589–96
10. Luu KT, Bergqvist S, Chen E, et al. A model-based approach to predicting the human pharmacokinetics of a monoclonal antibody exhibiting target-mediated drug disposition. J Pharmacol Exp Ther 2012;341(3):702–8
11. Zhang L, Mager DE. Physiologically-based pharmacokinetic modeling of target-mediated drug disposition of bortezomib in mice. J Pharmacokinet Pharmacodyn 2015;42(5):541–52
12. Page KR, Mezzalana E, MacDonald AJ, et al. Temporal pharmacokinetic/pharmacodynamic interaction between human CD3ε antigen-targeted monoclonal antibody otelixizumab and CD3ε binding and expression in human peripheral blood mononuclear cell static culture. J Pharmacol Exp Ther 2015;355(2):199–205
13. Plowchalk DR, Andersen ME, deBethizy JD. A physiologically based pharmacokinetic model for nicotine disposition in the Sprague-Dawley rat. Toxicol Appl Pharmacol 1992;116(2):177–88
14. Yang RSH, Thomas RS, Gustafson DL, et al. Approaches to developing alternative and predictive toxicology based on PBPK/PD and QSAR modeling. Environ Health Perspect 1998;106(6):1385–93
15. Knaak JB, Dary CC, Power F, et al. Physicochemical and Biological Data for the Development of Predictive Organophosphorus Pesticide QSARs and PBPK/PD Models for Human Risk Assessment. Critical reviews in toxicology. 2004. 143-207 p
16. Price K, Krishnan K. An integrated QSAR-PBPK modelling approach for predicting the inhalation toxicokinetics of mixtures of volatile organic chemicals in the rat. SAR QSAR Environ Res 2011;22(1–2):107–28
17. Van Der Graaf PH, Nilsson J, Van Schaick EA, et al. Multivariate quantitative structure-pharmacokinetic relationships (QSPKR) analysis of adenosine A1 receptor agonists in rat. J Pharm Sci 1999;88(3):306–12
18. Westen GJP Van, Hoven OO Van Den, Pijl R Van Der, et al. Identifying Novel Adenosine Receptor Ligands by Simultaneous Proteochemometric Modeling of Rat and Human Bioactivity Data. J Med Chem 2012;55:7010–20
19. Unterthiner T. Deep Learning as an Opportunity in Virtual Screening. Workshop on Deep Learning and Representation Learning 2014. p. 1–9
20. Christmann-Franck S, Van Westen GJP, Papadatos G, et al. Unprecedently Large-Scale Kinase Inhibitor Set Enabling the Accurate Prediction of Compound-Kinase Activities: A Way toward Selective Promiscuity by Design? J Chem Inf Model 2016;56(9):1654–75
21. Gaulton A, Bellis LJ, Bento AP, et al. ChEMBL: a large-scale bioactivity database for drug discovery. Nucleic Acids Res 2012;40(D1):D1100–7
22. Papadatos G, Gaulton A, Hersey A, et al. Activity, assay and target data curation and quality in the ChEMBL database. J Comput Aided Mol Des 2015;29(9):885–96
23. Mackie K. Cannabinoid receptors: Where they are and what they do. J Neuroendocrinol 2008;20(SUPPL. 1):10–4
24. Miller LKL, Devi L a. The highs and lows of cannabinoid receptor expression in disease: mechanisms and their therapeutic implications. Pharmacol Rev 2011;63(3):461–70
25. Pertwee RG, Howlett a C, Abood ME, et al. International Union of Basic and Clinical Pharmacology . LXXIX . Cannabinoid Receptors and Their Ligands : Beyond CB 1 and CB 2. Pharmacol Rev 2010;62(4):588–631
26. Bird MK, Lawrence AJ. The promiscuous mGlu5 receptor - a range of partners for therapeutic possibilities? Trends Pharmacol Sci 2009;30(12):617–23
27. Brotchie JM. CB1 cannabinoid receptor signalling in Parkinson's disease. Curr Opin Pharmacol 2003;3(1):54–61
28. Terzian ALB, Aguiar DC, Guimarães FS, et al. Modulation of anxiety-like behaviour by Transient Receptor Potential Vanilloid Type 1 (TRPV1) channels located in the dorsolateral periaqueductal gray. Eur

Neuropsychopharmacol 2009;19(3):188–95
29. Johnson K a, Conn PJ, Niswender CM. Glutamate receptors as therapeutic targets for Parkinson's disease. CNS Neurol Disord Drug Targets 2009;8(6):475–91
30. Team Rs. RStudio: Integrated Development Environment for R. Boston, MA; 2016.
31. R Core Team. R: A language and environment for statistical computing. R Found Stat Comput Vienna, Austria URL http//wwwR-project.org/ 2013;
32. Dassault Systèmes BIOVIA Pipeline Pilot. San Diego; 2017.
33. Heinemann A, Wischhusen F, Püschel K, et al. Standard Liver Volume in the Caucasian Population. Liver Transplant Surg 1999;5(5):366–8
34. Lüders E, Steinmetz H, Jäncke L. Brain size and grey matter volume in the healthy human brain. Neuroreport 2002;13(17):2371–4
35. Llinas RR, Walton KD, Lang EJ. Cerebellum. The Synaptic Organization of the Brain 2004. p. "Cerebellum"
36. Petryszak R, Keays M, Tang YA, et al. Expression Atlas update — an integrated database of gene and protein expression in humans, animals and plants. Nucleic Acids Res 2016;44:746–52
37. Levitt DG, Schnider TW. Human physiologically based pharmacokinetic model for propofol. BMC Anesthesiol 2005;5(1):4
38. Makris N, Swaab DF, van der Kouwe A, et al. Volumetric Parcellation Methodology of the Human Hypothalamus in Neuroimaging: Normative Data and Sex Differences. Neuroimage 2013;69(April):1–10
39. Yamamoto Y, Välitalo PA, van den Berg D-J, et al. A Generic Multi-Compartmental CNS Distribution Model Structure for 9 Drugs Allows Prediction of Human Brain Target Site Concentrations. Pharm Res 2017;34(2):333–51
40. Breivogel CS, Sim LJ, Childers SR. Regional differences in cannabinoid receptor/G-protein coupling in rat brain. J Pharmacol Exp Ther 1997;282(3):1632–42
41. Patel S, Hamill TG, Connolly B, et al. Species differences in mGluR5 binding sites in mammalian central nervous system determined using in vitro binding with [18F]F-PEB. Nucl Med Biol 2007;34(8):1009–17
42. Han P, Korepanova A V., Vos MH, et al. Quantification of TRPV1 protein levels in rat tissues to understand its physiological roles. J Mol Neurosci 2013;50(1):23–32
43. Costes N, Merlet I, Zimmer L, et al. Modeling [18 F]MPPF Positron Emission Tomography Kinetics for the Determination of 5-Hydroxytryptamine(1A) Receptor Concentration With Multiinjection. J Cereb Blood Flow Metab 2002;22(6):753–65
44. Glass M, Faull RLM, Dragunow M. Cannabinoid receptors in the human brain: a detailed anatomical and quantitative autoradiographic study on the fetal, neonatal and adult human brain. Neuroscience 1997;77(2):299–318
45. Liu P, Hamill TG, Chioda M, et al. Discovery of MK-3168: A PET tracer for imaging brain fatty acid amide hydrolase. ACS Med Chem Lett 2013;4(6):509–13
46. Szabo T, Biro T, Gonzalez AF, et al. Pharmacological characterization of vanilloid receptor located in the brain. Mol Brain Res 2002;98(1–2):51–7
47. Albe K, Butler MH, Wright B. Cellular concentrations of enzymes and their substrates. J Theor Biol 1990;143(2):163–95
48. Undén A, Tatemoto K, Mutt V, et al. Neuropeptide Y receptor in the rat brain. Eur J Biochem 1984;145(3):525–30
49. Milo R. What is the total number of protein molecules per cell volume? A call to rethink some published values. Bioessays 2013;35(12):1050–5
50. Poulin P, Theil FP. A priori prediction of tissue: Plasma partition coefficients of drugs to facilitate the use of physiologically-based pharmacokinetic models in drug discovery. J Pharm Sci 2000;89(1):16–35
51. Ghose AK, Viswanadhan VN, Wendoloski JJ. Prediction of Hydrophobic (Lipophilic) Properties of Small Organic Molecules Using Fragmental Methods : An Analysis of ALOGP and CLOGP Methods. J Phys Chem A 1998;5639(98):3762–72
52. Hornik K. The Comprehensive R Archiv Network. WIREs Comput Stat 2012;4:394–8
53. Bento AP, Gaulton A, Hersey A, et al. The ChEMBL bioactivity database: an update. Nucleic Acids Res 2014;42(D1):D1083–90
54. Kalliokoski T, Kramer C, Vulpetti A, et al. Comparability of Mixed IC 50 Data – A Statistical Analysis. PLoS One 2013;8(4)
55. Rogers D, Hahn M. Extended-Connectivity Fingerprints. J Chem Informatics Model 2010;50:742–54
56. Sventnik V, Liaw A, Tong C, et al. Random forest: a tool for classification and regression in compound classification and QSAR modeling. J Chem Inf Comput Sci 2003;43(6):1947–58
57. Golbraikh A, Tropsha A. Beware of q^2! J Mol Graph Model 2002;20(4):269–76
58. Tropsha A, Gramatica P, Gombar V. The Importance of Being Earnest: Validation is the Absolute Essential for Successful Application and Interpretation of QSPR Models. QSAR Comb Sci 2003;22(1):69–77
59. Kramer C, Kalliokoski T, Gedeck P, et al. The Experimental Uncertainty of Heterogeneous Public Ki Data. J Med Chem 2012;55:5165–73

60. Yassen A, Olofsen E, Romberg R, et al. Mechanism-based PK/PD modeling of the respiratory depressant effect of buprenorphine and fentanyl in healthy volunteers. Clin Pharmacol Ther 2007;81(1):50–8
61. Schaick EA Van, Tukker HE, Roelen HCPF, et al. Selectivity of action of 8-alkylamino analogues of N6-cyclopentyladenosine in vivo: haemodynamic versus anti-lipolytic responses in rats. Br J Pharmacol 1998;124:607–18
62. van der Graaf PH, Schaick EA Van, Visser SAG, et al. Mechanism-Based Pharmacokinetic-Pharmacodynamic Modeling of Antilipolytic Effects of Adenosine A 1 Receptor Agonists in Rats : Prediction of Tissue-Dependent Efficacy. J Pharmacol 1999;290(2):702–9
63. Walawalkar YD, Vaidya Y, Nayak V. Alteration in transforming growth factor-β receptor expression in gallbladder disease: implications of chronic cholelithiasis and chronic Salmonella typhi infection. Gastroenterol Insights 2016;7(1):39–42
64. Epling-burnette PK, Painter JS, Chaurasia P, et al. Dysregulated NK receptor expression in patients with lymphoproliferative disease of granular lymphocytes Dysregulated NK receptor expression in patients with lymphoproliferative disease of granular lymphocytes. Blood 2011;103(9):3431–9
65. Atkinson H, England JA, Rafferty A, et al. Somatostatin receptor expression in thyroid disease. Int J Exp Pathol 2013;94(3):226–9
66. Conn PJ, Christopoulos A, Lindsley CW. Allosteric modulators of GPCRs: a novel approach for the treatment of CNS disorders. Nat Rev drug Discov 2010;8(1):41–54
67. Westen GJP Van, Gaulton A, Overington JP. Chemical, Target, and Bioactive Properties of Allosteric Modulation. PLoS Comput Biol 2014;10(4)
68. Wennerberg M, Balendran A, Clapham JC, et al. Unravelling the complex dissociation of [3H]-rimonabant from plated CB1 cannabinoid receptor-expressing cells. Fundam &Clinical Pharmacol 2010;24:181–7
69. Wennerberg M, Cheng L, Hjorth S, et al. Binding properties of antagonists to Cannabinoid receptors in intact cells. Fundam Clin Pharmacol 2011;25:200–10
70. Packeu A, Wennerberg M, Balendran A, et al. Estimation of the dissociation rate of unlabelled ligand-receptor complexes by a “two-step” competition binding approach. Br J Pharmacol 2010;161(6):1311–28
71. Kågedal M, Cselényi Z, Nyberg S, et al. Non-linear mixed effects modelling of positron emission tomography data for simultaneous estimation of radioligand kinetics and occupancy in healthy volunteers. Neuroimage 2012;61(4):849–56
72. Kennedy DN, Lange N, Makris N, et al. Gyri of the Human Neocortex : An MRI-based Analysis of Volume and Variance. Cereb cortex 1998;8(4):372–84

Supplemental 1

A. Model I

$$\frac{dac}{dt} = -ack_a$$
$$\frac{dbl}{dt} = ack_a + k_{outbt}bt + k_{outnbt}nbt + k_{outli}li - bl(k_{inbt} + k_{innbt} + k_{inli})$$
$$\frac{dbt}{dt} = k_{inbt}bl - k_{outbt}bt - k_{on1}bt\left(Rtot1 - \frac{RL1}{V_{bt}}\right) + k_{off}1RL1 - k_{on2}bt\left(Rtot2 - \frac{RL2}{V_{bt}}\right) + k_{off2}$$
$$\frac{dnbt}{dt} = k_{innbt}bl - k_{outnbt}nbt$$
$$\frac{dli}{dt} = k_{inli}bl - k_{outli}li - kFli$$
$$\frac{dRL1}{dt} = k_{on1}bt\left(Rtot1 - \frac{RL1}{V_{bt}}\right) - k_{off1}RL1$$
$$\frac{dRL2}{dt} = k_{on2}bt\left(Rtot2 - \frac{RL2}{V_{bt}}\right) - k_{off2}RL2$$

Table S1. Input paramters for model I. k_{in} is the inwards distribution rate constant, V is volume, kF is the forward rate of elimination constant, k_a is the absorption rate constant, bt is binding tissue, nbt is nonbinding tissue, li is liver, bl is blood.

Parameter	**Value**	**Unit**
k_{inbt}	8.6	h^{-1}
k_{innbt}	25	h^{-1}
k_{inli}	27	h^{-1}
Vbl	5.5	L
Vbt	1.4	L
Vnbt	61	L
Vli	1.8	L
kF	100	h^{-1}
k_a	0.25	h^{-1}

B. Model II

$$\frac{dac}{dt} = -ack_a$$
$$\frac{dbl}{dt} = ack_a + k_{outbt}bt + k_{outnbt}nbt + k_{outli}li - bl(k_{inbt1} + k_{inbt2} + k_{innbt} + k_{inli})$$
$$\frac{dbt1}{dt} = k_{inbt1}bl - k_{outbt1}bt - k_{on}bt1\left(Rtot1 - \frac{RL1}{V_{bt1}}\right) + k_{off}RL1$$
$$\frac{dbt2}{dt} = k_{inbt2}bl - k_{outbt2}bt - k_{on}bt2\left(Rtot2 - \frac{RL2}{V_{bt2}}\right) + k_{off}RL2$$
$$\frac{dnbt}{dt} = k_{innbt}bl - k_{outnbt}nbt$$
$$\frac{dli}{dt} = k_{inli}li - k_{outli}li - kFli$$
$$\frac{dRL1}{dt} = k_{on}bt1\left(Rtot1 - \frac{RL1}{V_{bt}1}\right) - k_{off}RL1$$
$$\frac{dRL2}{dt} = k_{on}bt2\left(Rtot2 - \frac{RL2}{V_{bt2}}\right) - k_{off}RL2$$

i. Fast distribution

Table S2. Input parameters for the fast distribution simulations in model II. k_{in} is the inwards distribution rate constant, V is volume, kF is the forward rate of elimination constant, k_a is the absorption rate constant, bt is binding tissue, nbt is nonbinding tissue, li is liver, bl is blood, Rtot is receptor concentration, k_{on} is the ligand-target association rate constant.

Parameter	**Value**	**Unit**
$k_{inbt}1$	8.6	h^{-1}
$k_{inbt}2$	8.6	h^{-1}
k_{innbt}	17	h^{-1}
k_{inli}	27	h^{-1}
Vbl	5.5	L
Vbt1	1.4	L
Vbt2	1.4	L
Vnbt	60	L
Vli	1.8	L
kF	100	h^{-1}
Rtot1	25	nM
Rtot2	0.25	nM
k_{off}	10	$nM^{-1}h^{-1}$

ii. Slow distribution

Table S3. Input parameters for the slow distribution simulations in model II. k_{in} is the inwards distribution rate constant, V is volume, kF is the forward rate of elimination constant, k_a is the absorption rate constant, bt is binding tissue, nbt is nonbinding tissue, li is liver, bl is blood, Rtot is receptor concentration, k_{on} is the ligand-target association rate constant.

Parameter	**Value**	**Unit**
$k_{inbt}1$	8.6	h^{-1}
$k_{inbt}2$	8.6	h^{-1}
k_{innbt}	17	h^{-1}
k_{inli}	27	h^{-1}
Vbl	5.5	L
Vbt1	1.4	L
Vbt2	1.4	L
Vnbt	60	L
Vli	1.8	L
kF	100	h^{-1}
Rtot1	25	nM
Rtot2	0.25	nM
k_{off}	10	$nM^{-1}h^{-1}$

C. Model III

$$\frac{dac}{dt} = -ack_a$$

$$\frac{dbl}{dt} = ack_a + Q_{cer}\frac{{cer}/{V_{cer}}}{P_{cer}} + Q_{fc}\frac{{fc}/{V_{fc}}}{P_{fc}} + Q_{hyp}\frac{{hyp}/{V_{hyp}}}{P_{hyp}}Q_{cer} + \frac{{nbt}/{V_{nbt}}}{P_{nbt}} + Q_{li}\frac{{li}/{V_{li}}}{P_{li}} - Q_{bl}\frac{bl}{V_{bl}}$$

$$\frac{dnbt}{dt} = Q_{nbt}\left(\frac{bl}{V_{bl}} - \frac{{nbt}/{V_{nbt}}}{P_{nbt}}\right)$$

$$\frac{dcer}{dt} = Q_{cel}\left(\frac{bl}{V_{bl}} - \frac{{cer}/{V_{cer}}}{P_{cer}}\right) - k_{onCB1}cer\left(CB1_{cer} - \frac{CB1RL_{cer}}{V_{cer}}\right) + k_{offCB1}CB1RL_{cer} - k_{onmGlu5}cer\left(mGlu5_{cer} - \frac{mGlu5RL_{cer}}{V_{cer}}\right) + k_{offmGlu5}mGlu5RL_{cer} - k_{onTRPV1}cer\left(TRPV1_{cer} - \frac{TRPV1RL_{cer}}{V_{cer}}\right) + k_{offTRPV1}TRPV1RL_{cer} - k_{onHT1a}cer\left(HT1a_{cer} - \frac{HT1aRL_{cer}}{V_{cer}}\right) + k_{offHT1a}HT1aRL_{cer}$$

$$\frac{dhyp}{dt} = Q_{hyp}\left(\frac{bl}{V_{bl}} - \frac{{hyp}/{V_{hyp}}}{P_{hyp}}\right) - k_{onCB1}hyp\left(CB1_{hyp} - \frac{CB1RL_{hyp}}{V_{hyp}}\right) + k_{off}CB1RL_{hyp} - k_{onmGlu5}hyp\left(mGlu5_{hyp} - \frac{mGlu5RL_{hyp}}{V_{hyp}}\right) + k_{offmGlu5}mGlu5RL_{hyp} - k_{onTRPV1}hyp\left(TRPV1_{hyp} - \frac{TRPV1RL_{hyp}}{V_{hyp}}\right) + k_{offTRPV1}TRPV1RL_{hyp} - k_{onHT1a}hyp\left(HT1a_{hyp} - \frac{HT1aRL_{hyp}}{V_{hyp}}\right) + k_{offHT1a}HT1aRL_{hyp}$$

$$\frac{dfc}{dt} = Q_{fc}\left(\frac{bl}{V_{bl}} - \frac{{fc}/{V_{fc}}}{P_{fc}}\right) - k_{onCB1}fc\left(CB1_{fc} - \frac{CB1RL_{fc}}{V_{fc}}\right) + k_{offCB1}CB1RL_{fc} - k_{onmGlu5}fc\left(mGlu5_{fc} - \frac{mGlu5RL_{fc}}{V_{fc}}\right) + k_{offmGlu5}mGlu5RL_{fc} - k_{onTRPV1}fc\left(TRPV1_{fc} - \frac{TRPV1RL_{fc}}{V_{fc}}\right) + k_{offTRPV1}TRPV1RL_{fc} - k_{onHT1a}fc\left(HT1a_{fc} - \frac{HT1aRL_{fc}}{V_{fc}}\right) + k_{offHT1a}HT1aRL_{fc}$$

$$\frac{dli}{dt} = k_{inli}li - k_{outli}li - kFli$$

$$\frac{dCB1RL_{cer}}{dt} = k_{onCB1}cer\left(CB1_{cer} - \frac{CB1RL_{cer}}{V_{cer}}\right) - k_{offCB1}CB1RL_{cer}$$

$$\frac{dmGlu5RL_{cer}}{dt} = k_{onmGlu5}cer\left(mGlu5_{cer} - \frac{mGlu5RL_{cer}}{V_{cer}}\right) - k_{offmGlu5}mGlu5RL_{cer}$$

$$\frac{dTRPV1_{RLcer}}{dt} = k_{onTRPV1}cer\left(TRPV1_{cer} - \frac{TRPV1RL_{cer}}{V_{cer}}\right) - k_{offTRPV1}TRPV1RL_{cer}$$

$$\frac{dHT1aRL_{cer}}{dt} = k_{onHT1a}cer\left(HT1a_{cer} - \frac{HT1aRL_{cer}}{V_{cer}}\right) - k_{offHT1a}HT1aRL_{cer}$$

$$\frac{dCB1RL_{hyp}}{dt} = k_{onCB1}hyp\left(CB1_{hyp} - \frac{CB1RL_{hyp}}{V_{hyp}}\right) - k_{offCB1}CB1RL_{hyp}$$

$$\frac{dmGlu5RL_{hyp}}{dt} = k_{onmGlu5}hyp\left(mGlu5_{hyp} - \frac{mGlu5RL_{hyp}}{V_{hyp}}\right) - k_{offmGlu5}mGlu5RL_{hyp}$$

$$\frac{dTRPV1RL_{hyp}}{dt} = k_{onTRPV1}hyp\left(TRPV1_{hyp} - \frac{TRPV1RL_{hyp}}{V_{hyp}}\right) - k_{offTRPV1}TRPV1RL_{hyp}$$

$$\frac{dHT1aRL_{hyp}}{dt} = k_{onHT1a}hyp\left(HT1a_{hyp} - \frac{HT1aRL_{hyp}}{V_{hyp}}\right) - k_{offHT1a}HT1aRL_{hyp}$$

$$\frac{dCB1RL_{fc}}{dt} = k_{onCB1}fc\left(CB1_{fc} - \frac{CB1RL_{fc}}{V_{fc}}\right) - k_{offCB1}CB1RL_{fc}$$

$$\frac{dmGlu5RL_{fc}}{dt} = k_{onmGlu5}fc\left(mGlu5_{fc} - \frac{mGlu5RL_{fc}}{V_{fc}}\right) - k_{offmGlu5}mGlu5RL_{fc}$$

$$\frac{dTRPV1RL_{fc}}{dt} = k_{onTRPV1}fc\left(TRPV1_{fc} - \frac{TRPV1RL_{fc}}{V_{fc}}\right) - k_{offTRPV1}TRPV1RL_{fc}$$

$$\frac{dHT1aRL_{fc}}{dt} = k_{onHT1a}fc\left(HT1a_{fc} - \frac{HT1aRL_{fc}}{V_{fc}}\right) - k_{offHT1a}HT1aRL_{fc}$$

The clearances from brain extra-cellular fluid to the cerebrospinal fluid presented by Yamamoto *et al* are 0.0556, 0.0250, 0.0598, 0.0200,0.0248, 0.0133, 0.0237, 0.0176 and 0.0254 ml/min, resulting in a mean value of 0.0295 ml/min. These values were allometrically scaled to humans by multiplying this value by $(70/0.25)^{0.75}$, resulting in a value of 2.02 ml/min, which equals to 0.121 L/h. In this study, the ECF volume in humans was reported as 0.240 L. Given that the equation for clearance is $CL = V * k_{out}$, k_{out} can be calculated as 0.121 (L/h)/0.240 (L), resulting in a value of 0.504 h^{-1}. By multiplying this value by the tissue volume, the effective flow through the target site (cerebellum, hypothalamus, frontal cortex) is obtained.

Table S4. Model parameters for model III. Q is blood flow, P is the partition coefficient, V is volume, k_{off} is the ligand-target dissociation rate constant, kF is the forward rate of elimination constant, k_a is the absorption rate constant, bl is blood, nbt is nonbinding tissue, cer is cerebellum, hyp is hypothalamus, fc is frontal cortex, li is liver.

Parameter	**Value**	**Unit**	**References**
Qbl	335	L/h	[37]
Qnbt	335-0.504*(Vcer+Vhyp+Vfc)-108	L/h	
Qcer	Vcer*0.504	L/h	[39]
Qhip	Vhyp*0.504	L/h	[39]
Qfc	Vfc*0.504	L/h	[39]
Qli	27	L/h	[37]
Pnbt	46		
Pcer	13		
Phyp	13		
Pfc	13		
Pli	9.4		
Vbl	5.5	L	[37]
Vnbt	62	L	[37]
Vcer	0.15	L	[35]
Vhyp	$1.4*10^{-2}$	L	[38]
Vfc	0.27	L	[72]
Vli	1.8	L	[37]
k_{off}	10	h^{-1}	
kF	100	h^{-1}	
k_a	0.25	h^{-1}	
Dose	$5.0*10^{4}$	nM	

Supplemental 2

Table S5. Receptor density values obtained from literature. CB1 is cannabinoid 1 receptor, TRPV1 is vanilloid 1 receptor, 5-HT1a is serotonin 1a receptor, mGlu5 is metabotropic glutamate receptor 5. All these values are obtained from rat studies, unless otherwise specified

	CB1	**CB1**[a]	**mGlu5**[b]	**TRPV1**	**TRPV1**[c]	**5-HT1a**[b]
	Bmax (pmol/mg protein)	**Bmax (nM)**	**Bmax (nM)**	**Protein level (ng/mg lysate)**	**Protein level (nM)**	**Bmax (nM)**
cerebellum	5.27	**527**	**5.1**	4.03	**19**	**0.01**[d]
(frontal) cortex	5.29	**529**	**25**	2.53	**12**	**1.70**
hypothalamus	2.48	**248**	**16**[e]	2.76	**13**	**2.37**[f]
References	[40]		[41]	[42]		[43]

[a] Conversion from pmol/mg protein to nM was obtained by multiplying with an assumed protein concentration of 100 mg/ml tissue.[48]

[b] Values from humans.

[c] These values were obtained by multiplying the protein level in ng/mg lysate with the ratio of protein level in pmol/mg protein[46] and in ng/mg lysate[42] and subsequent multiplication with an assumed protein concentration of 100 mg/ml tissue.[48]

[d] This value was too low to be identified in the reference and was therefore set to a low concentration.

[e] The Bmax value was calculated as the average of the cortex, caudate-putamen and cerebellum.

[f] The reported value for the limbic average was used for the hypothalamus.

Supplemental 3

A. Physicochemical Properties

Table S6. Physicochemical properties for the partition coefficient calculations in the Integrated QSAR-RF PBPK-TMDD model. P is the octanol-water partition coefficient, Sw is the solubility in water, So is the solubility in octanol.

Ligand	**logP**	**logSw**	**P**	**Sw**	**So**
Δ^8-THC	6.109	-6,152	$12*10^5$	$7.05*10^{-7}$	0.91
Rimonabant	6.613	-8,112	$41*10^5$	$7.73*10^{-9}$	0.03
CP-55940	6.162	-7,244	$14*10^5$	$5.70*10^{-8}$	0.08

B. Volume Fractions

Table S7. Volume fractions of water, neutral lipids and phospholipids in human tissues. Nbt is nonbinding tissue.

	Water	Neutral lipid	Phospholipid
Blood	0.8	0.0044	0.0021
Liver	0.72	0.039	0.028
Nbt	0.56	0.21	0.071
Brain	0.79	0.0462	0.0638

Supplemental 4

A. Compare Binding

i. Within

Table S8. Statistical analysis of the pChEMBL value deviations within measurements of the same bioactivity value and all bioactivity values together. Mean Δ is the mean difference between measurements of the same ligand at the same target. K_D is the dissociation rate constant, K_i is the inhibitory constant, IC_{50} is the half-maximal inhibitory constant ions, and EC_{50} is the half-maximal effective concentration.

	K_D - K_D	K_i - K_i	IC_{50} - IC_{50}	EC_{50} - EC_{50}	Any - Any
Mean Δ	0.32	0.44	0.61	0.50	0.61
Mean pChEMBL value	6.56 ± 0.14	7.29 ± 0.20	6.83 ± 0.29	6.74 ± 0.23	6.90 ± 0.28

ii. Between

Table S9. Statistical analysis of the pChEMBL value deviations between measurements of different bioactivity values. Mean Δ is the mean difference between measurements of the same ligand at the same target. K_D is the dissociation rate constant, K_i is the inhibitory constant, IC_{50} is the half-maximal inhibitory constant ions, and EC_{50} is the half-maximal effective concentration

	K_D - K_i	**K_i - IC_{50}**	**K_i - EC_{50}**	**IC_{50} - EC_{50}**
Mean Δ	0.16	0.50	0.52	0.21
Mean pChEMBL value	7.16 ± 0.19	6.93 ± 0.28	7.21 ± 0.23	6.83 0.29

B. Out-of-bag validation

i. R^2

Table S10. The R^2 values of the out-of-bag validation of the QSAR-RF model trained on seven different datasets. The R^2 values are reported per training of the model on a data set obtained using a different split seed.

Seed		**CB1**	**TRPV1**	**ADORA2a**	**mGlu5**	**5-HT1a**
	111	0.62	0.61	0.67	0.59	0.62
	222	0.64	0.59	0.67	0.67	0.57
	333	0.65	0.61	0.68	0.70	0.59
	444	0.66	0.63	0.66	0.63	0.58
	555	0.64	0.64	0.68	0.68	0.58
	666	0.62	0.62	0.67	0.67	0.59
	777	0.63	0.61	0.68	0.64	0.59
STDEV		0.016	0.015	0.0076	0.038	0.015
AVG		0.64	0.62	0.67	0.65	0.59

ii. RMSE

Table S11. The RMSE values of the out-of-bag validation of the QSAR-RF model trained on seven different datasets. The root-mean squared error (RMSE) values are reported per training of the model on a dataset obtained using a different split seed.

Seed	**CB1**	**TRPV1**	**ADORA2a**	**mGlu5**	**5-HT1a**
111	0.67	0.66	0.67	0.83	0.68
222	0.66	0.68	0.67	0.69	0.70
333	0.65	0.67	0.67	0.73	0.70
444	0.64	0.66	0.68	0.81	0.70
555	0.65	0.65	0.66	0.76	0.70
666	0.67	0.64	0.67	0.77	0.69
777	0.66	0.67	0.66	0.75	0.69
STDEV	0.013	0.013	0.0076	0.047	0.0085
AVG	0.66	0.66	0.67	0.76	0.69

External Validation

i. R^2

Table S12. The R^2 values of external validation of the QSAR-RF model trained on seven different datasets. The R^2 values are reported per training of the model on a dataset obtained using a different split seed. The external validation was performed as a regression validation, using a validation dataset, containing only data which was not exposed to the model before validation.

	CB1	**TRPV1**	**ADORA2a**	**mGlu5**	**5-HT1a**
111	0.65	0.66	0.70	0.73	0.57
222	0.59	0.60	0.72	0.62	0.62
333	0.57	0.63	0.64	0.52	0.61
444	0.59	0.50	0.68	0.68	0.60
555	0.60	0.52	0.63	0.58	0.61
666	0.63	0.56	0.67	0.62	0.57
777	0.62	0.5	0.69	0.65	0.58
STDEV	0.028	0.056	0.031	0.070	0.020
AVG	0.61	0.58	0.68	0.63	0.60

ii. RMSE

Table S13. The RMSE values of the out-of-bag validation of the QSAR-RF model trained on seven different datasets. The root-mean squared error (RMSE) values are reported per training of the model on a dataset obtained using a different split seed. The external validation was performed as a regression validation, using a validation dataset, containing only data which was not exposed to the model before validation.

	CB1	TRPV1	ADORA2a	mGlu5	5-HT1a
111	0.66	0.64	0.65	0.72	0.68
222	0.68	0.70	0.64	0.75	0.66
333	0.7	0.66	0.69	0.90	0.67
444	0.71	0.74	0.64	0.74	0.69
555	0.70	0.73	0.70	0.85	0.69
666	0.67	0.76	0.67	0.79	0.69
777	0.67	0.68	0.66	0.87	0.7
STDEV	0.019	0.045	0.021	0.071	0.015
AVG	0.68	0.70	0.66	0.80	0.68

C. Prediction errors for Rimonabant at the CB1 receptor

In Figure S1**,** it can be seen that all predicted pChEMBL values for Rimonabant at the CB1 receptor fall within the confidence interval of pChEMBL values which are reported in the ChEMBL database. Although the structure of Rimonabant was present in the training set, this is indicative of a reliable prediction of the K_D values (at the CB1 receptor) used in this study.

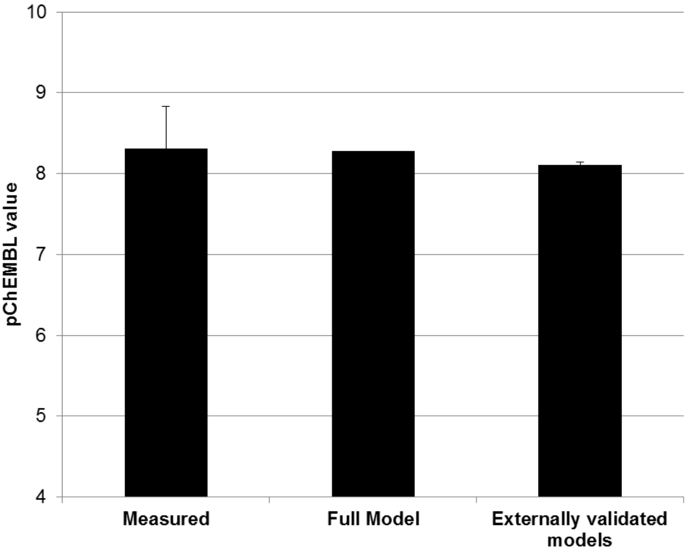

Figure S1. All model predictions for the binding affinity of Rimonabant at the CB1 receptor fall within measured range. The average pChEMBL value and the standard deviation are reported. Measured pChEMBL values include all the reported pChEMBL values for Rimonabant at the CB1 receptor in the ChEMBL database after filtering to obtain a high-quality dataset. Measured: average pChEMBL value is 8.3 with a standard deviation of 0.52. The full model predicted a pChEMBL value of 8.28 for Rimonabant at the CB1 receptor. The average pChEMBL value as predicted by the externally validated models is 8.11 with a standard deviation of 0.03.

Supplemental 5

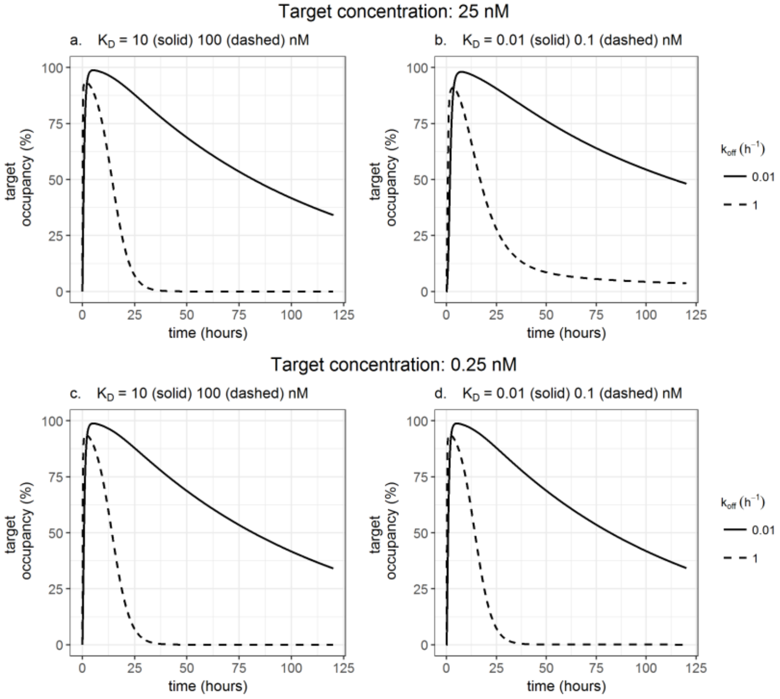

Figure S2. Target concentration and K_D determine the extent of in vivo kinetic target selectivity in Model I. Target selectivity is characterised by a difference in target occupancy between target 1 (solid) and target 2 (dashed). The parameter values for these simulations can be found in Supplemental 1.

Supplemental 6

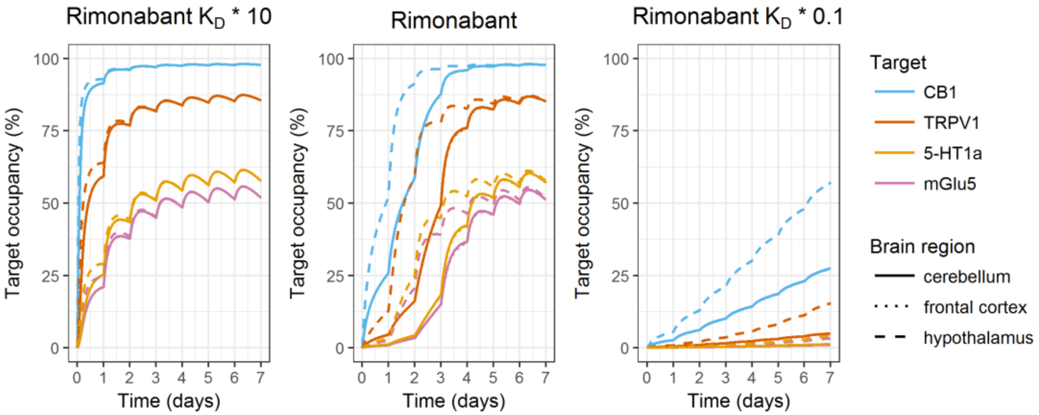

Figure S3. The simulated influence of K_D on the Rimonabant selectivity profile in Model III. Predicted K_D values of Rimonabant at the CB1, 5-HT1a, mGlu5 and TRPV1 receptor were used in these simulations, and multiplied by 10 or 0.1. k_{off} values were assumed to be 10 h^{-1}. A dose of 10^4 nmol was administered every 24 hours. $R_{tot,cer,CB1}$ = 527 nM, $R_{tot,cer,mGlu5}$ = 5.1 nM, $R_{tot,cer,TRPV1}$ = 19 nM, $R_{tot,cer,5\text{-}HT1a}$ = 0.01, $R_{tot,hyp,CB1}$ = 248 nM, $R_{tot,hyp,mGlu5}$ = 16 nM, $R_{tot,hyp,TRPV1}$ = 13 nM, $R_{tot,hyp,5\text{-}HT1a}$ = 2.37, $R_{tot,fc,CB1}$ = 529 nM, $R_{tot,fc,mGlu5}$ = 25 nM, $R_{tot,fc,TRPV1}$ = 12 nM, $R_{tot,fc,5\text{-}HT1a}$ = 1.7.

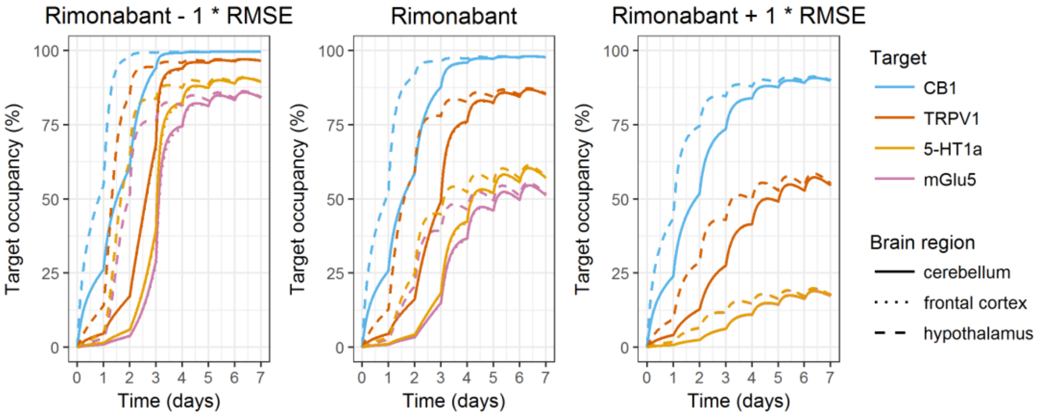

Figure S4. The influence of prediction errors on the simulated Rimonabant selectivity profile in Model III. Predicted K_D values of Rimonabant at the CB1, 5-HT1a, mGlu5 and TRPV1 receptor were used in these simulations. The RMSE values obtained from the external model validation of the QSAR were added or substracted from the predicted pChEMBL value and then converted to the K_D value in nM ($10^{-\text{pChEMBL value}} * 10^9$). k_{off} values were assumed to be 10 h^{-1}. A dose of 10^4 nmol was administered every 24 hours. $R_{tot,cer,CB1}$ = 527 nM, $R_{tot,cer,mGlu5}$ = 5.1 nM, $R_{tot,cer,TRPV1}$ = 19 nM, $R_{tot,cer,5\text{-}HT1a}$ = 0.01, $R_{tot,hyp,CB1}$ = 248 nM, $R_{tot,hyp,mGlu5}$ = 16 nM, $R_{tot,hyp,TRPV1}$ = 13 nM, $R_{tot,hyp,5\text{-}HT1a}$ = 2.37, $R_{tot,fc,CB1}$ = 529 nM, $R_{tot,fc,mGlu5}$ = 25 nM, $R_{tot,fc,TRPV1}$ = 12 nM, $R_{tot,fc,5\text{-}HT1a}$ = 1.7.

Chapter 7. Modelling the delay between PK and EEG effects of morphine in rats; binding kinetic *versus* effect compartment models

Wilhelmus E.A. de Witte[1], Vivi Rottschäfer[2], Meindert Danhof[1], Piet H. van der Graaf[1,3], Lambertus A. Peletier[2], Elizabeth C.M. de Lange[1*].

[1] Division of Pharmacology, Leiden Academic Centre for Drug Research, Leiden University, 2333 CC Leiden, The Netherlands

[2] Mathematical Institute, Leiden University, 2333, CA Leiden, The Netherlands.

[3] Certara Quantitative Systems Pharmacology, Canterbury Innovation Centre, Canterbury CT2 7FG, United Kingdom

* Correspondence: ecmdelange@lacdr.leidenuniv.nl

Manuscript under revision for the Journal of Pharmacokinetics and Pharmacodynamics

Abstract

Introduction. Drug-target binding kinetics (as determined by association and dissociation rate constants, k_{on} and k_{off}) can be an important determinant of the kinetics of drug action. However, the effect compartment model is used most frequently instead of a target binding model to describe hysteresis. Here we investigate when the drug-target binding model should be used in lieu of the effect compartment model.

Methods. We tested the utility of the effect compartment (EC), the target binding kinetics (TB) and the combined effect compartment-target binding kinetics (EC-TB) model on either plasma (EC_{PL}, TB_{PL} and EC-TP_{PL}) or brain extracellular fluid (EC_{ECF}, TB_{ECF} and EC-TP_{ECF}) morphine concentrations and EEG amplitude in rats. We also analyzed when a significant shift in the time to maximal target occupancy ($Tmax_{TO}$) with increasing dose, the discriminating feature between the TB and EC model, occurs in the TB model. All TB models assumed a linear relationship between target occupancy and drug effect on the EEG amplitude.

Results. We found that all three model types performed similarly in describing the morphine PD data, although the EC model provided the best statistical result. Our analysis of the shift in $Tmax_{TO}$ ($\Delta Tmax_{TO}$) as a result of increasing dose revealed that $\Delta Tmax_{TO}$ is decreasing towards zero if the k_{off} is much smaller than the elimination rate constant or if the target concentration is larger than the initial morphine concentration.

Discussion and Conclusion. Our results for the morphine PKPD modelling and the analysis of $\Delta Tmax_{TO}$ indicate that the EC and TB models do not necessarily lead to different drug effect *versus* time curves for different doses if a delay between drug concentrations and drug effect (hysteresis) is described. Drawing mechanistic conclusions from successfully fitting one of these two models should therefore be avoided. Since the TB model can be informed by *in vitro* measurements of k_{on}, either plasma (a target binding model should be considered more often for mechanistic modelling purposes

Abbreviations: AIC: Akaike Information Criterion, CNS: Central Nervous System, DE: Direct Effect, ECF: Extracellular Fluid, EC: Effect Compartment, IE: Indirect Effect, GOF: Goodness Of Fits, IIV: Inter-Individual Variability, OFV: Objective Function Value, PD: Pharmacodynamics, Pgp: P-glycoprotein, PK: Pharmacokinetics, PD: Pharmacodynamics, TB: Target binding, $Tmax_{PD}$: Time between dosing and maximal drug effect, $Tmax_{TO}$: Time between dosing and maximal target occupancy, $\Delta Tmax_{TO}$: $Tmax_{TO}$ of the lower dose - $Tmax_{TO}$ of the higher dose, VPC: Visual Predictive Check

Introduction

Drug-target binding kinetics is an important criterion in the selection of drug candidates, as it can be a determinant of the time course and the selectivity of drug effect.[1–4]

However, the *in vivo* time course of drug action is influenced by multiple factors including plasma pharmacokinetics, target site distribution, target binding kinetics, competition with endogenous ligands, turnover of the target, signal transduction kinetics and the kinetics of homeostatic feedback. As a consequence, the influence of binding kinetics on drug action can only be understood in conjunction with these kinetic processes and its relevance is still not fully understood and subject to an ongoing debate.[3,5–8]

One of the arguments against an important role of binding kinetics for *in vivo* drug action is that binding kinetics are most often not required to get a good fitting PKPD model for small molecules. However, numerous examples are available were binding kinetic models have been successfully applied, and binding kinetics are routinely incorporated in models for biologics and PET data.[9–17] The sparsity of target binding PKPD models for small molecules can be explained by the relatively fast binding kinetics of many drugs currently on the market, compared to their pharmacokinetics.[3] In addition, when a delay between drug concentrations and effect is observed, this delay is often described by an effect compartment or indirect response model.[18,19]

Here we study the difference between the effect compartment (EC) model, the target binding (TB) model the direct effect (DE) and the indirect effect (IE) model which are described below. The EC model describes the delay between pharmacokinetics (PK) and pharmacodynamics (PD) by including first order distribution of the drug into and out of a hypothetical target-site (biophase) compartment, which drives the PD mostly in a nonlinear fashion.[20] The indirect effect (IE) model describes the delay between PK and PD by the zero order synthesis and first order degradation of an effector molecule which represents the PD, mostly in a linear fashion.[21] The target binding (TB) model describes the delay between PK and PD by the second order drug-target association and first order dissociation of the drug-target complex, which drives the effect in a linear or nonlinear fashion, depending on the efficacy and receptor reserve.[22–24] The DE model describes no delay between the PK and PD and links the drug concentration directly to the effect measurements in a linear or nonlinear fashion.

These models thus result in a zero, first and second order formation of the compounds that drives the PD, being the drug concentration in the effect compartment, the target-bound drug concentrations and the endogenous effector molecule in the EC, TB and IE model, respectively. This results in different dose dependencies of the time to the maximal effect $Tmax_{PD}$. As a current paradigm, the shift in $Tmax_{PD}$ ($\Delta Tmax_{PD}$) in a PKPD dataset as a consequence of a change in the dose, identifies the appropriate PKPD model to describe the data: with increasing dose, the $Tmax_{PD}$ can increase for the indirect response model, decrease for the TB model and is constant for the EC model.[25–27]

However, in contrast to common belief, the indirect response model does not always result in an increasing $Tmax_{PD}$ with increasing doses but can also give rise to a decreasing $Tmax_{PD}$ with increasing doses, as shown by Peletier et al.[28] A comprehensive analysis of the conditions for which a shift in $Tmax_{TO}$ for changing doses occurs in a TB model is currently not available. It might be that EC models have been used while TB models could have been applied equally well to describe the data in previous PKPD studies.

One example in which performance of TB and EC models has been investigated indicates comparable performance in describing the data of eight calcium channel blockers, but this study used only one dose level for all drugs[14] and therefore cannot be used to validate the relationship between dose and $\Delta Tmax_{PD}$. An additional complexity in choosing the most appropriate PKPD model to describe PKPD data is that, for most drugs, factors as target site distribution, drug-target binding and turnover of signaling molecules occur in parallel. It is not always needed to incorporate all these factors in the PKPD model, as only the rate limiting mechanism is required for a proper model fit that describes the observed data. However, leaving out such factors will never lead to understanding of the individual contributions and the interplay between these factors. Combined EC-TB models[13,29,30] as well as combined IE-TB models[10] have been applied successfully to discriminate between the contributions of separate factors. However, this discrimination is not always possible if one of the factors is relatively fast and does not contribute significantly to the delay between PK and PD.[31–33]. In short, the relevance of drug-target binding kinetics cannot be excluded if one of the other models is successfully fitted to a dataset, and there is a need to generate more insight into the difference between the TB model and the EC model.

The aim of the current study is to investigate if the TB and EC model can give similar drug effect *versus* time curves and under what conditions this will occur. In this study, we used a historical PKPD dataset for morphine [34] to compare the goodness of fit for the TB model with the EC model and the combined EC-TB model in describing the time course of the EEG effect following administration of 3 different doses of morphine (4, 10 and 40 mg/kg). Both plasma and brain ECF drug concentrations were measured and tested in this study to be connected to the PD via an EC, TB or EC-TB model. Subsequently, a more general insight in the shift of $Tmax_{TO}$ for different dose levels in the drug-target binding model is obtained to identify for what parameter values the TB model can be discriminated from the EC model based on the $\Delta Tmax_{TO}$. To that end, we performed comprehensive simulations and mathematical model analysis for a wide range of drug-target association and dissociation rate constants, for various plasma elimination rate constants, target concentrations, and dose levels.

Methods

Pharmacokinetic and pharmacodynamic (PKPD) data of morphine in rats

All PK and PD data used in this study were obtained from the experiments described earlier.[35] In short: Morphine was intravenously administered to Male Wistar rats, during a 10-minute infusion, in 4 different dose groups: 0, 4, 10 or 40 mg/kg with 5, 29, 11 and 14 animals, respectively. The P-glycoprotein (Pgp) inhibitor GF120918 or vehicle was given as a continuous infusion. In the group of 29 animals that received 4 mg/kg morphine, 9 animals received GF120918, the other 20 animals received the vehicle. Furthermore, while plasma concentrations were measured in all animals, brain ECF concentrations were measured with microdialysis in 29 animals, of which 15 received 4 mg/kg, 0 received 10 mg/kg, 9 received 40 mg/kg and 5 received 0 mg/kg morphine.

For the modelling data set, all data entries without time recordings, without concentration data or with concentration data equal to 0 were removed from the dataset. The lower limit of quantification for morphine in plasma samples was 88 nM and 1.75 nM for morphine in ECF samples. The PD of morphine was measured as the amplitude in the δ frequency range (0.5-4.5 Hz) of the EEG, and recorded every minute. The EEG data were further averaged for every 3-minute interval to reduce the noise and decrease the model fitting time.

General model fitting methods

Data fitting was based on minimization of the Objective Function Value (OFV = − 2*log likelihood) as implemented in NONMEM 7.3.[36] To account for the number of parameters for the comparison of non-nested models, the Akaike Information Criterion (AIC) was calculated by adding two times the number of estimated parameters to the OFV.[37] Variability in the data was described by IIV (Inter Individual Variability: variability in parameter values between animals) and a residual error term. IIV was implemented assuming a log-normal distribution according to equation 1:

$$P_i = P_{pop} * e^{\eta_i} \qquad (1)$$

In which P_i is the individual parameter value, P_{pop} is the typical parameter value in the population and η_i is normally distributed around a mean of zero with variance ω^2 according to equation 2:

$$\eta_i \sim N(0, \omega^2) \tag{2}$$

The remaining variation between the data and the model predictions are incorporated as residual error for which both a proportional (equation 3) and a combined proportional and additive (equation 4) error model were tested.

$$obs_{ij} = pred_{ij} * (1 + \varepsilon_{prop,ij}) \tag{3}$$

$$obs_{ij} = pred_{ij} * (1 + \varepsilon_{prop,ij}) + \varepsilon_{add,ij} \tag{4}$$

In these equations, obs_{ij} is the observation, $pred_{ij}$ is the model prediction, $\varepsilon_{prop,ij}$ is the proportional error and $\varepsilon_{add,ij}$ is the additive error for individual *i* at time point *j*. Both $\varepsilon_{prop,ij}$ and $\varepsilon_{add,ij}$ are normally distributed around a mean of zero with variance σ^2 according to equation 5 and 6:

$$\varepsilon_{prop,ij} \sim N(0, \sigma^2) \tag{5}$$

$$\varepsilon_{add,ij} \sim N(0, \sigma^2) \tag{6}$$

Morphine plasma PK modelling

One-compartment, two-compartment and three-compartment models were fitted to the plasma PK data, with both proportional and additive plus proportional error models, and with IIV on the various parameters. The best fits (based on AICs) of each structural model were compared for their GOFs (Goodness Of Fits) and AICs. Since the purpose of the plasma PK modelling was to get the best possible input for the PD modelling, GOF was assessed by the AIC and by individual fits. Over- or underestimation of IIV and population parameter estimates and high uncertainties in population parameter estimates were not regarded as problematic, since only the right individual parameter estimates were required for PD modeling.

Morphine brain ECF PK Modelling

The individual parameter estimates that were estimated to describe the plasma PK were used as fixed parameters to describe the plasma PK profile as input for the brain ECF concentrations. To describe the ECF concentrations, we thus assumed that the distribution of the drug into and out of the ECF did not lead to a change in plasma concentrations. The best fits, based on the AICs, of each structural model were compared for their GOFs (Goodness Of Fits) and AICs. Since the purpose of the brain ECF PK modelling was to get the best possible input for the PD modelling, GOF was assessed by the AIC and by individual fits. Over- or underestimation of IIV and population parameter estimates and high uncertainties in population parameter estimates were not regarded as problematic, since only the right individual parameter estimates were required for PD modeling.

EEG PD modelling

To maximize the identifiability of the PD model parameters, all pharmacokinetic parameters were used as fixed parameters to describe the plasma and brain ECF concentrations as input for all the described PD models to describe EEG effects.[38] The different type of models that were tested are outlined in Table 1. For each model, the most informative variations on the model structure are given in the results section.

Table 1. Overview of the different model types, the data that were used and the model numbers as used in this manuscript. EC = Effect compartment, TB = target binding, EC-TB = effect compartment – target binding. IE = indirect effect, DE = direct effect and ECF = brain extracellular fluid.

Model type	Concentrations linked to effect	Model number
EC	PLasma	$EC_{PL}1 – EC_{PL}4$
EC	ECF	$EC_{ECF}1$
TB	PLasma	$TB_{PL}1 – TB_{PL}5$
TB	ECF	$TB_{ECF}1$
EC-TB	PLasma	$ECTB_{PL}1 – ECTB_{PL}5$
IE	ECF	$IE_{ECF}1$
DE	ECF	$DE_{ECF}1$

To compare structural models that linked plasma or brain ECF concentrations directly to the PD, the models that used plasma PK were fitted to the reduced dataset that only contained animals with plasma PK, brain ECF and EEG measurements. Model comparison was based on the AIC, visual inspection of the GOF and a VPC (Visual Predictive Check) to check if the IIV was captured appropriately.

Drug-target binding model simulations

Simulations with a one-compartment binding model with IV administration were performed for a wide range of k_{on} and k_{off} values and for a variety of elimination rate constants, target concentrations and drug dose levels. The $Tmax_{TO}$ was compared for 2 different doses to determine the influence of the drug dose on the $Tmax_{TO}$. The $\Delta Tmax_{TO}$ values were calculated by subtracting the $Tmax_{TO}$ of the highest dose from the $Tmax_{TO}$ of the lowest dose and $\Delta Tmax_{TO}$ was plotted against k_{on} and k_{off}.

Results

Morphine PK modelling

Modelling of morphine pharmacokinetic data in plasma and brain ECF as described in Supplement S 1 identified very similar model structures as previously described for pharmacokinetic modelling of the same dataset by Groenendaal and coworkers.[35] In short, the plasma concentrations were described by a 3-compartment model and the ECF concentrations were described by passive distribution into and out of the brain combined with saturable active influx and first-order efflux.

EEG PD modelling

EC_{PL} model fitting

EC and TB models have been applied to the morphine data to describe the relationship between the observed plasma concentrations and EEG amplitude and direct effect (DE) indirect effect (IE), EC and TB models have been applied to brain ECF and EEG amplitude data. The differential equations for these models are given in Supplement S 1. Firstly, the originally published EC_{PL} model structure was optimized by adding a slope parameter which describes the linear decline of EEG amplitude over time during the experiment independent of the drug effect, and including IIV on the baseline EEG amplitude only. For this model, a transit compartment was required between the plasma and the effect compartment.[34] An overview of the different variations on this basic model structure is given in Table 2. The structure of all EC_{PL} is identical and is depicted in Figure 1. Based on the AIC, the parameter estimates and the GOF, model $EC_{PL}1$ was chosen as the best parameterization for the effect compartment model in Figure 1.

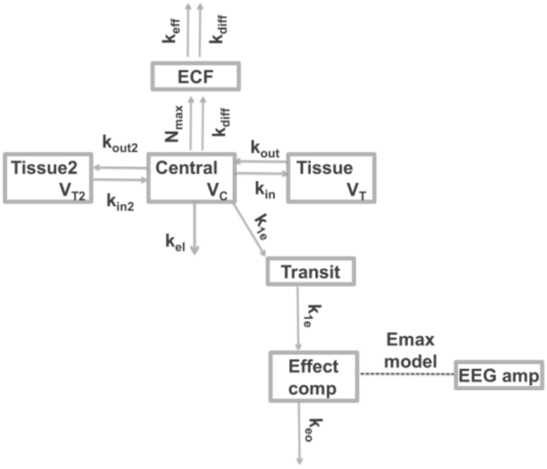

Figure 1. Schematic representation of the EC$_{PL}$ model structure that was used to describe the morphine EEG amplitudes over time. k_{ie} = first-order in- and outward distribution rate constant for the transit compartment. k_{eo} first-order outward distribution rate constant from the effect compartment. The effect compartment concentrations were linked to the EEG amplitude by a sigmoidal Emax model. The distribution from plasma to the tissue compartments and the brain ECF compartment is described in Supplement S 1. The arrows indicate morphine flows, the dotted line indicates a direct relationship.

Table 2. Parameter values and objective function values of the tested EC models describing the EEG data based on plasma concentrations. CV denotes the coefficient of variation as percentage. OFV denotes the Objective Function Value, AIC denotes the Akaike Information Criterion. ω^2 and σ^2 denote the variances of the exponential IIV distribution and the error distribution, respectively.

	EC$_{PL}$1 selected model	**EC$_{PL}$2 no slope**	**EC$_{PL}$3 $k_{1e} = k_{eo}$**	**EC$_{PL}$4 no Pgp effect**
OFV	44748.0	45084.2	44853.3	44868.4
AIC	44770.0	45104.2	44871.3	44886.4
parameter	**Value (%CV)**	**Value (%CV)**	**Value (%CV)**	**Value (%CV)**
k_{1e}(/min)	0.0393 (18)	0.0432 (10)	0.0403 (10)	0.0375 (8)
k_{eo}(/min)	0.0382 (14)	0.0458 (9)	-	0.0375 (8)
k_{1e} -Pgp (/min)	0.0565 (44)	0.0661 (38)	0.0295 (18)	-
k_{eo} -Pgp (/min)	0.016 (46)	0.0203 (20)	-	-
E_0 (µV)	45.1 (4)	42.2 (4)	45.8 (4)	45.9 (4)
E_{max} (µV)	27.9 (23)	25.3 (16)	26.1 (18)	27.0 (18)
EC_{50} (nM)	1270 (52)	1220 (31)	912 (37)	1000 (37)
N_H	1.44 (43)	2.02 (27)	1.46 (36)	1.37 (33)
slope (µV/min)	-0.024 (22)	0 FIX	-0.0263 (15)	-0.0267 (15)
ω^2 E_0 (µV)	0.111 (20)	0.125 (19)	0.115 (20)	0.116 (20)
σ^2 proportional	0.0554 (7)	0.0584 (7)	0.0562 (6)	0.0564 (6)

TB$_{PL}$ model fitting

The TB$_{PL}$ model was applied to describe target binding from plasma, all TB$_{PL}$ models in Table 3 shared the same structure as represented in Figure 2. The parameter estimation results are given in Table 3. Since the target concentration is of influence only if it is similar to the drug concentration (which is mostly above 100 nM in plasma and in brain ECF, as shown in Supplement S 1), the target concentration could not be estimated in this model and was fixed to an arbitrary low value of 1 nM in the model estimations. This low target concentration prevents the influence of the target concentration on the EEG amplitude in the model. The influence of blocking Pgp has been incorporated by estimating separate parameter values with and without the presence of Pgp blocker. While the influence of blocking Pgp on the k_{off} or K_D is mechanistically not plausible, the improved model fits for the models which incorporate these influences might indicate that the estimated k_{off} and K_D values refer to apparent values which include not only the molecular properties. The target occupancy is linearly related to the EEG amplitude in model $TB_{PL}1$ - $TB_{PL}5$, as nonlinear relationships could not be identified accurately in this study. On basis of the objective function values, model $TB_{PL}4$ was selected as the best drug-target binding model. It should be noted that the AIC of model $TB_{PL}4$ is 338 points higher than model $EC_{PL}1$, which means that model $EC_{PL}1$ performs better in fitting the data. All TB_{PL} models have one compartment less than the transit-EC models $EC_{PL}1$ - $EC_{PL}4$. Therefore, the combined EC-TB_{PL} models EC-$TB_{PL}1$ - EC-$TB_{PL}5$ were developed.

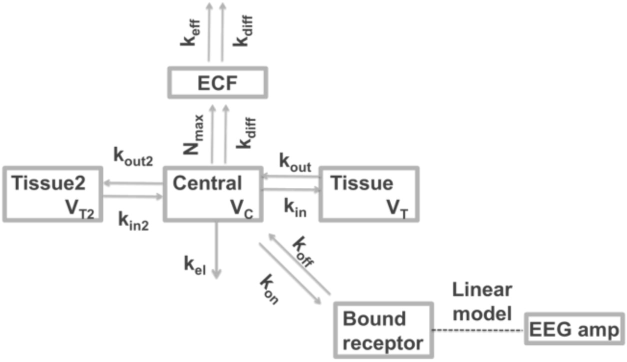

Figure 2. Schematic representation of the TB_{PL} model structure that was used to describe the morphine EEG amplitudes over time. k_{on} is the second-order drug-target association rate constant. k_{off} is the first-order drug-target dissociation rate constant. Target occupancy is linearly related to the EEG amplitude. The distribution from plasma to the tissue compartments and the brain ECF compartment is described in Supplement S 1. The arrows indicate morphine flows, the dotted line indicates a direct relationship.

Table 3. Parameter values and objective function values of the tested TB_{PL} models describing the EEG data based on plasma concentrations. CV denotes the coefficient of variation as percentage. OFV denotes the Objective Function Value, AIC denotes the Akaike Information Criterion. ω^2 and σ^2 denote the variances of the exponential IIV distribution and the error distribution, respectively.

	$TB_{PL}1$ no Pgp effect slope = 0	**$TB_{PL}2$ no Pgp effect**	**$TB_{PL}3$ Pgp on k_{off}**	**$TB_{PL}4$ Selected model**	**$TB_{PL}5$ slope = 0**
OFV	45677.7	45170.1	45166.6	45092.1	45536.9
AIC	45689.7	45184.1	45182.6	45108.1	45550.9
parameter	**Value (%CV)**	**Value (%CV)**	**Value (%CV)**	**Value (%CV)**	**Value (%CV)**
k_{off} (/min)	0.017 (8)	0.0103 (13)	0.0109 (17)	0.009 (26)	0.0149 (15)
k_{off} -Pgp (/min)	-	-	0.0087 (26)	-	-
K_D (nM)	1980 (37)	995 (36)	935 (37)	1570 (59)	3610
K_D -Pgp (nM)				381 (88)	715
E_0 (µV)	42.4 (4)	45.9 (4)	45.8 (4)	45.4 (4)	42.2
E_{max} (µV)	32.2 (14)	29.3 (13)	28.9 (13)	32.9 (20)	38.9
R_{tot} (nM)	1 FIX	1 FIX	1 FIX	1 FIX	1 FIX
slope (µV/min)	0 FIX	-0.0313 (13)	-0.0315 (12)	-0.0299 (12)	0 FIX
ω^2 E_0 (µV)	0.135 (18)	0.117 (20)	0.117 (20)	0.113 (19)	0.13 (17)
σ^2 proportional	0.0639 (6)	0.059 (6)	0.059 (6)	0.0584 (6)	0.0626 (6)

EC-TB$_{PL}$ model fitting

The EC-TB$_{PL}$ model structure that was tested to describe the EEG data is shown in Figure 3. The parameter values, OFVs and AICs are given in **Table 4**. Model EC-TB$_{PL}$1 was selected as best model on basis of the AIC, but this AIC is still 39 points higher than Model EC$_{PL}$1. The uncertainty in the parameter estimate of the K_D in the presence of the Pgp blocker (K_D –Pgp) is rather high with 93%, but this was allowed to test the conclusion that none of the binding models (TB$_{PL}$1 - TB$_{PL}$5 and EC-TB$_{PL}$1 - EC-TB$_{PL}$5) yielded lower AICs than the best effect compartment model (EC$_{PL}$1) in a conservative manner.

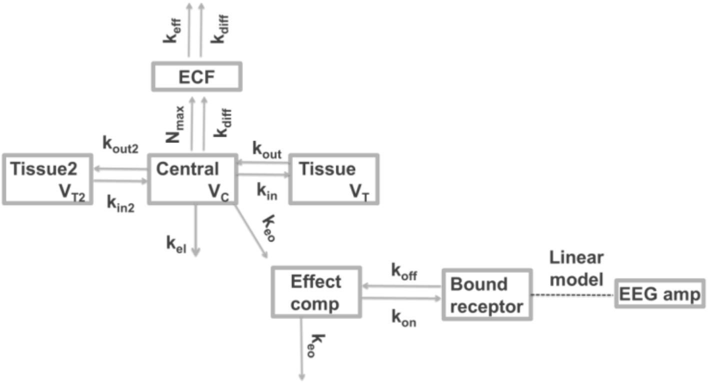

Figure 3. Schematic representation of the EC-TB$_{PL}$ model structure that was used to describe the morphine EEG amplitudes over time. k_{on} is the second-order drug-target association rate constant. k_{off} is the first-order drug-target dissociation rate constant. k_{eo} is the first-order distribution rate constant into and out of the effect compartment. Target occupancy is linearly related to the EEG amplitude. The distribution from plasma to the tissue compartments and the brain ECF compartment is described in Supplement S 1. The arrows indicate morphine flows, the dotted line indicates a direct relationship.

Table 4. Parameter values and objective function values of the tested EC-TB$_{PL}$ models describing the EEG data based on plasma concentrations. CV denotes the coefficient of variation as percentage. OFV denotes the Objective Function Value, AIC denotes the Akaike Information Criterion. ω^2 and σ^2 denote the variances of the exponential IIV distribution and the proportional error distribution, respectively.

	EC-TB$_{PL}$1 Selected model	**EC-TB$_{PL}$2 no Pgp effect**	**EC-TB$_{PL}$3 Pgp on k_{eo}**	**EC-TB$_{PL}$4 k_{off} = 1**	**EC-TB$_{PL}$5 slope = 0**
OFV	44790.9	44880.3	44873.8	45008.2	45235.3
AIC	44808.9	44896.3	44891.8	45024.2	45251.3
parameter	**Value (%CV)**	**Value (%CV)**	**Value (%CV)**	**Value (%CV)**	**Value (%CV)**
k_{off} (/min)	0.0275 (14)	0.0243 (14)	0.0247 (14)	1 FIX	0.0400 (9)
k_{eo} (/min)	0.0327 (17)	0.0365 (12)	0.0389 (14)	0.0162 (28)	0.036 (13)
k_{eo} -Pgp (/min)	-	-	0.0265 (31)	-	-
K_D (nM)	1520 (34)	1150 (30)	1110 (30)	2110 (50)	3150 (36)
K_D -Pgp (nM)	296 (93)	-	-	385 (78)	594 (47)
E_0 (µV)	45.0 (4)	45.7 (4)	45.6 (4)	45.2 (4)	41.9 (4)
E_{max} (µV)	31.8 (11)	30.7 (11)	30.5 (11)	34.4 (18)	37.3 (12)
R_{tot} (nM)	1 FIX	1 FIX	1 FIX	1 FIX	1 FIX
slope (µV/min)	-0.0276 (15)	-0.0296 (13)	-0.0296 (13)	-0.0273 (14)	0 FIX
ω^2 E_0 (µV)	0.111 (20)	0.116 (20)	0.116 (20)	0.111 (19)	0.129 (18)
σ^2 proportional	0.057 (7)	0.0565 (7)	0.0565 (7)	0.0576 (7)	0.0597 (7)

EC_{ECF}, TB_{ECF}, IE_{ECF} and DE_{ECF} model fitting

The last models that were fitted to the EEG data were based on the ECF concentrations instead of the plasma concentrations. Various model structures were tested, as shown in Figure 4. To compare the model fits based on ECF concentrations ($EC_{ECF}1$, $TB_{ECF}1$, $IE_{ECF}1$ and $DE_{ECF}1$) with the model fits that were based on plasma concentrations (EC_{PL}, TB_{PL} and EC-TB_{PL}), the best plasma model ($EC_{PL}1$) was fitted to the limited dataset that included only animals with ECF data. This model fit was compared to the ECF-based model fits on basis of their AICs, as shown in **Table 5**.

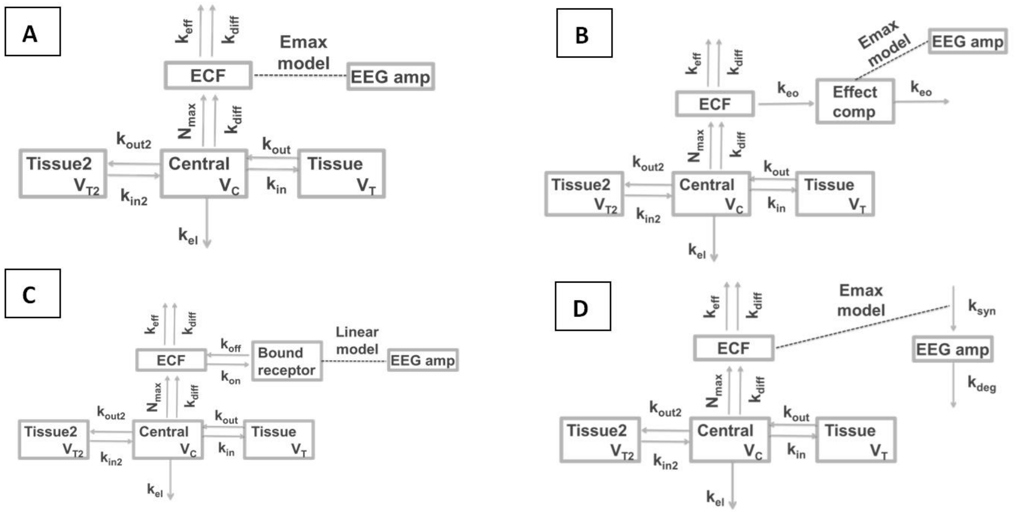
A
k_{eff}
k_{diff}
Emax model
ECF
EEG amp
N_{max}
k_{diff}
k_{out2}
k_{out}
Tissue2 V_{T2}
Central V_C
Tissue V_T
k_{in2}
k_{in}
k_{el}
B
Emax model
EEG amp
k_{eff}
k_{diff}
k_{eo}
Effect comp
k_{eo}
ECF
N_{max}
k_{diff}
k_{out2}
k_{out}
Tissue2 V_{T2}
Central V_C
Tissue V_T
k_{in2}
k_{in}
k_{el}
C
k_{eff}
k_{diff}
k_{off}
Bound receptor
Linear model
ECF
EEG amp
k_{on}
N_{max}
k_{diff}
k_{out2}
k_{out}
Tissue2 V_{T2}
Central V_C
Tissue V_T
k_{in2}
k_{in}
k_{el}
D
k_{eff}
k_{diff}
Emax model
k_{syn}
ECF
EEG amp
k_{deg}
N_{max}
k_{diff}
k_{out2}
k_{out}
Tissue2 V_{T2}
Central V_C
Tissue V_T
k_{in2}
k_{in}
k_{el}

Figure 4. Schematic representation of the EC_{ECF}, TB_{ECF}, IE_{ECF} and DE_{ECF} model structures that were used to describe the EEG data based on brain ECF concentrations. The different structures represent A) the DE_{ECF} model, B) the EC_{ECF} model, C) the TB_{ECF} model and D) the IE_{ECF} model, with k_{syn} being the zero-order effect generation rate constant, and k_{deg} being the first-order effect degradation rate constant. The distribution from plasma to the tissue compartments and the brain ECF compartment is described in Supplement S 1. The arrows indicate morphine flows, the dotted line indicates a direct relationship.

Table 5. Parameter values and objective function values of the tested models describing the EEG data based on ECF concentrations. CV denotes the coefficient of variation as percentage. OFV denotes the Objective Function Value, AIC denotes the Akaike Information Criterion. ω^2 and σ^2 denote the variances of the exponential IIV distribution and the proportional error distribution, respectively.

[a] This value was estimated as the maximal k_{syn} minus baseline k_{syn} (calculated from E_0 and k_{deg}) and

	$EC_{PL}1$ ref. model	**$TB_{ECF}1$ binding model**	**$DE_{ECF}1$ direct effect**	**$EC_{ECF}1$ effect compartment**	**$IE_{ECF}1$ indirect effect**
OFV	25996.1	26284.1	26284.0	26255.1	26240.3
AIC	26118.1	26300.1	26300.0	26273.1	26258.3
parameter	**Value (%CV)**	**Value (%CV)**	**Value (%CV)**	**Value (%CV)**	**Value (%CV)**
k_{1e}(/min)	0.0457 (35)	-	-	-	-
k_{eo}(/min)	0.0377 (41)	-	-	0.161 (40)	-
k_{1e} -Pgp (/min)	0.0647 (36)	-	-	-	-
k_{eo} -Pgp (/min)	0.0155 (77)	-	-	-	-
E_0 (μV)	47.6 (6)	48.9 (6)	48.9 (6)	49.1 (6)	49.1 (6)
E_{max} (μV)	27.5 (20)	32.7 (17)	23.4 (18)	24.9 (19)	25.4[a] (36)
E_{max} –Pgp (μV)	-		41.6 (14)	43.2 (15)	43.3 (42)
EC_{50} (nM)	1100 (87)	-	173 (22)	182 (26)	182 (25)
N_H	2.05 (49)		2.3 (41)	2.02 (43)	2.07 (43)
slope (μV/min)	-0.0235 (34)	-0.0400 (17)	-0.0359 (17)	-0.0373 (19)	-0.0377 (19)
k_{off} (/min)	-	0.0932 (37)	-	-	-
K_D	-	283 (40)	-	-	-
K_D -Pgp	-	55.9 (15)	-	-	-
k_{deg} (/min)					0.124 (34)
ω^2 E_0 (μV)	0.0668	0.0668 (26)	0.072 (25)	0.0696 (26)	0.0961 (26)
σ^2 proportional	0.0550 (10)	0.0598 (10)	0.0598 (10)	0.0593 (10)	0.059 (10)

calculated by dividing the estimated value by the k_{deg}.

Of all the models that are described above, model $EC_{PL}1$ has the lowest AIC. To evaluate its performance in more detail, the most relevant diagnostic plots are given in Figure S 6 to Figure S 10. These diagnostic plots indicate that the main trend of the data is captured, although the obtained fit is not optimal (which is especially clear from Figure S 10). The small difference in AIC between the best combined EC-TB model (EC-$TB_{PL}1$) and the best EC model ($EC_{PL}1$) is also reflected by very similar VPC results, as shown in Figure S 11. Moreover, the best model with only binding from plasma($TB_{PL}4$) also provided a similar VPC result (see Figure S 12).

Dose-dependency of $Tmax_{TO}$ in a TB_{PL} model

Our simulations of drug-target binding in a TB_{PL} model for the range of the most relevant binding kinetics demonstrated that the observable influence of dose on $Tmax_{TO}$, which discriminates the TB model from the EC model, is limited to a confined range of k_{on} and k_{off} combinations. As visualized in Figure 5, if the k_{off} has a value around the elimination rate constant of 0.03/hr $\Delta Tmax_{TO}$ is maximal. Also, the initial drug concentration C0 should not be above a specific threshold value which is approximately equal to the target concentration. The absolute $\Delta Tmax_{TO}$ for different doses (as shown in Figure 5) will be most relevant for the identification of the dose-dependent $\Delta Tmax_{TO}$ in a PKPD modelling study. However, for the understanding of the underlying determinants of this shift in $\Delta Tmax_{TO}$, the ratio of the $\Delta Tmax_{TO}$ values belonging to the 2 doses should also be considered, as shown in Figure 6. For example, if the two different $Tmax_{TO}$ values obtained from the two doses are 1 and 3 minutes, their ratio is 3, but the absolute difference is 2 minutes. If the two $Tmax_{TO}$ values are 1 and 3 hours, their ratio is still 3, but the difference is now 2 hours. In this latter case, the influence of the dose on the $Tmax_{TO}$ will be more easily identified. Representative example simulations that can help to understand the characteristics of Figure 5 are provided in Supplement S 2.

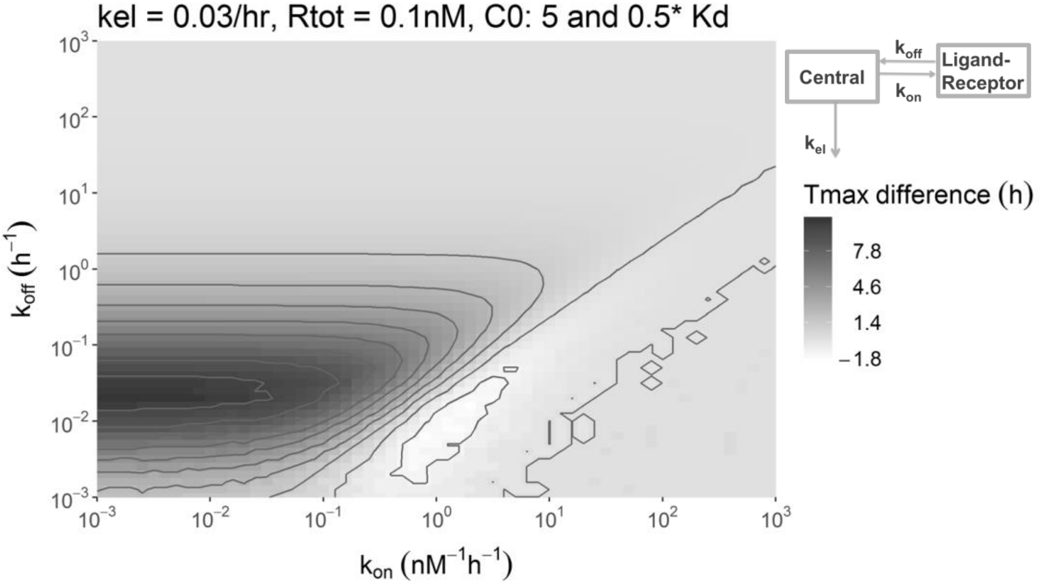

Figure 5. Overview of the shift in $Tmax_{TO}$ that was observed in the simulations with the TB_{PL} model (see upper-right corner) as a result of the change in the affinity-normalized dose (leading to an initial concentration of 5 and 0.5 times the K_D). The elimination rate constant k_{el} was 0.03/hr and the target concentration was 0.1 nM for all simulations in this figure.

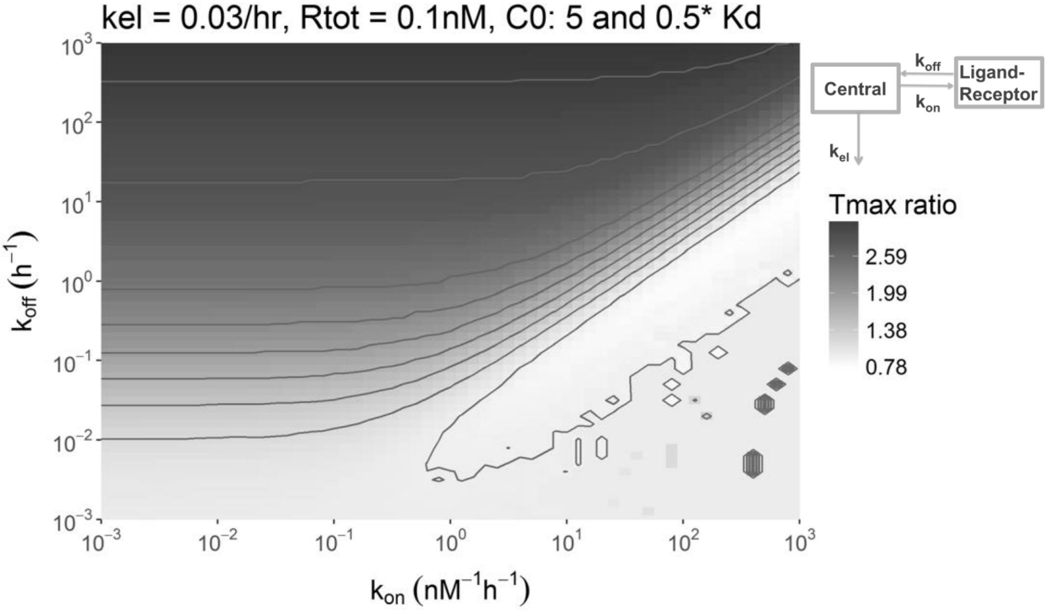

Figure 6. Overview of the ratio of $Tmax_{TO}$ values that was observed in the simulations with the TB_{PL} model (see inset) as a result of the change in the affinity-normalized dose (leading to an initial concentration of 5 and 0.5 times the K_D). The elimination rate constant k_{el} was 0.03/hr and the target concentration was 0.1 nM for all simulations in this figure.

Interestingly, the relationship between the $\Delta Tmax_{TO}$, the elimination rate constant, the target concentration and the dose could be approximated mathematically for the upper region, the lower-left region and the lower-right region of Figure 5 as presented in Supplement S 3. From this analysis, it follows that for the upper half of Figure 5, where the k_{off} is much larger than the k_{el}, $Tmax_{TO}$ is always small, and a significant $\Delta Tmax_{TO}$ will thus not be observed. For the lower and the lower-right part of Figure 5, where the k_{off} is much smaller than the k_{el}, it is found that $Tmax_{TO}$ does not depend on the dose. More specifically, when the initial drug concentration is much lower than the target concentration (and k_{off} is smaller than k_{el}), the $Tmax_{TO}$ is merely determined by the k_{el}. On the other hand, when the initial drug concentration is much larger than the target concentration (and k_{off} is smaller than k_{el}), the $Tmax_{TO}$ is given by a relation between k_{off} and k_{el}. This relationship between the $\Delta Tmax_{TO}$, the elimination rate constant, the target concentration and the dose is illustrated in Figure 7.

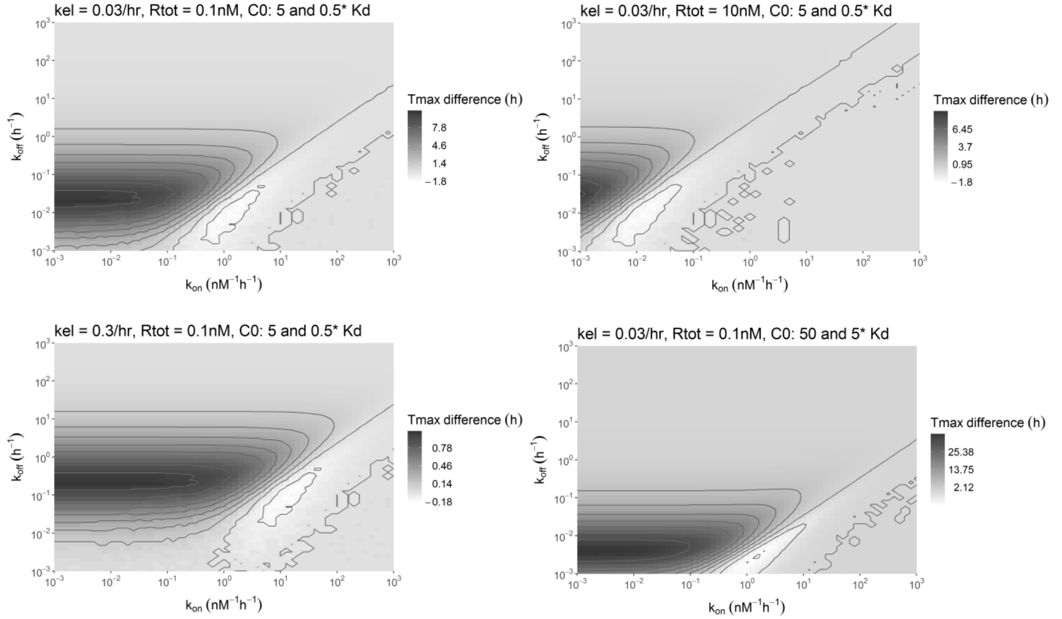

Figure 7. Overview of the $\Delta Tmax_{TO}$ that was observed in the simulations as a result of the change in the affinity-normalized dose for different combinations of parameter values as indicated above the panels. All panels vary only one parameter compared to the upper left panel.

Discussion

In this study, we compared TB and EC models to describe the delay between morphine plasma concentrations and EEG effects for 3 different dose levels. We found that model discrimination was difficult to obtain and that selection of the best model (the EC_{PL} model in this study) was only possible on basis of the objective function value differences. Moreover, our simulation study with the TB_{PL} model showed that a shift in $Tmax_{TO}$ with increasing doses, the distinctive future of the TB model compared to the EC model, only occurs for a limited range in parameter values. Both a k_{off} value much smaller and much larger than the k_{el} value and a target concentration larger than the initial drug concentration decrease this shift in $Tmax_{TO}$ towards zero.

Since our model simulations show that the $Tmax_{TO}$ does not depend on the dose for k_{off} values much lower than the k_{el} and target concentrations much higher than the initial drug concentration, this means that the TB_{PL} model for these parameter values behaves like an EC_{PL} model, with a first order increase and decrease in the concentration that is linked to the effect. Together with the small differences in EC and TB model fits to the morphine EEG data, this shows that for many parameter combinations, a TB model gives rise to similar drug effect profiles as an EC model. This means that neither a successful fit of a TB or EC model necessarily supports the relevance of target binding or target site distribution, respectively, while a single successful fit is often presented as such support[11,23,39]. To obtain support for one of the two mechanisms, both models should be fitted to the data and compared on basis of objective metrics such as the AIC. This approach demonstrated the added value of the combined EC-TB_{PL} model compared to the EC_{PL} and the TB_{PL} model for buprenorphine and AR-HO47108.[13,29] However, this method also demonstrated that the TB_{PL} model performed similarly as the EC_{PL} model for eight calcium antagonists[14] and that the EC model performed similarly as the EC-TB_{PL} model for fentanyl [13]. This demonstrates that even if objective metrics are used, discrimination between two models is not always possible. Moreover, obtained model discrimination strictly informs on the data fit of each model, not directly on the plausibility of the represented mechanism. The TB model should be considered and tested more often as alternative to the EC model, as its parameters can be measured *in vitro*/*ex vivo*, which enables a better *in vitro-in vivo* extrapolation (IVIVE).

In this study, we also found that the models based on brain ECF concentrations did not perform better than the models based on plasma concentrations. One would expect that the brain ECF concentrations would reflect the target site concentration better than the plasma concentrations, especially if brain distribution is relatively slow and nonlinear, as it was in this study. The inferior performance of the brain ECF-based models might be explained by the extremely high variability in the brain ECF data of the 4 mg/kg dose group, as shown in Figure S 5. However, a direct effect model ($DE_{ECF}1$) could be identified from the brain ECF concentrations and showed an only 39 points higher AIC than the best model $IE_{ECF}1$, while such a model fit could not be obtained from the plasma concentrations, indicating that the ECF concentrations reflect the target site concentration more closely compared to the plasma concentrations. This is in line with the relevance of drug concentrations in the brain for CNS effects that has been demonstrated by several other studies[40–43] and the difference between plasma and brain concentrations that has been identified for several compounds[44]. In all our target binding models, a linear target occupancy-effect relationship had to be assumed to keep the model parameters identifiable. Such a linear relationship has been observed and can be expected unless for full agonists in tissues with relatively high target concentrations compared to the concentration of signal transduction molecules (i.e. for a high receptor reserve).[24]

Only a one compartment pharmacokinetic model was used in this study in combination with the simplest TB_{PL} model to investigate the $\Delta Tmax_{TO}$. We expect that the same principles apply if the TB_{PL} model has a two-compartment or three compartment pharmacokinetic models or with target turnover or signal transduction models, but the parameter range for which $Tmax_{TO}$ shifts with a change in dose might be different compared to the model used in our simulations. In analogy to Figure 7, for the combined EC-TB model one would expect that to obtain a significant $\Delta Tmax_{TO}$ and to identify the TB model in addition to the EC model, the k_{e0} should be in the same order of magnitude as the k_{off} if the maximal drug concentration is around or below the K_D. This is indeed the case for the two successful examples of a EC-TB_{PL} fit: for buprenorphine, the k_{e0} was 0.0242 min^{-1} and the k_{off} was 0.0731 min^{-1}[13] and for AR-HO47108, the k_{e0} was 0.0351 for the drug and 0.00749 for its metabolite and the k_{off} was 0.00303 min^{-1} and 0.00827 min^{-1}, respectively[29]. On the other hand, the combined EC-TB model EC-$TB_{PL}1$ that was identified in this study for morphine also showed a similar value for k_{e0} and k_{off} (0.0327 and 0.275, respectively), but this model was not better than the EC model $EC_{PL}1$. In comparison with our one compartment PK model with intravenous dosing, especially the absorption or the distribution phase into the target site could pose additional limiting factors that prevent a shift in $Tmax_{TO}$ with increasing doses.

One of the most important advantages of the EC model is that it only requires one parameter, k_{e0}. However, the EC model most often needs to be combined with an Emax model, which also requires two or three parameters, Emax, EC_{50} and possibly the hill factor. The binding model has 3 parameters, k_{on}, k_{off} and R_{tot}, and needs at least 1 additional parameter, Emax, to convert occupancy predictions to effect predictions. One or two additional parameters might be required to describe a nonlinear target occupancy-effect relationship, which is required in case of a high efficacy and receptor reserve[24]. The discrimination between the two nonlinearities in such cases might be hard or impossible to obtain. However, k_{on} and k_{off}

can be obtained from in vitro experiments and R_{tot} from *ex vivo* experiments. Especially the identification of R_{tot} from *ex vivo* data can help to reduce the difficulties with parameter identifiability as often associated with the TB model [45].

In summary, the limited difference between TB and EC models should be taken into account in the evaluation of historical and the design of new modelling studies. By informing the TB models with *in vitro* data, TB models can help to translate between *in vitro* and *in vivo* studies. The combination of parameter values for which the $Tmax_{TO}$ in the target binding model is dependent on the dose is limited to k_{off} values around the elimination rate constant and to target concentrations lower than the initial drug concentration. Although the combination of multi-compartment PK models, TB models and target turnover models might affect the parameter range were the $Tmax_{TO}$ is dependent on the dose, our study is a first indication that such limitations should be taken into account for understanding TB models.

Conclusion

In this study, we have shown that successful fitting of a TB or EC model is not enough support to assume the relevance of target binding or target site distribution. Moreover, we have shown for a one-compartment pharmacokinetic model with target binding that the $\Delta Tmax_{TO}$ for changing doses can only be identified if the k_{off} has a value around the pharmacokinetic elimination rate constant and the target concentration is lower than the initial drug concentration. We have thus identified that the $Tmax_{TO}$ is determined by the rate of target binding relative to the decline rate of unbound drug and unbound target concentrations. Our findings indicate that the relatively sparse occurrence of target binding models in literature does not discredit the relevance of target binding kinetics. Our study also shows that a TB and EC model might be similar for the tested dose range and pharmacokinetic conditions, while extrapolation to different conditions might result in different effect *versus* time profiles for the TB and EC model. We conclude that identification of the appropriate model is important and that target binding models should be tested more often to increase the translation between *in vitro* and *in vivo* studies and to increase the predictive power of developed PKPD models.

References

1. Copeland RA, Pompliano DL, Meek TD. Drug-target residence time and its implications for lead optimization. Nat Rev Drug Discov 2006;5(9):730–9
2. Lu H, Tonge PJ. Drug-Target Residence Time: Critical Information for Lead Optimization. Curr Opin Chem Biol 2011;14(4):467–74
3. Dahl G, Akerud T. Pharmacokinetics and the drug-target residence time concept. Drug Discov Today 2013;18(15–16):697–707
4. Schuetz DA, de Witte WEA, Wong YC, et al. Kinetics for Drug Discovery: an industry-driven effort to target drug residence time. Drug Discov Today 2017;22(6):896–911
5. de Witte WEA, Wong YC, Nederpelt I, et al. Mechanistic models enable the rational use of in vitro drug-target binding kinetics for better drug effects in patients. Expert Opin Drug Discov 2016;11(1):45–63
6. de Witte WEA, Danhof M, van der Graaf PH, et al. In vivo Target Residence Time and Kinetic Selectivity: The Association Rate Constant as Determinant. Trends Pharmacol Sci 2016;37(10):831–42
7. Vauquelin G, Bostoen S, Vanderheyden P, et al. Clozapine, atypical antipsychotics, and the benefits of fast-off D2 dopamine receptor antagonism. Naunyn Schmiedebergs Arch Pharmacol 2012;385(4):337–72
8. Sahlholm K, Zeberg H, Nilsson J, et al. The fast-off hypothesis revisited: A functional kinetic study of antipsychotic antagonism of the dopamine D2 receptor. Eur Neuropsychopharmacol 2016;26(3):467–76
9. Ramsey SJ, Attkins NJ, Fish R, et al. Quantitative pharmacological analysis of antagonist binding kinetics at CRF1 receptors in vitro and in vivo. Br J Pharmacol 2011;164(3):992–1007
10. Jiang XL, Samant S, Lewis JP, et al. Development of a physiology-directed population pharmacokinetic and pharmacodynamic model for characterizing the impact of genetic and demographic factors on clopidogrel response in healthy adults. Eur J Pharm Sci 2016;82:64–78
11. Hong Y, Gengo FM, Rainka MM, et al. Population pharmacodynamic modelling of aspirin- and ibuprofen-induced inhibition of platelet aggregation in healthy subjects. Clin Pharmacokinet 2008;47(2):129–37
12. Äbelö A, Holstein B, Eriksson UG, et al. Gastric acid secretion in the dog: A mechanism-based pharmacodynamic model for histamine stimulation and irreversible inhibition by omeprazole. J Pharmacokinet Pharmacodyn 2002;29(4):365–82
13. Yassen A, Olofsen E, Dahan A, et al. Pharmacokinetic-Pharmacodynamic Modeling of the Antinociceptive Effect of Buprenorphine and Fentanyl in Rats : Role of Receptor Equilibration Kinetics. J Pharmacol Exp Ther 2005;313(3):1136–49
14. Shimada S, Nakajima Y, Yamamoto K, et al. Comparative Pharmacodynamics of Eight Calcium Channel Blocking Agents in Japanese Essential Hypertensive Patients. Biol Pharm Bull 1996;19(3):430–7
15. Dua P, Hawkins E, van der Graaf P. A Tutorial on Target-Mediated Drug Disposition (TMDD) Models. CPT Pharmacometrics Syst Pharmacol 2015;4(6):324–37
16. Lammertsma AA, Hume SP. Simplified reference tissue model for PET receptor studies. Neuroimage 1996;4:153–8
17. Liefaard LC, Ploeger BA, Molthoff CFM, et al. Population pharmacokinetic analysis for simultaneous determination of Bmax and KD in vivo by positron emission tomography. Mol imaging Biol 2005;7(6):411–21
18. Louizos C, Yáñez JA, Forrest ML, et al. Understanding the hysteresis loop conundrum in pharmacokinetic / pharmacodynamic relationships. J Pharm Pharm Sci 2014;17(1):34–91
19. Upton R, Mould D. Basic Concepts in Population Modeling, Simulation, and Model-Based Drug Development: Part 3—Introduction to Pharmacodynamic Modeling Methods. CPT Pharmacometrics Syst Pharmacol 2014;3(1)
20. Holford NHG, Sheiner LB. Understanding the Dose-Effect Relationship: Clinical Application of Pharmacokinetic-Pharmacodynamic Models. Clin Pharmacokinet 1981;6:429–53
21. Jusko WJ, Ko HC. Physiologic indirect response models characterize diverse types of pharmacodynamic effects. Clin Pharmacol Ther 1994;56(4):406–19
22. Paton WDM. A theory of drug action based on the rate of drug-receptor combination. Proc R Soc London Ser B Biol Sci 1961;154(954):21–69
23. Perry DC, Mullis KB, Oie S, et al. Opiate antagonist receptor binding in vivo: evidence for a new receptor binding model. Brain Res 1980;199(1):49–61
24. Ruffolo RR. Important Concepts of Receptor Theory. J Auton Pharmacol 1982;2(4):277–95
25. Wakelkamp M, Alvá N G, Paintaud G. The time of maximum effect for model selection in pharmacokinetic–pharmacodynamic analysis applied to frusemide. Br J Clin Pharmacol 1998;45:63–70
26. Ploeger BA, Van Der Graaf PH, Danhof M. Incorporating Receptor Theory in Mechanism-Based Pharmacokinetic-Pharmacodynamic (PK-PD) Modeling. Drug Metab Pharmacokinet 2009;24(1):3–15
27. N.L.Dayneka, Garg V, W.J.Jusko. Comparison of four basic models of indirect pharmacodynamic responses. J Pharmacokinet Biopharm 1993;21(4):457–77
28. Peletier LA, Gabrielsson J, Haag J Den. A dynamical systems analysis of the indirect response model with special emphasis on time to peak response. J Pharmacokinet Pharmacodyn 2005;32(3–4):607–54

29. Äbelö A, Andersson M, Holmberg AA, et al. Application of a combined effect compartment and binding model for gastric acid inhibition of AR-HO47108: A potassium competitive acid blocker, and its active metabolite AR-HO47116 in the dog. Eur J Pharm Sci 2006;29(2):91–101
30. Yassen A, Olofsen E, Kan J, et al. Animal-to-human extrapolation of the pharmacokinetic and pharmacodynamic properties of buprenorphine. Clin Pharmacokinet 2007;46(5):433–47
31. Cleton A, de Greef HJ, Edelbroek PM, et al. Application of a combined "effect compartment/indirect response model" to the central nervous system effects of tiagabine in the rat. J Pharmacokinet Biopharm 1999;27(3):301–23
32. Jusko WJ, Ko HC, Ebling WF. Convergence of direct and indirect pharmacodynamic response models. J Pharmacokinet Biopharm 1995;23(1):5–8
33. Hutmacher MM, Mukherjee D, Kowalski KG, et al. Collapsing mechanistic models: An application to dose selection for proof of concept of a selective irreversible antagonist. J Pharmacokinet Pharmacodyn 2005;32(3–4):501–20
34. Groenendaal D, Freijer J, de Mik D, et al. Influence of biophase distribution and P-glycoprotein interaction on pharmacokinetic-pharmacodynamic modelling of the effects of morphine on the EEG. Br J Pharmacol 2007;151(5):713–20
35. Groenendaal D, Freijer J, de Mik D, et al. Population pharmacokinetic modelling of non-linear brain distribution of morphine: influence of active saturable influx and P-glycoprotein mediated efflux. Br J Pharmacol 2007;151:701–12
36. Beal S, Sheiner LB, Boeckmann A, et al. NONMEM 7.3.0 Users Guides. (1989-2013). Icon Development Solutions,;
37. Akaike H. Information Theory and an Extension of the Maximum Likelihood Principle. In: Kotz S, Johnson NL, editors. Breaktroughs in Statistics, Vol I, Foundations and Basic Theory New York; 1992. p. 610–24
38. Zhang L, Beal SL, Sheiner LB. Simultaneous vs . Sequential Analysis for Population PK / PD Data I: Best-case Performance. J Pharmacokinet Pharmacodyn 2003;30(6):387–404
39. Walkup GK, You Z, Ross PL, et al. Translating slow-binding inhibition kinetics into cellular and in vivo effects. Nat Chem Biol 2015;11(6):416–23
40. Stevens J, Ploeger BA, Hammarlund-Udenaes M, et al. Mechanism-based PK-PD model for the prolactin biological system response following an acute dopamine inhibition challenge: quantitative extrapolation to humans. J Pharmacokinet Pharmacodyn 2012;39(5):463–77
41. Larsen MS, Keizer R, Munro G, et al. Pharmacokinetic/Pharmacodynamic Relationship of Gabapentin in a CFA-induced Inflammatory Hyperalgesia Rat Model. Pharm Res 2016;33(5):1133–43
42. Danhof M, Levy G. Kinetics of Drug Action in Disease States. I. Effect of Infusion Rate on Phenobarbital Concentrations in Serum, Brain and Cerebrospinal Fluid of Normal Rats at Onset of Loss of Righting Reflex1. J Pharmacol Exp Ther 1984;229(1):44–50
43. Balerio GN, Rubio MC. Pharmacokinetic-Pharmacodynamic Modeling of the antinociceptive effect of baclofen in mice. Eur J Drug Metab Pharmacokinet 2002;27(3):163–9
44. Yamamoto Y, Välitalo PA, van den Berg D-J, et al. A Generic Multi-Compartmental CNS Distribution Model Structure for 9 Drugs Allows Prediction of Human Brain Target Site Concentrations. Pharm Res 2017;34(2):333–51
45. Janzén DLI, Bergenholm L, Jirstrand M, et al. Parameter identifiability of fundamental pharmacodynamic models. Front Physiol 2016;7(DEC):1–12
46. Tummino PJ, Copeland RA. Residence Time of Receptor-Ligand Complexes and Its Effect on Biological Function. Biochemistry 2008;47(20):5481–92

Supplement S 1. Morphine PK and PD model fits, GOF plots and VPCs

Plasma concentration modelling

A three-compartment model (Figure S 1) was identified as the best model with respect to the AIC and the individual fits. The goodness of fit of this model is illustrated in Figure S 2 and Figure S 3.

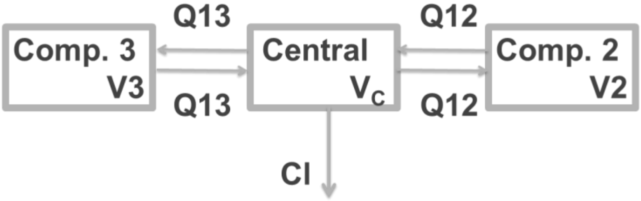

Figure S 1. Schematic representation of the three-compartment model structure that was used to describe the morphine plasma concentrations over time.

The differential equations of the model in Figure S 1 are given in equations 1-3. In these equations, A_c, A_2 and A_3 represent the amount of drug in the central, second and third compartment, respectively. k_{el} k_{12}, k_{21} k_{13} and k_{31} represent the first order rate constants of elimination and distribution between the compartments. The relation between the parameters in equations 1-3 and the estimated parameters as given in Table S 1 is shown in equation 4-8. V_c, V_2 and V_3 represent the volumes of the respective compartments and CL, Q12 and Q13 represent the clearances of elimination and distribution between compartments.

1. $\frac{dA_c}{dt} = -\ k_{el} \cdot A_c - k_{12} \cdot A_c - k_{13} \cdot A_c + k_{21} \cdot A_2 + k_{31} \cdot A_3$
2. $\frac{dA_2}{dt} = k_{12} \cdot A_c - k_{21} \cdot A_2$
3. $\frac{dA_3}{dt} = k_{13} \cdot A_c - k_{31} \cdot A_3$
4. $k_{el} = \frac{CL}{V_c}$
5. $k_{12} = \frac{Q12}{V_c}$
6. $k_{13} = \frac{Q13}{V_c}$
7. $k_{21} = \frac{Q12}{V_2}$
8. $k_{31} = \frac{Q13}{V_3}$

The goodness of fit of this model is illustrated in Figure S 2 and Figure S 3. Inter individual variability (IIV) was estimated for 4 of the estimated model parameters. Attempts to add IIV on more parameters resulted in a failing covariance step while the drop in OFV was limited (9 points). Comparison to the 2-compartment model with the lowest OFV value that was tested demonstrated better individual fits and a 109-points lower OFV for the 3-compartment model.

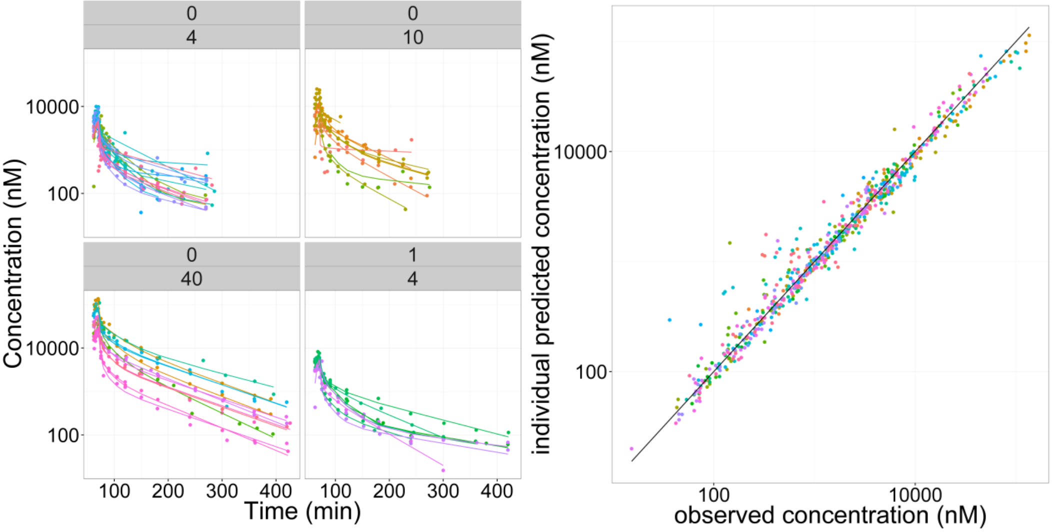

Figure S 2. Diagnostic plots of the plasma concentration fits. Left panel: Overview of observed (dots) and predicted (lines) concentrations. Upper panel labels indicate the dose in mg/kg and lower panel labels the presence (1) or absence (0) of Pgp inhibitor GF120918. Right panel: relation between observed and individual predicted plasma concentrations on a double logarithmic scale.

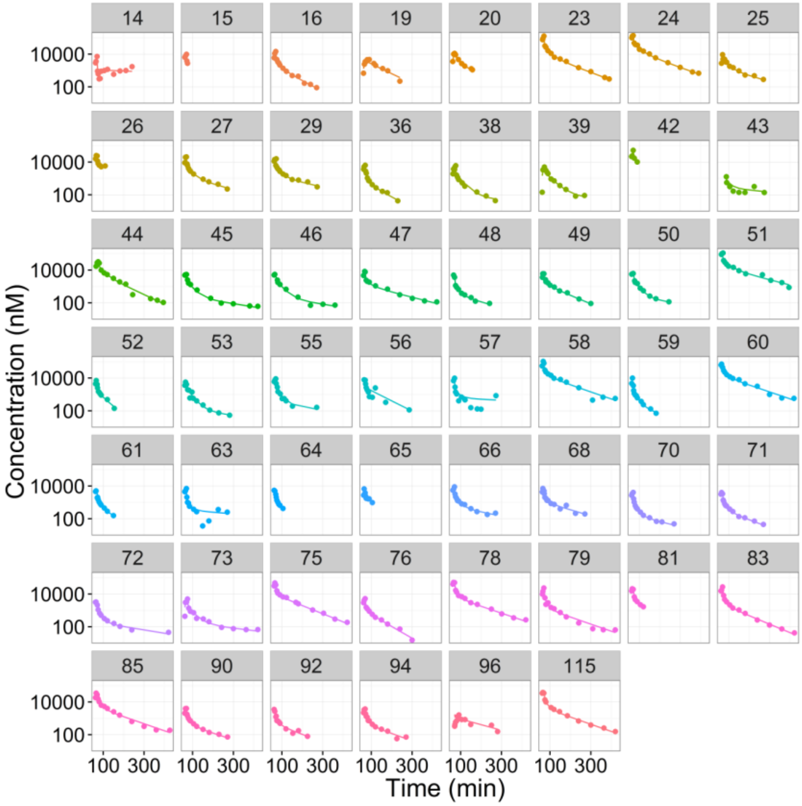

Figure S 3. Individual profiles of observed (dots) and predicted (lines) concentrations on a semi-logarithmic scale. Panel labels indicate the animal ID number.

Table S 1. Parameter values and objective function values of the tested models for the plasma concentrations. CV denotes the coefficient of variation as percentage. OFV denotes the Objective Function Value. ω^2 and σ^2 denote the variances of the exponential IIV distribution and the error distribution, respectively.

	2-cmp model	**3-cmp model** **4 IIV parameters**	**3-cmp model** **5 IIV parameters**
OFV	9314	9205	9194
parameter	**Value (CV)**	**Value (CV)**	**Value (CV)**
CL (L/min)	0.0300 (8)	0.028 (22)	0.028
V1 (L)	0.200 (11)	0.17 (49)	0.12
Q12 (L/min)	0.0432 (10)	0.019 (66)	0.056
V2 (L)	1.15 (10)	1.3 (48)	0.51*
Q13 (L/min)	-	0.031 (30)	0.020
V3 (L)	-	0.36 (32)	1.4*
ω^2 CL	0.34 (23)	0.33 (25)	0.35
ω^2 V1	0.55 (27)	0.63 (35)	0.15
ω^2 Q12	0.28 (39)	0.62 (33)	0.72
ω^2 V2	0.32 (31)	0.66 (28)	0 FIX
ω^2 Q13			0.79
ω^2 V3			0.57
σ^2 proportional	0.0766 (15)	0.79 (14)	0.071
σ^2 additive	1710 (28)	0 FIX	7.2

* To get the best model fit, V2 and V3 were estimated here as the ratio of V2 and V1 and the ratio of V3 and V2, respectively. The displayed values in this table are derived from the estimated ratios. CV = coefficient of variation as percentage.

ECF concentration modelling

Various structural models were tested for the description of the ECF concentrations, including a two-compartent model (ECF and "deep brain") and a target binding model (ECF-unbound and ECF bound). The best combination of OFV, parameter estimate uncertainty and diagnostic plots was obtained with the original one compartment ECF model, with passive first-order in- and outward distribution, saturable influx and first-order efflux (Figure S 4). As the parameters for the plasma concentrations were fixed, the only additional equation is given in equation 9, in which A_{ECF} and V_{ECF} refer to the amount and volume of the ECF compartment, respectively, k_{diff} and k_{eff} represent first order influx and efflux rate constants, Nmax represents the maximal saturable influx rate and C_{50} is the plasma concentration at which the saturable influx is half-maximal.

$$9. \quad \frac{d\frac{A_{ECF}}{V_{ECF}}}{dt} = k_{diff} \cdot \left(\frac{A_1}{V_1} - \frac{A_{ECF}}{V_{ECF}}\right) + \frac{N_{max} \cdot \frac{A_1}{V_1}}{C_{50} + \frac{A_1}{V_1}} - k_{eff} \cdot \frac{A_{ECF}}{V_{ECF}}$$

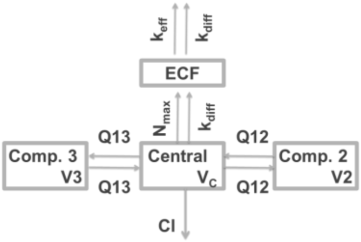

Figure S 4. Schematic representation of the model structure that was used to describe the morphine ECF concentrations over time. k_{diff} = first-order in- and outward distribution rate constant. k_{eff} first-order efflux rate constant. Nmax = zero-order maximal saturable influx rate constant.

Different versions of this model were tested in which the inter-individual variability was tested on different parameters and the influence of Pgp was estimated. Estimating the influence of Pgp did not reduce the OFV enough, so the final model did not include the influence of Pgp and had IIV estimated for k_{diff} and N_{max}. The diagnostic plots for the evaluation of the fit of this model is given in Figure S 5.

Table S 2. Parameter values and objective function values of the tested models for the ECF concentrations. CV denotes the coefficient of variation as percentage. OFV denotes the Objective Function Value. ω^2 and σ^2 denote the variances of the exponential IIV distribution and the error distribution, respectively.

	IIV on k_{diff}, N_{max}	**IIV on k_{diff}, k_{eff}**	**IIV on k_{diff}, k_{eff} Pgp on N_{max}**	**IIV on k_{diff}, N_{max} Pgp on N_{max}**
OFV	-1126	-1096	-1104	-1128
parameter	**Value (CV)**	**Value (CV)**	**Value (CV)**	**Value (CV)**
k_{diff}(/min)	0.0025 (17)	0.0027 (19)	0.0027 (17)	0.0025 (16)
k_{eff}(/min)	0.020 (11)	0.021 (20)	0.0213 (24)	0.019 (12)
N_{max} (nM/min)	2.6 (21)	3.0 (38)	2.2 (34)	2.2 (29)
N_{maxPgp} (nM/min)	-	-	4.45 (52)	3.15 (28)
ω^2 k_{diff}	0.36 (39)	0.44 (47)	0.44 (45)	0.35 (39)
ω^2 k_{eff}	0 FIX	0.35 (108)	0.31 (71)	0 FIX
ω^2 N_{max}	0.42 (55)	0 FIX	0 FIX	0.39 (52)
σ^2 proportional	0.11 (18)	0.11 (22)	0.11 (22)	0.11 (20)

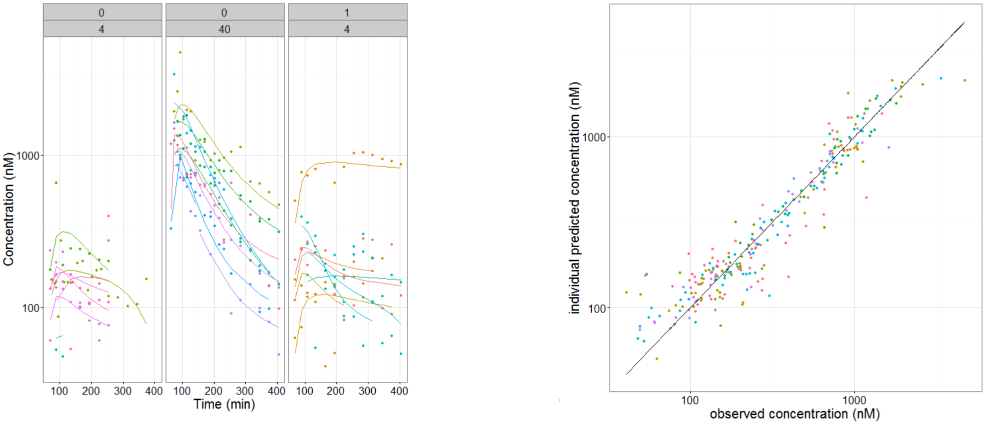

Figure S 5. Diagnostic plots of the ECF concentration fits. Left panel: Overview of observed (dots) and predicted (lines) concentrations. lower panel labels indicate the dose in mg/kg and upper panel labels the presence (1) or absence (0) of Pgp inhibitor GF120918. Right panel: relation between observed and individual predicted plasma concentrations on a double logarithmic scale.

EEG effect modelling

Model equations, Goodness of fit and VPC for model EC$_{PL}$1

The model equations for the connection between plasma concentrations and EEG effect are given in equations 10-12, where A$_{TRANS}$ and V$_{TRANS}$ refer to the amount of drug and the volume of the transit compartment, A$_{EFF}$ and V$_{EFF}$ refer to the amount of drug and the volume of the effect compartment k$_{1e}$ and k$_{e0}$ refer to the first order distribution rate constants into and out of the transit and effect compartment, E0 is the baseline EEG amplitude, slope is the linear change of the EEG amplitude during the experiment without morphine treatment, Emax is the maximal increase in EEG amplitude due to morphine, N$_H$ is the hill coefficient and EC$_{50}$ is the morphine plasma concentration that leads to the half-maximal increase in EEG amplitude.

$$10.\quad \frac{d\frac{A_{TRANS}}{V_{TRANS}}}{dt} = k_{1e} \cdot \left(\frac{A_1}{V_1} - \frac{A_{TRANS}}{V_{TRANS}}\right)$$

$$11.\quad \frac{d\frac{A_{EFF}}{V_{EFF}}}{dt} = k_{1e} \cdot \left(\frac{A_{TRANS}}{V_{TRANS}}\right) - k_{e0} \cdot \frac{A_{EFF}}{V_{EFF}}$$

$$\mathbf{12.}\quad Effect\ (EEG\ amplitude) = E_0 + slope * t + \frac{E_{max} \cdot \left(\frac{A_{EFF}}{V_{EFF}}\right)^{N_H}}{{EC_{50}}^{N_H} + \left(\frac{A_{EFF}}{V_{EFF}}\right)^{N_H}}$$

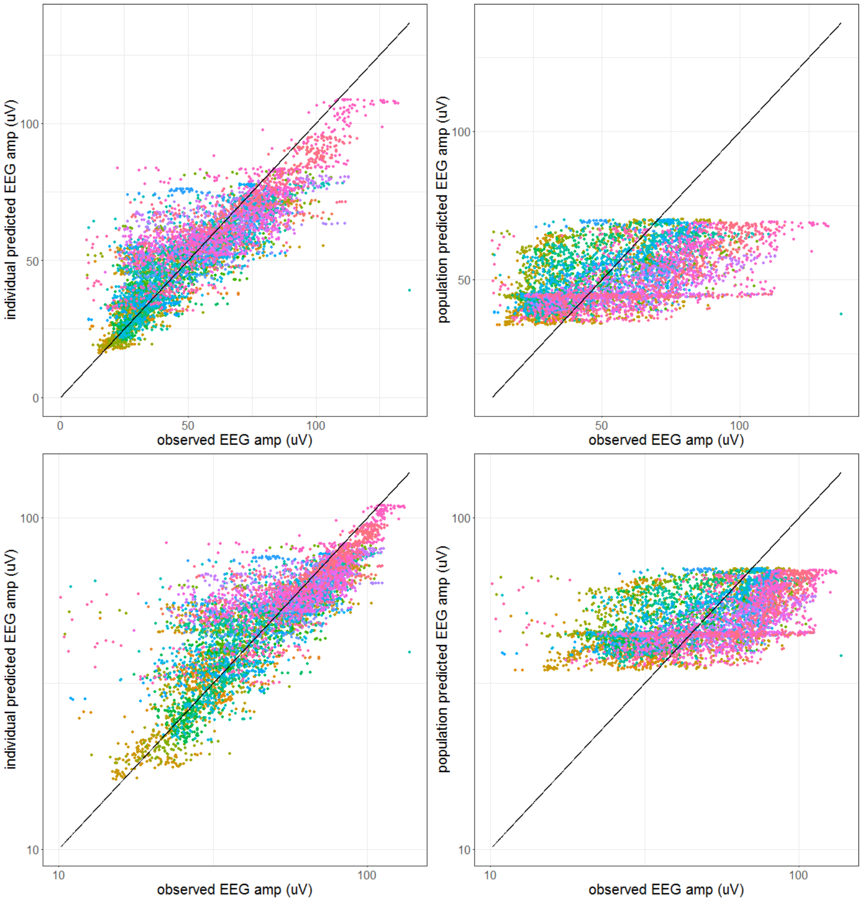

Figure S 6. Population (right panels) and individual (left panels) observed versus predicted EEG data as obtained from the model fit of model EC$_{PL}$1. The upper panels have a linear scale and the lower panels have a logarithmic scale.

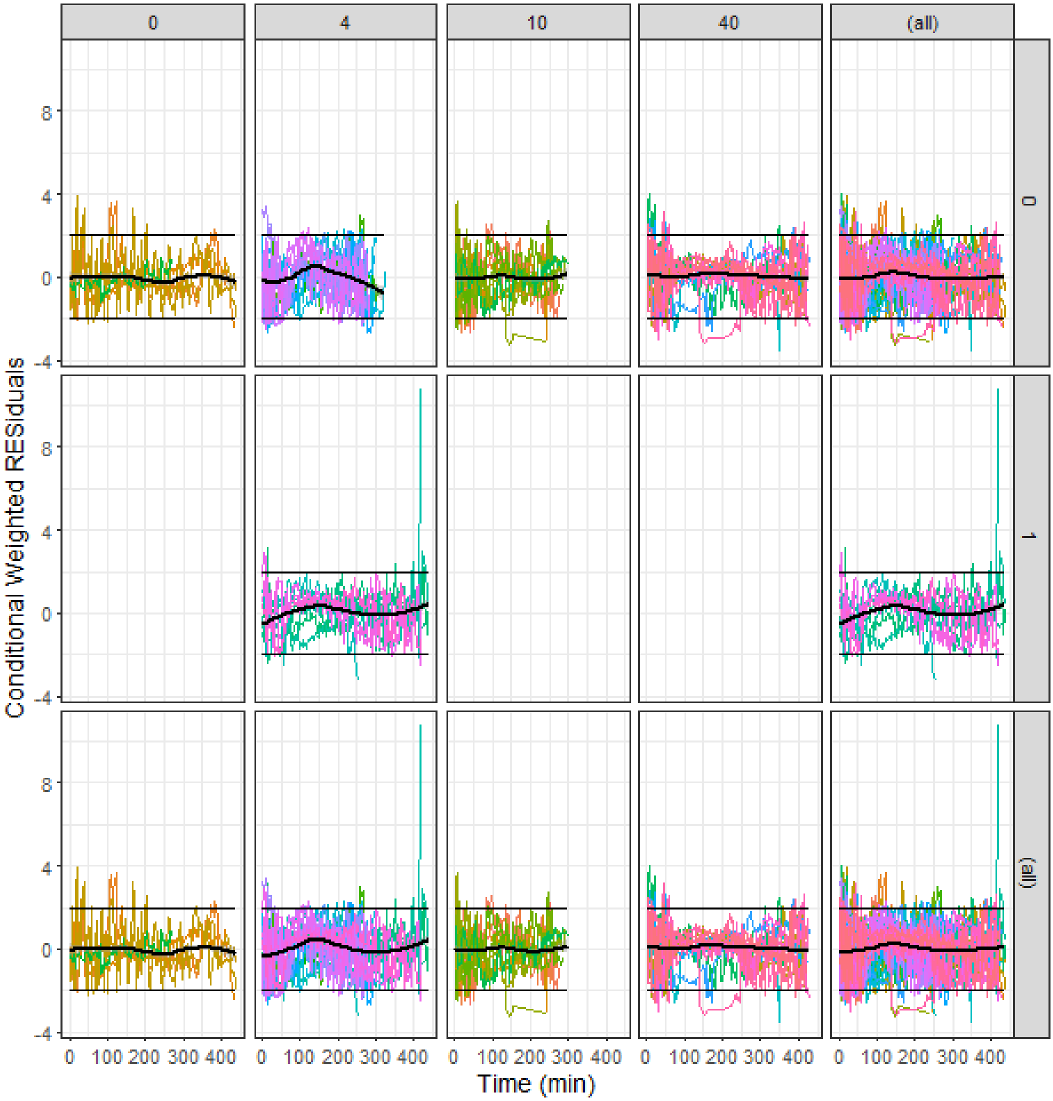

Figure S 7. Conditional weighted residuals versus time for the different dose groups and dose group combinations in the model fit of EC$_{PL}$1. The top labels indicate the morphine dose in mg/kg. The side labels indicate the absence (0) or presence (1) of Pgp inhibitor GF120918. The columns and rows indicated with (all) display the combination of all dose groups or all Pgp inhibitor groups, respectively.

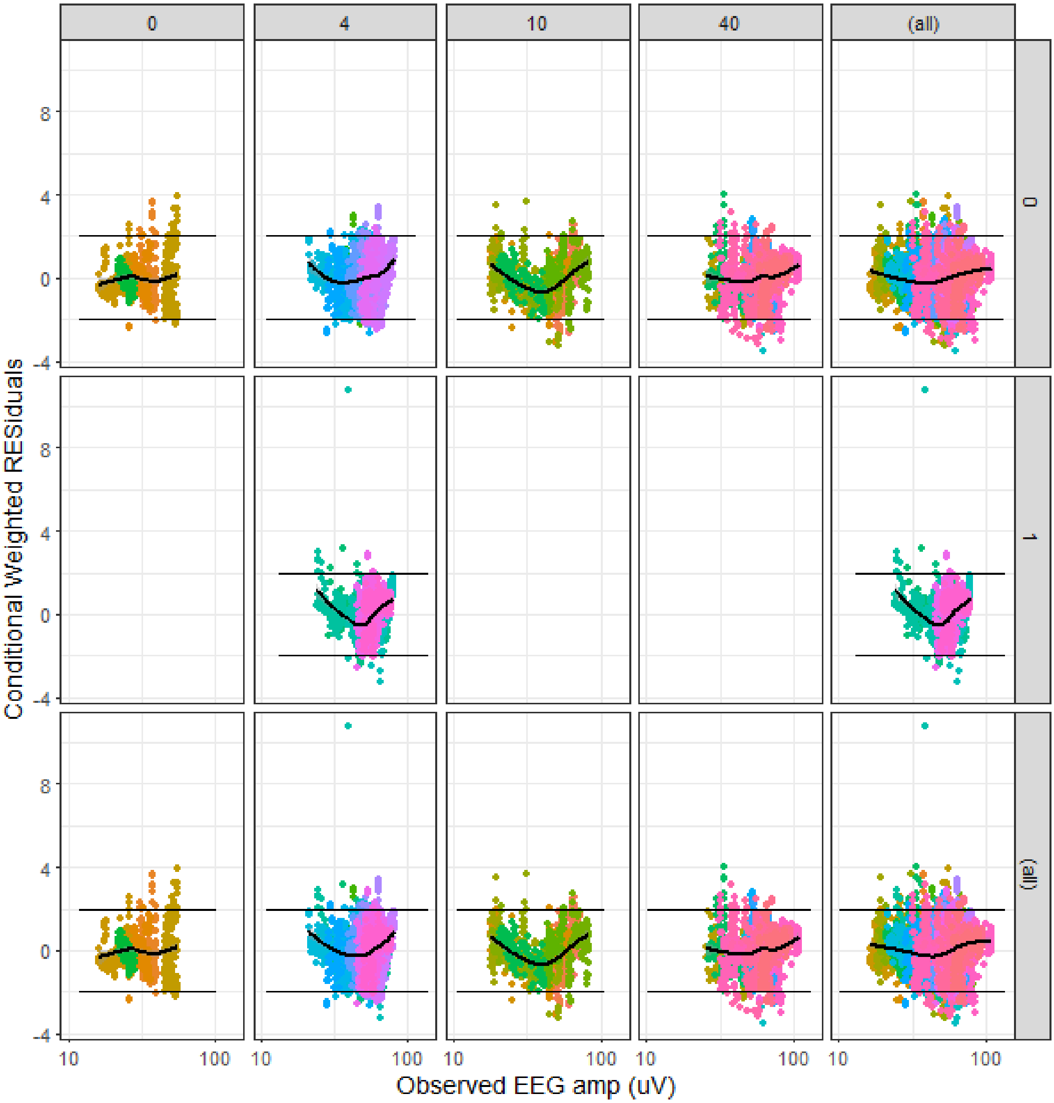

Figure S 8. Conditional weighted residuals versus observed EEG amplitudes. for the different dose groups and dose group combinations in the model fit of $EC_{PL}1$*. The top labels indicate the morphine dose in mg/kg. The side labels indicate the absence (0) or presence (1) of Pgp inhibitor GF120918. The columns and row indicated with (all) display the combination of all dose groups or all Pgp inhibitor groups, respectively.*

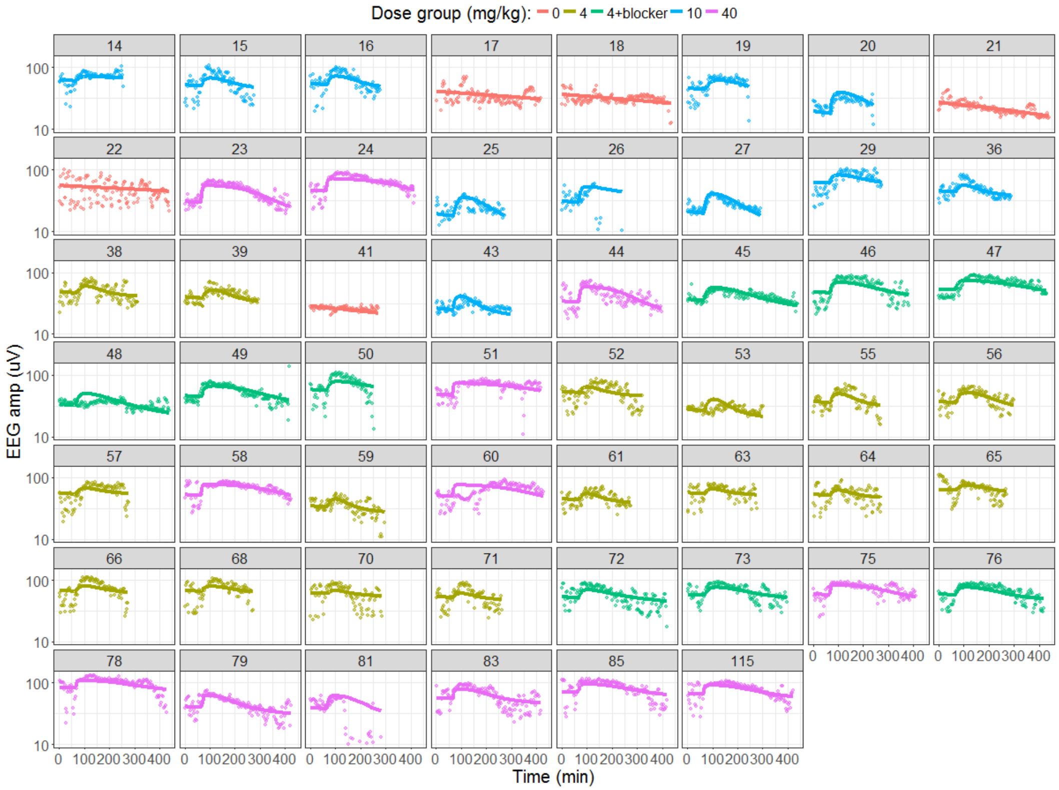

Figure S 9. Individual model fits of model EC$_{PL}$1 to the EEG data. The colors represent the different dose groups. Dots represent the observations, lines the model predictions.

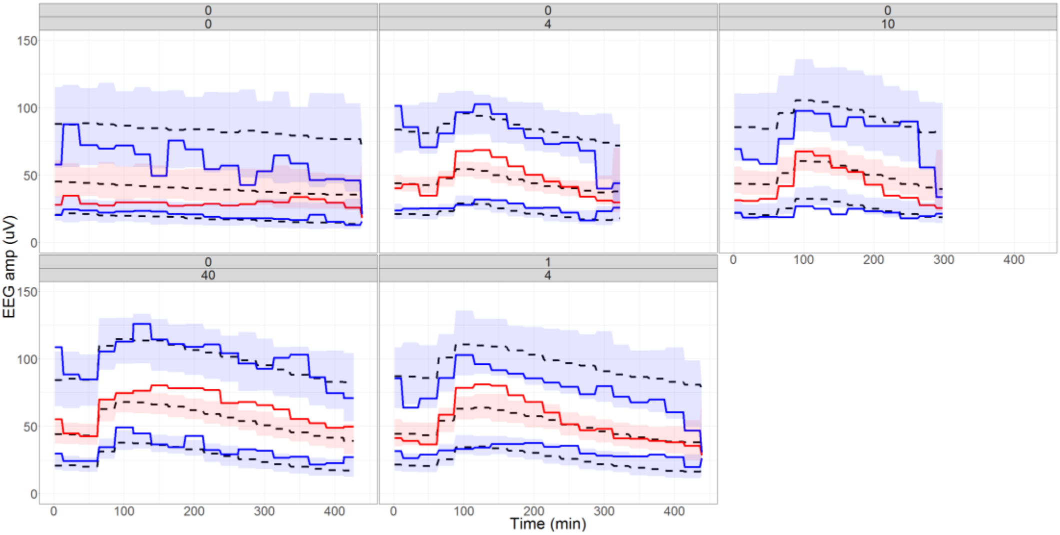

Figure S 10. Visual predictive check of the model fit of model EC$_{PL}$1. The upper labels indicate the absence (0) or presence (1) of Pgp inhibitor GF120918. The lower labels indicate the morphine dose in mg/kg. The solid lines represent the observed 5%, 50% and 95% quantiles of the data. The dashed lines represent the median of the 5%, 50% and 95% quantiles of the simulated datasets. The shaded areas represent the 5%-95% percent interval of the 5%, 50% and 95% quantiles of the simulated datasets.

Model equations and VPC for model EC-TB$_{PL}$1

The model equations for the EC-TB$_{PL}$ model are provided in equations 13-15. In these equations, A_{EFF} and V_{EFF} refer to the amount and volume of the effect compartment, respectively. A_{RL} and V_{RL} refer to the amount and volume of the drug-target complex compartment, respectively. A_{Rtot} and V_{Rtot} refer to the amount and volume of the bound plus unbound target compartment, respectively. The rate constants k_{e0} and k_{off} are first order rate constants of distribution and dissociation, respectively. k_{on} is the second order association rate constant. E_0 is the baseline EEG amplitude, slope is the linear decline of the EEG amplitude per time unit, independent of the drug effect and Emax is the maximal drug effect.

$$13.\quad \frac{d\frac{A_{EFF}}{V_{EFF}}}{dt} = k_{e0} \cdot \left(\frac{A_{EFF}}{V_{EFF}} - \frac{A_1}{V_1}\right)$$

$$14.\quad \frac{d\frac{A_{RL}}{V_{RL}}}{dt} = k_{on} \cdot \frac{A_{EFF}}{V_{EFF}} \cdot \left(Rtot - \frac{A_{RL}}{V_{RL}}\right) - k_{off} \cdot \frac{A_{RL}}{V_{RL}}$$

$$\mathbf{15.}\quad Effect\ (EEG\ amplitude) = E_0 + slope * t + \frac{E_{max} \cdot \frac{A_{RL}}{V_{RL}}}{\frac{A_{Rtot}}{V_{Rtot}}}$$

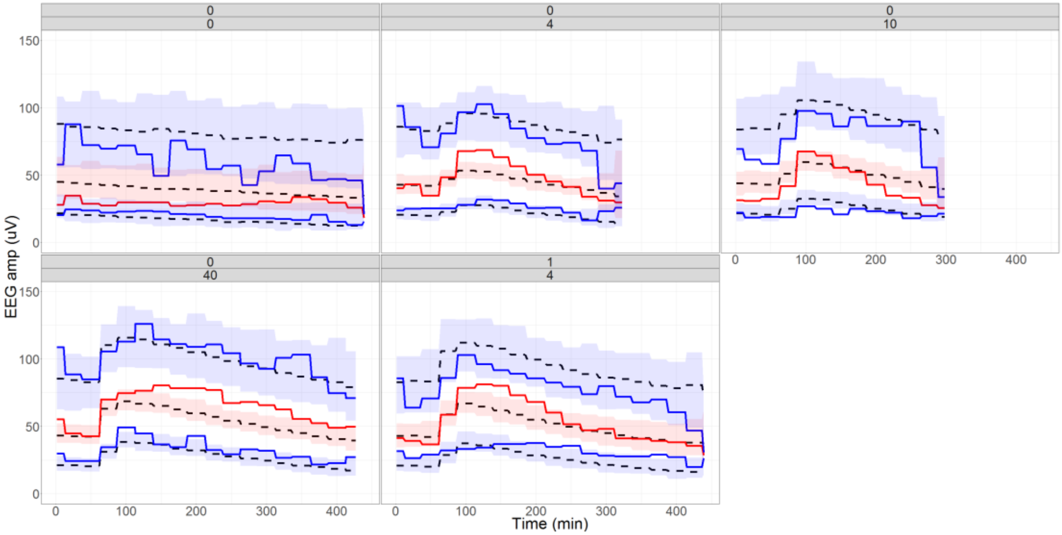

Figure S 11. Visual predictive check of the model fit of model EC-TB$_{PL}$1. The upper labels indicate the absence (0) or presence (1) of Pgp inhibitor GF120918. The lower labels indicate the morphine dose in mg/kg. The solid lines represent the observed 5%, 50% and 95% quantiles of the data. The dashed lines represent the median of the 5%, 50% and 95% quantiles of the simulated datasets.

Model equations and VPC for model TB$_{PL}$4

The model equations for the combined TB$_{PL}$ model are provided in equations 16 and 17. In these equations, A_{RL} and V_{RL} refer to the amount and volume of the drug-target complex compartment, respectively. A_{Rtot} and V_{Rtot} refer to the amount and volume of the bound plus unbound target compartment, respectively. The rate constants k_{off} is the first order rate constants of drug-target dissociation. k_{on} is the second order association rate constant. E_0 is the baseline EEG amplitude, slope is the linear decline of the EEG amplitude per time unit, independent of the drug effect and Emax is the maximal drug effect.

$$16.\quad \frac{d\frac{A_{RL}}{V_{RL}}}{dt} = k_{on} \cdot \frac{A_C}{V_C} \cdot \left(Rtot - \frac{A_{RL}}{V_{RL}}\right) - k_{off} \cdot \frac{A_{RL}}{V_{RL}}$$

$$\textbf{17.}\quad Effect\ (EEG\ amplitude) = E_0 + slope * t + \frac{E_{max} \cdot \frac{A_{RL}}{V_{RL}}}{\frac{A_{Rtot}}{V_{Rtot}}}$$

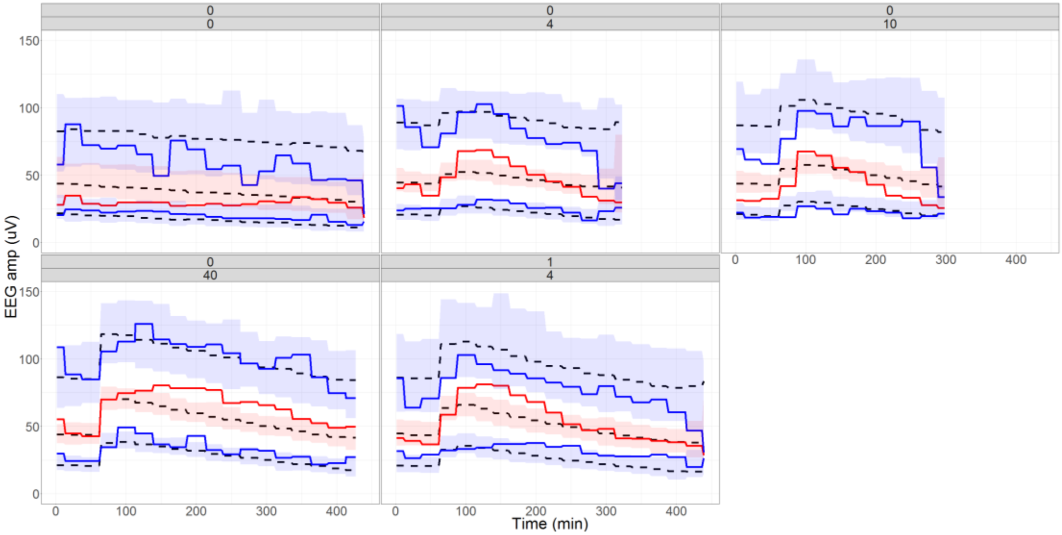

Figure S 12. Visual predictive check of the model fit of model $TB_{PL}4$. The upper labels indicate the absence (0) or presence (1) of Pgp inhibitor GF120918. The lower labels indicate the morphine dose in mg/kg. The solid lines represent the observed 5%, 50% and 95% quantiles of the data. The dashed lines represent the median of the 5%, 50% and 95% quantiles of the simulated datasets.

Supplement S 2. Dose-dependency of Tmax_{TO} in a TB_{PL}.

To obtain a better understanding of the influence of dose on the Tmax_{TO} in a TB_{PL} model, some of the underlying simulations for Figure 5 are shown in this section. In Figure S 13, the simulation with the lowest values of k_{on} and k_{off} is showing that in this situation, the Tmax_{TO} has a high value, but also that there is no difference between the two doses. This can be understood by comparing the rate of equilibration in a situation with a constant ligand concentration with the rate of elimination.

The rate of equilibration (k_{obs}) for a constant ligand concentration [L] can be calculated by equation 1 [46]:

$$k_{obs} = kon * [L] + koff \qquad (1)$$

Since the ligand concentration in our simulations is normalized for the value of K_D, equation 1 can be rewritten as equation 2, in which c is the ratio $[L]/K_D$:

$$k_{obs} = kon * c * koff/kon + koff = koff*(c + 1) \qquad (2)$$

From equation 2, it can be observed that a low value of koff leads to slow equilibration, unless the ligand concentration is much higher than the affinity. If the equilibration rate is slow, the Tmax_{TO} is mainly determined by the elimination rate constant, which is independent on the dose/ligand concentration. Thus, a low value of koff gives similar Tmax_{TO} values for different doses, as confirmed in Figure S 13.

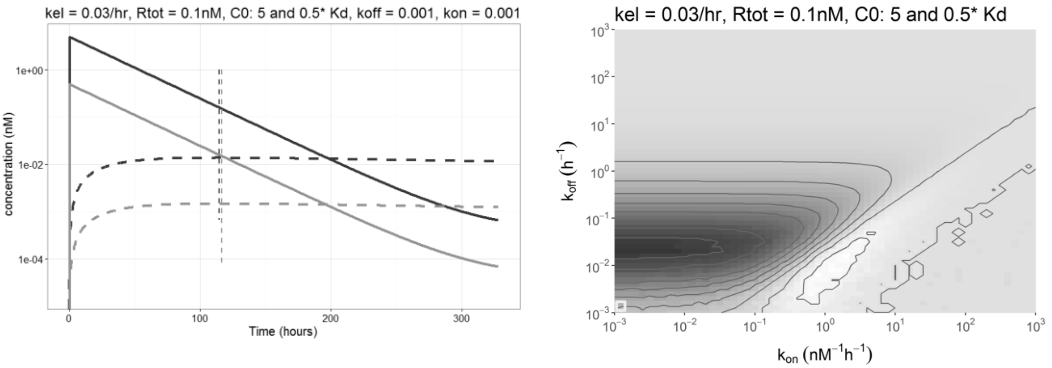

Figure S 13. Simulation of drug target binding for two different doses. The solid lines indicate plasma concentrations for the high (dark grey line) dose and the low (light grey line) dose. The dashed lines indicate target-bound drug concentrations. The vertical dotted lines indicate the time point of the maximal target-bound concentration for each dose. In this simulation, the elimination rate constant k_{el} was 0.03/hr and the target concentration was 0.1 nM. The initial concentrations for the high and the low dose corresponded to 5 and 0.5 times the K_D, respectively. The k_{on} and k_{off} values were 0.001 nM^{-1} h^{-1} and 0.001 h^{-1}, respectively, representing the area of Figure 5 that is indicated with the square in the right panel.

A high value of k_{off} gives rise to fast equilibration and a significant influence of the dose on the equilibration time, because equilibration is now much faster than elimination, and thus determining the $Tmax_{TO}$. However, because of the fast equilibration, the decrease in $Tmax_{TO}$ with increasing doses is difficult to detect because all $Tmax_{TO}$ values are low, and the absolute difference is low as well, as illustrated in Figure S 14.

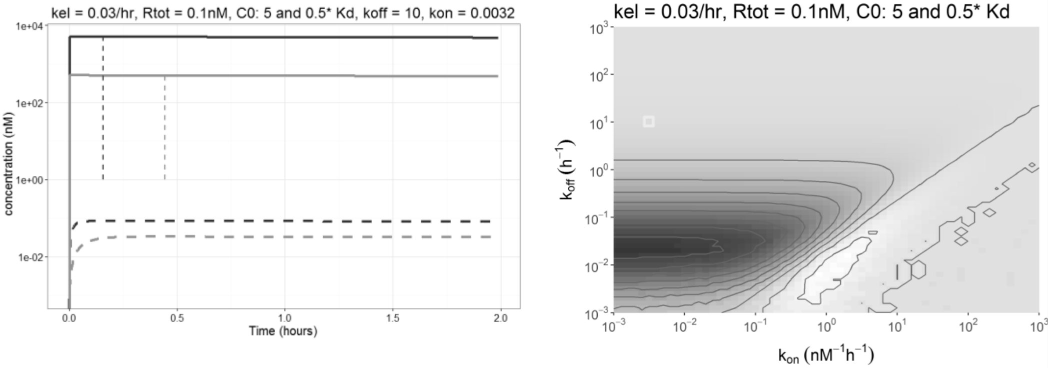

Figure S 14. Simulation of drug target binding for two different doses. The solid lines indicate plasma concentrations for the high (dark grey line) dose and the low (light grey line) dose. The dashed lines indicate target-bound drug concentrations. The vertical dotted lines indicate the time point of the maximal target-bound concentration for each dose. In this simulation, the elimination rate constant k_{el} was 0.03/hr and the target concentration was 0.1 nM. The initial concentrations for the high and the low dose corresponded to 5 and 0.5 times the K_D, respectively. The k_{on} and k_{off} values were 0.0032 nM^{-1} h^{-1} and 10 h^{-1}, respectively, representing the area of Figure 5 that is indicated with the square in the right panel.

A low value of the K_D (and therefore a low dose) will also lead to a difference in $Tmax_{TO}$ which is negligibly small or sometimes even negative (i.e. the highest dose leads to the highest $Tmax_{TO}$ value). In this area the assumption of a constant ligand concentration does not hold anymore, even when there is no elimination of the drug. This is caused by the depletion of ligand as a result of drug-target binding. When the ligand concentration is much lower than the target concentration, the equilibration rate can now be approximated by assuming the target concentration (Rtot) is constant, according to equation 3:

$$k_{obs} = kon * [Rtot] + koff \qquad (3)$$

From equation 3, it should be observed that there is no influence of the ligand concentration any more, and therefore the dose does not influence the $Tmax_{TO}$ anymore. The small band in Figure 5 where the difference in $Tmax_{TO}$ values is negative can be explained by the situation where the lowest dose has the same target concentration and drug concentration. In this case, both the target and the drug concentration decline upon drug-target binding and equilibration is twice as fast compared to the situation with a constant target or ligand concentration. This can make the equilibration of the lowest dose faster than that of the highest dose. An example of such a situation is shown Figure S 15.

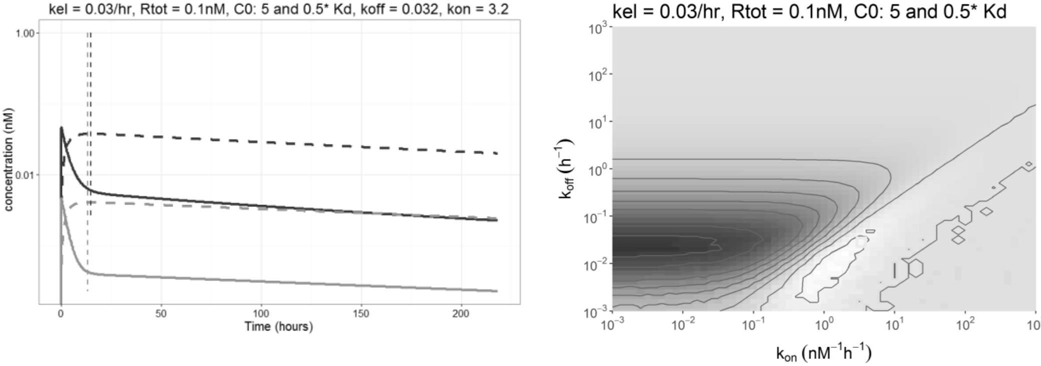

Figure S 15. Simulation of drug target binding for two different doses. The solid lines indicate plasma concentrations for the high (dark grey line) dose and the low (light grey line) dose. The dashed lines indicate target-bound drug concentrations. The vertical dotted lines indicate the time point of the maximal target-bound concentration for each dose. In this simulation, the elimination rate constant k_{el} was 0.03/hr and the target concentration was 0.1 nM. The initial concentrations for the high and the low dose corresponded to 5 and 0.5 times the K_D, respectively. The k_{on} and k_{off} values were 3.2 nM^{-1} h^{-1} and 0.032 h^{-1}, respectively, representing the area of Figure 5 that is indicated with the yellow square in the right panel.

To observe a change in $Tmax_{TO}$, it follows from the previous examples that the value of k_{off} should be low enough to make the change in $Tmax_{TO}$ observable, but it should not be so low that the elimination of the drug determines the $Tmax_{TO}$. Moreover, the initial concentration of the drug should not be lower than the target concentration. An example of such a situation is given in Figure S 16. Additionally, the lines $k_{off} = k_{el}/(c+1)$ and $K_D = Rtot/(c+1)$ align reasonably well with the middle and the diagonal end of the area where $Tmax_{TO}$ is most significant, where c represents the initial concentration/K_D ratio for the lowest dose as shown in Figure S 17.

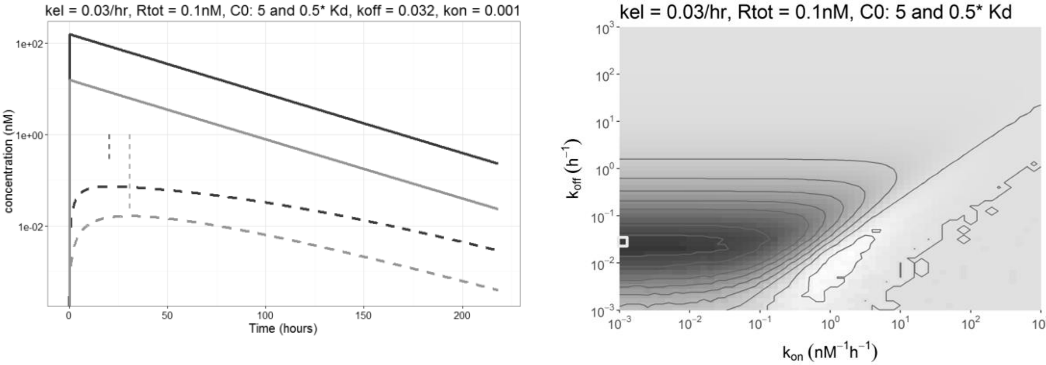

Figure S 16. Simulation of drug target binding for two different doses. The solid lines indicate plasma concentrations for the high (dark grey) dose and the low (light grey) dose. The dashed lines indicate target-bound drug concentrations. The vertical dotted lines indicate the time point of the maximal target-bound concentration for each dose. In this simulation, the elimination rate constant k_{el} was 0.03/hr and the target concentration was 0.1 nM. The initial concentrations for the high and the low dose corresponded to 5 and 0.5 times the K_D, respectively. The k_{on} and k_{off} values were 0.001 nM^{-1} h^{-1} and 0.032 h^{-1}, respectively, representing the area of Figure 5 that is indicated with the yellow square in the right panel.

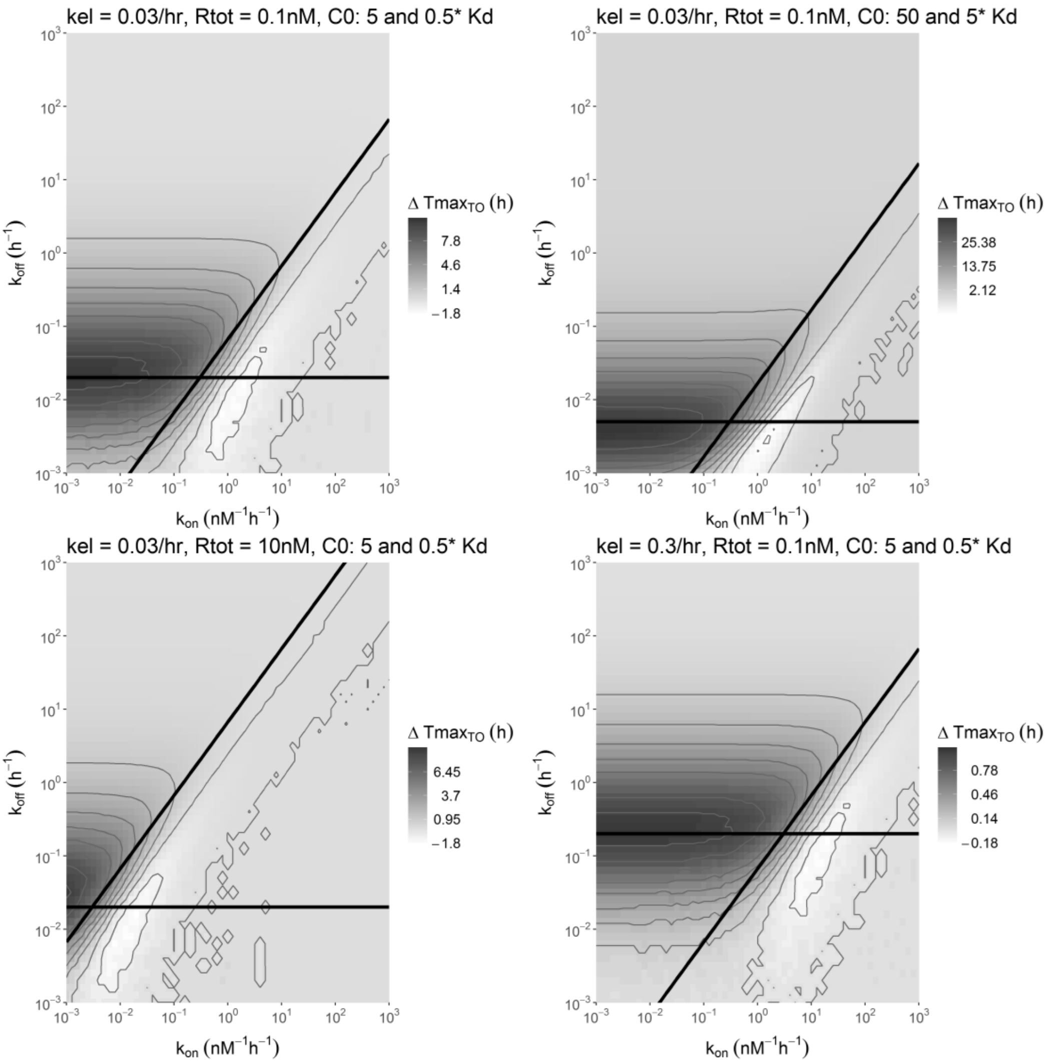

Figure S 17. Overview of the ΔTmax$_{TO}$ that was observed in the simulations as a result of the change in the affinity-normalized dose for different combinations of parameter values as indicated above the panels. All panels vary only one parameter compared to the upper left panel. The horizontal and diagonal lines represent the equations $k_{off} = k_{el}/(c+1)$ and $K_D = Rtot/(c+1)$, respectively, where c represents the initial concentration/K_D ratio for the lowest dose.

Supplement S 3. Asymptotic analysis of $Tmax_{TO}$ and its dependency on the dose.

1 One compartment model with drug-target binding

The model for drug-target binding is given by

$$\frac{dL}{dt} = -k_{el}L - k_{on}LR + k_{off}B$$

$$\frac{dB}{dt} = k_{on}LR - k_{off}B,$$

where

- L is the drug concentration,
- R is the **free** receptor concentration,
- B is the concentration of bound complex of L and R : $[LR]$,
- k_{on} is the rate constant at which L binds to free receptors,
- k_{off} is the rate constant at which L unbinds,
- k_{el} is the elimination rate constant.

Now, we use that the **total** receptor concentration is described by R_{tot} so that $R + B = R_{tot}$, and hence, $R = R_{tot} - B$. Then, after substituting this expression for R, the system becomes

$$\frac{dL}{dt} = -k_{el}L - k_{on}L(R_{tot} - B) + k_{off}B$$

$$\frac{dB}{dt} = k_{on}L(R_{tot} - B) - k_{off}B,$$

and hence,

$$\frac{dL}{dt} = -(k_{on}R_{tot} + k_{el})L + (k_{on}L + k_{off})B$$

$$\frac{dB}{dt} = k_{on}R_{tot}L - (k_{on}L + k_{off})B.$$

We study this system together with the initial conditions $L(0) = c\frac{k_{off}}{k_{on}} = cK_D$ and $B(0) = 0$.

The aim of this analysis is to determine the value of t where B attains a maximum for general c. We denote this maximum by $Tmax_{TO}(c)$. Furthermore, the interest is to determine the difference in $Tmax_{TO}(c)$ for two (different) values of c. More specifically for $c = c_1$ and $c = c_2$ where $c_2 > c_1$, we want to determine $Tmax_{TO}(c_2) - Tmax_{TO}(c_1)$.

2. Rescaling the system

In order to be able to analyse system (1.1), we rescale it by using the fact that both L and B can maximally reach certain concentrations. From the initial conditions it follows that the drug L is limited by drug dose $L(0) = cK_D = c\frac{k_{off}}{k_{on}}$. Also, the bound complex is limited by the total receptor concentration R_{tot}. This suggests to rescale L with cK_D and B with R_{tot}, and therefore, set $L = cK_D u$ and $B = R_{tot}v$. Then system (1.1) becomes

$$\frac{du}{dt} = -k_{el}u + k_{on}R_{tot}[-u + (u + \frac{1}{c})v]$$

$$\frac{dv}{dt} = ck_{off}[u - (u + \frac{1}{c})v],$$

with $u(0) = 1$ and $v(0) = 0$. In this system u corresponds to L and v to B.

Next, we study system (2.1) in different parameter regions and determine the value of t for which v attains a maximum.We use the different sets of coefficients present in system (2.1) to determine the various regions. In these regions, we use asymptotic analysis to determine an asymptotic expansion for v from which we determine the leading order of $Tmax_{TO}(c)$.

To define the regions, we look at the groups of parameters present in system (2.1) and set them to be equal. This gives us the following lines

$$ck_{off} = k_{el}$$

$$k_{off} = k_{el}$$

$$k_{off} = k_{on}R_{tot}$$

$$ck_{off} = \frac{k_{on}R_{tot}}{c}$$

$$k_{on}R_{tot} = k_{el}$$

$$k_{on}R_{tot} = ck_{el}.$$

In the following analysis, we assume that c is of order 1, hence $c = \mathrm{O}(1)$, then we define various regions

$$I. \quad ck_{off} = \mathrm{O}(k_{el}) \ and \ R_{tot} << K_D$$

$$II. \quad k_{el} << k_{off} \ and \ R_{tot} << K_D$$

$$III. \quad k_{off} << k_{el} \ and \ R_{tot} << K_D$$

$$IV. \quad k_{el} << k_{off} \ and \ R_{tot} >> K_D$$

$$V. \quad k_{off} << k_{el} \ and \ R_{tot} >> K_D.$$

Note that since $c = \mathrm{O}(1)$, not all the lines in (2.2) are needed when defining these regions. On the other hand, when *c* >> 1, the different lines are essential.

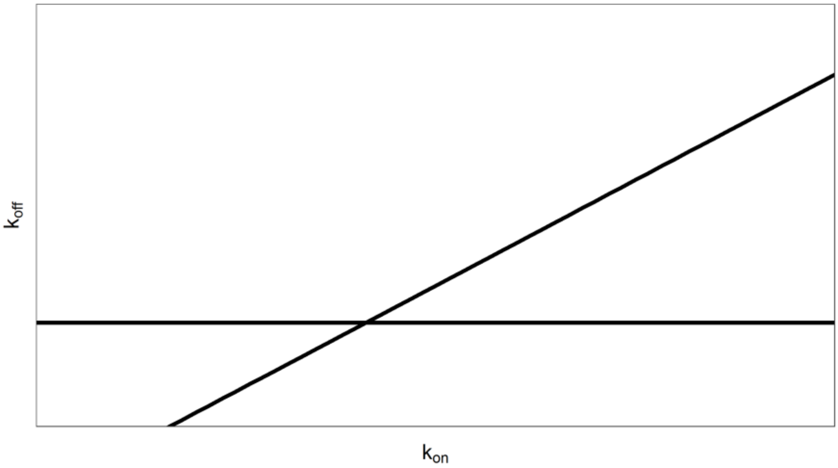

Figure S18: Sketch of the different regions in the (k_{on}, k_{off}) *-plane and the lines* $k_{off} = k_{el}$ *and* $R_{tot} = K_D$ *for* $c > 1$.

In these regions, we can find an asymptotic expression for v and determine the leading order expression for $Tmax_{TO}$. Here, we summarise the results.

In region I, we find that $Tmax_{TO}$ must satisfy an implicit relation depending on the different parameters. We introduce $a = \frac{ck_{off}}{k_{el}} = \mathrm{O}(1)$ then $Tmax_{TO} = \frac{\tau}{k_{el}}$, where τ must satisfy

$$a(c+e^{\tau})e^{a(ce^{-\tau}-\tau)}\int_0^{\tau} e^{-ace^{-s}+(a-1)s}ds = 1.$$

In the other regions we can determine the leading order of $Tmax_{TO}$ explicitly, this yields:

$$II. \quad Tmax_{TO} = -\frac{1}{(c+1)k_{off}}\log\left(\frac{k_{el}}{(c+1)^2 k_{off}}\right)$$

$$III. \quad Tmax_{TO} = -\frac{1}{k_{el}}\log\left(\frac{k_{off}}{k_{el}}\right)$$

$$IV. \quad Tmax_{TO} = -\frac{1}{k_{on}R_{tot}}\log\left((c+1)\frac{k_{off}}{k_{on}R_{tot}}\right)$$

$$V. \quad Tmax_{TO} = \frac{1}{k_{el}}.$$

Note that we denote with log the natural logarithm, $\ln$.

Hence, we find that when $k_{off} << k_{el}$ (in regions III and V) that $Tmax_{TO}$ **does not depend on** c, and therefore, is independent of the dosis, to leading order. For $k_{off} >> k_{el}$ (in regions II and IV), we find from the above expressions that $Tmax_{TO}$ **is small**, and so the dependence on the dose does also not play a role.

Note that the above results are not true for $c >> 1$. We briefly study that case in section 5.

To show how we obtain the above results, we give the details of the asymptotic analysis in two of the regions in the next sections.

3. The analysis in region III

We choose the parameters to lie in region III such that $R_{tot} << K_D$ and $k_{off} << k_{el}$. Then, we rescale time as $\tau = k_{el}t$ in this region and system (2.1) becomes

$$\frac{du}{d\tau} = -u + \delta[-u + (u + \frac{1}{c})v]$$

$$\frac{dv}{d\tau} = \varepsilon[u - (u + \frac{1}{c})v].$$

where $\delta = \frac{k_{on}R_{tot}}{k_{el}}$ and $\varepsilon = \frac{ck_{off}}{k_{el}}$. From the choice of the relation between the parameters, we find that $\delta << \varepsilon << 1$. Now, we assume the following asymptotic expansions for u and v

$$u = u_0 + \varepsilon u_{10} + \delta u_{01} + \textit{higher order terms},$$

$$v = v_0 + \varepsilon v_{10} + \delta v_{01} + \textit{higher order terms}.$$

And, from the initial conditions for system (2.1), it follows that $u_0(0)=1, u_{ij}(0)=0$, $v_{ij}(0)=0$ for all i, j.

In the following we assume that δ and ε^2 are not of the same order. Next, we substitute the above expansions into system (3.1), collect terms at different orders and solve the corresponding equations at each level.

At $O(1)$, we find that

$$\frac{du_0}{d\tau} = -u_0$$

$$\frac{dv_0}{d\tau} = 0.$$

This can be solved and, together with the initial conditions, this leads to $v_0 = 0$ and $u_0 = e^{-\tau}$.

Next, at $O(\varepsilon)$ we obtain

$$\frac{du_{10}}{d\tau} = -u_{10}$$

$$\frac{dv_{10}}{d\tau} = u_0 - (u_0 + \frac{1}{c})v_0 = u_0.$$

Together with the initial conditions, this gives $u_{10} = 0$ and $v_{10} = 1 - e^{-\tau}$. Since this v_{10} does not attain a maximum, we need to determine higher order terms in the expansion of v.

Then, at $O(\delta)$ we find

$$\frac{du_{01}}{d\tau} = -u_{01} - u_0 + (u_0 + \frac{1}{c})v_0$$

$$\frac{dv_{01}}{d\tau} = 0,$$

which yields $v_{01} = 0$. It turns out we don't need u_{01} to determine $Tmax_{TO}$ so we refrain from giving that here.

At $O(\varepsilon^2)$ we obtain

$$\frac{dv_{20}}{d\tau} = u_{10} - (u_0 + \frac{1}{c})v_{10} - u_{10}v_0$$

$$= -(e^{-\tau} + \frac{1}{c})(1 - e^{-\tau})$$

$$= e^{-2\tau} + \frac{1-c}{c}e^{-\tau} - \frac{1}{c}.$$

From this, we find

$$v_{20} = \frac{1}{2}(1 - e^{-2\tau}) - \frac{\tau}{c} + \frac{1-c}{c}(1 - e^{-\tau}).$$

Since we do not need u_{20} for further analysis, we also do not give that here.

Now, collecting the various terms, we find that

$$v(\tau) = \varepsilon(1 - e^{-\tau}) + \varepsilon^2\left(\frac{1}{2}(1 - e^{-2\tau}) + \frac{1-c}{c}(1 - e^{-\tau}) - \frac{\tau}{c}\right)$$

to leading order. Using this expression, we can obtain a leading order expression for $Tmax_{TO}$. Differentiating we find

$$\frac{dv}{d\tau} = \varepsilon e^{-\tau} + \varepsilon^2\left(e^{-2\tau} + \frac{1-c}{c}e^{-\tau} - \frac{1}{c}\right).$$

Setting this expression to zero, we can find $Tmax_{TO}$ from a balance between the first and the last term. Hence, we set $\varepsilon e^{-\tau} = \varepsilon^2 \frac{1}{c}$ which leads to

$$\tau = -\log(\frac{\varepsilon}{c}).$$

Rescaling back to original variables and parameters, we obtain

$$Tmax_{TO} = -\frac{1}{k_{el}}\log(\frac{k_{off}}{k_{el}}).$$

4. The analysis in region V

In this section, we choose the parameters to lie in region V such that $k_{off} << k_{el}$ and $K_D << R_{tot}$. We rescale time as $\tau = k_{on}R_{tot}t$ in this region and system (2.1) becomes

$$\frac{du}{d\tau} = -\delta u - u + (u + \frac{1}{c})v$$

$$\frac{dv}{d\tau} = \varepsilon[u - (u + \frac{1}{c})v],$$

where $\delta = \frac{k_{el}}{k_{on}R_{tot}}$ and $\varepsilon = \frac{ck_{off}}{k_{on}R_{tot}}$. From the choice of the relation between the parameters, we find that $\varepsilon << \delta << 1$. Now, we assume the following asymptotic expansions for u and v

$$u = u_0 + \delta u_{01} + \varepsilon u_{10} + higher\,order\,terms,$$

$$v = v_0 + \delta v_{01} + \varepsilon v_{10} + higher\,order\,terms.$$

From the initial conditions for system (2.1), it follows that $u_0(0) = 1, u_{ij}(0) = 0$, $v_{ij}(0) = 0$ for all i, j.

In the following we assume that δ^2 and ε are not of the same order. Next, we substitute the above expansions into system (4.1), collect terms at different orders and solve the corresponding equations at each level.

At $O(1)$ we find that

$$\frac{du_0}{d\tau} = -u_0 + (u_0 + \frac{1}{c})v_0$$

$$\frac{dv_0}{d\tau} = 0.$$

This can be solved and, together with the initial conditions, this leads to $v_0 = 0$ and $u_0 = e^{-\tau}$.

Next, at $O(\delta)$ we find

$$\frac{du_{01}}{d\tau} = -u_{01} - u_0 + (u_0 + \frac{1}{c})v_{01}$$

$$\frac{dv_{01}}{d\tau} = 0,$$

which yields $v_{01} = 0$. Solving for u_{01} leads to

$$u_{01} = -\tau e^{-\tau}.$$

At $O(\varepsilon)$ we obtain

$$\frac{du_{10}}{d\tau} = -u_{10} + (u_0 + \frac{1}{c})v_{10} + u_{10}v_0$$

$$\frac{dv_{10}}{d\tau} = u_0 - (u_0 + \frac{1}{c})v_0 = u_0.$$

Together with the initial conditions, this gives $v_{10} = 1 - e^{-\tau}$. We do not give u_{10} since we will not need it in the further analysis. Again, v_{10} does not attain maximum, and therefore, we need higher order terms in the expansion of v.

At $O(\delta^2)$ we find that $v_{02} = 0$ and so we need to go to $O(\varepsilon\delta)$ where

$$\frac{dv_{11}}{d\tau} = u_{01} - (u_0 + \frac{1}{c})v_{01} - u_{10}v_0$$

$$= -\tau e^{-\tau}.$$

Hence,

$$v_{11} = (\tau + 1)e^{-\tau} - 1,$$

and the expansion for v reads

$$v = \varepsilon\left(1 - e^{-\tau} + \delta((\tau+1)e^{-\tau} - 1)\right),$$

to leading order. Differentiating leads to

$$\frac{dv}{d\tau} = \varepsilon\left(e^{-\tau} - \delta\tau e^{-\tau}\right),$$

which becomes zero when

$$\tau = \frac{1}{\delta}.$$

Rescaling back to original variables and parameters, we obtain

$$Tmax_{TO} = \frac{1}{\delta k_{on} R_{tot}} = \frac{1}{k_{el}}.$$

5. The case when $c >> 1$.

Next, we briefly look at the case when $c >> 1$. Then, the results are different from before. One essential difference is that the regions now depend on c where $c >> 1$.

We will only give results for region I. Note that this region shifts down in the (k_{on}, k_{off}) -plane compared to before.

We do still find that $Tmax_{TO}$ must satisfy an implicit relation depending on the different parameters. We find that $Tmax_{TO} = \dfrac{\tau}{k_{el}}$, where τ must satisfy

$$e^{a(e^{-\tau}-1)-\tau} - \frac{1}{c}\left(1 - e^{a(e^{-\tau}-1)} + ae^{ae^{-\tau}-\tau}(\tau e^{-b} - \int_0^{\tau} e^{-ae^{-s}} ds)\right) = 0,$$

and $a = \dfrac{ck_{off}}{k_{el}} = \mathrm{O}(1)$.

Chapter 8. *In vitro* and *in silico* analysis of the influence of D_2 antagonist target binding kinetics on the cellular response to fluctuating dopamine concentrations

Wilhelmus E. A. de Witte[1], Joost W. Versfelt[1], Maria Kuzikov[2], Solene Rolland[3], Victoria Georgi[3], Philip Gribbon[2], Sheraz Gul[2], Dymphy Huntjens[4], Piet Hein van der Graaf[1,5], Meindert Danhof[1], Amaury Fernández-Montalván[3], Gesa Witt[2], Elizabeth C. M. de Lange[1*].

[1] Division of Pharmacology, Leiden Academic Centre for Drug Research, Leiden University, 2333 CC Leiden, The Netherlands

[2] Fraunhofer Institute for Molecular Biology and Applied Ecology, ScreeningPort, Hamburg, Germany

[3] Bayer Healthcare Pharmaceuticals, Global Drug Discovery, Berlin, Germany

[4] Janssen R&D, Janssen Pharmaceutica, Beerse, Belgium

[5] Certara Quantitative Systems Pharmacology, Canterbury Innovation Centre, Canterbury CT2 7FG, United Kingdom

* Correspondence: ecmdelange@lacdr.leidenuniv.nl

Manuscript under revision for the British Journal of Pharmacology

Abstract

Introduction

Target binding kinetics can influence the time course of the drug effect (pharmacodynamics) both I) directly, by affecting the time course of target occupancy, driven by the pharmacokinetics of the drug, competition with endogenous ligands and target turnover, and II) indirectly, by affecting signal transduction and homeostatic feedback at the cellular and systems level. For dopamine D_2 antagonists, it has been hypothesized that fast receptor binding kinetics cause fewer side effects, because part of the dynamics of the dopaminergic system is preserved by displacement of these antagonists.

Methods

Target binding kinetics of D_2 antagonists and agonists and signal transduction after dopamine and D_2 antagonist exposure were measured *in vitro*. These data were integrated by mechanistic modeling, taking into account competitive binding of endogenous dopamine and the antagonist, the turnover of the second messenger cyclic adenosine monophosphate (cAMP), and negative feedback by phosphodiesterase turnover.

Results

The proposed signal transduction model successfully described the cellular cAMP response for 17 D_2 antagonists with widely different binding kinetics. Simulation of the response to fluctuating dopamine concentrations revealed that a significant effect of the target binding kinetics on the dynamics of the signaling only occurs at endogenous dopamine concentration fluctuations with frequencies below 1/min.

Conclusion

Signal transduction and feedback are important determinants of the time course of drug effects. The influence of the D_2 antagonist dissociation rate constant (k_{off}) is limited to the maximal rate of fluctuations in dopamine signaling as determined by the dopamine k_{off} and the cAMP turnover.

Abbreviations: cAMP: cyclic adenosine monophosphate, DMR: Dynamic Mass Redistribution, PDE: Phosphodiesterase, PPHT: poly-3-phenylhydrazone thiophene, RT: room temperature

Introduction

The potential influence of drug-target association and dissociation kinetics on the time course of drug effects (pharmacodynamics) has led to an increasing interest in the use of binding kinetic parameters as a criterion in the selection of drug candidates.[1–6] Although the influence of binding kinetics on the time course of target occupancy has been studied, its exact role in the complex relation between drug dosing and drug effect is potentially complex and not completely understood.[7,8]

Under distinct circumstances, target binding kinetics can influence the pharmacodynamics directly by affecting the time course of the target occupancy. To what extent this occurs depends on values of the rate constants of target association(k_{on}) and dissociation(k_{off}), relative to the pharmacokinetic rate constants characterizing the rates of tissue distribution and elimination. In this regard, additional factors to be taken into consideration are the rate constants characterizing the turnover of the target and the competition with endogenous target ligands. In addition to these direct effects of target binding on the pharmacodynamics, variation in k_{on} and k_{off} can also indirectly influence the pharmacodynamics via signal transduction and homeostatic feedback mechanisms, both at the cellular and the systems level.[7–11] The possible influence of the drug-target dissociation rate constant (k_{off}) on signal transduction has been suggested previously, based on observed *in vitro* efficacy measurements that correlated with k_{off}, but not with the equilibrium dissociation constant K_D.[12,13]

One target for which the influence of drug-target binding kinetics on *in vivo* drug effects is thought to be relevant is the dopamine D_2 receptor. Almost two decades ago, the influence of drug-target binding kinetics on the safety of dopamine D_2 antagonists has been suggested, based on the correlation between low values of k_{off} and the lack of typical side effects, such as extrapyramidal symptoms (i.e. atypicality).[14] This observation led to the hypothesis that quickly dissociating antagonists induce less side effects by allowing displacement from the receptor by fluctuating dopamine concentrations and thus preserving part of the dopamine dynamics, which we will refer to as the “fast-off hypothesis” in this study.[15–18] To understand the influence of dopamine D_2 antagonist binding kinetics on their efficacy and safety, it should be noted that the fluctuations in dopamine concentrations occur at various time scales, ranging from hours to microseconds.[16,19,20] The influence of these target binding kinetics needs to be studied in comparison to dopamine fluctuations at all these time scales.

The dopamine D_2 receptor belongs to the class of inhibitory G-protein coupled receptors (GPCRs). Thus, receptor activation is known to inhibit cAMP production and cAMP in turn is known to stimulate active PDE production, while active PDE stimulates degradation of cAMP. Moreover, GPCR receptor activation can lead to receptor phosphorylation and desensitization as described quantitatively for the β_2-Adrenergic receptor.[21] The production of cAMP is thus regulated by a negative feedback loop, which is a common feature in signal transduction pathways[22].

In this respect, it should be noted that the distinction between agonists and antagonist is often based on historical data and does not always take into account the classification of partial agonists and inverse agonists. One example of this is the study in which Remoxipride was introduced as D_2 antagonist based on its *in vivo* antidopaminergic action and the lack of *in vitro* adenylyl cyclase inhibition in rat striatum homogenate. [23] This study does not report the possibility of adenylyl cyclase stimulation, and inverse agonism is thus not excluded. Moreover, the occurrence of inverse agonism and partial agonism can be influenced by the experimental system and cannot directly be translated across systems. Many D_2 binding drugs that have initially been classified as antagonist have been reported to function as inverse agonists.[24,25] For convenience, we only apply the terms agonist and antagonist in this study, but we assume that the antagonists can have inverse agonistic activities.

In this study, *in vitro* and *in silico* methods were combined to elucidate the influence of D_2 antagonist target binding kinetics on the cellular response to fluctuating dopamine concentrations and to investigate the fast-off hypothesis. Firstly, experimental methods were developed to quantify the binding kinetics of D_2 agonists and antagonists to investigate if the binding kinetics were different for these two types of D_2 ligands.

Secondly, to investigate the fast-off hypothesis with respect to the competition between antagonists and dopamine, the cellular response kinetics after subsequent exposure to dopamine and D_2 receptor antagonists with varying binding kinetics at different levels of the signaling pathway were measured. A minimal mechanistic model combining D_2 receptor binding kinetics, D_2 receptor turnover, cAMP and active PDE turnover was established to describe cAMP concentration *versus* time curves in response to D_2 antagonist exposure. Thirdly, the model was used to identify the role of binding kinetics on drug effect for fluctuating dopamine concentrations. The physiological range of dopamine fluctuation time scales was taken into account by using a frequency response analysis [22,26]. For a more general insight in the influence of binding kinetics on signal transduction, this analysis was expanded to a range of hypothetical turnover rates of cAMP and active PDE.

Methods

This study consists of three parts:

I) *In vitro* measurements of target binding and signal transduction kinetics: drug-target binding parameters of 17 dopamine D_2 antagonists and 12 agonists were measured at room temperature (RT) and at 37°C. Only for the antagonists, the *in vitro* response after dopamine pre-incubation was measured for two different biomarkers: cAMP concentrations over time as second messenger and Dynamic Mass Redistribution (DMR) as a composite signaling marker.

II) Model-based analysis of the *in vitro* cAMP antagonist response curves: A minimal mechanistic model was developed to describe the cAMP responses of the antagonists, based on the target binding kinetics as determined in part I).

III) Frequency Response Analysis: Simulations of the predicted in vivo response to fluctuating dopamine concentrations: The mechanistic model was used to simulate the cAMP response to dopamine concentrations that fluctuate according to a sine-wave pattern with a range of physiologically relevant frequencies between $2 * 10^{-6}$ min^{-1} and 7 min^{-1}. The fluctuation amplitude of cAMP, compared to dopamine, was used to summarize the cAMP response.

I) *In vitro* measurements of target binding and signal transduction kinetics

Equilibrium and Kinetic Probe Competition Assay (ePCA and kPCA)

Affinity and kinetic binding parameters for the 17 studied antagonists and the additional 12 agonists (see Table 1) were measured with a homogeneous time-resolved fluorescence energy transfer (TR-FRET) method as previously described for the Histamine H1 and the GnRH receptors [27,28]. In this study, Tag-lite® Dopamine D_2 labeled cells and a poly-3-phenylhydrazone thiophene (PPHT)-based Dopamine D_2 receptor red antagonist Fluorescent Ligand (both from Cisbio, Codolet, France) were used as receptor-tracer pair to be competed with unlabeled test compounds (Tocris bioscience, TRC, Sigma-Aldrich, Biotrend Chemicals AG or provided by Janssen). Briefly, frozen cells containing the terbium (Tb^{2+}) labeled D_2 receptor, were thawed, spun down and re-suspended in Tag-lite® buffer (Cisbio, Codolet, France) to the concentration indicated by the manufacturer and dispensed into Greiner black small volume 384-well microtiter plates already containing the fluorescent tracer (10 nM end concentration) and the test compounds (antagonists/agonists). These compounds were diluted and transferred to the test plates following the procedures described previously [27].

Starting concentrations of the D_2 antagonist/agonist dilution series were adapted according to their expected affinity, in order to cover a meaningful dose range (see Figure S 1). The ePCA and kPCA experiments as described above were performed at RT and 37°C, for which steady state assay plates were kept in standard tissue culture incubators, whereas for kinetic assays the temperature control function of the PHERAstar FS™ microtiter plate reader was used. For ePCA, tracer and D_2 labeled cells were dispensed to the ready-to-use compound plates to a final volume of 5 µL, and the mixture was incubated for 1-2 h prior to acquisition of the steady state TR-FRET ratiometric signals (665/620 nm) upon excitation at 337 nm. Normalized values were fitted to a logistic 4-parameter model using the Genedata Screener™ software, and

Ki values calculated using the Cheng-Prusoff relationship [29]. For kPCA, the tracer was dispensed to the ready-to-use compound plates prior to introducing them into the PHERAstar FS^{TM} microtiter plate reader. Then the D_2 labeled cells were added to wells to a final volume of 10 µL using the injector system of the instrument, and kinetic TR-FRET readings were made at time zero and every 21-sec or 100-seconds (depending on whether faster or slower compounds were being measured) for the times indicated in Figure S 1. Baseline-normalized kinetic traces were analyzed with a competitive binding kinetics model [30] adapted to deal with normalized- instead of blank-subtracted curves using the Genedata Screener^{TM} software. Prior to D_2 agonist/antagonist testing, binding saturation and kinetic association and dissociation curves for the Dopamine D_2 receptor red antagonist Fluorescent Ligand were recorded as described previously [27,28]. Subsequently, these curves were fitted to the corresponding models using Graph Pad Prism^{TM} in order to obtain the affinity and kinetic constants used as parameters in the Cheng-Prusoff and Motulsky and Mahan models.[29]

cAMP assay

CHO/hD2L and wt-CHO cells were grown in DMEM/F12 with Glutamine (without phenol red, Gibco), 1 % heat inactivated FCS, 1 x Penicillin/ Streptomycin, 400 µg/mL G418. Cells were cultured in humidified atmosphere at 37°C and 5 % CO_2 in air.
To gain insight in the activity of known antagonists after binding to the D2-receptor, changes in the cellular cAMP level were analyzed. To allow real time kinetic measurement, a cAMP-biosensor variant pGloSensor™-22F (Promega Corporation) was used, which consists of a cAMP binding domain (cAMP binding domain B from human PKA regulatory subunit type II β) fused to mutant luciferase. Binding of cAMP results in a conformational change and an increase in luminescence signal. The use of the biosensor system provides a method for a real-time measurement of changes in the cAMP level in a non-lytic assay format. Cells from a Chinese Hamster Ovary (CHO) cell line stably transfected with the long isoform of the human Dopamine 2 receptor, CHO/hD_2L cells, were kindly provided by Janssen Pharmaceutica.

CHO/hD_2L cells (15,000/50 µL) were transiently transfected with the pGloSensor™-22F plasmid (2ng/µL i.a.) using FuGeneHD transfection reagent (3 µL FuGeneHD: 1 µg DNA plasmid, Promega, Madison, USA). By reaching 70-80% confluency, cells were harvested using Trypsin/EDTA and resuspended in DMEM/F-12/ HEPES medium supplemented with 1% fetal calf serum (FCS), Pen/Strep and 1 mg/ml G418. Prior to addition of the pGloSensor™-22F plasmid to cells, it was incubated for 20 min with the FuGeneHD transfection reagent at room temperature. By the end of incubation time, the cells and transfection solution were combined, mixed and plated in white, solid bottom 384 well assay plates (Greiner CELLSTAR® 384 well plates). After 24 h of incubation the transfection mixture was replaced by 20 µL/well DMEM/F-12/HEPES medium with 9% Glo-substrate followed by 2 h incubation at room temperature. To achieve a good signal window, CHO/hD_2L cells were treated with 3 µM forskolin for 30 min. Forskolin was used as an activator of the adenylate cyclase and therefore for a receptor-independent increase of the cellular cAMP level. In order to monitor antagonist activity against the natural receptor ligand, cells were incubated with 15 nM dopamine for 20 min prior to addition of antagonists. D_2 receptor antagonists were tested in a 10-point dose response (top concentration 10 µM, 1:4 dilutions). Signal kinetics was detected for a total period of 1h every 2min. All compounds were dissolved in dimethyl sulfoxide (Carl Roth GmbH + Co. K, Karlsruhe, Germany).

Dynamic mass redistribution (DMR) Assay

For DMR measurements[31], 10 µl/ well cell culture media(DMEM/ F12 without phenol red, Gibco) were transferred into an EnSpire-LFC 384– fibronectin coated plate (PerkinElmer, Waltham, USA) and incubated for 30 min. A suspension of CHO/hD_2L cells in cell culture media was prepared and cells were seeded into the label-free cellular (LFC) plate (1.5 x 10^4 cells/well), resulting in a final volume of 30 µl/ well. The LFC plate was incubated overnight in a humidified atmosphere at 37°C and 5 % CO2 in air.
On the next day, label-free assay buffer (HBSS (Sigma Aldrich), 20 mM HEPES (Sigma Aldrich), 0.5 % (v/v) DMSO, 0.05 % v/v Pluronic (AnaSpec)) was prepared. Dopamine was diluted in label-free assay buffer (5 uM, final assay concentration) and dispensed into an intermediate plate (Polypropylen 384 well microplate

(Greiner Bio-One GmbH, Frickenhausen, Germany)). Of each antagonist, a dilution series in dimethyl sulfoxide was prepared and transferred into an intermediate plate. Label free assay buffer was added to the intermediate plate to dilute the antagonists further.

The media was removed from the LFC plate by washing the wells four times with label-free assay buffer (25 µl/ well). The total assay volume after the washing step was 30 µl/ well. The LFC plate was placed in an EnSpire multimode reader equipped with Corning® Epic® Label-free technology (PerkinElmer). After 2 h, a baseline was recorded (10 minutes) followed by the addition of Dopamine or vehicle control (10 µl/well) from the intermediate plate. Antagonist dispensing and mixing was automated using a Janus Workstation (PerkinElmer). A 20-min kinetic DMR measurement was recorded on the EnSpire multimode reader. Directly afterwards, the D_2R antagonists were transferred from the intermediate plate to the LFC plate (10 µl/well) and a 90-min kinetic DMR measurement was initiated on the EnSpire multimode reader.

II) Model-based analysis of the *in vitro* cAMP antagonist response curves

Modeling procedure

To obtain a detectable cAMP signal, adenylyl cyclase was activated first by forskolin. The dynamics of this activation was recorded in a separate experiment. Since the cAMP response to forskolin addition was measured separately from the cAMP response to the D_2 receptor antagonists, the D_2 antagonist response measurements were normalized to the average cAMP response before antagonist addition (baseline). A mechanistic model, based on previous models and mechanistic information from literature [21,24,25,32–34], combining dopamine-receptor binding kinetics, antagonist-receptor binding kinetics, and cAMP as well as active PDE turnover to describe the generation of the cAMP response was used to simultaneously fit the cAMP data of all compounds. A diversity of models, with differences in mechanistic detail (Table 2), was tested for their utility to describe the cAMP responses. Model fitting was performed in NONMEM v7.3 using ADVAN9. All values of k_{off}, including the k_{off} of dopamine, were fixed to the values that were measured according to the methods described above, while the K_D values were estimated. Models were selected based on the objective function value (OFV) and visual inspection of the individual fits of the experiments. A schematic overview of the final model structure that was fitted to the cAMP response data (model 1) is given in Figure 1.

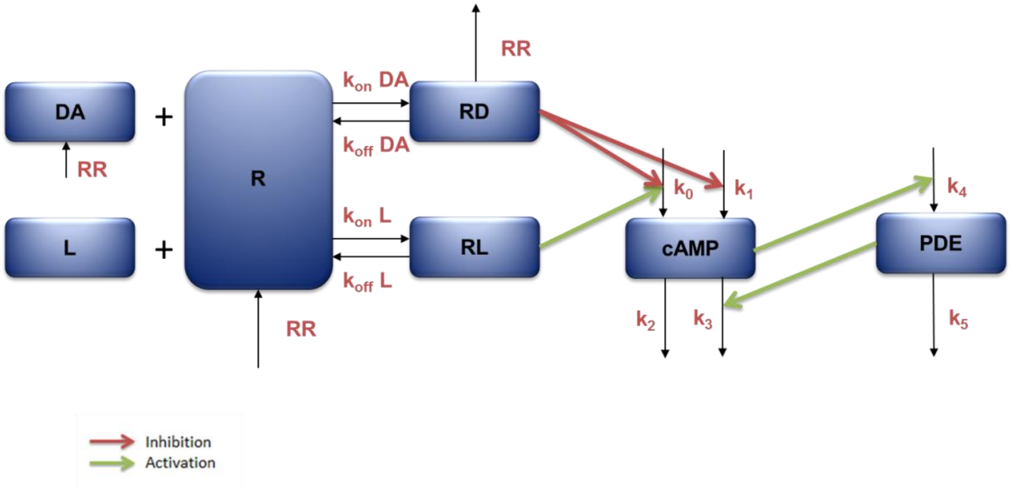

Figure 1. Schematic overview of the structure of the final model (Model 1). DA denotes dopamine, L denotes the antagonist, R denotes the D_2 receptor RD the D_2 receptor-dopamine complex, RL the receptor antagonist complex. RR indicates receptor recycling; the internalization (or degradation) of the dopamine-receptor complex and the resurfacing (or synthesis) of the unbound receptor and dopamine. Black arrows denote mass transfer, green arrows an activating interaction, red arrows an inhibiting interaction. The equations of Model 1 are given in Supplement S 3.

III) Frequency Response Analysis: Simulations of the predicted *in vivo* response to fluctuating dopamine concentrations

Dopamine concentrations were varied over time according to a sine wave with various frequencies and an amplitude of 10 nM. This dopamine fluctuation induces fluctuations in the cAMP concentrations, but the amplitude of these fluctuations is dependent on the frequency of the dopamine fluctuations. To get a complete analysis of the cAMP response to fluctuating dopamine concentrations in the presence of an antagonist and to cover all physiologically relevant frequencies [16,19,20], a wide frequency range was tested between $2 * 10^{-6}$ min^{-1} and 7 min^{-1}. After the cAMP concentration had reached constant fluctuation around the average steady state (i.e. the mean of the minimal and maximal concentration), the amplitudes of both the dopamine and the cAMP concentrations were converted amplitudes relative to their average steady state values and their ratio was defined as the “cAMP gain”, according to equation 1. This gain is a measure for the degree in which dopamine fluctuations results in cAMP fluctuations. All simulations were performed in Rstudio using the deSolve package and the lsoda differential equation solving method.[35,36]

$$Gain\ cAMP = \frac{\frac{amplitude\ cAMP}{average\ steady\ state\ cAMP}}{\frac{amplitude\ dopamine}{average\ steady\ state\ dopamine}} \qquad \text{Eq. 1}$$

Results

I) *In vitro* measurements of target binding and signal transduction kinetics

We have used a novel TR-FRET based assay technology to measure the K_D, k_{on} and k_{off} values of 17 dopamine D_2 antagonists and 12 agonists at both room temperature and 37°C. The results (shown in Figure 2, Table 1, Table S 1 and Table S 2) are in good agreement with previous literature reports that used radioligand binding [17,18,37–46]. Figure 2 shows that both the D_2 antagonists and agonists in this study had diverse combinations of k_{on} and k_{off} values, and that none of them had a combined low k_{on} and low k_{off} value. Figure 2 also shows that the investigated agonists tend to have higher k_{off} values and lower k_{on} values compared to the investigated antagonists. For compounds with higher dissociation rates than the competing fluorescent ligand ($k_{off} \geq 0.01$ s^{-1}) the precision of their k_{off} estimates is limited, or only the lower limit could be identified. However, for the experiments and model fits in this study, the exact value of the k_{off} has less influence on the cAMP concentration for fast compared to slow dissociating compounds and a low precision for high k_{off} values is thus acceptable for the scope of this study.

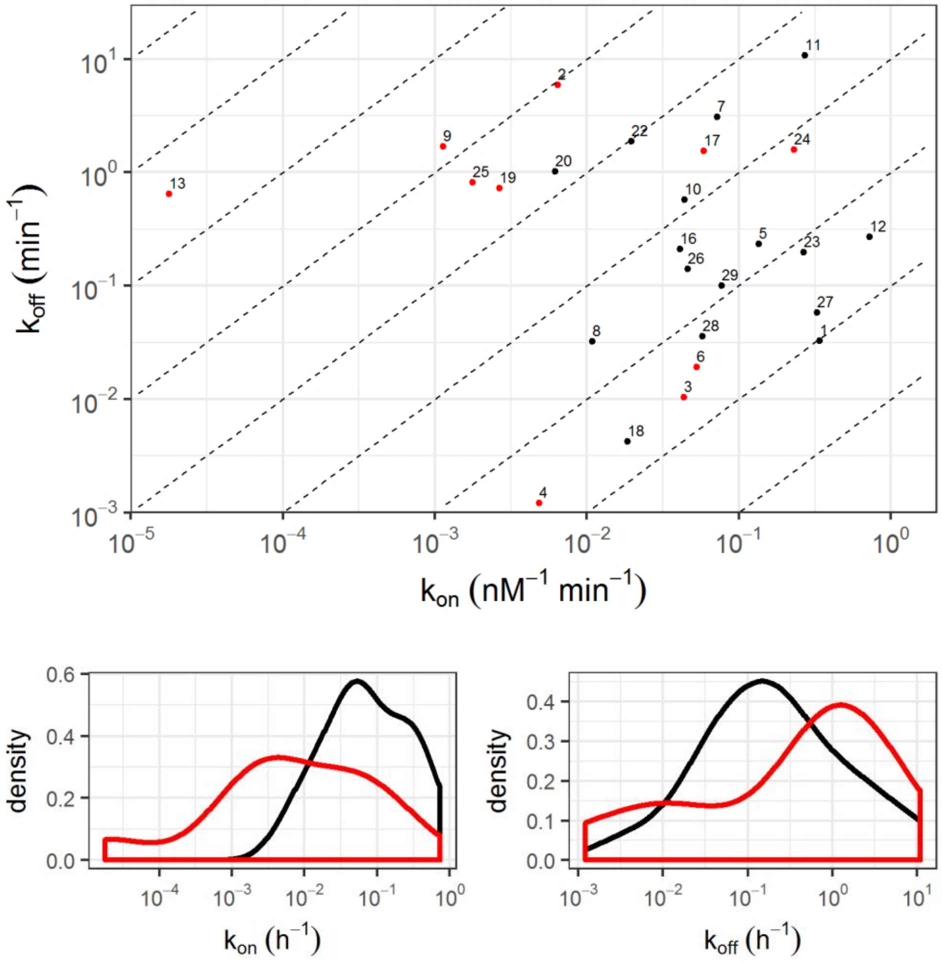

Figure 2. In vitro measurements of k_{on} and k_{off} for each of the measured D_2 antagonists from the kPCA assay at room temperature. Red symbols/lines represent agonists, black symbols/lines antagonists. Upper panel: The numbers refer to the compound numbers in Table 1. Lower panel: distribution of k_{on} and k_{off} for agonists compared to antagonists, plotted as the estimated probability density function.

Table 1. *In vitro* measurement of k_{on}, k_{off}, their standard deviation (SD) and the calculated K_D for each of the measured D_2 antagonists from the kPCA assay at room temperature. NA: not available, NPA: N-n-Propyl Apomorphine

Compound ID	#	K_D [M]	SD	k_{on} [1/(M*s)]	SD	k_{off} [1/s]	SD
(-)-Nemonapride	1	9.58E-11	3.26E-12	5.66E+06	2.73E+05	5.43E-04	4.46E-05
(-)-Quinpirole	2	7.80E-07	6.28E-07	1.07E+05	4.77E+04	9.82E-02	1.04E-01
Aripiprazole	3	2.39E-10	4.40E-13	7.24E+05	3.17E+05	1.73E-04	7.52E-05
Bromocriptine	45	2.19E-10	1.96E-10	8.09E+04	2.54E+04	2.02E-05	1.80E-05
Bromperidol	5	1.89E-09	7.49E-10	2.26E+06	9.57E+05	3.91E-03	1.21E-04
Cabergoline	6	4.26E-10	2.13E-10	8.80E+05	5.13E+05	3.21E-04	3.15E-05
Clozapine	7	5.05E-08	1.28E-08	1.20E+06	1.44E+06	5.13E-02	5.74E-02
Domperidone	8	3.04E-09	5.08E-10	1.81E+05	5.26E+04	5.37E-04	6.75E-05
Dopamine	9	1.27E-06	5.56E-07	1.88E+04	2.16E+04	2.82E-02	3.01E-02
JNJ-37822681	10	9.32E-09	2.71E-09	7.33E+05	NA	9.54E-03	NA
JNJ-39269646	11	4.87E-08	8.35E-09	4.53E+06	4.51E+06	1.79E-01	1.64E-01
Haloperidol	12	3.82E-10	4.98E-11	1.21E+07	5.18E+06	4.48E-03	1.37E-03
Memantine	13	2.61E-05	9.91E-06	2.98E+02	NA	1.07E-02	NA
NPA	14	NA	NA	NA	NA	NA	NA
Olanzapine	15	8.58E-09	3.38E-09	> 7.30E+05	NA	> 1.00E-02	NA
Paliperidone	16	5.45E-09	2.07E-09	6.81E+05	1.83E+05	3.52E-03	4.14E-04
Pergolide	17	2.44E-08	1.24E-08	9.81E+05	NA	2.59E-02	NA
Pimozide	18	2.55E-10	6.74E-11	3.10E+05	2.45E+05	7.08E-05	4.17E-05
Piribedil	19	2.23E-07	5.90E-08	4.43E+04	9.30E+03	1.21E-02	4.18E-03
Quetiapine	20	1.50E-07	6.94E-08	1.03E+05	2.04E+04	1.69E-02	6.07E-03
R-(-)-Apomorphine	21	1.70E-07	7.68E-08	> 8.85E+04	NA	> 1.00E-02	NA
Remoxipride	22	8.31E-08	3.47E-08	3.28E+05	NA	3.14E-02	NA
Risperidone	23	7.56E-10	7.62E-11	4.43E+06	8.54E+05	3.31E-03	3.09E-04
Rotigotine	24	7.82E-09	2.86E-09	3.84E+06	3.78E+06	2.65E-02	2.75E-02
S-(+)-Apomorphine	25	3.33E-07	1.15E-07	2.94E+04	NA	1.36E-02	NA
Sertindole	26	4.07E-09	2.23E-09	7.70E+05	7.00E+05	2.35E-03	1.13E-03
Spiperone	27	1.79E-10	4.11E-12	5.44E+06	1.11E+06	9.70E-04	1.76E-04
S-(+)-Raclopride	28	6.34E-10	1.15E-10	9.57E+05	1.81E+05	5.96E-04	4.62E-06
Ziprasidone	29	1.31E-09	8.40E-11	1.29E+06	2.01E+05	1.67E-03	1.55E-04

Our cAMP and DMR measurement provide a new and extensive set of signal transduction data for 17 D_2 antagonists. Figure 3 shows the measured cAMP concentrations during the complete time course of a typical experiment with and a control experiment without dopamine D_2 receptor transfection. For comparison, the DMR responses are given in Supplement S 2, Figure S 3. In Figure 4, the complete set of measured cAMP time courses for all 17 D_2 antagonists at 10 different concentrations is given, together with their model fits. The data in Figure 4 show that the antagonists with lower k_{off} values (pimozide, domperidone, raclopride) induce cAMP concentration-time curves for the lower antagonist concentrations, with later and lower peak concentrations, compared to faster dissociating compounds (JNJ-39269646, Clozapine, Olanzapine). However, this trend was not observed in the DMR data (see Supplement S 2).

II) Model-based analysis of the *in vitro* cAMP antagonist response curves

Model selection

A series of related model structures, which differed in mechanistic detail, was evaluated for their utility to describe the cAMP responses (Table 2). From these models, Model 1 was selected as the final model for further analyses. This model selection was based on the lowest Objective Function Value (OFV) and on the goodness of fit, as described in the methods. In Model 1, all antagonists also functioned as inverse agonists by stimulating cAMP production (see Figure 1), and the inverse agonism efficacy was estimated by the model for each antagonist. Model 1 was compared with alternative models to ensure that Model 1 was the optimal model:

Model 2 incorporated more mechanistic detail compared to Model 1 by including the role of PKA in linking the cAMP concentrations to active PDE concentrations. The performance of Model 2 was identical to the performance of the simpler Model 1. In addition, the estimated value of PKA turnover was high compared to cAMP and active PDE turnover, which means that the PKA addition to the model did not introduce any further delay in the response kinetics.

Models 3 and 4 were simplified models compared to Model 1 that excluded inverse agonism and receptor recycling, respectively. Model 3 and 4 clearly performed worse than Model 1, as indicated by the much higher OFVs.

Model 5 included dopamine elimination/degradation, but this did not improve the model fit.

Model 6 used a fixed value for k_5 which was set to 0. This model performed slightly better than Model 1. The value of k_5 (0.0005 min^{-1}) in the final model (Model 1) was chosen for a combination of physiological and numerical reasons: setting k_5 to zero as in Model 6 would mean that active PDE is only synthesized and not degraded, which would result in a physiologically implausible infinite increase in active PDE concentrations. Moreover, all other parameter values than k_5 differed maximally 5% between Model 6 and Model 1.

Finally, Model 7 demonstrates the contribution of slow binding kinetics to the model fit of the final model, as the exclusion of slow binding kinetics (k_{off} was set to 10 min^{-1} for all antagonists in Model 7) resulted in a large increase of the OFV, compared to Model 1.

Table 2. Overview of the Objective Function Values (OFVs) of the final model and the tested alternative models. The changes compared to Model 1 are indicated by the mechanistic detail that was added (+) or removed (-) from Model 1.

#	Model	OFV	model fit
1	Final model	62404	successful
2	+ PKA	62411	successful
3	- inverse agonism (k0)	102215	terminated
4	- receptor recycling (RR)	81594	terminated
5	+ degradation of dopamine	62404	successful
6	- active PDE degradation (k_5)	62307	successful
7	+ assumption of fast binding kinetics	67468	successful

Model fitting

The model fits of Model 1 in Figure 4 demonstrate that the general shape of the cAMP concentration-time curve and the concentration-dependency of the antagonist effect on the cAMP concentration are well captured by the model for all compounds. The equations of Model 1 are given in Supplement S 3. For a few compounds (i.e. Clozapine, Bromperidol) the peak cAMP concentration or the cAMP concentrations in the terminal phase for the highest antagonist concentrations are underpredicted. The parameter estimates that were the same for all antagonists are given in Table 3 and all parameter estimates are given in Supplement S 3, Table S 3. The uncertainty in the parameter estimates is low, as indicated by the small residual standard errors.

Table 3. Estimates for the system-specific parameters and their uncertainties from fitting Model 1 to the cAMP response data. Naming of the parameters corresponds to Figure 1. $DAFR_{50}$ denotes the ratio of the total receptor concentration divided by the dopamine-bound receptor concentration that inhibits the maximal cAMP synthesis to 50%, R_{tot} denotes the total receptor concentration, k_{0max} denotes the maximal value of k_0. h denotes the hill factor of the non-linear relationship between D_2 receptor occupancy and cAMP synthesis (k_0). The dopamine k_{off} was based on the *in vitro* measurements and the chosen values for k_4 and k_5 are described in the text. RSE: Relative Standard Error.

Parameter	**Value (unit)**	**RSE (%)**
K_D dopamine	10.3 (nM)	4.0
k_{off} dopamine	1.69 (min^{-1})	Input parameter
$DAFR_{50}$	2.25	2.4
R_{tot}	1.74 (nM)	1.3
RR	0.238 (min^{-1})	2.2
k_{0max}	20.5 ($AU \cdot min^{-1}$)	0.50
k_1	4.12 ($AU \cdot min^{-1}$)	0.80
k_2 (active PDE-independent)	0.0334 (min^{-1})	11
k_3 (active PDE-dependent)	0.00882 ($nM^{-1} \cdot min^{-1}$)	0.20
k_4	0.00882 (min^{-1})	defined as identical to k_3
k_5	0.0005 (min^{-1})	input parameter
h	1.77	0.40

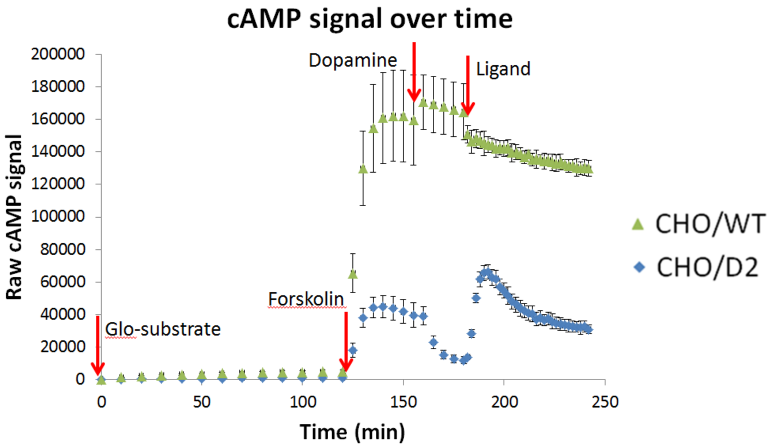

Figure 3. Measured cAMP response during a typical experiment of the cAMP assay (see Methods). The arrows indicate addition of Glo-substrate, Forskolin, Dopamine and the tested ligand. The light grey data points were measured in wild type CHO cells, while the dark grey data points were measured in CHO cells transfected with the dopamine D2 receptor.

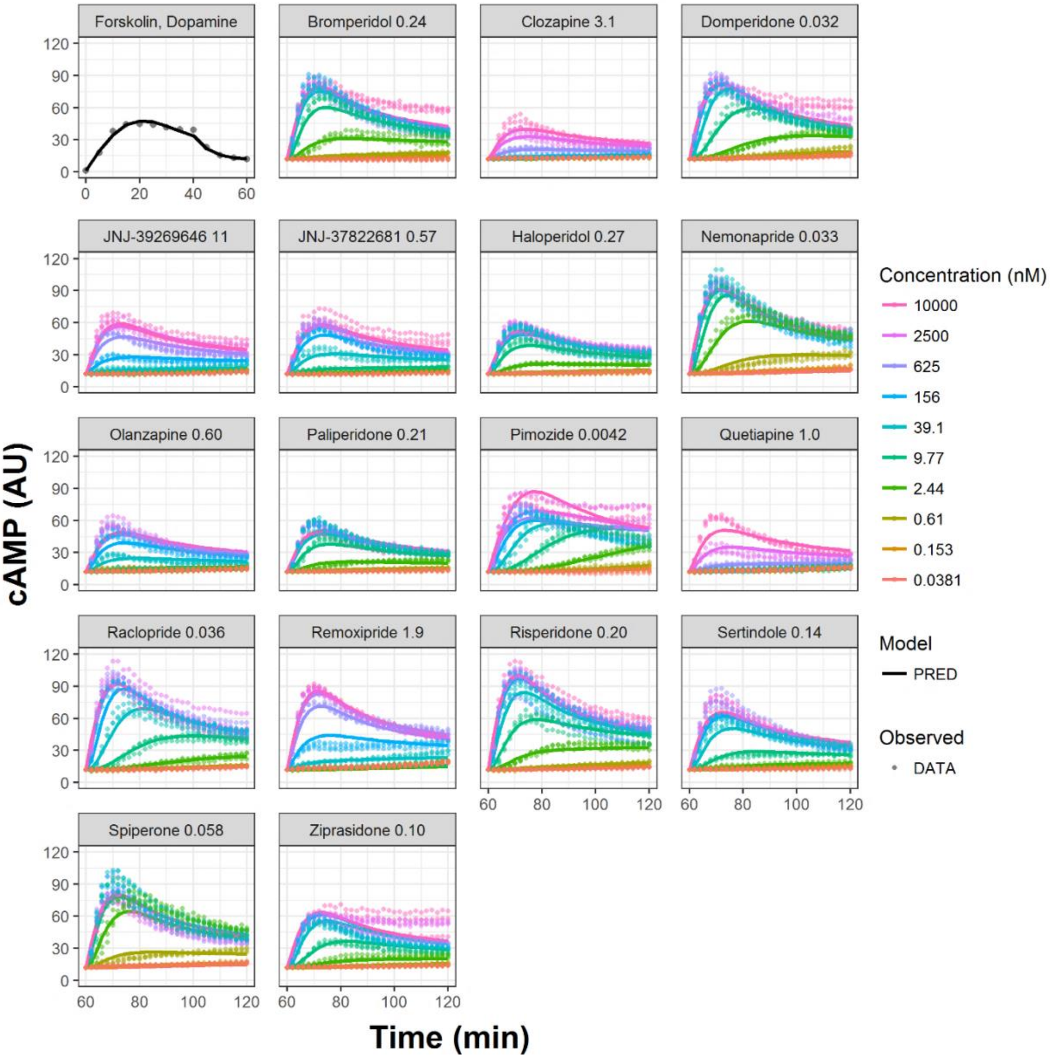

Figure 4. Model fits for all in vitro cAMP data as measured in transfected CHO cells. Both the observed (dots) and model-predicted (lines) cAMP signals are included. The order of the lines and symbols correspond to the order of the concentrations in the legend. The top-left panel shows the cAMP measurements and model predictions for the first 60 minutes in between forskolin addition and antagonist addition. The lower panels only show the time points after antagonist addition.

III) Frequency Response Analysis: Simulations of the predicted in vivo response to fluctuating dopamine concentrations

The simulations of the response to fluctuating dopamine concentrations resulted in a fluctuation pattern of cAMP over time for each dopamine fluctuation frequency that was tested. The cAMP fluctuation amplitude was dependent on the frequency, as illustrated in Figure 5.

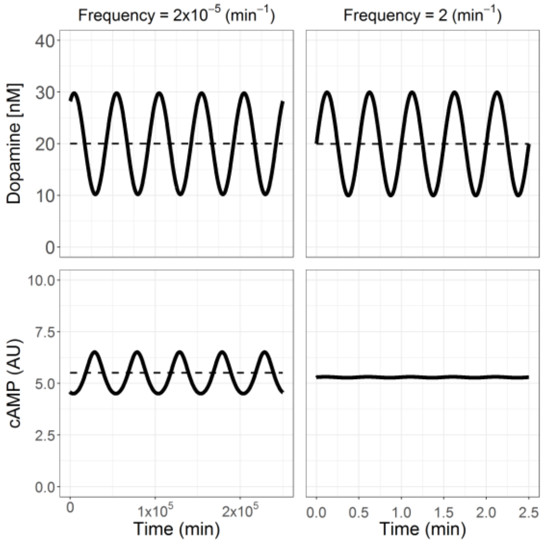

Figure 5. Example simulations of fluctuations in dopamine concentration for a low frequency (left-hand plots) and a high frequency (right-hand plots). The dashed lines indicate the average steady state values of the fluctuations, which is calculated as the mean of the maximal and the minimal concentration. Note the different time scales on the left compared to the right plots. The antagonist k_{off} was 2.5 min^{-1} for these simulations.

From these dopamine and cAMP fluctuations, the relative amplitudes and the ratio of these relative amplitudes could be calculated to obtain the cAMP gain (Equation 1, see Methods) as illustrated in Figure 6. The two simulations in Figure 5 and Figure 6 thus provide two points on the line for an antagonist k_{off} of 2.5 min^{-1} in the graph of Figure 7; at a frequency of 2 x 10^{-5} min^{-1} and 2 min^{-1}, the cAMP gain is 0.36 and 0.0080, respectively.

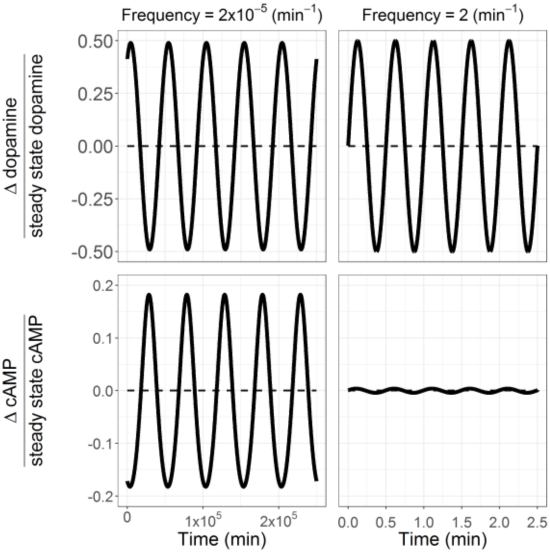

Figure 6. Converted dopamine and cAMP concentrations into relative fluctuations compared to average steady state. The delta sign refers to the difference between the concentration and the average steady state concentration. From this data, the gain can be identified according to equation 1, which is approximately 0.36 for the left-hand plots and 0.0080 for the right-hand plots. The antagonist k_{off} was 2.5 min^{-1} for these simulations.

From the Frequency Response Analysis as shown in Figure 7, the following was observed:

If dopamine fluctuations occur slowly, the cAMP response has a steady gain (i.e. the cAMP fluctuations have a constant amplitude) for frequencies lower than $1*10^{-5}$ min^{-1} in Figure 7. This gain is increased for intermediate frequencies (between $1*10^{-4}$ and 0.1/min) and decreases steeply for higher frequencies. The influence of drug-target binding kinetics on the transduction of dopamine fluctuations into cAMP fluctuations is limited to intermediate frequencies between $1*10^{-4}$ and 0.1/min of dopamine fluctuations.

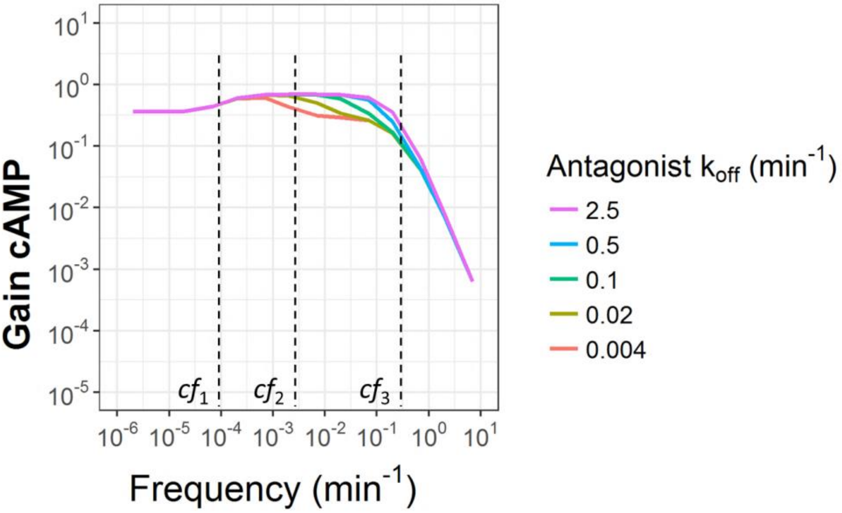

Figure 7. Frequency response analysis of the relative amplitude of cAMP fluctuations normalized to the relative amplitude of dopamine fluctuations (gain). The frequency on the x-axes denotes the frequency of the dopamine concentration sine wave that has been used as input for the simulations. The different colors represent different dissociation rate constants (k_{off}) for the antagonist. The applied antagonist concentration was 14 nM while the antagonist K_D was 6.9 nM for all simulations in both plots. The applied dopamine concentrations had a median value of 20 nM and an amplitude of 10 nM. The value of k_{on} changed simultaneously with k_{off} such that the K_D was constant. The dashed lines indicate characteristic frequencies for the line where k_{off} = 0.004 min^{-1} at which the gain increases (cf_1) and decreases (cf_2) to new plateau values and decreases linearly with increasing frequencies (cf_3). The order of the lines follows the order of the legend.

The model-based frequency response analysis allowed characterization of the cAMP response to a wide range of dopamine fluctuation frequencies (as shown in Figure 7). This analysis identified the influence of each model parameter on the cAMP response. The cAMP gain versus dopamine fluctuation frequency graphs as shown in Figure 7 are dependent on the antagonist k_{off} and can have up to three characteristic frequencies around which the gain changes. The positions of the characteristic frequencies are dependent on the parameter values, as discussed below, and have been derived empirically from the gain *versus* frequency plot as the frequencies at which the cAMP gain starts to change. These frequencies were numbered cf_1, cf_2, and cf_3, as indicated in Figure 7. From the lowest dopamine fluctuation frequencies to cf_1, the cAMP gain is independent of the antagonist k_{off} and does not change with increasing frequency, until cf_1 is reached where the gain increases towards a new plateau value. The frequency at which the cAMP gain declines to a new plateau value, cf_2, is dependent on the antagonist k_{off} and cannot be observed for high-k_{off} antagonists, which is the case for k_{off} values between 0.5 and 2.5 min^{-1} (Figure 7). The third characteristic frequency, cf_3, is independent of the antagonist k_{off} and introduces a decline in the cAMP gain that is linear with the increasing frequency.

The influence of the model parameters on the characteristic frequencies was identified by repeating the FRA for different values of each model parameter, as shown in Supplement S 5. As illustrated by Figure S 5, the value of cf_1 depends on the value of the active PDE turnover rate constant k_5. This can be understood by considering that the increase in cAMP gain is caused by a reduced negative feedback if the turnover of active PDE is to slow, relative to the fast fluctuations of cAMP. The second characteristic frequency, cf_2, is influenced by the antagonist k_{off} and by the antagonist concentration, as illustrated in Figure S 8. The role of the antagonist k_{off} can be explained by the slow displacement of antagonists with a low k_{off} value and the consequently reduced fluctuation of dopamine receptor occupancy. The role of the antagonist concentration can be explained by the higher antagonist receptor occupancy and the relatively lower influence of fluctuating dopamine concentrations on the antagonist receptor occupancy for higher antagonist concentrations. The third characteristic frequency, cf_3, is determined by both the cAMP turnover and the dopamine k_{off}, as shown in Figure S 6 and Figure S 7, respectively. These parameters determine the turnover of cAMP and dopamine receptor occupancy, respectively, and the slowest turnover is thus rate-limiting for the eventual turnover of cAMP and the maximal frequency of dopamine fluctuations that can be translated into cAMP fluctuations without a declining fluctuation amplitude. In summary, if k_5 (active PDE turnover) increases, cf_1 increases, if the antagonist concentration or k_{off} increases, cf_2 increases and if k_3 (cAMP turnover) increases, cf_3 increases

Overall, the translation of fluctuating dopamine concentrations into fluctuation of cAMP concentrations is inhibited to a larger extent by antagonists with a low k_{off} value compared to antagonists with a high k_{off} value. However, this role of the antagonist k_{off} is only present if the dopamine fluctuation frequency is not too high (i.e. higher than cf_3) to be translated and not too slow (i.e. lower than cf_2) to be able to displace even a slow dissociating antagonist.

Discussion

In this study, we developed a minimal mechanistic model that describes the cellular effects of dopamine D_2 antagonism on cAMP turnover, including both dopamine and antagonist receptor binding kinetics as well as active PDE turnover. The model was able to describe successfully *in vitro* binding and cAMP concentration-time profiles data obtained for 17 D2 antagonists. Compared to fast dissociating antagonists, slowly dissociating D_2 antagonists lead to a reduced response to fluctuating dopamine concentrations as previously suggested in the fast-off hypothesis (see below) for dopamine antagonists. However, this influence of antagonist binding kinetics is only observed when the dopamine fluctuations have a frequency in the range of 1/min to 1/hour. This range is determined by the cAMP turnover, the dopamine k_{off} and the antagonist k_{off}.

Insight into the influence of target binding kinetics on dopamine D_2 antagonism

According to the fast-off hypothesis for dopamine D_2 antagonists, it is beneficial if dopamine can displace D2 antagonists receptor binding, to avoid extrapyramidal side effects.[15] Since the dopamine fast-off hypothesis only applies to D_2 antagonists, one would expect more antagonists with a high k_{off} value, compared to agonists, for which a high k_{off} value is not considered beneficial. However, our results in Figure 2 show that the k_{off} of agonists tends to be higher compared to antagonists. The k_{off} values that would be necessary for the displacement of dopamine according to the fast-off hypothesis were analyzed previously, [16] but the kinetics of signal transduction were not taken into account in that study. Here we show that the displacement of D_2 antagonists by dopamine is not generating a fluctuating response if the frequency of fluctuation in dopamine D_2 occupancy is higher than what the endogenous signal transduction can translate into a cellular signal, such as cAMP fluctuation. In this study, it is indicated that the rate of endogenous signal transduction is limited both by the dopamine k_{off} and by the cAMP turnover. It was found that D_2 antagonists that dissociate faster than haloperidol (a typical antipsychotic) will lead to a similar signal transduction of fluctuating dopamine concentrations as haloperidol. However, this is in conflict with the fast-off hypothesis.[15] Moreover, this fast-off hypothesis has been challenged recently by *in vitro* electrophysiology measurements that revealed only moderate differences (6.4-2.5 fold) in recovery rates of the electrophysiological response to dopamine in oocytes between atypical antagonists and the typical antagonist haloperidol [47].

Extrapolation of *in vitro* to *in vivo* antagonism and signal transduction

Our analysis demonstrates that the fast-off hypothesis for D_2 antagonists is only relevant for a limited range of antagonist k_{off} values and not applicable to sub-second pulses of dopamine release in the synaptic cleft. Moreover, this study reveals how the relevance of the D_2 antagonist k_{off} depends on the kinetics of signal transduction and negative feedback. Although we provide a quantitative estimate of the maximal value of k_{off} that could decrease the inhibited transduction of dopamine fluctuations, it should be noted that this value cannot be translated directly into the *in vivo* situation.

Firstly, the temperature at which the signal transduction experiments were performed, room temperature, is not the physiological temperature, and most reactions (including drug-target binding kinetics) will be faster at 37°C. However, the difference in binding kinetics between these temperatures is moderate, although highly variable: the ratio of the k_{off} values for the measured D_2 antagonists in this study at 37°C divided by the k_{off} at room temperature was 3.2 fold on average and between 0.10 and 7.4 in the whole dataset, while for k_{on} this ratio was 2.5 on average and between 0.038 and 6.7 (see Supplement S 1). Therefore, we expect that the kinetics of signal transduction will be different at 37°C compared to our measurements at room temperature, but we do not expect differences of more than one order of magnitude.

Secondly, the analysis of Model 1 in this study only incorporates signal transduction into cAMP and active PDE levels, while in the clinical *in vivo* situation, more transduction steps are involved before the antipsychotic effect of D_2 antagonists is obtained. The differences between the time curves of cAMP and cellular optical density as measured by DMR (Supplement S 2), provide a first indication of possible differences between the cAMP response and downstream signaling, but the mechanistic interpretation of cellular optical density requires more advanced experimental designs.[48]

Thirdly, the analysis of the cAMP response data with Model 1-7 is not sufficient to obtain a conclusive and comprehensive description of the mechanism(s) underlying the observed cAMP responses. Although various mechanisms were represented by Model 1-7 and fitted to the data, some of these models provide similar fits (e.g. Model 1 and Model 5) and the true mechanism cannot be identified based on these fits alone. Also, the transfected CHO cells used in the in vitro measurements of CAMP are not brain cells, and the system-specific parameter values as obtained by the model fit in this study might therefore be different from the in vivo situation.

All of these factors might explain why the receptor recycling rate constant as identified here (0.238 min^{-1}) does not correspond to previous more direct estimates of the D_2 receptor degradation rate constant from rat striatum (0.0001 min^{-1})[49,50]. However, the critical elements in the structure of Model 1 are well supported by previous studies: Inverse agonism has been reported for many of the D_2 antagonists as described in the introduction [24,25]. The active PDE-independent degradation of cAMP has been described before in a more extensive GPCR signaling model [21] and is also supported by the different molecules that can hydrolyze cAMP [33,34]. The two cAMP production rate constants represent the constitutive receptor activity, which is inhibited by inverse agonism [32], and the remaining cAMP production.

Finally, the frequency response analysis that was used here is based on a sine-wave function while the dopamine fluctuations in the brain occur with a more variable frequency and amplitude.[16,19].

Although the absolute limit of the influence of binding kinetics on antagonist effects cannot be translated directly into the *in vivo* situation, our findings demonstrate that such a limitation likely exists in the *in vivo* situation as well, and may be expected to be in the order of minutes. These results make it highly unlikely that sub-second dopamine fluctuations can be translated into cAMP fluctuations and that sub-second k_{off} values are required to minimize extrapyramidal side effects. This also indicated that it is highly unlikely that antagonists with sub-second dissociation half-lives yield different inhibition of dopamine signaling compared to antagonists with dissociation half-lives in the second-minute range, as suggested before.[16]

We have shown that for a common transduction system including an indirect effect and a negative feedback loop, the relevance of fast drug-target dissociation is limited by the target dissociation of the endogenous ligand and the turnover of the second messenger. The rate constants for dopamine dissociation from the D_2 receptor and cAMP turnover that we have obtained in this study challenge the fast-off hypothesis. Our study demonstrates that the influence of target binding kinetics on drug effects cannot be fully understood without taking into account signal transduction and feedback kinetics, especially if fluctuating endogenous ligand concentrations are present.

Conclusion

The cellular cAMP response to dopamine D_2 antagonists could be described using a minimal mechanistic model including *in vitro* measured dopamine and antagonist D_2 binding kinetics, in conjunction with synthesis and degradation of cAMP and active PDE. This model revealed that slowly dissociating D_2 antagonists show a reduced transduction of dopamine fluctuations into cAMP fluctuations, compared to fast dissociating antagonists. However, this influence of the dissociation rate constant is limited to dopamine fluctuations that are faster than the k_{off} value of the drug but slower than the dopamine k_{off} value and the cAMP turnover. In general, we conclude that the influence of drug-target binding kinetics on drug effect kinetics is dependent on the dynamics of signal transduction kinetics and that both the turnover of second messengers and the k_{off} value of endogenous ligands limit the discrimination between fast and slowly dissociating antagonists.

Acknowledgements

This research is part of the K4DD (Kinetics for Drug Discovery) consortium which is supported by the Innovative Medicines Initiative Joint Undertaking (IMI JU) under grant agreement no. 115366. The IMI JU is a project supported by the European Union's Seventh Framework Programme (FP7/2007–2013) and the European Federation of Pharmaceutical Industries and Associations (EFPIA).

References

1. Copeland RA, Pompliano DL, Meek TD. Drug-target residence time and its implications for lead optimization. Nat Rev Drug Discov 2006;5(9):730–9
2. Zhang R, Monsma F. Binding kinetics and mechanism of action: toward the discovery and development of better and best in class drugs. Expert Opin Drug Discov 2010;5(11):1023–9
3. Lu H, Tonge PJ. Drug-Target Residence Time: Critical Information for Lead Optimization. Curr Opin Chem Biol 2011;14(4):467–74
4. Dahl G, Akerud T. Pharmacokinetics and the drug-target residence time concept. Drug Discov Today 2013;18(15–16):697–707
5. Vauquelin G. Impact of target binding kinetics on in vivo drug efficacy: k off , k on and rebinding. Br J Pharmacol 2016;173(15):2319–34
6. Copeland RA. The drug-target residence time model: a 10-year retrospective. Nat Rev Drug Discov 2016;15(2):87–95
7. de Witte WEA, Wong YC, Nederpelt I, et al. Mechanistic models enable the rational use of in vitro drug-target binding kinetics for better drug effects in patients. Expert Opin Drug Discov 2016;11(1):45–63
8. Yin N, Pei J, Lai L. A comprehensive analysis of the influence of drug binding kinetics on drug action at molecular and systems levels. Mol Biosyst 2013;9(6):1381–9
9. Landersdorfer CB, He Y-L, Jusko WJ. Mechanism-based population modelling of the effects of vildagliptin on GLP-1, glucose and insulin in patients with type 2 diabetes. Br J Clin Pharmacol 2012;73(3):373–90
10. Kleinbloesem CH, van Brummelen P, Danhof M, et al. Rate of increase in the plasma concentration of nifedipine as a major determinant of its hemodynamic effects in humans. Clin Pharmacol Ther 1987;41(1):26–30
11. Francheteau P, Steimer JL, Merdjan H, et al. A mathematical model for dynamics of cardiovascular drug action: Application to intravenous dihydropyridines in healthy volunteers. J Pharmacokinet Biopharm 1993;21(5):489–514
12. Guo D, Mulder-Krieger T, IJzerman AP, et al. Functional efficacy of adenosine A_2A receptor agonists is positively correlated to their receptor residence time. Br J Pharmacol 2012;166(6):1846–59
13. Sykes DA, Dowling MR, Charlton SJ. Exploring the mechanism of agonist efficacy: a relationship between efficacy and agonist dissociation rate at the muscarinic M3 receptor. Mol Pharmacol 2009;76(3):543–51
14. Meltzer HY. What's atypical about atypical antipsychotic drugs? Curr Opin Pharmacol 2004;4(1):53–7
15. Kapur S, Seeman P. Does Fast Dissociation From the Dopamine D 2 Receptor Explain the Action of Atypical Antipsychotics ?: A New Hypothesis. Am J Psychiatry 2001;158(3):360–9
16. Vauquelin G, Bostoen S, Vanderheyden P, et al. Clozapine, atypical antipsychotics, and the benefits of fast-off D2 dopamine receptor antagonism. Naunyn Schmiedebergs Arch Pharmacol 2012;385(4):337–72
17. Langlois X, Megens A, Lavreysen H, et al. Pharmacology of JNJ-37822681, a specific and fast-dissociating D2 antagonist for the treatment of schizophrenia. J Pharmacol Exp Ther 2012;342(1):91–105
18. Kapur S, Seeman P. Antipsychotic agents differ in how fast they come off the dopamine D2 receptors. Implications for atypical antipsychotic action. J Psychiatry Neurosci 2000;25(2):161–6
19. Schultz W. Multiple dopamine functions at different time courses. Annu Rev Neurosci 2007;30(1):259–88
20. Young AMJ, Ahier RG, Upton RL, et al. Increased extracellular dopamine in the nucleus accumbens of the rat during associative learning of neutral stimuli. Neuroscience 1998;83(4):1175–83
21. Violin JD, DiPilato LM, Yildirim N, et al. beta2-adrenergic receptor signaling and desensitization elucidated by quantitative modeling of real time cAMP dynamics. J Biol Chem 2008;283(5):2949–61
22. Ingalls BP. Mathematical Modeling in Systems Biology: an introduction [Internet]. MIT Press; 2013. 1-396 p
23. Ögren SO, Hall H, Köhler C, et al. Remoxipride, a new potential antipsychotic compound with selective anti-dopaminergic actions in the rat brain. Eur J Pharmacol 1984;102:459–74
24. Hall DA, Strange PG. Evidence that antipsychotic drugs are inverse agonists at D2 dopamine receptors. Br J Pharmacol 1997;121(4):731–6
25. Bond RA, IJzerman AP. Recent developments in constitutive receptor activity and inverse agonism, and their potential for GPCR drug discovery. Trends Pharmacol Sci 2006;27(2):92–6
26. Ang J, Ingalls B, McMillen D. Probing the inputoutput behavior of biochemical and genetic systems: System identification methods from control theory [Internet]. 1st ed. Methods in Enzymology. Elsevier Inc.; 2011. 279-317 p
27. Schiele F, Ayaz P, Fernández-Montalván A. A universal, homogenous assay for high throughput determination of binding kinetics. Anal Biochem 2014;468:42–9
28. Nederpelt I, Georgi V, Schiele F, et al. Characterization of 12 GnRH peptide agonists - A kinetic perspective. Br J Pharmacol 2016;173(1):128–41
29. Cheng Y-C, Prusoff WH. Relationship between the inhibition constant (KI) and the concentration of inhibitor which causes 50 per cent inhibition (I50) of an enzymatic reaction. Biochem Pharmacol 1973;22(23):3099–108

30. Motulsky HJ, Mahan LC. The Kinetics of Competitive Radioligand Binding Predicted Mass Action by the Law of Mass Action. Mol Pharmacol 1984;25(1):1–9
31. Fang, Frutos, Verklereen. Label-free cell-based assays for GPCR screening. Comb Chem High Throughput Screen 2008;11(5):357–69
32. de Ligt RAF, Kourounakis AP, IJzerman AP. Inverse agonism at G protein-coupled receptors: (patho)physiological relevance and implications for drug discovery. Br J Pharmacol 2000;130(1):1–12
33. Cherry JA, Pho V. Characterization of cAMP Degradation by Phosphodiesterases in the Accessory Olfactory System. Chem Senses 2002;27(7):643–52
34. Keravis T, Lugnier C. Cyclic nucleotide phosphodiesterase (PDE) isozymes as targets of the intracellular signalling network: benefits of PDE inhibitors in various diseases and perspectives for future therapeutic developments. Br J Pharmacol 2012;165:1288–305
35. R Core Team. R: A language and environment for statistical computing. R Found Stat Comput Vienna, Austria URL http//wwwR-project.org/ 2013;
36. Soetaert K, Petzoldt T, Setzer RW. Solving Differential Equations in R: Package deSolve. J Stat Softw 2010;33(9):1–25
37. Burstein ES, Ma J, Wong S, et al. Intrinsic Efficacy of Antipsychotics at Human D 2 , D 3 , and D 4 Dopamine Receptors : Identification of the Clozapine Metabolite N -Desmethylclozapine as a D 2 / D 3 Partial Agonist. J Pharmacol Exp Ther 2005;315(3):1278–87
38. Wood M, Dubois V, Scheller D, et al. Rotigotine is a potent agonist at dopamine D_1 receptors as well as at dopamine D_2 and D_3 receptors. Br J Pharmacol 2015;172(4):1124–35
39. Kroeze WK, Hufeisen SJ, Popadak BA, et al. H1-Histamine Receptor Affinity Predicts Short-Term Weight Gain for Typical and Atypical Antipsychotic Drugs. Neuropsychopharmacology 2003;28(3):519–26
40. Toll L, Berzetei-Gurske IP, Polgar WE, et al. Standard binding and functional assays related to medications development division testing for potential cocaine and opiate narcotic treatment medications. NIDA Res Monogr 1998;178:440–66
41. Seeman P, Tallerico T. Antipsychotic drugs which elicit little or no parkinsonism bind more loosely than dopamine to brain D2 receptors, yet occupy high levels of these receptors. Mol Psychiatry 1998;3(2):123–34
42. Richelson E, Souder T. Binding of antipsychotic drugs to human brain receptors focus on newer generation compounds. Life Sci 2000;68(1):29–39
43. Leysen JE, Gommeren W. Drug-Receptor Dissociation Time , New Tool for Drug Research : Receptor Binding Affinity and Drug-Receptor Dissociation Profiles of Serotonin-S2 , Dopamine-D2 , Histamine-HI Antagonists , and Opiates. Drug Dev Res 1986;131:119–31
44. Kongsamut S, Kang J, Chen XL, et al. A comparison of the receptor binding and HERG channel affinities for a series of antipsychotic drugs. Eur J Pharmacol 2002;450(1):37–41
45. Klein Herenbrink C, Sykes DA, Donthamsetti P, et al. The role of kinetic context in apparent biased agonism at GPCRs. Nat Commun 2016;7:10842
46. Freedman SB, Patel S, Marwood R, et al. Expression and pharmacological characterization of the human D3 dopamine receptor. J Pharmacol Exp Ther 1994;268(1):417–26
47. Sahlholm K, Zeberg H, Nilsson J, et al. The fast-off hypothesis revisited: A functional kinetic study of antipsychotic antagonism of the dopamine D2 receptor. Eur Neuropsychopharmacol 2016;26(3):467–76
48. Schröder R, Janssen N, Schmidt J, et al. Deconvolution of complex G protein–coupled receptor signaling in live cells using dynamic mass redistribution measurements. Nat Biotechnol 2010;28(9):943–9
49. Zou L-L, Cai S-T, Jin G-Z. Chronic treatment with (-)-stepholidine alters density and turnover of D1 and D2 receptors in striatum. Acta Pharmacol Sin 1996;17(6):485–9
50. Dewar KM, Paquet M, Reader TA. Alterations in the turnover rate of dopamine D1 but not D2 receptors in the adult rat neostriatum after a neonatal dopamine denervation. Neurochem Int 1997;30(6):613–21

Supplemental information

Supplement S 1. Measurements of binding kinetics and equilibrium binding for antagonists and agonist at room temperature and at 37 °C.

Table S 1. Binding equilibrium (ePCA) and binding kinetics (kPCA) measurements at 37°C. NA: not available, NPA: N-n-Propyl Apomorphine

	ePCA		kPCA					
Compound ID	**K_I [M]**	SD	**K_D [M]**	SD	**k_{on} [1/(M*s)]**	SD	**k_{off} [1/s]**	SD
(-)-Nemonapride	2.11E-10	5.96E-11	4.96E-11	3.54E-11	1.79E+07	1.95E+06	8.54E-04	5.38E-04
(-)-Quinpirole	> 8.71E-07	NA	3.83E-06	2.84E-06	5.35E+04	2.42E+04	1.45E-01	1.47E-01
Aripiprazole	1.03E-09	4.29E-10	5.58E-10	4.90E-11	1.77E+06	6.03E+05	1.00E-03	4.23E-04
Bromocriptine	1.75E-09	4.04E-10	5.86E-10	3.22E-12	2.40E+05	8.64E+04	1.41E-04	5.14E-05
Bromperidol	3.24E-09	1.55E-09	2.52E-09	8.27E-10	2.67E+06	1.04E+06	7.42E-03	2.68E-03
Cabergoline	8.22E-10	1.03E-10	7.38E-10	6.89E-11	2.11E+06	4.75E+05	1.54E-03	2.06E-04
Clozapine	3.12E-08	1.96E-09	5.39E-08	1.33E-08	8.35E+05		2.88E-02	
Domperidone	5.06E-09	8.69E-10	3.15E-09	3.92E-10	6.87E+05	2.62E+05	2.12E-03	5.56E-04
Dopamine	> 8.71E-07		1.07E-06	4.99E-07	1.02E+04	6.02E+03	9.36E-03	1.32E-03
JNJ-37822681	1.61E-08	1.89E-09	1.93E-08	3.99E-09	1.24E+06	9.63E+05	2.19E-02	1.36E-02
JNJ-39269646	7.22E-08	1.18E-08	9.14E-08	1.37E-08	1.71E+05	NA	1.84E-02	NA
Haloperidol	9.48E-10	2.96E-10	3.86E-10	9.95E-11	7.23E+07	NA	3.30E-02	NA
Memantine	> 8.71E-07	NA	1.01E-05	2.59E-07	1.99E+03	1.37E+03	2.41E-02	9.94E-03
NPA	3.40E-08	8.42E-09	1.77E-07	6.90E-08	NA	NA	NA	NA
Olanzapine	1.39E-08	1.29E-09	2.17E-08	9.44E-09	1.61E+06	1.00E+06	3.61E-02	5.99E-03
Paliperidone	8.18E-09	1.56E-09	9.25E-09	2.71E-09	1.92E+06	1.56E+06	1.36E-02	5.91E-03
Pergolide	1.30E-08	6.53E-09	2.87E-08	1.11E-08	3.27E+06	NA	7.89E-02	NA
Pimozide	6.62E-10	3.27E-10	5.82E-10	1.40E-10	9.38E+05	5.11E+05	5.10E-04	1.66E-04
Piribedil	2.99E-07	4.02E-08	4.22E-07	5.13E-08	2.23E+04	NA	8.25E-03	NA
Quetiapine	1.63E-07	3.84E-09	1.60E-07	9.72E-08	6.74E+05	4.03E+05	1.03E-01	5.98E-02
R-(-)-Apomorphine	1.69E-07	7.42E-09	2.71E-07	2.11E-07	> 5.92E+04	NA	> 1.00E-02	NA
Remoxipride	1.23E-07	2.81E-08	1.35E-07	2.86E-08	1.10E+06	4.54E+05	1.30E-01	7.94E-02
Risperidone	1.67E-09	9.11E-10	1.30E-09	7.52E-10	8.41E+06	5.96E+06	1.07E-02	5.02E-03
Rotigotine	1.67E-08	4.25E-09	5.69E-09	1.68E-09	3.18E+06	8.05E+05	1.74E-02	7.63E-04
S-(+)-Apomorphine	5.16E-07	6.50E-08	5.47E-07	1.75E-07	2.13E+04	NA	9.94E-03	NA
Sertindole	6.80E-09	1.86E-09	7.52E-09	5.87E-10	1.33E+06	NA	9.45E-03	NA
Spiperone	5.09E-10	2.29E-10	6.58E-11	1.77E-11	2.03E+07	7.02E+06	1.45E-03	6.22E-04
S-(+)-Raclopride	2.19E-09	1.85E-09	1.29E-09	1.18E-10	2.43E+06	8.68E+05	3.08E-03	8.32E-04
Ziprasidone	1.65E-09	2.93E-10	2.28E-09	2.12E-10	3.54E+06	1.38E+06	7.92E-03	2.31E-03

Table S 2. Binding equilibrium (ePCA) and binding kinetics (kPCA) measurements at room temperature. NA: not available, NPA: N-n-Propyl Apomorphine

	ePCA		**kPCA**					
Compound ID	**K_I [M]**	**SD**	**K_D [M]**	**SD**	**k_{on} [1/(M*s)]**	**SD**	**k_{off} [1/s]**	**SD**
(-)-Nemonapride	2.70E-10	5.96E-12	9.58E-11	3.26E-12	5.66E+06	2.73E+05	5.43E-04	4.46E-05
(-)-Quinpirole	> 8.53E-07	NA	7.80E-07	6.28E-07	1.07E+05	4.77E+04	9.82E-02	1.04E-01
Aripiprazole	1.01E-09	3.46E-10	2.39E-10	4.40E-13	7.24E+05	3.17E+05	1.73E-04	7.52E-05
Bromocriptine	5.04E-09	1.98E-09	2.19E-10	1.96E-10	8.09E+04	2.54E+04	2.02E-05	1.80E-05
Bromperidol	3.09E-09	3.22E-10	1.89E-09	7.49E-10	2.26E+06	9.57E+05	3.91E-03	1.21E-04
Cabergoline	9.58E-10	2.89E-10	4.26E-10	2.13E-10	8.80E+05	5.13E+05	3.21E-04	3.15E-05
Clozapine	3.42E-08	3.93E-09	5.05E-08	1.28E-08	1.20E+06	1.44E+06	5.13E-02	5.74E-02
Domperidone	4.18E-09	1.08E-09	3.04E-09	5.08E-10	1.81E+05	5.26E+04	5.37E-04	6.75E-05
Dopamine	> 8.53E-07		1.27E-06	5.56E-07	1.88E+04	2.16E+04	2.82E-02	3.01E-02
JNJ-37822681	1.24E-08	2.14E-09	9.32E-09	2.71E-09	7.33E+05	NA	9.54E-03	NA
JNJ-39269646	3.96E-08	2.10E-09	4.87E-08	8.35E-09	4.53E+06	4.51E+06	1.79E-01	1.64E-01
Haloperidol	9.88E-10	1.55E-10	3.82E-10	4.98E-11	1.21E+07	5.18E+06	4.48E-03	1.37E-03
Memantine	> 8.53E-07	NA	2.61E-05	9.91E-06	2.98E+02	NA	1.07E-02	NA
NPA	2.42E-08	3.80E-09	NA	NA	NA	NA	NA	NA
Olanzapine	1.37E-08	9.41E-10	8.58E-09	3.38E-09	> 7.30E+05	NA	> 1.00E-02	NA
Paliperidone	7.39E-09	9.15E-10	5.45E-09	2.07E-09	6.81E+05	1.83E+05	3.52E-03	4.14E-04
Pergolide	1.33E-08	6.02E-09	2.44E-08	1.24E-08	9.81E+05	NA	2.59E-02	NA
Pimozide	1.22E-09	4.23E-10	2.55E-10	6.74E-11	3.10E+05	2.45E+05	7.08E-05	4.17E-05
Piribedil	2.26E-07	2.77E-08	2.23E-07	5.90E-08	4.43E+04	9.30E+03	1.21E-02	4.18E-03
Quetiapine	1.26E-07	3.48E-08	1.50E-07	6.94E-08	1.03E+05	2.04E+04	1.69E-02	6.07E-03
R-(-)-Apomorphine	1.13E-07	1.88E-08	1.70E-07	7.68E-08	> 8.85E+04	NA	> 1.00E-02	NA
Remoxipride	7.01E-08	1.08E-08	8.31E-08	3.47E-08	3.28E+05	NA	3.14E-02	NA
Risperidone	1.05E-09	4.07E-10	7.56E-10	7.62E-11	4.43E+06	8.54E+05	3.31E-03	3.09E-04
Rotigotine	1.16E-08	3.55E-11	7.82E-09	2.86E-09	3.84E+06	3.78E+06	2.65E-02	2.75E-02
S-(+)-Apomorphine	2.65E-07	8.49E-08	3.33E-07	1.15E-07	2.94E+04	NA	1.36E-02	NA
Sertindole	6.15E-09	3.21E-09	4.07E-09	2.23E-09	7.70E+05	7.00E+05	2.35E-03	1.13E-03
Spiperone	2.96E-10	1.43E-10	1.79E-10	4.11E-12	5.44E+06	1.11E+06	9.70E-04	1.76E-04
S-(+)-Raclopride	1.35E-09	9.97E-10	6.34E-10	1.15E-10	9.57E+05	1.81E+05	5.96E-04	4.62E-06
Ziprasidone	1.76E-09	4.12E-10	1.31E-09	8.40E-11	1.29E+06	2.01E+05	1.67E-03	1.55E-04

Figure S1a

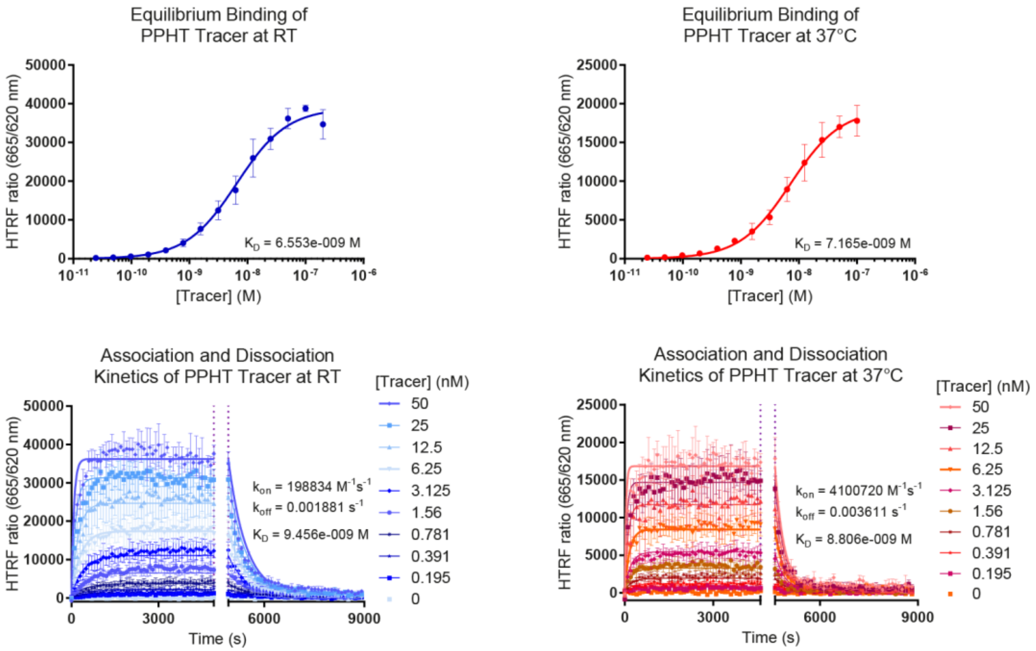

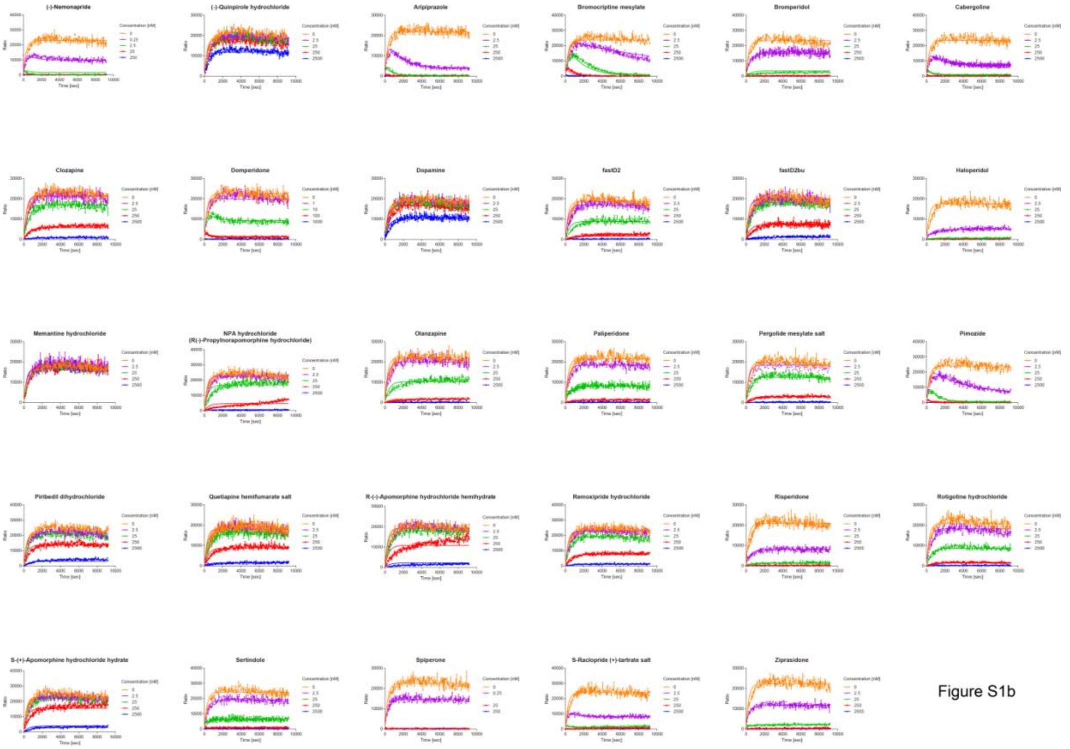

Figure S1b

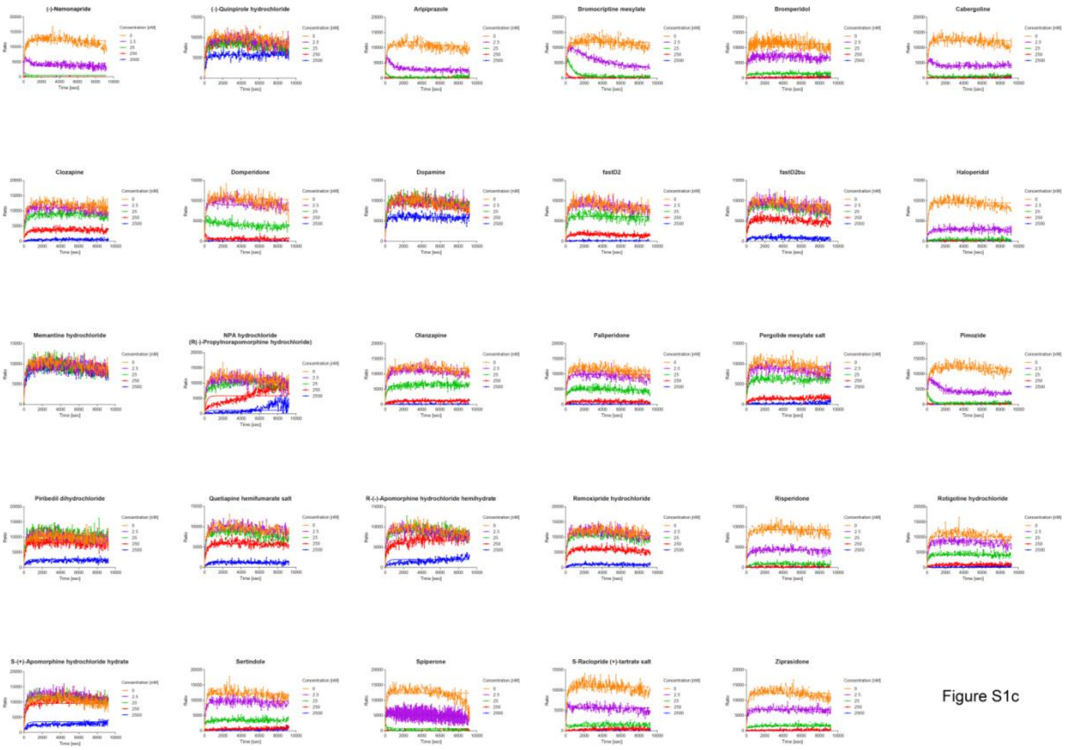

Figure S1c

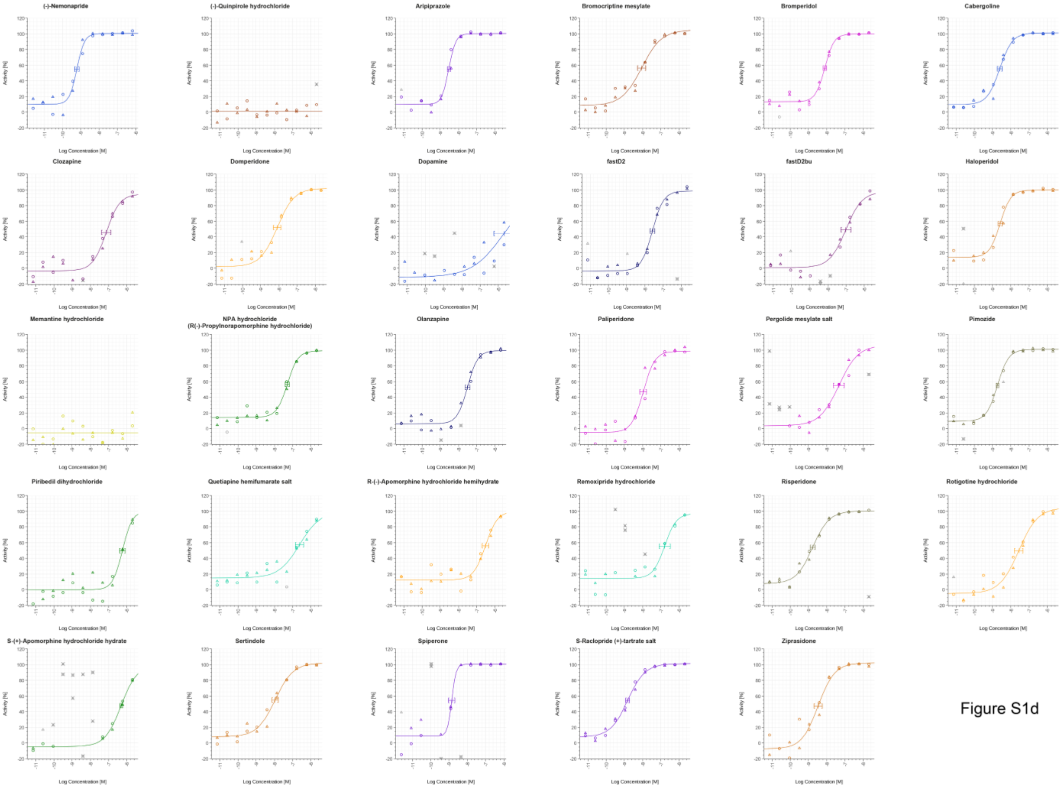

Figure S1d

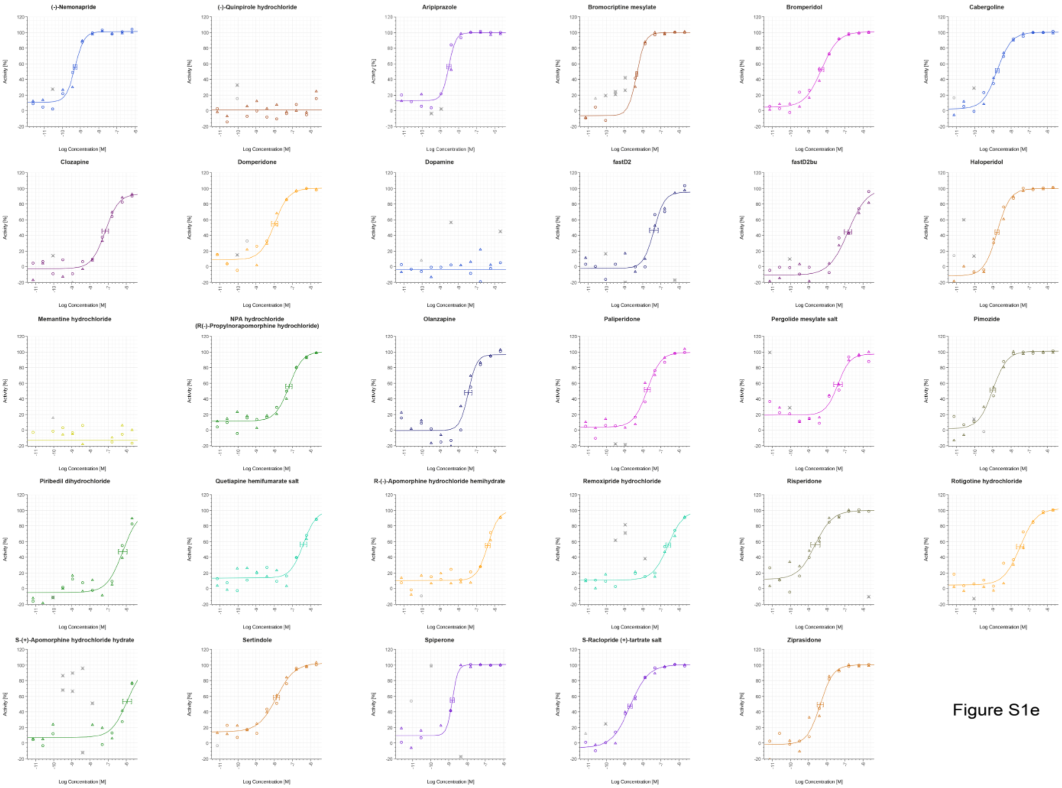
(-)-Nemonapride, (-)-Quinpirole hydrochloride, Aripiprazole, Bromocriptine mesylate, Bromperidol, Cabergoline

Clozapine, Domperidone, Dopamine, fastD2, fastD2bu, Haloperidol

Memantine hydrochloride, NPA hydrochloride (R(-)-Propylnorapomorphine hydrochloride), Olanzapine, Paliperidone, Pergolide mesylate salt, Pimozide

Piribedil dihydrochloride, Quetiapine hemifumarate salt, R-(-)-Apomorphine hydrochloride hemihydrate, Remoxipride hydrochloride, Risperidone, Rotigotine hydrochloride

S-(+)-Apomorphine hydrochloride hydrate, Sertindole, Spiperone, S-Raclopride (+)-tartrate salt, Ziprasidone

Figure S1e

Figure S 1. Determination of affinity and kinetic parameters for the binding of Dopamine D2 receptor drugs using the TagLite® homogeneous time resolved fluorescence (HTRF) technology and the equilibrium and kinetic Probe Competition Assays (ePCA and kPCA). Symbols represent the measured data and lines the fits to the corresponding binding models. The compounds indicated with fastD2 and fastD2bu refer to JNJ-37822681 and JNJ-39269646, respectively. These figures are also available as separate supplemental files to allow better readability.

a) Characterization of the PPHT tracer used in ePCA and kPCA at room temperature and at 37°C. The upper panel shows representative steady state titration curves, and the lower panel kinetic association- and dissociation curves at increasing tracer concentrations. HTRF signals were fit to the models specified in the methods section and the resulting binding parameters are indicated in the graphs.

b-c) Representative kPCA traces of the compounds listed in Table S1 at room temperature (b) and 37°C (c). Compound names are indicated on top of the graphs and dosing on the right-hand side.

d-e) Representative ePCA curves of the compounds listed in Table S1 at room temperature (d) and 37°C (e). Compound names are indicated on top of the graphs and dosing on the right-hand side. Grey crosses indicate data points excluded from the analysis. The different symbols represent different dilution series.

Supplement S 2. DMR experimental overview and results for all D_2 antagonists.

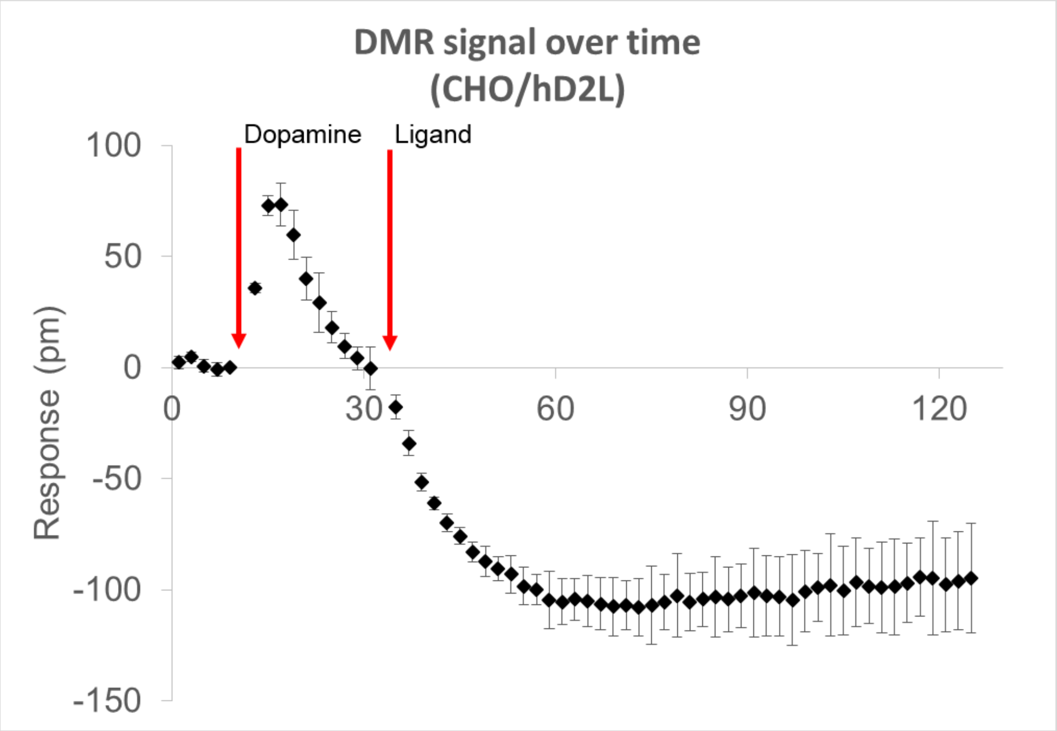

Figure S 2 Example of the complete DMR versus time curve for 10 µM haloperidol. The time points of addition of dopamine and the ligand (haloperidol in this case) are indicated with the red arrows.

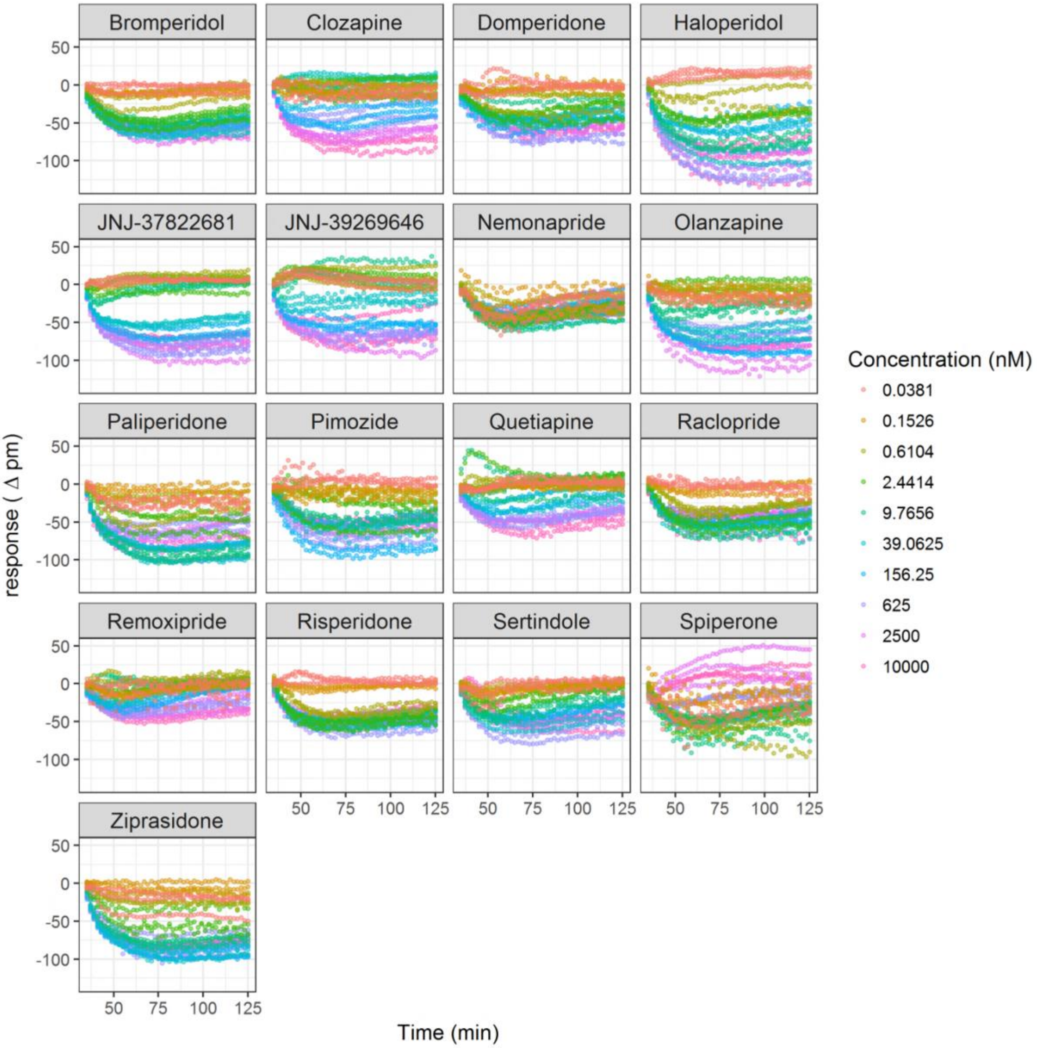

Figure S 3. Normalized Dynamic Mass Redistribution (DMR) responses as change in DMR response in picometer compared to the dopamine response after addition of various concentrations of the indicated antagonists. Normalization was performed by subtracting the response per well/replicate at the latest time point after dopamine addition and before antagonist addition (t = 31 min) from the raw DMR traces. Normalization for the dopamine + buffer was performed for each time point by subtracting the mean dopamine + buffer in each experiment/well plate from the normalized DMR traces.

Supplement S 3. Model 1 equations and parameter estimates for all dopamine D_2 antagonists.

To describe dopamine and antagonist binding to the D_2 receptor, a simple drug-target binding model with competition between antagonist and dopamine was developed. This model assumed a constant total receptor concentration. This was represented as a single conservation equation of total receptor (R_t), where the receptor can have 3 different states: free receptor (R), antagonist bound to receptor (RL) and dopamine bound to receptor (RDA). Receptor recycling (RR) was added to this model as well, which describes internalization of the receptor-agonist complex, dissociation of this complex return of the free receptor to the cell membrane. This model is given by the following equations (equation 1-5):

$$\frac{d[L]}{dt} = -k_{onL}[R][L] + k_{offL}[RL]$$

(Eq. 1)

$$\frac{d[DA]}{dt} = -k_{onDA}[R][DA] + k_{offDA}[RDA] + RR[RDA]$$

(Eq. 2)

$$\frac{\mathrm{d[RL]}}{\mathrm{dt}} = k_{onL}[R][L] - k_{offL}[RL]$$

(Eq. 3)

$$\frac{\mathrm{d[RDA]}}{\mathrm{dt}} = k_{onDA}[R][DA] - k_{offDA}[RDA] - RR[RDA]$$

(Eq. 4)

$$[R] = [R_t] - [RL] - [RDA]$$

(Eq. 5)

In these equations, [L] represents the free antagonist concentration, [DA] represents the free dopamine concentration, [R_t] represents the total receptor concentration, [R] represents the free receptor concentration, [RL] represents the concentration of the receptor—antagonist complex and [RDA] represents the concentration of the receptor—dopamine complex. k_{onL} and k_{onDA} represent the second-order association rate constants of receptor with the antagonist and with dopamine, respectively. k_{offL} and k_{offDA} represent the first order dissociation rate constants of the antagonist and dopamine from the receptor-bound complex, respectively. The receptor binding part of the model as described above was connected to cAMP concentrations in a mechanistic manner according to the following equations (equation 6 and 7).

$$\frac{d[cAMP]}{dt} = \left(k_1 + \frac{k_{0,max}[RL]^n}{EC50^n + [RL]^n}\right)\left(1 - \frac{[RDA]^n}{IC50^n + [RDA]^n}\right) - k_2[cAMP] - k_3[cAMP][PDE]$$

(Eq. 6)

Here, $k_{0,max}$ represents the maximum rate constant for inverse agonism by the receptor-antagonist complex, where n is the hill coefficient. Additionally, k_1 represents the rate constant for baseline synthesis of cAMP by adenylyl cyclase. Furthermore, the total cAMP synthesis is inhibited by the receptor dopamine complex (RDA) in a nonlinear manner, where n is the hill coefficient as well. k_2 is the rate constant for cAMP elimination independent of active PDE, and k_3 is the rate constant of active PDE-mediated cAMP elimination. active PDE synthesis is dependent on the cAMP concentration, and active PDE degradation is determined by the first order rate constant k_5 as in equation 7.

$$\frac{d[PDE]}{dt} = k_4[cAMP] - k_5[PDE]$$

(Eq. 7)

Table S 3. Parameter estimates from fitting the final model to the cAMP response data. Asterisks indicate parameter values that were not estimated but used as input parameter values. $DAFR_{50}$ denotes the ratio of the total receptor concentration divided by the dopamine-bound bound receptor concentration that inhibits the cAMP synthesis to 50%, LFR_{50} denotes the ratio of the total receptor concentration divided by the antagonist bound receptor concentration that generates the half-maximal antagonist-dependent cAMP synthesis (i.e. k_0 equals 0.5 * k_{0max}), R_{tot} denotes the total receptor concentration, k_{0max} denotes the maximal value of k_0.

Parameter (unit)	**Value**	**RSE**
k_{off} Bromperidol (min^{-1})	0.235*	
k_{off} Clozapine (min^{-1})	3.08*	
k_{off} Domperidone (min^{-1})	0.0322*	
k_{off} JNJ-39269646 (min^{-1})	10.7*	
k_{off} JNJ-37822681 (min^{-1})	0.573*	
k_{off} Haloperidol (min^{-1})	0.269*	
k_{off} Nemonapride (min^{-1})	0.0326*	
k_{off} Olazapine (min^{-1})	0.600*	
k_{off} Paliperidone (min^{-1})	0.211*	
k_{off} Pimozide (min^{-1})	0.0042*	
k_{off} Quetiapine (min^{-1})	1.01*	
k_{off} Raclopride (min^{-1})	0.0358*	
k_{off} Remoxipride (min^{-1})	1.89*	
k_{off} Risperidone (min^{-1})	0.199*	
k_{off} Sertindole (min^{-1})	0.141*	
k_{off} Spiperone (min^{-1})	0.0582*	
k_{off} Ziprasidone (min^{-1})	0.1*	
K_D Bromperidol (nM)	2.04	2.0%
K_D Clozapine (nM)	440	2.1%
K_D Domperidone (nM)	1.72	2.1%
K_D JNJ-39269646 (nM)	104	1.9%
K_D JNJ-37822681 (nM)	19.5	1.9%
K_D Haloperidol (nM)	1.72	2.4%
K_D Nemonapride (nM)	0.454	2.2%
K_D Olazapine (nM)	22.7	2.3%
K_D Paliperidone (nM)	1.61	2.4%
K_D Pimozide (nM)	291	2.8%
K_D Quetiapine (nM)	942	2.2%
K_D Raclopride (nM)	8.29	2.2%
K_D Remoxipride (nM)	118	2.7%
K_D Risperidone (nM)	10.5	4.6%

K_D Sertindole (nM)	6.89	2.0%
K_D Spiperone (nM)	0.19	2.5%
K_D Ziprasidone (nM)	3.56	1.8%
K_D Dopamine (nM)	10.3	3.9%
k_{off} Dopamine (min^{-1})	1.69*	
R_{tot} [D2 Receptor concentration] (nM)	1.74	1.3%
k_{0max}: Maximum cAMP synthesis induced by inverse agonism (min^{-1})	20.5	0.5%
k_1: Baseline cAMP synthesis (min^{-1})	4.12	0.8%
k_2: cAMP degradation independent from active PDE (min^{-1})	0.0334	10.8%
k_3: cAMP degradation by active PDE (nM^{-1} min^{-1})	0.00882	0.2%
k_4: active PDE synthesis (min^{-1})	0.00882[a]	
k_5: active PDE degradation (min^{-1})	0.0005*	
$DAFR_{50}$ Dopamine	2.25	2.4%
Hill coefficient	1.77	0.4%
LFR_{50} Bromperidol	1.54	0.6%
LFR_{50} Clozapine	0.504	0.7%
LFR_{50} Domperidone	1.71	0.6%
LFR_{50} JNJ-39269646	0.856	0.5%
LFR_{50} JNJ-37822681	0.823	0.4%
LFR_{50} Haloperidol	0.699	0.5%
LFR_{50} Nemonapride	2.47	1.1%
LFR_{50} Olazapine	0.628	0.6%
LFR_{50} Paliperidone	0.657	0.5%
LFR_{50} Pimozide	618	1.9%
LFR_{50} Quetiapine	0.827	0.9%
LFR_{50} Raclopride	2.68	1.2%
LFR_{50} Remoxipride	1.95	1.4%
LFR_{50} Risperidone	5.37	3.6%
LFR_{50} Sertindole	1.02	0.5%
LFR_{50} Spiperone	1.56	0.6%
LFR_{50} Ziprasidone	0.959	0.4%
Receptor Turnover (min^{-1})	0.238	2.2%
Proportional error	0.01	0.3%

[a] k_4 was set to have the same value as k_3.

Supplement S 4. explanation of frequency response analysis results (FRA)

In a frequency response analysis, the dynamic behavior of a system is investigated by providing a harmonic oscillation as input signal, described by a sine wave with a variable frequency. Subsequently, the amplitude and the phase of the resulting sine wave are compared to that of the original sine wave. This frequency response analysis is often applied to a linear or linearized system and is derived analytically from the system's differential equations, but can also be derived from experimental data or simulations [26]. Dopamine concentrations are released in a pulsatile manner with a frequency of around 1 s^{-1}, but also show more slowly fluctuating levels caused by transient activity. Therefore, a frequency response analysis with fluctuating dopamine concentrations as input is reflective of the relevant context of drug action for dopamine antagonists.

Here we show the intermediate steps that lead to the eventual calculation of gain in cAMP amplitude. Firstly, we show in the top row of Figure S 4 three examples of different input frequencies, for which the different line colors all have the same overlaying sine wave characteristics and are not influenced by the drug-target k_{off}.

The second row of Figure S 4 shows how the dopamine occupancy follows the dopamine concentrations (in a non-linear fashion) until the frequency gets too high, as visible for the highest frequency, and the amplitude of the dopamine occupancy fluctuation declines. The slight influence of the antagonist k_{off} on dopamine occupancy for the intermediate occupancy can be explained by the competitive binding of the antagonist and dopamine and the influence of the koff on antagonist binding, as shown in the third row of Figure S 4.

The third row of Figure S 4 shows how all antagonists can be displaced by dopamine binding for the slowest frequency (hence the fluctuating occupancy), while for the intermediate frequency only the fast dissociating drug can be displaced fast enough to keep the original amplitude. Finally, for the highest frequency, none of the antagonists can be displaced fast enough and the fluctuation in dopamine concentrations and dopamine occupancy is not reflected in the antagonist-receptor occupancy.

The bottom row of Figure S 4 shows how the differences in dopamine and antagonist occupancy are translated into cAMP concentrations in a frequency-dependent manner (note the increased gain for the intermediate frequency that is not reflected in the occupancy profiles).

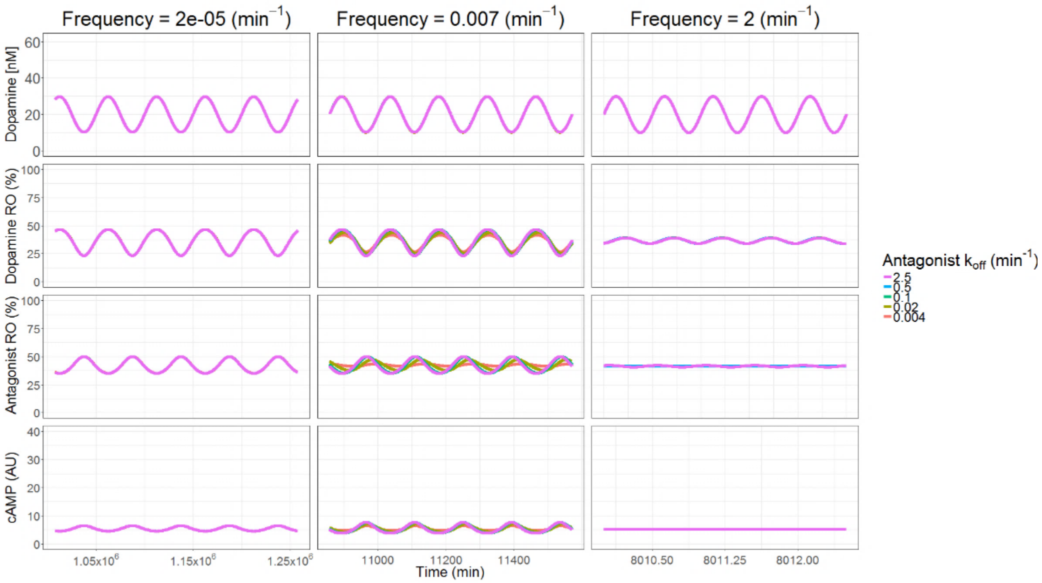

Figure S 4. Example of input frequencies for dopamine as used in the simulations (top panels) and the simulated responses (lower panels). The second row shows the dopamine receptor occupancy, the third row the antagonist receptor occupancy and the bottom row the cAMP response for each simulation with the fluctuating dopamine concentrations from the corresponding top row panels. The different line colors represent different simulations for which the dissociation rate constant of the antagonist-receptor complex is changed. The dopamine fluctuation frequencies are indicated above the panels and by the different time scales on the x-axis.

Supplement S 5. Identification of the influence of system-specific parameters on the frequency response analysis results.

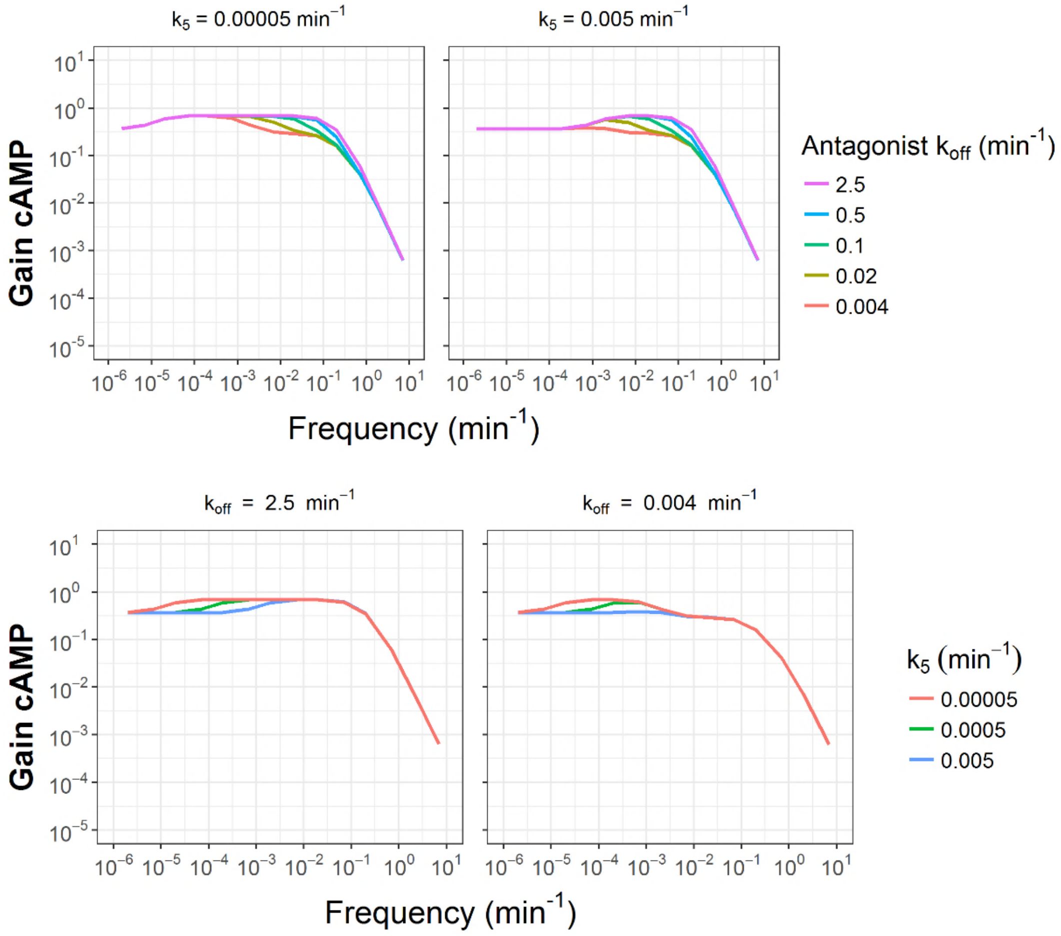

Figure S 5. Frequency response analysis for 3 different active PDE turnover rate constants and 5 different antagonist k_{off} values. The upper plots show the influence of k_{off} for two different active PDE turnover rate constants, and the lower plots show the influence of the active PDE turnover rate constants for two different koff values. The input signal was a sine wave of free dopamine with an amplitude of 10nM and baseline of 20 nM, at the frequencies indicated on the x-axis. At each active PDE turnover rate, 5 different antagonist k_{off} values were simulated, which are represented by the different line colors. The k_{on} values were changed simultaneously with k_{off}, which means that the K_D was constant at 6.93 nM. The antagonist concentration was 14 nM, the LFR_{50} was 1.03 and all system-specific parameters were identical to Table 3. The order of the lines in the legend follows the order of the lines in the graph.

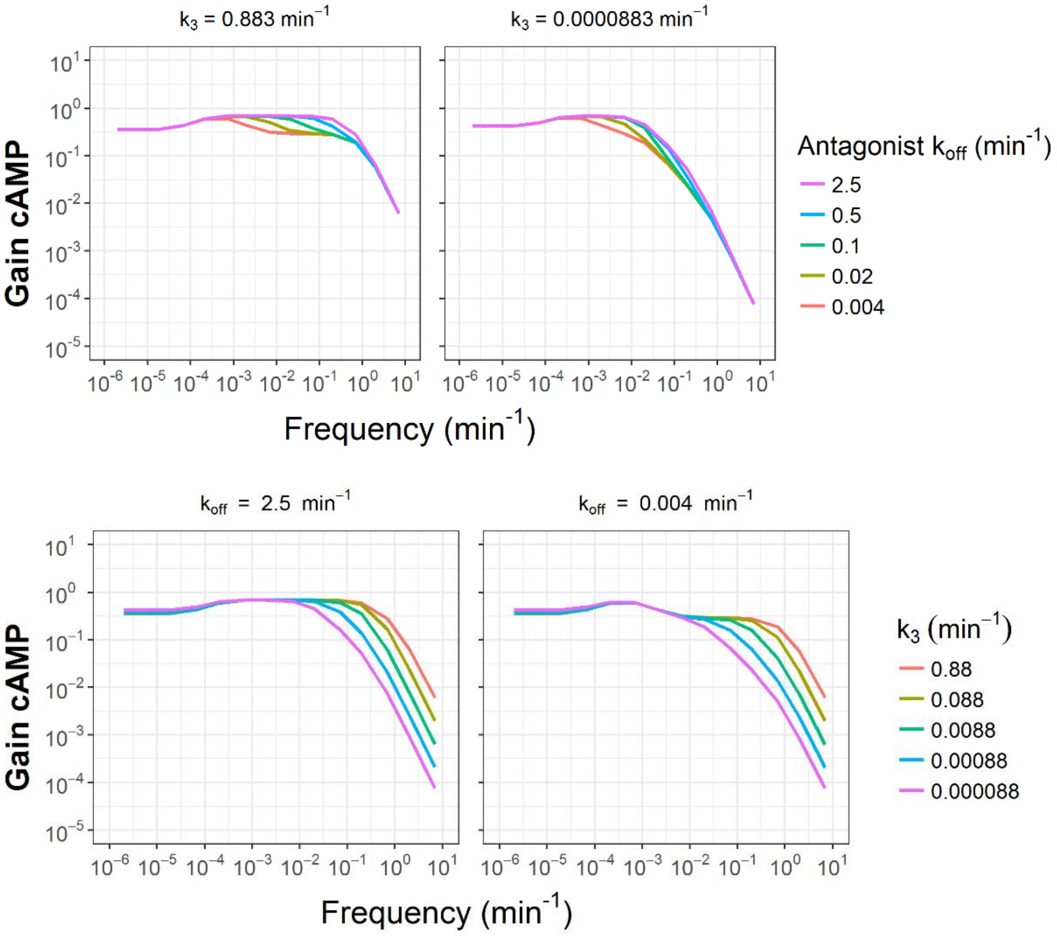

*Figure S 6. Frequency response analysis for active PDE-dependent cAMP turnover rate constants (k_3) of 0.883 min^{-1} (left) and 0.883*10^{-4} min^{-1} (right). The input signal was a sine wave of free dopamine with an amplitude of 10nM and baseline of 20 nM, at the frequencies indicated on the x-axis. At each cAMP turnover rate, 5 different antagonist k_{off} values were simulated, which are represented by the different line colors. The k_{on} values were changed simultaneously with k_{off}, which means that the K_D was constant at 6.93 nM. The antagonist concentration was 14 nM, the LFR_{50} was 1.03 and all system-specific parameters were identical to* Table 3. *The order of the lines in the legend follows the order of the lines in the graph.*

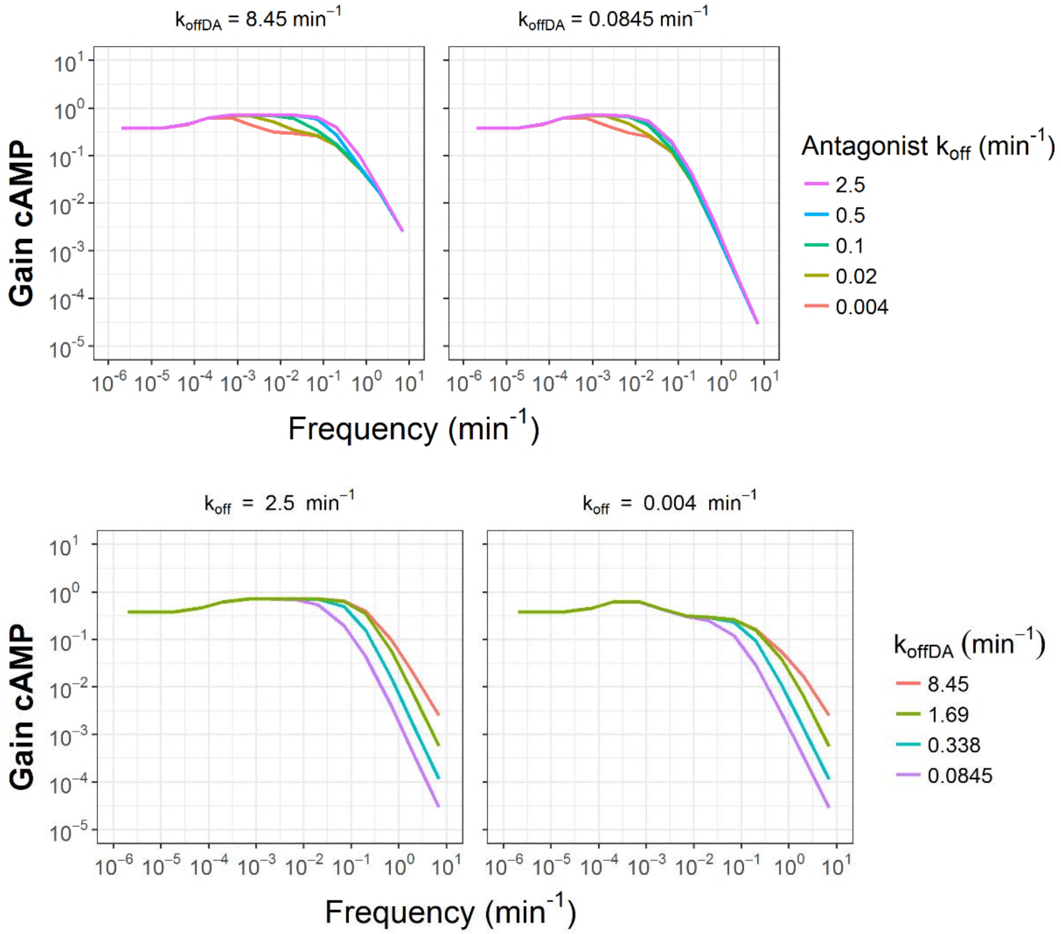

Figure S 7. Frequency response analysis for dopamine-receptor dissociation rate constants (k_{offDA}) of 8.45 min^{-1} (left) and 0.0845 min^{-1} (right). The input signal was a sine wave of free dopamine with an amplitude of 10nM and baseline of 20 nM, at the frequencies indicated on the x-axis. At each dopamine dissociation rate constant, 5 different antagonist k_{off} values were simulated, which are represented by the different line colors. The k_{on} values were changed simultaneously with k_{off}, which means that the K_D was constant at 6.93 nM. The antagonist concentration was 14 nM, the LFR_{50} was 1.03 the receptor recycling rate constant was switched to 0 and all other system-specific parameters were identical to Table 3*. The order of the lines in the legend follows the order of the lines in the graph.*

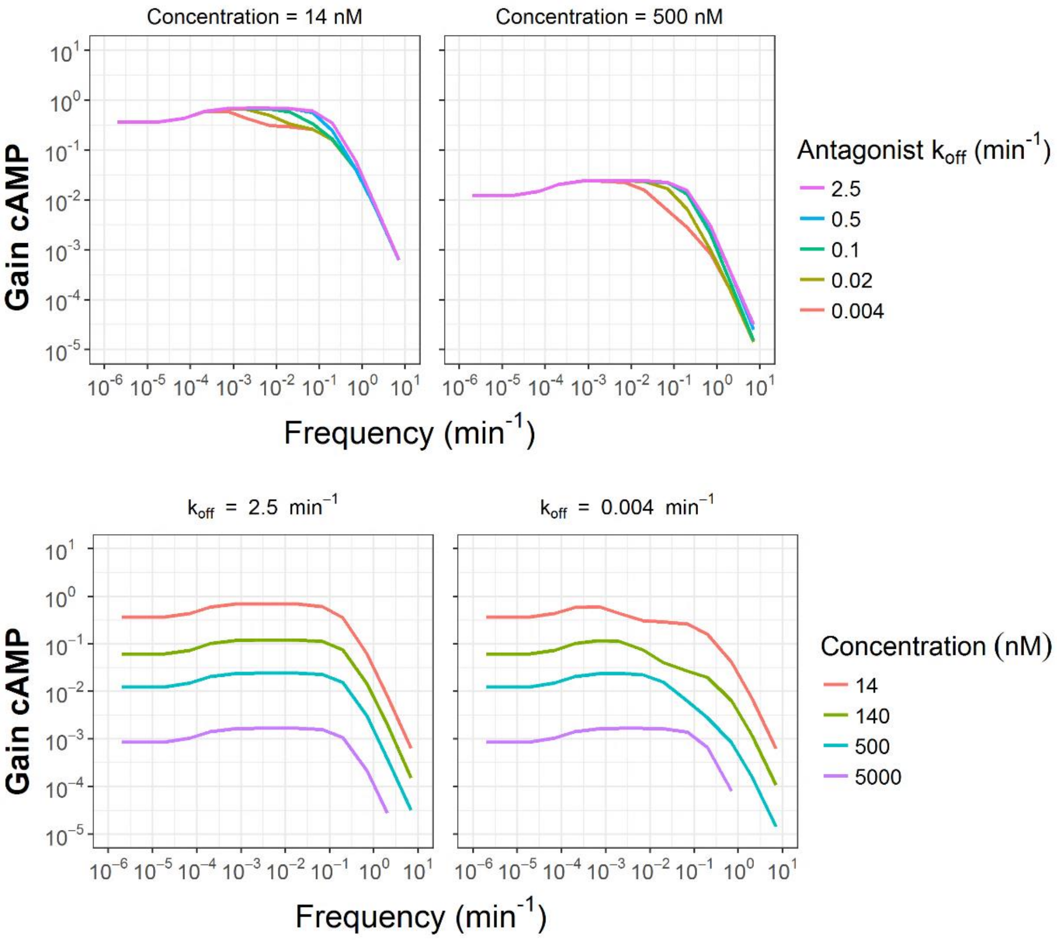

Figure S 8. Frequency response analysis for antagonist concentrations of 14 nM (left) and 500 nM (right). The input signal was a sine wave of free dopamine with an amplitude of 10nM and baseline of 20 nM, at the frequencies indicated on the x-axis. At each antagonist concentration, 5 different antagonist k_{off} values were simulated, which are represented by the different line colors. The k_{on} values were changed simultaneously with k_{off}, which means that the K_D was constant at 6.93 nM. The antagonist concentration was 14 nM, the LFR_{50} was 1.03 and all system-specific parameters were identical to Table 3. The order of the lines in the legend follows the order of the lines in the graph.

Chapter 9. Mechanistic modelling of drug target binding kinetics as determinant of the time course of drug action *in vivo*

Discussion, perspectives and conclusion

abbreviations: BF: Target fraction bound, k_{off}: drug-target dissociation rate constant, k_{on}: drug-target association rate constant, k_{el}: drug-target elimination rate constant, $t_{1/2z}$-pl: terminal plasma, elimination half-life, $t_{1/2}$-diss: drug-target dissociation half-life

For any drug that is administered to patients or that is being developed, is essential that the time course of its effects can be predicted to ensure rational drug therapy and drug development. After its administration, the time course of the effect of a drug can be influenced by all processes that constitute the complex system of the human body. The most common processes that determine the time course of drug action can be categorised as related to either target site exposure, target binding, signal transduction or homeostatic feedback mechanisms, as indicated in *Figure **1***. For the development of new drugs, it is critical to predict the time course of drug action as early as possible. To this end, the *in vitro* measurement and *in silico* prediction of the critical process of target binding provides a valuable selection criterion to identify potential drug candidates.

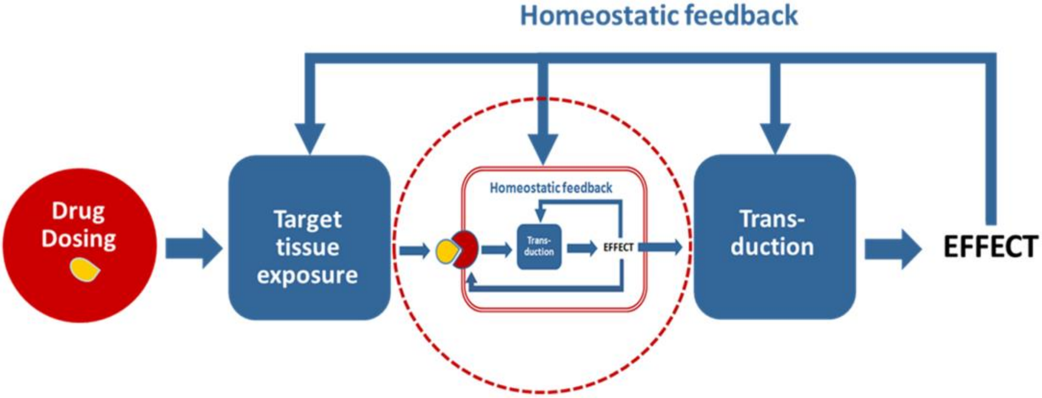

Figure 1. The causal chain from drug dosing to drug effect. The drug is indicated by the yellow shape and the drug target is indicated by the complimentary red shape. Adapted by E.C.M. de Lange from Danhof, 2016.[1]

To use target binding as selection criterion in drug discovery, the measurement of target binding under equilibrium conditions has been traditionally used to determine a single drug-specific parameter for the drug-target affinity, being the drug target dissociation constant K_D. However, the kinetics of this target binding (drug-target binding kinetics), has often been demonstrated to influence the time course of drug action.[2–10] More than half a century ago, it has even been postulated that the strength of a drug effect is proportional to the rate of drug-target dissociation (rate theory), rather than to the occupancy of the target (occupancy theory).[11] Together with new technologies to determine drug-target binding kinetics and new compound series with varying binding kinetics, this has sparked a new interest in the application of especially the drug target dissociation rate constant k_{off} as selection criterion in drug discovery.[12] However, drug-target binding kinetics is only a single step in the long chain of events from drug dosing to drug effect and many other processes influence the kinetics of drug action *in vivo* as discussed above. To understand the role of drug-target binding kinetics, to predict its influence on the time course of drug action, and to use it to develop better drugs, one should study drug-target binding kinetics in relation to the other determinants of the time course of drug action.

In this thesis, we studied a wide range of pharmacokinetic-pharmacodynamic (PKPD) models that include expressions to describe target binding kinetics by simulation for a wide range of their parameter values and, where possible, application to *in vitro* and *in vivo* pharmacokinetic and pharmacodynamic data. The main question in these studies was how the drug-target binding kinetics, in conjunction with plasma pharmacokinetics, tissue distribution kinetics, endogenous ligand competition, signal transduction kinetics and homeostatic feedback determine the *in vivo* time course of drug action. In this chapter, we first discuss how our findings contribute to our understanding of the influence of drug-target binding kinetics on the time course of drug action. Next, we discuss how our findings can be applied in drug discovery, drug development and in clinical practice. Finally, we provide suggestions for future research and conclude this thesis.

The added value of drug target binding kinetics as selection criterion in drug discovery is relatively new and subject to an ongoing debate.[13] As described in **chapter 1 and 3**, the considerations regarding the role of drug-target binding kinetics, especially the dissociation rate constant k_{off}, on the time course of drug effect *in vivo* fall into four categories:

I) a low k_{off} value can result in prolongation of target occupancy [3,14,15],
II) a low k_{off} value for the therapeutic target compared to the secondary-targets can give rise to an increase in selectivity over time [3,16,17],
III) a low k_{off} value will lead to a more constant blocking of endogenous ligand binding and thus block the endogenous signalling more effectively [18,19] and
IV) a low k_{off} value can yield a more efficient coupling to signal transduction, leading to a higher efficacy.[20,21]

In this thesis, we have investigated the validity and the limiting conditions of the first three of the considerations that support the relevance of drug-target binding kinetics. The fourth consideration is beyond the scope of this work. Below, we will shortly summarise and discuss our findings for each of these three arguments.

I. Target dissociation kinetics as determinant of the time course of target occupancy.

The first consideration on the influence of the k_{off} value on the duration of target occupancy was investigated in relation to i) plasma pharmacokinetics, ii) tissue distribution kinetics and iii) the concentration of the target, in **chapter 2, 4 and 5**. Simulations on the basis of a one-compartment pharmacokinetic model with target binding showed that the time course of target occupancy is only affected by the value of k_{off} if both the k_{off} is lower than the product of the elimination rate constant (k_{el}) and unbound target fraction (1-*BF*) and the k_{on} is lower than the ratio of k_{el}/R_{tot} as illustrated in ***Figure 2***. If the k_{off} is lower than the product of the elimination rate constant and unbound target fraction and the k_{on} is higher than the ratio of k_{el}/R_{tot}, the duration of target occupancy is equally influenced by the k_{off} and the k_{on}.

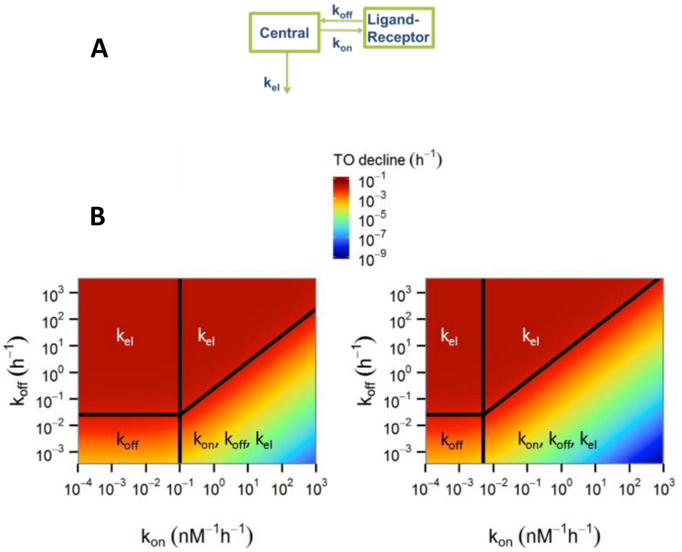

Figure 2. Approximation of the decline in target occupancy as function of k_{off} and k_{on} using a simple one compartment model with target binding. A: schematic representation of the approximated model. B: Approximation results for a total target concentration 1 nM (left panel) and 20 nM (right panel) an elimination rate constant of 0.1/h and a target fraction bound of 0.75, to represent a clinically relevant degree of target occupancy. Colours represent the decrease of target occupancy. The vertical line is given by $K_{RLon} = k_{el} / (R_{tot} * k_{on}) = 1$, the horizontal line is given by $K_{RLoff}(BF) = k_{el} * (1-BF)/k_{off} = 1$ and the diagonal line is given by the equation $k_{off} = k_{on} * R_{tot} * (1-BF)$. In these equations, k_{el} is the elimination rate constant, R_{tot} is total target concentration and BF is the bound fraction of the target. The annotations indicate which parameters influence the decrease in target occupancy in the corresponding segment of the plot.

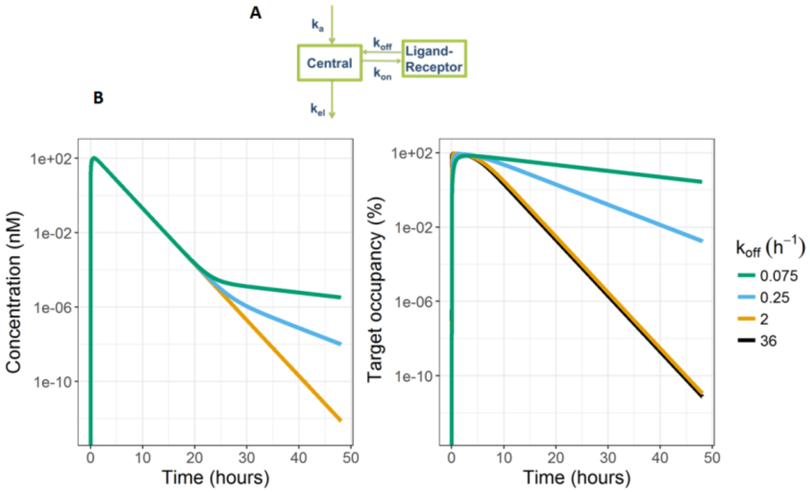

Figure 3. Simulations with a one compartment pharmacokinetic model with drug target binding demonstrate the parallel terminal phase of the pharmacokinetic and target occupancy curves. A: schematic representation of the model that was used for these simulations. For these simulations, the first order absorption rate constant k_a was 3 hr^{-1}, the first order pharmacokinetic elimination rate k_{el} was 0.693 hr^{-1}, the target concentration was 0.001 nM and the K_D was 10 nM.

When drug distribution out of the target site is slow compared to its elimination from plasma, the distribution can also become the rate-limiting step in the decline of target occupancy, which leads to an equal influence of k_{on} and k_{off} on the duration of target occupancy. These findings contrast with studies that suggested that the role of the k_{off} value is independent of the K_D and the concentration of the target[4,15,22], but are in line with studies on rebinding, in which also a clear influence of the target concentration on the duration of target occupancy has been observed.[14,23,24] In **chapter 4**, we have shown that k_{off} values, even when these are much lower than the pharmacokinetic elimination rate constant, lead to equilibrium between free target site and target-bound drug concentrations for high target concentration/K_D ratios. This finding is in line with the equilibrium binding and steady-state assumptions, which require free and bound drug concentration to be in equilibrium, which are often successfully incorporated in drug target binding models.[25–27] Moreover, our findings in **chapter 4** showed that the decline of plasma concentrations eventually parallels the decline of target occupancy on semi-log scale, even if drug-target dissociation is the rate-limiting step for the decline of target occupancy. This parallel decline is illustrated in *Figure **3*** for an extremely low target concentration of 0.001 nM and a K_D of 10 nM. This low target concentration/K_D ratio causes this parallel decline to appear only at the late time points and at an extremely low plasma concentration, but these simulations show that even in this case both plasma pharmacokinetics and target occupancy curves are eventually parallel.

This parallel decline in drug concentration and target occupancy makes that the comparison of the terminal plasma half-life ($t_{1/2z}$-pl) and target dissociation half-life ($t_{1/2}$-dis) is only informative if the $t_{1/2}$-dis is much shorter than the $t_{1/2z}$-pl. If both half-lives have similar values, this does not necessarily dispute the influence of k_{off} on the decline rate of target occupancy. This influence of the drug-target dissociation rate on the $t_{1/2z}$-pl might not be observed, because of the lower limit of quantification of the assays for determining drug concentrations in plasma. However, Dahl et al. [15] calculated the ratio of the $t_{1/2z}$-pl and the $t_{1/2}$-dis for a series of marketed drugs and observed that the $t_{1/2}$-dis is often shorter than the $t_{1/2z}$-pl. While this observation supports the conclusion of the authors that the $t_{1/2}$-dis does not determine the duration of target occupancy, it should be noted that several of the studied drugs had a $t_{1/2}$-dis in the same order of magnitude as the $t_{1/2z}$-pl. As described above, if the target occupancy duration is determined by the $t_{1/2}$-dis, the $t_{1/2z}$-pl will be identical to the $t_{1/2}$-dis. Thus, the duration of target occupancy for the drugs with a $t_{1/2}$-dis in the same order of magnitude as the $t_{1/2z}$-pl in the study of Dahl et al. could have been determined as well by the $t_{1/2}$-dis.

So far, our description of the influence of plasma elimination, target site distribution and the target concentration on the duration of target occupancy did not take into account the role of target synthesis and degradation, distribution to non-target binding tissues, and protein binding. These latter factors need to be addressed as well, as they can influence the duration of target occupancy (**chapter 1**). While extensive distribution to non-target binding tissues and plasma protein binding can reduce the effective elimination rate of the drug from the plasma and thereby prolong drug-target binding, a fast target turnover can reduce the duration of target occupancy, even for a slow drug-target dissociation compared to the plasma drug elimination or target site distribution. Thus, whereas the pharmacokinetic rate of elimination of the drug functions as an upper limit for the values of k_{off} that influence the duration of target occupancy, the degradation rate constant of the drug-target complex functions as a lower limit for the values of k_{off} that influence the duration of target occupancy.

In summary, a low k_{off} value can prolong the duration of target occupancy, but this prolongation can only be predicted in conjunction with the pharmacokinetics, target concentration and target turnover.

II. The relation between the k_{off} value for different targets, target selectivity and tissue selectivity

The second consideration for the relevance of the k_{off} value for the time course of drug action is based on the differential duration of target occupancy between the therapeutic target and the off-target(s), as can be caused by different k_{off} values. In **chapter 6,** we distinguish between selective binding to the therapeutic target relative to off-targets caused by differential k_{off} values, which is commonly referred to as "*kinetic selectivity*" [3,16,17], and selective binding to a target in the therapeutic tissue, relative to tissues that mediate side effects, which is commonly referred to as "*tissue selectivity*"[28,29]. *Kinetic selectivity* is closely related to the time course of target occupancy for each target. Therefore, the principles for single target binding in one tissue as identified in **chapter 4** are likely to hold for *kinetic selectivity* as well. Our simulations in **chapter 6** were in line with **chapter 4**: a high target concentration/K_D ratio leads to a prolonged duration of target occupancy, which is caused by a slow decline of the drug concentration at the target site. As a consequence, all targets at the same target site will be exposed to drug concentrations that decline slowly and their duration of target occupancy will be equally long. On the other hand, any tissues with much lower target concentrations than the therapeutic tissue will be exposed to faster decline of drug concentrations and the target occupancy in those tissues will also decline faster. This results in *tissue selectivity*. This is illustrated in *Figure **4***, where target 2 has a much longer target occupancy duration in tissue 1 compared to tissue 2, while both tissues have the same distribution rate constants, the same concentration of target 2 and the same binding kinetics to target 2. The long duration of target occupancy in tissue 1 is caused by the high concentration of target 1, which causes retention of the drug in tissue 1, as reflected by the concentration profiles.

However, *tissue selectivity* decreases when K_D is extremely low and the concentration of the target is higher than the K_D in both therapeutic and non-therapeutic tissues, as compared to tissues with reasonably high K_D values. These results demonstrate that a high K_D value may result in a decrease in both *kinetic selectivity* and *tissue selectivity*. Moreover, the combination of target and tissue selectivity may lead to a reversal of selectivity over time if one of the targets has a high target concentration. We have shown that the use of mechanistic modelling and simulation combined with statistical Quantitative Structure Activity Relationship (QSAR) modelling can help to predict both target and tissue selectivity in the earliest stage of drug discovery. However, we also found that these predictions are dependent on the effective distribution of the target site and the target concentration. These latter parameters might be difficult to obtain with high precision, especially in the earliest phase of drug discovery.

In short, a low k_{off} value can result in *kinetic selectivity*, but only when the target concentration/K_D ratio is not high enough to induce a slow decline of local drug concentrations. Moreover, a high target concentration or low K_D value can increase tissue selectivity.

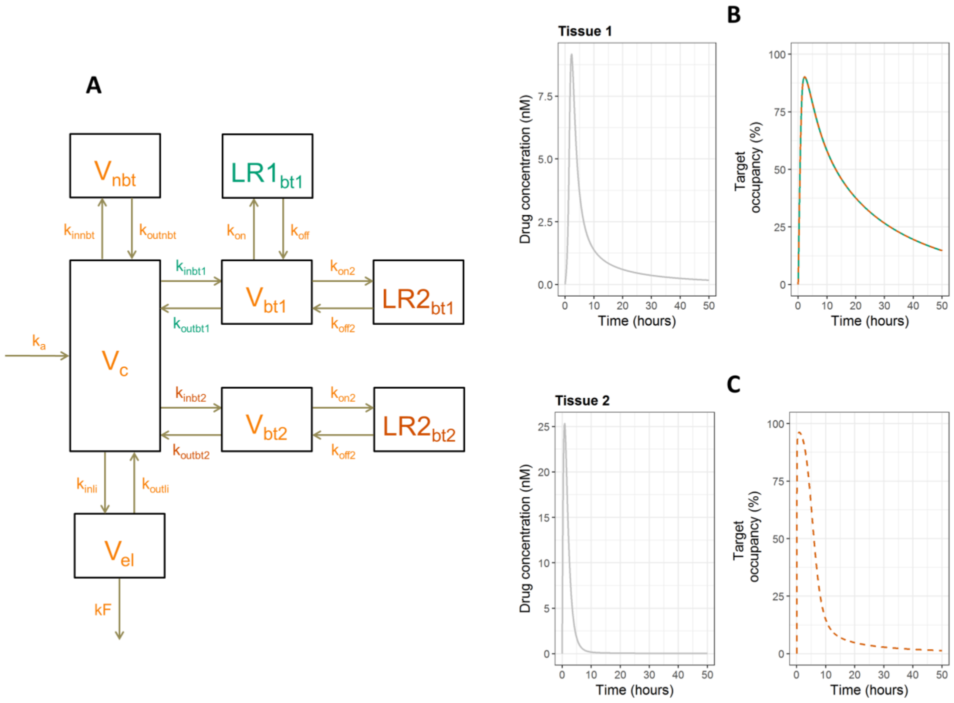

Figure 4. Simulation of simultaneous target and tissue selectivity and the influence of the target concentration. A: schematic representation of the applied model structure for these simulations. k_a = absorption rate constant, k_{in} = inwards distribution rate constant, k_{out} = outwards distribution rate constant, k_{on} = association rate constant, k_{off} = dissociation rate constant, kF = forward rate of elimination constant, LR = ligand-receptor complex, V = tissue volume (L), nbt = non-binding tissue, c = plasma compartment, bt = binding tissue, nbt = non-binding tissue, el = elimination tissue. The values for k_{on} and k_{off} were 10 nM^{-1} h^{-1} and 10 h^{-1}, respectively, for both targets. The values for k_{inbt} and k_{outbt} were 2.6 and 0.88 h^{-1}, respectively, and V_{bt} was 2 L for both tissues, the target concentration for target 1 was 100 nM and was 1 nM for target 2 in both tissues. The values of the other parameters were: k_a = 3 h^{-1}, k_{innbt} = 60 h^{-1}, k_{outnbt} = 5.5 h^{-1}, k_{inli} = 17 h^{-1}, k_{outli} = 54 h^{-1}, kF = 100 h^{-1}, V_c = 6 L, V_{nbt} = 66 L, V_{li} = 1.9 L B: Drug concentration and target occupancy of target 1 (solid line) and target 2 (dashed line) in tissue 1. Both target occupancy profiles are identical. C: Drug concentration and target occupancy of target 2 (dashed line) in tissue 1.

III. The relation between the k_{off} value, resilience to endogenous ligand binding, signal transduction and homeostatic feedback.

The third consideration that supports the relevance of the k_{off} value for the time course of drug action is related to the resilience to endogenous ligand competition. This idea has been raised in relation to dopamine D_2 antagonists [18], but the principle also holds for any other target where endogenous competition is important. In short, an endogenous signal in the form of a steep increase and decrease in the endogenous ligand concentration would normally lead to endogenous ligand binding to the target and further signal transduction. In the presence of a drug with a high k_{off} value that is bound to the target, this rise in endogenous ligand would still lead to binding of the endogenous ligand, albeit to a lesser degree depending on the concentration of the drug and its K_D. For a drug with a low k_{off} value, the endogenous ligand would not have enough time to displace the drug from the receptor before its concentrations go down to the basal level. As a result, for a drug with a relatively high k_{off} value, part of the physiological signalling is maintained, whereas for a compound with a relatively low k_{off} value the signalling would be completely blocked. In the case of the dopamine D_2 receptor, this extensive blocking of the dopaminergic signalling is considered to lead to side effects, and a low k_{off} value is therefore considered to be a disadvantage of a D_2 antagonist. In **Chapter 8**, we found that a low k_{off} value can indeed prolong the drug-target occupancy with fluctuating endogenous ligand concentrations. However, we also found that this influence of the drug k_{off} only occurs when the endogenous ligand k_{off} is high enough to result in rapid endogenous ligand binding. Moreover, if the turnover of the signal transduction molecules is not fast enough, the rapid increase and decrease of endogenous ligand target occupancy does not lead to rapid fluctuations in the concentrations of the signalling molecules. This limited influence of the k_{off} value on the drug effect to frequently fluctuating endogenous ligand concentrations for high k_{off} values was not identified in a previous study that did not take the endogenous ligand k_{off} and the signal transduction kinetics into account.[19] The limited translation of fluctuating endogenous ligand concentrations into fluctuating second messengers is in line with the concept of frequency encoding, which explains that the strength of biological signals can be translate into the frequency of the fluctuations in signalling molecules and *vice versa*. These fluctuations are therefore only representing the strength of a signal and eventually not translated into a fluctuating effect, but into a stable effect, the extent of which is dependent on the fluctuation frequency of the signalling molecules.[30]

In summary, the k_{off} value of a drug (especially an antagonist) is only relevant for the resilience to endogenous signalling if both the endogenous ligand k_{off} and the turnover of the signalling molecules are high enough to translate the endogenous ligand fluctuations into fluctuations in signalling strength.

Modelling the delay between pharmacokinetics and pharmacodynamics and the relevance of drug-target binding.

One of the considerations that disputes the relevance of the k_{off} value for the time course of drug action is that, on one hand, the drug-target binding kinetics are not generally required in PKPD models that give a good description of the observed drug concentration and effect data. On the other hand, target binding models are often required to adequately describe antibody pharmacokinetics, in so called Target Mediated Drug Disposition (TMDD) models, which can and have been applied to small molecules as well.[25,31,32]

The effect compartment model is typically used to explain hysteresis, rather than a target binding model.[33] However, this does not necessarily mean that drug-target binding kinetics does not influence the time course of drug action. In **Chapter 7**, we compared the target binding model and the more popular effect compartment model and found that these models do not lead to a different time course of the drug effect for all parameter values combinations that result in a delay between drug concentrations and drug effect. In other words, hysteresis between plasma drug concentrations and effect can be described equally well by an effect compartment and a target binding model for many of the parameter value combinations used in this study. Although this is not a finding that directly supports the relevance of drug target binding for the time course of drug action, it does suggest that the drug-target binding model should be tested more often to allow *prediction* of the time course of drug action*,* by the incorporation of *in vitro* data, and therewith to improve the *in vitro-in vivo* translation in drug discovery.

Perspectives for the development and application of pharmacotherapy

The centrality of the drug-target binding event in drug treatment makes our findings applicable across the whole range of pharmacotherapy, from drug discovery to clinical practice. The most general application of our work is that we obtained a better understanding of drug-target binding kinetics and its role in the complex chain between drug dosing and drug effect. Below, we discuss more specifically how our insights can be applied in drug discovery, drug development and clinical practice.

In drug discovery, the selection of the best drug candidates is essential because of the limited resources and the large number of molecules that enter the drug discovery phase, while only a limited number of tests can be performed. Therefore, these tests need to yield information on the most critical drug properties which can be easily translated into selection criteria for the best drug candidates. The current understanding of the value of drug-target binding kinetics as a selection criterion in drug discovery is limited and mostly focussed on obtaining drugs with low k_{off} values. In this thesis, we have shown that a low k_{off} value is only a beneficial drug property if the whole PKPD context favours the influence of the k_{off} on the time course of drug action. Therefore, our findings suggest that for any new disease/therapeutic indication, detailed knowledge on the system-specific parameters is required before knowledge of drug-target binding kinetics can be applied meaningfully. Such parameters include the concentration of the target, its degradation and synthesis rate constants, the perfusion of the target site and the concentration and binding kinetics of endogenous ligands. Subsequently, mechanistic PKPD modelling should be applied to identify the optimal drug properties, including the drug target k_{off} and K_D.

As a rule of thumb, targets that are expressed at a higher concentration than the K_D value of the drug and targets with a faster degradation rate constant than the k_{off} value of the drug are not expected to favour the relevance of the k_{off} value.

In drug development, the *in vitro – in vivo* translation of drug effects and the translation across animal species is essential to get the best drug candidates to the market. For this, the combination of *in vitro-in vivo* extrapolations (IVIVE) with physiologically based pharmacokinetic models can be used to predict drug effects across animal species and humans.[34,35] However, drug target binding kinetics are often not incorporated in these models. Our results suggest that the target concentrations, the perfusion of the target tissue and active processes in drug distribution to the target site are important and need to be included in these models to enable translation between species, especially for high affinity compounds.

In clinical practice, the prediction and understanding of the time course of drug action can be critical for effective and safe drug treatment. Our findings in **chapter 4 and 6** demonstrate that a delayed onset and offset of drug action can be caused by slow drug-target binding kinetics or binding to a target with a high target concentration. Importantly, if these mechanisms drive a delayed onset of the drug effect, this can be avoided by using higher drug doses. Thus, the combination of a high initial drug dose (loading dose) combined with lower subsequent doses (maintenance dose) can be used to achieve rapid drug action while still minimizing toxicity. Since our findings demonstrate the influence of the target concentration on the time course of drug action, these findings can also be used to individualize drug dosing based on target concentrations. This might be especially relevant for high target concentrations that are also highly variable between patients, such as HER2 concentrations in HER2-positive breast tumours.[36]

Future research

The findings described in this thesis present an improved understanding of the influence of drug-target binding kinetics on the time course of drug action in relation to the most important determinants of the time course of drug action. However, the complete biological system that determines drug action is too complex to understand completely or even to describe all elements and their relation with the role of drug-target binding kinetics. The main questions that remain elusive after the studies in this thesis are described below.

As mentioned in **chapter 1** and in the discussion above, the turnover of the target can be an important factor that influences the role of drug-target binding kinetics. Although target turnover is often referred to as a single parameter, its relation with drug-target binding kinetics is complex since the turnover of the unbound target can be different than the turnover of drug-target complex. This is schematically represented in *Figure 5*. The analysis of target turnover can be simplified by assuming that the turnover of the unbound target (k_{degT}) and the drug-target complex (k_{degC}) are equal, but differences between these two parameters of more than tenfold have been estimated from *in vivo* data.[37–39] In these studies k_{degT} has been observed to be both more than tenfold larger and more than tenfold smaller than k_{degC}. A consequence of a difference in k_{degT} and k_{degC} is that the total target concentration is not constant and depends on the amount of target binding. This makes the level of target occupancy and the drug-target affinity constant K_D less informative parameters [40] and makes mathematical analysis of the model less straightforward. Moreover, the pharmacological entity that drives the drug effect depends on the disease and the target: for an enzyme inhibitor, the concentration of the unbound target determines the drug effect, while for a receptor agonist, the concentration of the drug-target complex drives the drug effect. These complexities have not been investigated in this thesis and it would require further research to understand their relationship with drug-target binding kinetics.

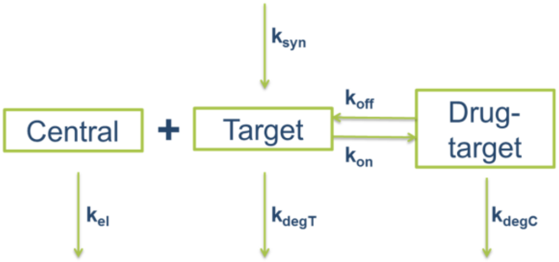

Figure 5. schematic representation of target turnover in relation to drug-target binding kinetics and pharmacokinetics. k_{el}, k_{degT}, k_{degC} *and* k_{off} *represent the first order rate constant of elimination of the drug from plasma, degradation of the unbound target, degradation of the drug-target complex and dissociation of the drug-target complex, respectively.* k_{on} *represents the second order drug-target association rate constant,* k_{syn} *represents the zero-order target synthesis rate constant.*

In addition to the influence of drug-target turnover, the translation from target occupancy to drug effect also requires further exploration. First of all, several authors have observed a correlation between the k_{off} and the efficacy of agonists.[21,41,42] Interestingly, these correlations all show a higher efficacy for agonists with lower k_{off} values, which is opposite to what Paton postulated in his rate theory in 1961.[11] The higher efficacy of slowly dissociating drugs can be explained by a more efficient coupling of activated receptors to signal transduction if they are active for a longer continuous period of time, which reduces the fraction of aborted signalling events.[21] This correlation between k_{off} and efficacy should be supported with more compound series for various targets and with the analysis of mechanistic signal transduction models.

Secondly, the occurrence of a non-linear target occupancy *versus* effect relationship (transducer function) can reduce the impact of a change in target occupancy levels and its rate.[43] If the transducer function, for example, has the classical sigmoidal shape, this means that a fast declining target occupancy does not lead to a fast decline of the drug effect if the target occupancy is close to 100%. In a clinical setting of continuously high target occupancies, this would make the decline rate of target occupancy less relevant for the duration of drug effects. It should be noted that this nonlinearity can have a similar influence on the time course of drug action as the nonlinearity between drug concentrations and target occupancy, as described in **chapter 2**. In addition, the occupancy versus effect relationship can have various profiles, including a parabolic profile [44,45], which further complicates the translation from target occupancy kinetics to drug effect kinetics. The signal transduction system that was analysed in **chapter 8** included the turnover of secondary messengers and regulation via a negative feedback loop. While we did observe the influence of the turnover of the feedback molecule on the transduction of fluctuating endogenous ligand concentration, we focused mainly on the fluctuation amplitude of the response in steady-state. The presence of homeostatic feedback mechanisms can also influence the initial response to a drug after its first administration and lead to a system with multiple steady-states.[46] Such a system can be sensitive to the rate of administration of a drug[47] which makes it more likely for the rate of drug-target association to influence which of the steady-states will be reached. Finally, signal transduction is often interlinked with an extensive signalling network with signalling cascades that are branched and result in simultaneous signal transduction at multiple levels, as identified for GnRH analogues.[48] Analysing the influence of drug-target binding kinetics on the drug effect in such complex networks would require additional research. The simulation-based frequency response analysis that was applied in **chapter 8** could also be applied to such signalling networks to unravel their dynamic behaviour and its determinants.

Conclusions

The research in this thesis has improved our understanding of the influence of drug-target binding kinetics on the time course of drug action. We have especially elucidated and quantified how drug-target binding kinetics relate to the other determinants of the time course of drug action, including pharmacokinetics, target turnover, endogenous competition and signal transduction. This research does not provide a complete understanding of all these factors and further research is especially required on the interaction between target turnover, signal transduction and binding kinetics. Nonetheless, our insights can be applied to the selection of better drug candidates, to improve translational research and to optimize and personalize clinical practice of pharmacotherapy.

References

1. Danhof M. Systems pharmacology - Towards the modeling of network interactions. Eur J Pharm Sci 2016;94:4–14
2. Yassen A, Olofsen E, Dahan A, et al. Pharmacokinetic-Pharmacodynamic Modeling of the Antinociceptive Effect of Buprenorphine and Fentanyl in Rats : Role of Receptor Equilibration Kinetics. J Pharmacol Exp Ther 2005;313(3):1136–49
3. Copeland RA, Pompliano DL, Meek TD. Drug-target residence time and its implications for lead optimization. Nat Rev Drug Discov 2006;5(9):730–9
4. Vauquelin G, Van Liefde I. Slow antagonist dissociation and long-lasting in vivo receptor protection. Trends Pharmacol Sci 2006;27(7):356–9
5. Ploeger BA, Van Der Graaf PH, Danhof M. Incorporating Receptor Theory in Mechanism-Based Pharmacokinetic-Pharmacodynamic (PK-PD) Modeling. Drug Metab Pharmacokinet 2009;24(1):3–15
6. Äbelö A, Andersson M, Holmberg AA, et al. Application of a combined effect compartment and binding model for gastric acid inhibition of AR-HO47108: A potassium competitive acid blocker, and its active metabolite AR-HO47116 in the dog. Eur J Pharm Sci 2006;29(2):91–101
7. Hong Y, Gengo FM, Rainka MM, et al. Population pharmacodynamic modelling of aspirin- and ibuprofen-induced inhibition of platelet aggregation in healthy subjects. Clin Pharmacokinet 2008;47(2):129–37
8. Äbelö A, Holstein B, Eriksson UG, et al. Gastric acid secretion in the dog: A mechanism-based pharmacodynamic model for histamine stimulation and irreversible inhibition by omeprazole. J Pharmacokinet Pharmacodyn 2002;29(4):365–82
9. Ramsey SJ, Attkins NJ, Fish R, et al. Quantitative pharmacological analysis of antagonist binding kinetics at CRF1 receptors in vitro and in vivo. Br J Pharmacol 2011;164(3):992–1007
10. Yamazaki S, Shen Z, Jiang Y, et al. Application of target-mediated drug disposition model to small molecule heat shock protein 90 inhibitors. Drug Metab Dispos 2013;41(6):1285–94
11. Paton WDM. A theory of drug action based on the rate of drug-receptor combination. Proc R Soc London Ser B Biol Sci 1961;154(954):21–69
12. Schuetz DA, de Witte WEA, Wong YC, et al. Kinetics for Drug Discovery: an industry-driven effort to target drug residence time. Drug Discov Today 2017;22(6):896–911
13. Folmer RHA. Drug target residence time: a misleading concept. Drug Discov Today 2017;6446(17)
14. Vauquelin G, Charlton SJ. Long-lasting target binding and rebinding as mechanisms to prolong in vivo drug action. Br J Pharmacol 2010;161(3):488–508
15. Dahl G, Akerud T. Pharmacokinetics and the drug-target residence time concept. Drug Discov Today 2013;18(15–16):697–707
16. Guo D, Dijksteel GS, Van Duijl T, et al. Equilibrium and kinetic selectivity profiling on the human adenosine receptors. Biochem Pharmacol 2016;105:34–41
17. Tonge PJ. Drug-Target Kinetics in Drug Discovery. ACS Chem Neurosci 2017;epub ahead of print
18. Kapur S, Seeman P. Does Fast Dissociation From the Dopamine D 2 Receptor Explain the Action of Atypical Antipsychotics ?: A New Hypothesis. Am J Psychiatry 2001;158(3):360–9
19. Vauquelin G, Bostoen S, Vanderheyden P, et al. Clozapine, atypical antipsychotics, and the benefits of fast-off D2 dopamine receptor antagonism. Naunyn Schmiedebergs Arch Pharmacol 2012;385(4):337–72
20. Guo D, Mulder-Krieger T, IJzerman AP, et al. Functional efficacy of adenosine A_2A receptor agonists is positively correlated to their receptor residence time. Br J Pharmacol 2012;166(6):1846–59
21. Sykes DA, Dowling MR, Charlton SJ. Exploring the Mechanism of Agonist Efficacy : A Relationship between Efficacy and Agonist Dissociation Rate at the Muscarinic M 3 Receptor. 2009;76(3):543–51
22. Copeland RA. The drug-target residence time model: a 10-year retrospective. Nat Rev Drug Discov 2016;15(2):87–95
23. DeLisi C. The biophysics of ligand-receptor interactions. Quaterly Rev Biophys 1980;13(2):201–30
24. Coombs D, Goldstein B. Effects of the geometry of the immunological synapse on the delivery of effector molecules. Biophys J 2004;87(4):2215–20
25. Dua P, Hawkins E, van der Graaf P. A Tutorial on Target-Mediated Drug Disposition (TMDD) Models. CPT Pharmacometrics Syst Pharmacol 2015;4(6):324–37
26. Liefaard LC, Ploeger BA, Molthoff CFM, et al. Population pharmacokinetic analysis for simultaneous determination of Bmax and KD in vivo by positron emission tomography. Mol imaging Biol 2005;7(6):411–21
27. Mager DE, Wyska E, Jusko WJ. Diversity of mechanism-based pharmacodynamic models. Drug Metab Dispos 2003;31(5):510–8
28. Klebanoff CA, Rosenberg SA, Restifo NP. Prospects for gene-engineered T cell immunotherapy for solid cancers. Nat Med 2016;22(1):26–36
29. Schaick EA Van, Tukker HE, Roelen HCPF, et al. Selectivity of action of 8-alkylamino analogues of N6-

cyclopentyladenosine in vivo: haemodynamic versus anti-lipolytic responses in rats. Br J Pharmacol 1998;124:607–18

30. Ingalls BP. Mathematical Modeling in Systems Biology: an introduction [Internet]. MIT Press; 2013. 1-396 p
31. Levy G. Pharmacologic target-mediated drug disposition. Clin Pharmacol Ther 1994;56(3):248–52
32. Landersdorfer CB, He YL, Jusko WJ. Mechanism-based population pharmacokinetic modelling in diabetes: Vildagliptin as a tight binding inhibitor and substrate of dipeptidyl peptidase IV. Br J Clin Pharmacol 2012;73(3):391–401
33. Louizos C, Yáñez JA, Forrest ML, et al. Understanding the hysteresis loop conundrum in pharmacokinetic / pharmacodynamic relationships. J Pharm Pharm Sci 2014;17(1):34–91
34. Rostami-Hodjegan A. Physiologically based pharmacokinetics joined with in vitro-in vivo extrapolation of ADME: a marriage under the arch of systems pharmacology. Clin Pharmacol Ther 2012;92(1):50–61
35. Yamamoto Y, Välitalo PA, van den Berg D-J, et al. A Generic Multi-Compartmental CNS Distribution Model Structure for 9 Drugs Allows Prediction of Human Brain Target Site Concentrations. Pharm Res 2017;34(2):333–51
36. Olsen DA, Østergaard B, Bokmand S, et al. HER1-4 protein concentrations in normal breast tissue from breast cancer patients are expressed by the same profile as in the malignant tissue. Clin Chem Lab Med 2009;47(8):977–84
37. Kagan L, Abraham AK, Harrold JM, et al. Interspecies scaling of receptor-mediated pharmacokinetics and pharmacodynamics of type I interferons. Pharm Res 2011;27(5):920–32
38. Le KN, Gibiansky L, Good J, et al. A Mechanistic Pharmacokinetic/Pharmacodynamic Model of Factor D Inhibition in Cynomolgus Monkeys by Lampalizumab for the Treatment of Geographic Atrophy. J Pharmacol Exp Ther 2015;355(November):288–96
39. Li H, Xu J, Fan X. Target-mediated pharmacokinetic/pharmacodynamic model based meta-analysis and dosing regimen optimization of a long-acting release formulation of exenatide in patients with type 2 diabetes mellitus. J Pharmacol Sci 2015;127(2):170–80
40. Stein AM, Ramakrishna R. AFIR: A Dimensionless Potency Metric for Characterizing the Activity of Monoclonal Antibodies. CPT Pharmacometrics Syst Pharmacol 2017;6(4):258–66
41. Guo D, Mulder-Krieger T, IJzerman AP, et al. Functional efficacy of adenosine A2A receptor agonists is positively correlated to their receptor residence time. Br J Pharmacol 2012;166(6):1846–59
42. Costa B, Da Pozzo E, Giacomelli C, et al. TSPO ligand residence time: a new parameter to predict compound neurosteroidogenic efficacy. Sci Rep 2016;6(August 2015):18164
43. Ruffolo RR. Important Concepts of Receptor Theory. J Auton Pharmacol 1982;2(4):277–95
44. Visser SAG. Neuroactive Steroids Differ in Potency but Not in Intrinsic Efficacy at the GABAA Receptor in Vivo. J Pharmacol Exp Ther 2002;303(2):616–26
45. Monastyrskaia K, Lundstrom K, Plahl D, et al. Effect of the umami peptides on the ligand binding and function of rat mGlu4a receptor might implicate this receptor in the monosodium glutamate taste transduction. Br J Pharmacol 1999;128(5):1027–34
46. Bakshi S, de Lange EC, van der Graaf PH, et al. Understanding the Behavior of Systems Pharmacology Models Using Mathematical Analysis of Differential Equations: Prolactin Modeling as a Case Study. CPT pharmacometrics Syst Pharmacol 2016;5(7):339–51
47. Kleinbloesem CH, van Brummelen P, Danhof M, et al. Rate of increase in the plasma concentration of nifedipine as a major determinant of its hemodynamic effects in humans. Clin Pharmacol Ther 1987;41(1):26–30
48. Röblitz S, Stötzel C, Deuflhard P, et al. A mathematical model of the human menstrual cycle for the administration of GnRH analogues. J Theor Biol 2013;321:8–27

Acknowledgements

I would like to acknowledge the contribution of anyone who has contributed to the content of this thesis. Firstly, I would like to thank professor Meindert Danhof, professor Piet Hein van der Graaf and dr. Liesbeth de Lange for their conceptual preparation, innovative ideas and critical review of all elements in this work.

Secondly, I would like to thank my colleagues at the pharmacology department for the numerous critical discussions that provided new ideas and refined the results regarding the pharmacokinetic/pharmacodynamic and the modelling aspects of this work. This research was part of the IMI consortium Kinetics for Drug Discovery (K4DD), which enabled frequent discussions and exchange of expertise. I would like to thank professor Ad IJzerman and dr. Anke Mueller-Fahrnow for their leadership in this consortium and professor Steve Hill for leading the fellow program. I would like to thank all colleagues in the K4DD consortium for their helpful insights and critical discussions regarding the binding kinetics aspects in this thesis, especially Laura Heitman, Indira Nederpelt and Eric Wong. I am also grateful for the numerous discussions with professor Bert Peletier and dr. Vivi Rottschäffer about the mathematical aspects of my results.

Thirdly, I would like to thank my Master students Michelle Laerke, Joost Versfelt and Anna Vlot for their contribution to these results and their discussions with me to refine the results and their representation.

Finally, I would like to thank Janneke Klop for her critical support of my research and the visual and textual representation thereof.

Curriculum Vitae Wilbert de Witte

Wilbert de Witte started his studies in Bio-Pharmaceutical sciences at Leiden University in 2007. As part of the Master of Science programme, he performed internships in Organic Chemistry at the division of Bio-Organic synthesis and in pharmacokinetic/pharmacodynamic modeling at the division of Pharmacology, both at Leiden University. In 2013, he started his PhD research in the Pharmacology division of the Leiden Academic Centre for Drug Research under supervision of dr. Liesbeth de Lange, professor Piet van der Graaf and professor Meindert Danhof, which resulted in this thesis. His research aimed to identify the influence of drug-target binding kinetics on *in vivo* drug action by using modelling and simulation techniques. To identify this influence, drug-target binding kinetics are integrated with the other drivers of *in vivo* drug effects. This research was part of the IMI Kinetics for Drug Discovery (K4DD) consortium, which is a public-private partnership with several European universities and pharma companies. In October 2017, he started to work at Ablynx in Ghent as Modeling & Simulation scientist.

List of publications

Publications related to this thesis:

Witte, W.E.A. de, Danhof, M., Graaf, P.H. van der, and Lange, E.C.M. de (2017). The long residing negligence of target saturation **Nat. Rev. Drug Disc.** *Manuscript under revision*.

Witte, W.E.A. de, Vauquelin, G., Graaf, P.H. van der, and Lange, E.C.M. de (2017). The influence of drug distribution and drug-target binding on target occupancy: The rate-limiting step approximation. **Eur. J. Pharm. Sci.** *Epub ahead of print.*

Witte, W.E.A. de, Danhof, M., Graaf, P.H. van der, and Lange, E.C.M. de (2016). In vivo Target Residence Time and Kinetic Selectivity: The Association Rate Constant as Determinant. **Trends Pharmacol. Sci.** *37*: 831–842.

Witte, W.E.A. de, Wong, Y.C., Nederpelt, I., Heitman, L.H., Danhof, M., Graaf, P.H. van der, et al. (2015). Mechanistic models enable the rational use of in vitro drug-target binding kinetics for better drug effects in patients. **Expert Opin. Drug Discov**. *11*: 45–63.

De Lange, E.C.M., Van den Brink, W., Yamamoto, Y., de Witte, W.E.A., Wong, Y.C. (2017). Novel CNS drug discovery and development approach: model-based integration to predict neuro-pharmacokinetics and pharmacodynamics. **Expert Opin. Drug Discov**. *Epub ahead of print.*

Bot, I., Ortiz Zacarías, N. V., Witte, W.E.A. de, Vries, H. de, Santbrink, P.J. van, Velden, D. van der, et al. (2017). A novel CCR2 antagonist inhibits atherogenesis in apoE deficient mice by achieving high receptor occupancy. **Sci. Rep.** *7*: 52.

Schuetz, D.A., Witte, W.E.A. de, Wong, Y.C., Knasmueller, B., Richter, L., Kokh, D.B., et al. (2017). Kinetics for Drug Discovery: an industry-driven effort to target drug residence time. **Drug Discov. Today** *22*: 896–911.

Publications unrelated to this thesis:

Dubois, V.F.S., Witte, W.E.A. De, Visser, S.A.G., Danhof, M., and Pasqua, O. Della (2016). Assessment of Interspecies Differences in Drug-Induced QTc Interval Prolongation in Cynomolgus Monkeys, Dogs and Humans. **Pharm. Res.** *33*: 40–51.

Delft, P. Van, Witte, W. De, Meeuwenoord, N.J., Heden Van Noort, G.J. Van Der, Versluis, F., Olsthoorn, R.C.L., et al. (2014). Design of a ribosyltriazole-annulated cyclooctyne for oligonucleotide labeling by strain-promoted alkyne-azide cycloaddition. **European J. Org. Chem.** 2014: 7566–7571.

Walvoort, M.T.C., Witte, W. de, Dijk, J. van, Dinkelaar, J., Lodder, G., Overkleeft, H.S., et al. (2011). Mannopyranosyl uronic acid donor reactivity. **Org. Lett.** *13*: 4360–3.

Samenvatting in het Nederlands

Op mechanisme gebaseerde modellering van de binding van geneesmiddelmoleculen aan het doelwit als bepalende factor voor het beloop van het effect *in vivo.*

Deel 1. Introductie

Zowel lichaamseigen stoffen als lichaamsvreemde geneesmiddelen kunnen alleen een effect in het lichaam bewerkstelligen als gevolg van het binden aan hun "bindingsplaats". Dit is meestal een eiwit zoals een receptor, een enzym of een ion kanaal. De snelheid van het binden van een geneesmiddel aan (associatie) en het weer loskomen van (dissociatie) het doelwit wordt bindingskinetiek genoemd. Deze bindingskinetiek kan een bepalende factor zijn voor het beloop van het effect na toediening van een geneesmiddel.

Van kandidaat geneesmiddelen wordt om die reden in toenemende mate de bindingskinetiek bepaald. De meest eenvoudige beschrijving van bindingskinetiek is weergegeven in vergelijking 1, waar k_{on} de tweede orde associatie snelheidsconstante, k_{off} de eerste orde dissociatie snelheidsconstante, L de concentratie van de stof die bindt aan het doelwit (het ligand), R de concentratie van het doelwit en LR de concentratie van het gebonden geneesmiddel-doelwit complex is. De ratio k_{off}/k_{on} is gelijk aan de dissociatie constante K_D.

$$L + R \underset{k_{off}}{\overset{k_{on}}{\rightleftarrows}} LR \qquad 1$$

De beschrijving van de bindingskinetiek van een geneesmiddel aan het doelwit, zoals gegeven in vergelijking 1, wordt in de praktijk toegepast om het beloop van concentraties van monoclonale antilichamen te beschrijven in zogenaamde wiskundige "target mediated drug disposition" (TMDD) modellen. Echter, in de selectie van kleine moleculen (dat wil zeggen stoffen met een molecuulgewicht kleiner dan 1000 Dalton) wordt de bindingskinetiek meestal niet meegenomen in de beschrijving van het beloop van de concentratie (de farmacokinetiek) en de optimalisatie tot geneesmiddelen. Bovendien wordt bij de beschrijving van de farmacokinetiek en van het effect (de farmacodynamiek) de snelheid van associatie en dissociatie meestal verwaarloosd, er van uit gaande dat deze snelheden zo hoog zijn in vergelijking met andere processen op het causale pad van toediening tot het effect, dat deze niet een snelheidsbepalende stap vormen.

Echter, sinds 2006 is er een nieuwe interesse ontstaan in het gebruik van de bindingskinetiek als selectie criterium bij het ontwikkelen van nieuwe kleine moleculen tot geneesmiddelen. Hierbij is er vooral aandacht voor de waarde van k_{off}, om de volgende vier redenen:

- Een lage k_{off} waarde kan resulteren in een langere bezetting van het doelwit en daarmee indirect een verlenging van de werkingsduur.
- Een lage k_{off} waarde kan resulteren in een meer selectieve bezetting van de gewenste bindingsplaats ten opzichte van ongewenste bindingsplaatsen, met als gevolg een gunstiger verhouding tussen de gewenste werking en mogelijke bijwerkingen.
- Een lage k_{off} waarde kan resulteren in een bezetting van het doelwit die minder gevoelig is voor competitie door wisselende concentraties van endogene stoffen die aan dezelfde bindingsplaats binden.
- een lage k_{off} waarde kan resulteren in efficiëntere koppeling tussen de binding en de verdere signaal overdracht.

Het onderzoek dat is beschreven in dit proefschrift is gericht op de relatie tussen de k_{off} en het beloop van de bezetting van het doelwit en het effect, zoals naar voren komt in de eerste drie van de bovengenoemde punten. Het vierde punt lag daarmee buiten het beoogde bereik van dit proefschrift.

De kinetiek van de binding van een geneesmiddel aan het doelwit is slechts één van de processen op het causale pad van toediening tot en met effect die het beloop van de werking *in vivo* bepalen. Dit is één van de redenen waarom het lastig is om *in vitro* metingen van bindingskinetiek te vergelijken met *in vivo* metingen, zoals besproken is in **hoofdstuk 1**. Andere factoren met een grote invloed op het tijdsverloop van geneesmiddeleffecten *in vivo* zijn o.a. de snelheid waarmee het geneesmiddel in het lichaam wordt opgenomen, zich verdeelt over de weefsels en uiteindelijk weer wordt afgebroken/verwijderd en de snelheid waarmee het geneesmiddel de plaats van werking bereikt en weer verlaat. Deze factoren bepalen het beloop van de concentratie in het lichaam en daarmee indirect ook het beloop van het effect.

Een andere belangrijke factor is de aanwezigheid van endogene stoffen. Deze binden aan dezelfde bindingsplaats als het geneesmiddel en kunnen door deze competitie de binding van het geneesmiddel aan de bindingsplaats verhinderen. Verder is ook de afbraaksnelheid van het doelwit een belangrijke factor die de werkingsduur van geneesmiddelen kan beïnvloeden, aangezien een doelwit dat snel wordt afgebroken bij voorbaat al geen lange duur van bezetting kan hebben.

Tenslotte is de snelheid waarmee na binding, en daarmee activatie of blokkering van de bindingsplaats, het signaal wordt overgedragen via signaalstoffen en de terugkoppelingsmechanismen die dit in gang zet ook van invloed op de tijdsduur van het effect.

Het doel van dit proefschrift was om de samenhang tussen enerzijds de kinetiek van de binding aan het doelwit en anderzijds het beloop van de bezetting van het doelwit en uiteindelijk het effect *in vivo* te onderzoeken. Dat is vooral, maar niet uitsluitend, belangrijk als de kinetiek van de binding de snelheidsbepalende stap is. Dit concept is bekend van chemische reactievergelijkingen waarbij de langzaamste reactie vaak de snelheidsbepalende stap wordt genoemd. Voor de duur van de bindingsplaats bezetting door het geneesmiddel kan de invloed van de k_{off} dan ook onderzocht worden door de afnamesnelheid van de doelwitbezetting te vergelijken met de snelheid van de andere processen, zoals de snelheid waarmee de geneesmiddelconcentraties afnemen.

Bij het bepalen van de snelheidsbepalende stap is een belangrijke factor dat de snelheid waarmee de doelwitbezetting afneemt niet constant is ten opzichte van de geneesmiddelconcentratie vanwege de niet-lineaire relatie tussen de concentratie van het geneesmiddel en de bezettingsgraad van het doelwit, waarbij bij hogere concentraties verzadiging van de binding aan het doelwit optreedt. Dit betekent, zoals beschreven in **hoofdstuk 2**, dat een halvering van de geneesmiddelconcentratie slechts zorgt voor een kleine afname in de bezettingsgraad van het doelwit wanneer de geneesmiddelconcentraties hoog zijn, terwijl bij een lage geneesmiddelconcentratie dit ook zorgt voor een halvering van de bezettingsgraad. Dit betekent dat bij een hoge bezettingsgraad van het doelwit pas bij een veel lagere waarde van de k_{off} de dissociatie van de bindingsplaats de snelheidsbepalende stap is. In **hoofdstuk 2** hebben we deze relatie verder gekwantificeerd.

Deel 2. Simulaties, modelanalyse en experimentele validatie van de invloed van bindingskinetiek op het beloop van de doelwit bezetting.

De relaties tussen enerzijds de kinetiek van de binding aan het doelwit en anderzijds het beloop van het effect zijn complex, omdat de verschillende processen op het causale pad niet onafhankelijk van elkaar zijn. Dit is vooral duidelijk bij de afname van geneesmiddelconcentraties en de dissociatie van het doelwit-geneesmiddel complex. Wanneer dit complex uiteenvalt komt er namelijk weer ongebonden geneesmiddel vrij die de dalende plasmaconcentraties aanvult, wat ervoor zorgt dat de afname van de geneesmiddelconcentratie langzamer gaat dan wanneer er geen geneesmiddel dissocieert van het doelwit. Om in deze situatie te bepalen wat de snelheidsbepalende stap is voor de afname van bindingsplaats bezetting, beschrijven we in **hoofdstuk 4** een integraal wiskundig model voor het beloop van de bezetting van het doelwit voor een systeem waarin het doelwit zich in het plasma compartiment of in een perifeer compartiment bevindt. Daarbij houden we zowel rekening met de verzadiging van de bindingsplaats als met de interactie tussen farmacokinetiek en doelwitbinding. Het resultaat van onze benadering is een algebraïsche formule voor de afname van de bezettingsgraad van het doelwit, als functie van de k_{el}, de k_{off}, de k_{on}, de concentratie van de bindingsplaats, de snelheidsconstanten die de distributiesnelheid naar de plaats van binding bepalen en de gebonden fractie van het doelwit. Met deze formule hebben we kunnen onderzoeken voor welke waarden van k_{on} en k_{off} de dissociatie van het doelwit de snelheidsbepalende stap voor het beloop van de bezettingsgraad van het doelwit is.

Onder de aanname van een relatief snelle distributie naar de bindingsplaats geldt volgens deze benadering dat dissociatie alleen de snelheidsbepalende stap is wanneer de k_{off} kleiner is dan $k_{el} * (1\text{-}BF)$ en k_{on} kleiner is dan k_{el}/R_{tot}. Hierbij is *BF* de gebonden fractie van de bindingsplaats en R_{tot} de concentratie van de bindingsplaats. Hieruit volgt dat voor een waarde van k_{on} groter dan k_{el}/R_{tot}, de dissociatie van het doelwit nooit de snelheidsbepalende stap is voor de afname van de doelwitbezettingsgraad, ongeacht hoe laag de waarde van k_{off} is. In dit geval heeft de k_{on} een even grote invloed op de afnamesnelheid van de doelwitbezetting als de k_{off}, aangezien de binding in evenwicht is en daarmee dus bepaald wordt door de K_D. In deze formules is ook duidelijk de belangrijke rol van de concentratie van het doelwit zichtbaar, terwijl hier vaak geen rekening mee wordt gehouden in het onderzoek naar de rol van bindingskinetiek. Wij concluderen dan ook dat het begrip van de rol van bindingskinetiek verbeterd is door rekening te houden met de concentratie van het doelwit en de invloed van binding op de farmacokinetiek.

In **hoofdstuk 5** concentreren we ons met name op de invloed van binding op lokale geneesmiddelconcentraties rondom de bindingsplaats (de concentraties in de zgn. "biofase"). Hiervoor spelen dezelfde principes een rol als beschreven in **hoofdstuk 4**, maar de lokale geneesmiddelconcentratie rondom de bindingsplaats, als gevolg van de binding aan het doelwit, is altijd hoger in vergelijking met de vrije concentraties elders in het weefsel of in het lichaam In dit hoofdstuk vergelijken we twee benaderingsmethoden voor de invloed van bindingsplaatsbinding op lokale concentraties: de "snelheidsbepalende stap" benadering, zoals beschreven in **hoofdstuk 4**, en de zogenaamde "evenwichtsbenadering", waarbij wordt aangenomen dat de lokale concentraties snel veranderen ten opzichte van de doelwitbinding. Deze twee methodes zijn beide algebraische benaderingen van hetzelfde volledige wiskundige model, dat bestaat uit differentiaalvergelijkingen. We hebben deze benaderingsmethoden dan ook vergeleken met het volledige model door met alle methoden de bezettingsgraad van het doelwit te simuleren. Uit deze simulaties bleek dat de "snelheidsbepalende stap" benadering de beste benadering geeft van de volledige set aan differentiaalvergelijkingen. De verschillen tussen beide benaderingen zijn vooral groot wanneer de dissociatie van het doelwit-geneesmiddel complex relatief snel gaat ten opzichte van de snelheid waarmee het geneesmiddel verdwijnt uit de omgeving van het doelwit (middels diffusie of actief transport) en de associatie aan het doelwit. Dit valt ook te begrijpen omdat deze evenwichtsaanname onder deze condities niet geldt. We concluderen dat de snelheidsbepalende stap benadering de voorkeur heeft voor het beschrijven van de invloed van binding op lokale geneesmiddel concentraties.

In **hoofdstuk 6** breiden we ons onderzoek uit naar de duur van bindingsplaats bezetting van zowel de gewenste bindingsplaats als van een ongewenste bindingsplaats. We bestuderen hier dus het verloop van selectiviteit over tijd en de beïnvloeding hiervan door de bindingskinetiek en de bindingsplaatsconcentratie. We onderzoeken twee soorten selectiviteit d.m.v. simulatiestudies: "bindingsplaatsselectiviteit" verwijst naar selectiviteit voor een bindingsplaats ten opzichte van andere bindingsplaatsen, en "weefselselectiviteit" verwijst naar selectiviteit voor een weefsel ten opzichte van andere weefsels. Uit deze simulatiestudies blijkt dat de invloed van de bindingskinetiek en de bindingsplaatsconcentratie zoals beschreven in **hoofdstuk 4** ook relevant is voor bindingsplaats- en weefselselectiviteit. Voor het verloop van bindingsplaatsselectiviteit over tijd wordt vaak gezegd dat een lagere k_{off} voor de gewenste bindingsplaats ten opzichte van de ongewenste bindingsplaats zorgt voor een toename van selectiviteit over tijd, ook wel "kinetische selectiviteit" genoemd. Uit onze simulaties blijkt dat een hoge bindingsplaats concentratie of een lage K_D deze kinetische selectiviteit vermindert, omdat dit zorgt voor een afname van de bezettingsgraad die niet door de dissociatie wordt bepaald. Verder zorgt een lage K_D juist voor een toename van weefselselectiviteit voor het weefsel met de hoogste bindingsplaats concentratie door retentie van het geneesmiddel in dit weefsel, tenzij de K_D zo laag wordt dat de geneesmiddel retentie ook in het weefsel met de laagste bindingsplaats concentratie plaatsvindt.

In **hoofdstuk 6** laten we tenslotte zien dat deze inzichten toegepast kunnen worden op drie bestaande geneesmiddelen en hun selectiviteit voor de CB1 receptor. Op basis van een nieuw ontwikkelde voorspelling van de K_D voor deze stoffen voor de CB1 receptor, 3 andere receptoren, en de receptorconcentraties in 3 verschillende hersengebieden, laten we zien dat de selectiviteit voor de verschillende hersengebieden wordt bepaald door de receptorconcentraties en K_D waardes. Bovendien blijkt uit deze simulaties dat het voor stoffen met een lage K_D meerdere dagen kan duren voordat een stabiele bezettingsgraad van de receptor bereikt wordt. We concluderen dat een lage K_D waarde niet altijd wenselijk is en dat er bij optimalisatie van de K_D en de bindingskinetiek rekening gehouden dient te worden met de concentraties van de bindingsplaatsen en de distributiesnelheid naar de verschillende weefsels.

Deel 3. Simulaties, modelanalyse en experimentele validatie van de invloed van bindingskinetiek op het tijdsverloop van geneesmiddel effecten.

Terwijl we in de voorgaande hoofdstukken vooral onderzochten hoe bindingskinetiek de bezettingsgraad van het doelwit beïnvloedt, beschrijven we in **hoofdstuk 7** de invloed van bindingskinetiek op het tijdsverloop van een geneesmiddeleffect. We focussen ons in dit hoofdstuk op het verschil in het tijdsverloop van een geneesmiddeleffect tussen de situatie waar de distributie naar de plaats van werking langzaam is en de situatie waar de binding aan de bindingsplaats langzaam is. De wiskundige modellen die deze situaties beschrijven hebben we gebruikt om een bestaande collectie meetgegevenste analyseren van het effect van morfine op het elektro-encefalogram (EEG) in ratten. Bij deze analyse zagen we dat het lastig was om het verschil in de beschrijving van de meetgegevens tussen beide modellen te zien en dat alleen een kwantitatieve analyse van de beschrijving van de meetgegevens voor beide modellen kon laten zien dat het model voor de langzame distributie naar de plaats van werking de data het best beschreef.

Om het verschil tussen beide modellen verder uit te zoeken hebben we ook geanalyseerd voor welke parameterwaardes het gebruik van verschillende doseringen leidt tot een verschil in de tijd tot het maximale geneesmiddeleffect in het bindingsmodel. Het verschuiven van de tijd tot het maximale geneesmiddeleffect is namelijk een belangrijke eigenschap die het verschil tussen het bindingsmodel en het distributiemodel bepaalt. Uit deze analyse bleek dat een k_{off} die veel kleiner is dan de k_{el} en een K_D die veel kleiner is dan de doelwitconcentratie zorgen voor een vermindering van het verschuiven van de tijd tot het maximale geneesmiddeleffect. Daardoor is onder deze voorwaarden het verschil tussen beide modellen klein en moeilijk te identificeren. De kleine verschillen tussen het bindings- en distributiemodel zorgen ervoor dat een beschrijving van experimentele gegevens met één van deze modellen niet voldoende is om de relevantie van het gebruikte mechanisme aan te tonen, terwijl deze denkstap in de literatuur wel vaak impliciet of expliciet gemaakt wordt. We pleiten dan ook voor het vaker testen van het bindingsmodel, ook omdat voor dit model *in vitro* gegevens kunnen worden gebruikt en zo een betere *in vitro - in vivo* vertaling kan worden verkregen. Bovendien kunnen op deze manier ook mogelijke interacties van stoffen die binden aan dezelfde bindingsplaats beter worden gekarakteriseerd.

In **hoofdstuk 8** komen de laatste onderwerpen uit dit proefschrift aan de orde: de invloed van de bindingskinetiek van endogene stoffen en de rol van signaaltransductie en terugkoppelingsmechanismen. Om dit te kunnen onderzoeken is eerst de bindingskinetiek van dopamine en 17 verschillende dopamine antagonisten *in vitro* bepaald. Vervolgens zijn de cyclisch adenosine monofosfaat (cAMP) responsprofielen gemeten na pre-incubatie met dopamine en toevoeging van de antagonisten. Deze gegevens zijn gebruikt om een minimaal mechanistisch model te ontwikkelen. Dit model beschrijft de competitieve binding van dopamine en de antagonist aan de dopamine D_2 receptor, de invloed van receptorbinding op de cAMP synthese en de negatieve terugkoppeling tussen cAMP en PDE (fosfodiësterase). Tenslotte beschrijven we de analyse van dit model middels een simulatie studie met fluctuerende dopamine concentraties. De endogene dopamineconcentraties fluctueren *in vivo* op verschillende tijdschalen variërend van seconden tot uren. Om dit na te bootsen hebben we de dopamineconcentraties laten variëren volgens een sinusfunctie, waarbij de frequentie van de sinusfunctie werd gevarieerd om zo een wijd bereik van frequenties te onderzoeken. Uit deze studie kwam naar voren dat voor hoge frequenties van dopamineconcentratiefluctuaties de binding van dopamine aan de receptor en de omzettingssnelheid van cAMP te laag zijn om deze concentratiefluctuaties om te zetten in fluctuaties van cAMP. Deze hoogfrequente dopaminefluctuaties resulteren in een stabiele, gemiddelde cAMP respons. Dit betekent ook dat de k_{off} van de dopamine agonisten geen invloed meer heeft op de gevoeligheid voor fluctuaties in dopamine concentraties zodra deze k_{off} hoger is dan de k_{off} van dopamine of de degradatiesnelheidsconstante van cAMP. In dit hoofdstuk hebben we dus laten zien dat de invloed van bindingskinetiek bestudeerd moet worden in verband met de bindingskinetiek van endogene stoffen, signaal overdracht en terugkoppelingsmechanismen.

In **hoofdstuk 9** bespreken we de bevindingen uit de voorgaande hoofdstukken en hoe deze bevindingen zich verhouden met de bestaande inzichten. Verder bespreken we de mogelijkheden voor vervolgonderzoek en vatten we de belangrijkste conclusies van het onderzoek samen. We laten in dit hoofdstuk zien dat de kinetiek van de binding aan het doelwit alleen onder specifieke omstandigheden een invloed heeft op het beloop van de bezettingsgraad en het geneesmiddeleffect. Tevens leveren we kwantitatieve richtlijnen over de parameterwaarden die leiden tot een grote invloed van de k_{off} op de werkingsduur van een geneesmiddel. In dit proefschrift hebben we ons vooral gericht op de relatie tussen bindingskinetiek, farmacokinetiek, competitie met endogene stoffen, signaal transductie en terugkoppelingsmechanismen. Eén van de onderwerpen die we wel deels hebben besproken maar nog verder onderzocht moet worden is de invloed van de omzettingssnelheid van het doelwit. Verder hebben we de invloed van signaaloverdracht slechts onderzocht voor één overdrachtssysteem met omzetting van een eerste signaalstof en negatieve terugkoppeling hierop. Dit zou verder onderzocht kunnen worden voor meer complexe systemen met positieve terugkoppeling en vertakte signaaloverdrachtssystemen.

In dit proefschrift is steeds gebleken dat de rol van bindingskinetiek alleen begrepen kan worden als andere relevante factoren, zoals de farmacokinetiek, ook meegewogen worden. We hebben niet alleen laten zien dat dit nodig is maar ook hoe dit bepaald kan worden. We concluderen dan ook dat de rol van bindingskinetiek alleen begrepen kan worden met inbegrip van de gehele farmacokinetische en farmacodynamische context. Alhoewel nog steeds meer onderzoek te verrichten valt kunnen de inzichten die wij hier hebben verkregen gebruikt worden om de beste geneesmiddelkandidaten te selecteren en verder te ontwikkelen.